WOODHEAD PUBLISHING IN TEXTILES

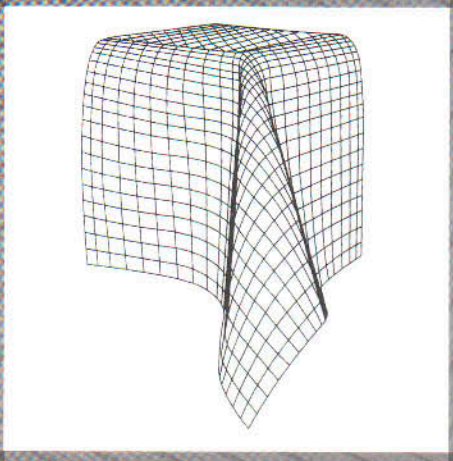

Structure and mechanics of woven fabrics

Jinlian HU

CRC

The Textile Institute

WP

Structure and mechanics of woven fabrics

Structure and mechanics of woven fabrics

Jinlian HU

The Textile Institute

CRC Press
Boca Raton Boston New York Washington, DC

WOODHEAD PUBLISHING LIMITED
Cambridge England

Published by Woodhead Publishing Limited in association with The Textile Institute
Woodhead Publishing Ltd
Abington Hall, Abington
Cambridge CB1 6AH, England
www.woodhead-publishing.com

Published in North America by CRC Press LLC
2000 Corporate Blvd, NW
Boca Raton FL 33431, USA

First published 2004, Woodhead Publishing Ltd and CRC Press LLC

British Library Cataloguing in Publication Data
A catalogue record for this book is available from the British Library.

Library of Congress Cataloging in Publication Data
A catalog record for this book is available from the Library of Congress.

Woodhead Publishing ISBN 1 85573 904 6
CRC Press ISBN 0-8493-2826-8
CRC Press order number: WP2826

The publisher's policy is to use permanent paper from mills that operate a sustainable forestry policy, and which have been manufactured from pulp which is processed using acid-free and elementary chlorine-free practices. Furthermore, the publisher ensures that the text paper and cover board used have met acceptable environmental accreditation standards.

Typeset by Replika Press Pvt Ltd, India
Printed by TJ International, Padstow, Cornwall, England

Contents

Preface

This book introduces fundamental and advanced fabric structure and mechanics. There are 10 chapters covering the general features of textile structure and mechanics. All the simple modes of deformation such as tensile, bending, shear and compression, and the complex, particularly drape deformation of fabrics (mainly woven), are discussed. Testing methods for the objective/instrumental measurement of fabric mechanical properties and structure parameters are also included.

I am grateful to my PhD supervisor, Dr Alan Newton, in the Textile Department of UMIST. He introduced me to fabric structure and mechanics and, through his extensive academic knowledge in this area, taught me the fascinating science of fibre assemblies.

From my own point of view, mechanics is the most difficult science. I achieved lower marks in this subject than in the other subjects I studied as a bachelor degree student. Fabric mechanics must be the most difficult of all areas of mechanics because all my predecessors and the people I have worked with have said so. It is funny to think that I have picked this area for my research. It is also a very rewarding area to work in for the following reasons:

1. I have benefited from the academic standards and professionalism of many outstanding people: Prof. John Hearle, Prof. Ron Postle, Prof. Ning Pan, Prof. George Stylios, Prof. Tongxi Yu and many more.
2. I have become more versatile and have been able to handle other areas of research much more easily because of my understanding and experience in fabric mechanics. This is because the challenges in this field have helped me to solve problems in other areas such as Shape Memory Materials and Textiles more conveniently and quickly.
3. I have made many friends by carrying out different projects and working with different people from all over the world, from India to Europe, from east to west, from students to outstanding scholars, from Hong Kong and China, and across various disciplines ranging from physics, mechanics, civil and structural mechanics, textiles and clothing, medicine, etc.
4. I feel I am a scientist rather than a textile technologist, and thus have no

psychological barriers in regards to working with people from different disciplines, such as chemistry and physics. This has helped me to open new research areas the past few years.

5. Fabric mechanics has become one of the most popular subjects for research students in the Institute of Textiles and Clothing in the Hong Kong Polytechnic University. This is evidenced by the fact that students continue to select this subject; I offer it every semester to different students.

Indeed, as I tell my students, mechanics is closely related to forces. Can anybody tell me what materials or products are used without applying a force? It is difficult to find any. Every researcher should know some basic facts about mechanics; every research student in clothing and textiles should know something about textile/fabric mechanics. Not only that, textiles have been used for many, many areas because of their unique characteristics, as introduced in Chapter 1. To apply textiles to these areas properly and optimally, an understanding of the structures and mechanics of fabrics is required. This book can be used by people working in many areas, including textile composites, geotextiles, medical textiles, transportation textiles, etc.

Thus, I hope this book will be useful for many people and benefit many sectors of scientific and technological development. In particular, people working in the areas of textiles, clothing, materials, fibrous composites and medical textiles will find this book useful as a reference and/or textbook for studying, research and teaching.

Dr Jinlian HU
Institute of Textiles and Clothing
The Hong Kong Polytechnic University
Hung Hom, Kowloon, Hong Kong
tchujl@polyu.edu.hk

Acknowledgements

This book is the effort of many people in addition to the author. I would like to take this opportunity to thank the following individuals:

- Dr Debbie Jiang Xiuying, who helped with editing the first version of this book;
- Mr Xin Binjie also helped in editing the final version of Chapters 2, 3, 8 and 9;
- Candy Wu, who helped in formatting the chapters.

The contents of the book are based on my intensive research work over the past 15 years starting from my PhD study in UMIST, Manchester, UK until now. During this time, my research students and research assistants at the Hong Kong Polytechnic University have helped me with many projects. They are:

- Dr Jane Chung Siu-Ping, whose research into seams is included;
- Dr Winnie Lo Wing-Man, whose study of the anisotropy of woven fabrics has been used in different chapters;
- Dr Chen Shuifu, whose work on the applications of finite-volume methods to the simulation of fabric drape is also included;
- Dr Fengjun Shi, who worked with me for about one year – his modelling of bending and wrinkling using viscoelastic properties is included in Chapter 5.

I have also worked with many outstanding people over the past few years for the work reported in this book. They are:

- Prof. John Hearle, who has helped me since I was a PhD student in UMIST;
- Prof. Ron Postle, who has been one of my PhD students' co-supervisors and from whom I learned particularly the methods of and cultivated a passion for supervision;
- Prof. Tongxi Yu and Prof. Jinguang Teng, who collaborated with me in the complex deformation of fabrics, including drape and wrinkle simulation.

Sections of the following articles have been included in this book and I wish to thank Dr Ludwig Rebenfeld, editor of the *Textile Research Journal*, for allowing us to include them here:

1. Bending hysteresis of plain woven fabrics in various directions, no. 70, pp. 237–242, March 2000.
2. Modeling the creasing properties of woven fabrics, no. 70, pp. 247–255, March 2000.
3. Bending behavior of woven fabrics with vertical seams, no. 70, pp. 148–153, February 2000.
4. The KES shear test for fabrics, no. 67, pp. 654–664, September 1997.
5. Shear properties of woven fabrics in various directions, no. 72, pp. 383–390, May 2002.
6. Modeling a fabric drape profile, no. 72, pp. 454–463, May 2002.
7. Numerical drape behavior of circular fabric sheets over circular pedestals, no. 70, pp. 593–603, July 2000.
8. Drape behavior of woven fabrics with seams, no. 68, pp. 913–919, December 1998.

In addition, I would like to express my appreciation to Woodhead Publishing Limited, represented by Emma Starr, and The Textile Institute, for giving me the opportunity to publish this book.

Dr Jinlian HU

1
Introduction

1.1 Role of woven fabric mechanics

The science and engineering of textiles and clothing have played an important role in one of the major technological transformations known to mankind: the computer revolution. For example, the Jacquard principle of weaving shares its basis with the binary system in the computer. Textile manufacture, particularly the woven fabric computer-aided design (CAD) system, is one of the earliest success stories in the development of CAD. Therefore, today's textile and clothing plant is significantly different from that of the past. The integration of the principal functions carried out in the production of textile materials and end products (fibres/yarns/fabrics/garments), namely product design, production planning and scheduling, manufacturing, material handling, and distribution, into a single entity is giving rise to the computer-integrated textile enterprise. The implementation of management philosophies, such as quick response and just-in-time, in the textile and apparel industries requires increased flexibility, higher quality and faster response times in new manufacturing systems. Automation and the linking of processes are two ways to reduce labour, improve quality and increase productivity. This trend towards automation and computerisation in textile and clothing manufacturing is not only inevitable but also beneficial.

However, there are still many problems preventing automation and the integration of processes for the textile and clothing industries. For example, automation of the handling and transport of apparel fabrics is of vital interest to researchers and industrialists, where the cost of labour is a significant portion of the total product cost. However, automated handling of textile materials is a difficult task because of their unique engineering properties and the variability of these properties in diverse product applications. Knowledge-based systems are required to control highly flexible automated devices for handling limp materials. These computer systems must be able to take fabric property information and predict the fabric bending behaviour or other mode deformation properties during the handling process. The computer

algorithm must be based on numerical models for predicting the deformations of typical fabrics.

In addition, as consumers have become increasingly sophisticated in their demand for quality textile products, this has led to a requirement for automatic and objective evaluation of fabric appearance with respect to such characteristics as pilling, hairiness, wrinkling, etc. All these issues add up to a need for greater knowledge and more thorough understanding together with mathematical models of fabric structure and mechanics, especially in low-stress mechanical responses and their relationship with fabric structure.

Indeed, woven fabrics are the end products of spinning and weaving, but they are also the raw materials for clothing and other industries such as composites and medical textiles. The study of fabric mechanics under the low-stress conditions which exist in ordinary manufacturing and wear/application processes should be applicable to different sectors, namely apparel manufacturing, wear performance and fabric formation, as well as technical textiles.

An understanding of the formation mechanisms of fabrics is useful for fabric design and process control, and includes investigation of the relationships between fibre properties, yarn structure, fabric construction and fabric physical properties. The constitutive laws of fabrics and other properties will be indispensable to the investigation of clothing construction, automation of clothing manufacturing, and computer-aided clothing design. In addition, low-stress mechanical responses are related to fabric hand, quality and performance; therefore, low-stress structural mechanics can be applied to quality control, process control, product development, process optimisation and product specification, clothing construction, automation of clothing manufacturing, and computer-aided clothing design.

1.2 General features of woven fabric mechanical behaviour

Textile materials differ considerably from conventional engineering materials in many ways. They are inhomogeneous, lack continuity and are highly anisotropic; they are easily deformed, suffering large strains and displacements even at low stress, under ordinary conditions or in normal use; they are non-linear and plastic even at low stress and at room temperature; they often achieve success rather than failure through buckling into shapes with double curvature without forming the sharp corners which appear in the case of paper when it is folded (Amirbayat and Hearle, 1989; Amirbayat, 1991). Thus they possess unique characteristics suitable especially for the human being's body movement, for the satisfaction of the human being's eyes and other physiological and psychological requirements.

1.2.1 Complicated geometric structure

The geometric structure of a fabric is extremely complicated. Figures 1.1 and 1.2 show photos of cross-sectional and surface images of a woven fabric. It is clear that each yarn in the fabric is crimped. The yarn cross-sectional

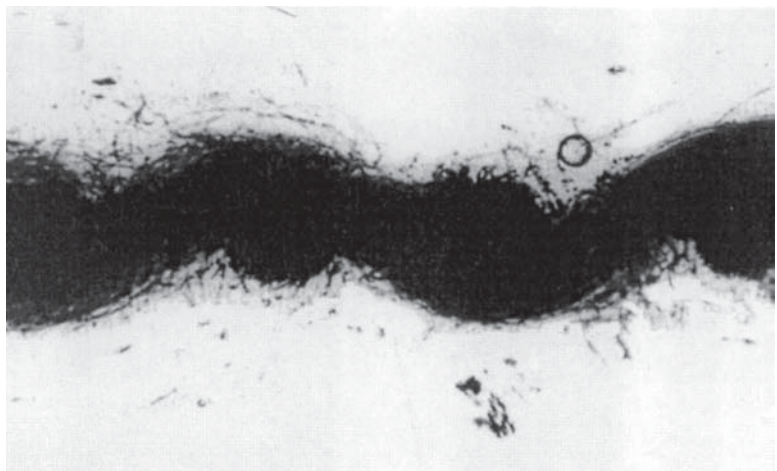

1.1 Cross-section image of a woven fabric.

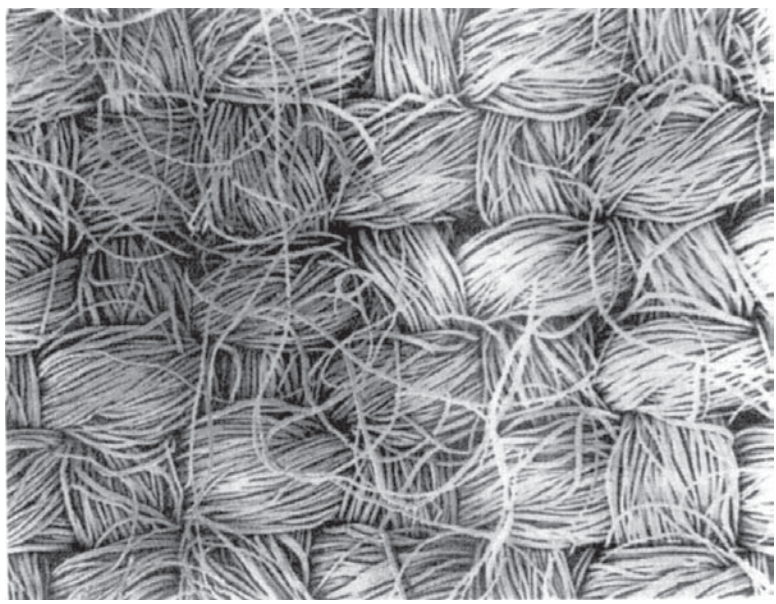

1.2 Surface image of a woven fabric.

shape is rather irregular. Moreover, there are also many fibres which protrude from the yarn surfaces.

Every piece of woven fabric is an integration of warp yarns and weft yarns through intersection. The extent of this intersection is largely dependent on the friction between fibres and yarns together with fibre entanglement, while the distance between two parallel adjacent yarns determines the porosity of a fabric structure. The existence of such a discrete porous structure is what differentiates a fabric from a continuum engineering structure such as a metal sheet.

The simplest theoretical model of yarn configuration is that developed by Peirce (1937). This contrasts with reality because in the theoretical study, the cross-sectional shape and physical properties of a yarn are always simplified and idealised. However, even for this simple model, the calculations required by the geometrical parameters still involve transcendental functions (see Chapter 3).

1.2.2 Large deformability

Figure 1.3 is a typical tensile stress–strain curve of woven fabrics, where the applied tensile force per unit length is plotted against tensile strain. Because fabric sheet is very thin, the usual practice of textile researchers is to use force and moment per unit length rather than stresses in plotting stress–strain curves. This figure shows that the membrane strain is quite large even at

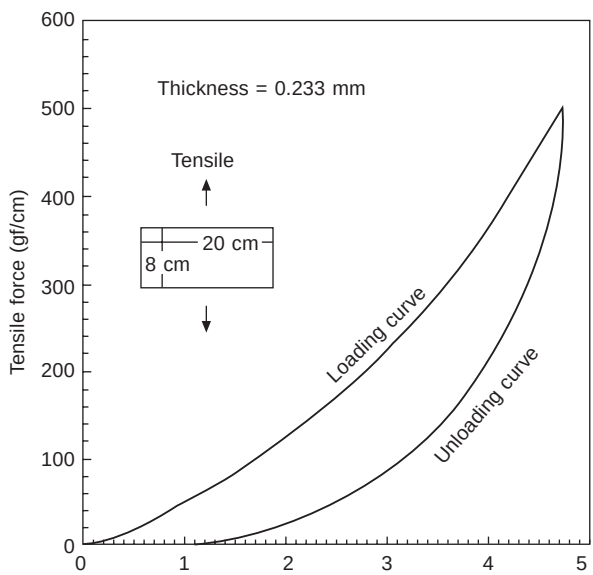

1.3 Tensile stress–strain curve of a woven fabric.

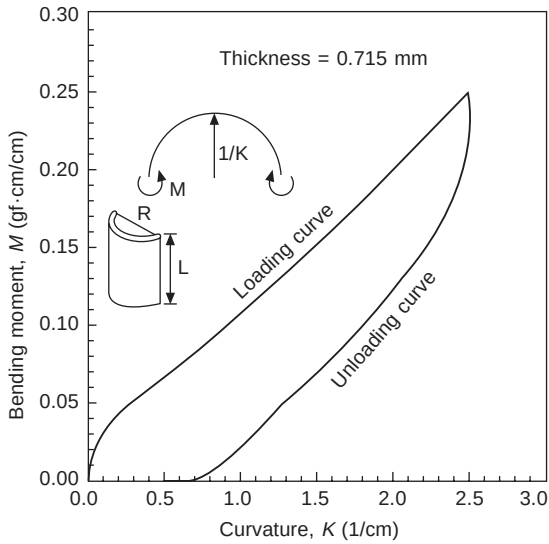

1.4 Moment–curvature curve of a woven fabric.

small forces, due to the straightening of the crimped configuration of the yarns within the fabric. The initial tensile modulus of a typical fabric is of the order of 10 MPa, compared to steel which has an elastic modulus of 2×10^5 MPa.

Compared to tensile deformations, fabrics are even more susceptible to bending deformations when under transverse loading, as shown by Fig. 1.4. Assuming that slippage between fibres is not constrained, we can easily work out the ratio of a yarn's bending stiffness to that of a solid rod of the same cross-section, i.e. $\alpha(\gamma/R)^2$, where α is the porosity ratio (the ratio of the summed area of fibres to that of the yarn cross-sectional area, and is always smaller than 1), R and γ are the radii of the yarn and its constituent fibres, respectively. For a typical yarn which contains 100 fibres, this ratio is ~1:10 000. This makes it possible to produce a thick yarn with great flexibility. In addition, due to the low thickness of fabric sheet, the ratio between bending stiffness and membrane stiffness is small. These factors contribute to the generation of a very low bending stiffness of fabrics, much lower even than their corresponding membrane (stretching) stiffness.

While large deformations can often be neglected in the engineering design of structures using stiff materials, at least in the service stage, they are required in the engineering of fabrics. Fabric under its own weight and/or external forces tends to move through these large deformations and buckle at very small in-plane compressive stresses in order to approach a state of membrane tension which it is better able to resist.

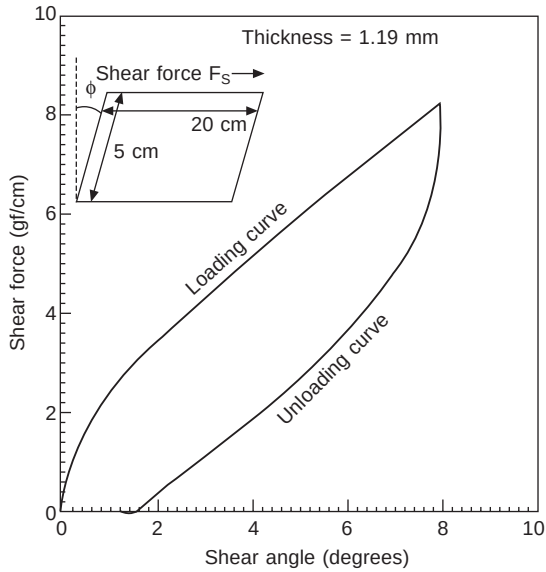

1.5 Shear behaviour of a woven fabric.

1.2.3 Non-linear stress–strain behaviour and inelasticity

Figures 1.3–1.5 show the typical stress–strain curves of woven fabrics (produced from different fabrics). For conventional engineering materials, low-stress deformations usually cause small strains which are related to stresses in a linear manner. By contrast, stress–strain curves of fabrics are complicated and generally non-linear in the low-stress range, becoming almost linear beyond a certain critical stress level. This critical value varies for different deformation modes. It is comparatively high for tension, but is very low and can be near zero for bending and shear.

This unique stress–strain behaviour of fabrics can be attributed to the porous, crimped and loosely connected structure of woven fabrics. Under tension, straightening of crimped yarns occurs at low stresses, and this is why the initial tensile stiffness is small. At high stresses when decrimping is nearly complete and inter-fibre friction is increased, the fabric structure becomes consolidated and the fibres better oriented. This leads to a stress–strain relationship close to linear, which is similar to a solid. In the intermediate range, the stress–strain curve is non-linear, reflecting the consolidation and yarn reorienting process. This behaviour makes an interesting comparison with the tensile behaviour of conventional engineering materials. For the latter, the microstructure of the material changes from order to disorder as the stresses increase. For fabrics, the applied stresses bring about order in the microstructure.

For bending and shear, when the applied stresses are low, inter-fibre friction provides a high initial resistance. However, inter-fibre slippage gradually dominates the behaviour once the frictional resistance between fibres is overcome by applied stresses, and this leads to a reduction in the stiffness as shown in Figs 1.4 and 1.5. Another interesting phenomenon observed from Figs 1.3–1.5 is that loops between loading and unloading curves exist even for low stresses, implying that irrecoverable deformations (inelasticity) occur for fabrics at small stresses. This differs from the situation for most conventional engineering materials for which inelastic deformations are usually associated with stresses which are so high that failure of the material may be imminent.

However, it is by no means the case that textile materials differ from conventional engineering materials in every way. For example, all terms such as inhomogeneous, anisotropical and non-linear come directly from conventional mechanics rather than being invented by the textile scientist. This suggests that such characteristics as non-linear, viscoelastic and inhomogeneous are problems of engineering materials. The view can be justified that the main difference between textile materials and conventional engineering materials is that the former show very complicated mechanical responses to external loads, even under ordinary conditions of low stress and at room temperature, while this happens to the latter usually under large stress, high temperature or other specific conditions. After recognition of this double identity of textile materials, it is reasonable to import conventional mechanical treatments into the study of textile in some circumstances.

1.3 Study of woven fabric mechanics

1.3.1 Summary of previous study

The study of woven fabric mechanics dates from very early work reported by Haas in the German aerodynamic literature in 1912 at a time of worldwide interest in the development of airships. In the English literature, the paper by Peirce (1937) presented a geometrical and a mathematical force model of the plain-weave structure, both of which have been used extensively and modified by subsequent workers in the field.

Considerable progress has been made over the last century in the development of the theory of geometrical structure and mechanical properties of fabrics. Responding to demands from industry, the investigation of the geometry and mechanical behaviour of fabrics has moved successively through observation, explanation and prediction. The main advances were included in the two books (Hearle *et al*., 1969; 1980) edited by the leading figures: Hearle, Grosberg, Backer, Thwaites, Amirbayat, Postle, and Lloyd. The maturity of textile mechanics, and thus of fabric mechanics, was highlighted at the workshop at the NATO Advanced Study Institute held in 1979 (Hearle *et al*.,

1980). One of the major achievements in this process has been the development of the Kawabata Evaluation System (KES) for fabric testing, which proved to be beneficial for the objective measurement of fabric and clothing manufacturing control as well as the development of new materials for apparel fabrics. Since the 1980s the focus for research has been empirical investigations examining the relationship between the parameters obtained from the KES (Kawabata, 1980; Kawabata *et al.*, 1982; Postle *et al.*, 1983; Barker *et al.*, 1985, 1986, 1987) and characteristics such as fabric handle and tailorability. The KES system can provide five modes of tests under low-stress conditions, 17 parameters with 29 values in warp and weft and five charts consisting of nine curves for one fabric. This large amount of data was intended to provide a full description of the fabric. As a whole, it can suit a wide range of purposes in research and applications.

Research in this field in terms of methods and emphasis has taken three directions. These are:

(1) **Component-oriented:** this direction was led by Hearle, Grosberg and Postle and starts from physical concepts and assumptions which are used to facilitate further deductions and for which the theoretical basis is Newton's third law, minimum energy principles and mathematical analysis of construction. The aim is to predict the mechanical responses of fabrics by combining yarn properties, inter-yarn interactions and fabric structures with these assumptions. Many pages of mathematics and personalised programs are involved.

(2) **Phenomena-oriented:** responses of fabrics to applied loads involve elastic, viscoelastic, frictional and plastic parts. Therefore, rheological models consisting of different combination of components, such as the spring that represents the elastic part or the dashpot which represents the frictional part, simulate combined responses of fabrics to applied forces. From these, general relationships of stress–strain could be deduced.

(3) **Results-oriented:** this can be contrasted with the component-oriented direction in that it starts not from assumptions and concepts but from a hypothesis – a function or a statement to describe the experimental results. It then goes back to find the relationship of this function with fabric components such as spacing, dash pot and simulated combined responses before finally subjecting it to further analysis. The theoretical background of this approach is more concerned with pure mathematics, especially numerical methods and statistics. This type of theory is helpful in the ordering of observations. It allows estimates to be made of purely mathematical operations, thus avoiding many subjective assumptions that may be misleading. As the analysis develops, further and more complex phenomena may be revealed and an effective and realistic approach may be developed from this.

There are several questionable features which have been noticed in previous analysis of woven fabric mechanics:

(1) In general, along with the well-established exchange of ideas and the qualitative consideration of experimental results, there is a perceptible worsening of the mutual communications and practical applications as mathematical models become more and more complicated and implicit. This can lead to misunderstandings and redundancy in theoretical research.
(2) There exist few specific investigations of the explicit mathematical expression of the stress–strain relationships (constitutive laws) of fabrics.
(3) In particular, although the KES system has received wide attention for fabric objective measurement in which the investigation and application of the system are confined to the parameters extracted from the test equipment (Kawabata, 1980, Barker *et al*., 1985, 1986, 1987), the interpretation of the charts recorded from each tester is strictly ignored. This apparent neglect of an area of important technological interest stems from the difficulties inherent in the complexity of curves themselves which are intrinsically non-linear.

Additionally, in practice, the information from the KES system is so comprehensive and extensive that it is too complicated to handle or to interpret. A technique of extracting information from massive amounts of data of this type is needed to explain the main features of the relationship hidden or implied in the data and charts.

1.3.2 Constitutive laws of fabric as a sheet

Fabric is a type of textile material and it shares the complexity characteristic of other textile materials. In order to reduce the complexity of fabric behaviour to manageable proportions, deformation must be separated into different modes.

To the first approximation, a fabric may be simulated as a sheet. In some cases, a fabric is approximated to an elastica – this was discussed by Lloyd *et al*. (1978). In engineering treatments, a simplified sheet can be subjected to four different modes of deformations which can be superposed by simple addition to give any more complicated form of deformation at a point on a sheet. In addition to two independent in-plane strains, i.e. tensile and shear strains, there are two out-of-plane deformations generated by bending and twist. In an orthogonally woven fabric, it is convenient to make use of structural axes. The desirable features of textile materials, such as double curvature, may be synthesised from the above mentioned modes of deformations. No matter how complex a fabric deformation is, constitutive laws always apply. A stress–strain relationship is usually called a constitutive equation, or constitutive law.

1.3.2.1 Basic framework

One of the simplest constitutive equations is the linear equation from the infinitesimal-elasticity theory that is applicable to the Hookean elastic body under the assumption of infinitesimal strain. Woven fabrics, however, as pointed out above, are not Hookean bodies but accord typical non-linear stress–strain relationships. Nevertheless, based on the basic frame of the infinitesimal elastic theory of a sheet, the complicated mechanical behaviour of fabric can be explored.

In the most general case, the stress–strain relationships, or constitutive laws, of a linearly elastic plate (an initially flat) sheet are as follows:

$$\begin{matrix} \text{Tensile stress} \rightarrow \\ \text{Tensile stress} \rightarrow \\ \text{Shear stress} \rightarrow \\ \text{Bending stress} \rightarrow \\ \text{Bending stress} \rightarrow \\ \text{Twist strain} \rightarrow \end{matrix} \left\{ \begin{matrix} T_1 \\ T_2 \\ T_{12} \\ M_1 \\ M_2 \\ M_{12} \end{matrix} \right\}$$

$$= \begin{bmatrix} A_{11} & A_{12} & A_{13} & B_{14} & B_{15} & B_{16} \\ & A_{22} & A_{23} & B_{24} & B_{25} & B_{26} \\ & & A_{33} & B_{34} & B_{35} & B_{36} \\ & & & D_{44} & D_{45} & D_{46} \\ & & & & D_{55} & D_{56} \\ & & & & & D_{66} \end{bmatrix} \left\{ \begin{matrix} \varepsilon_1 \\ \varepsilon_2 \\ \varepsilon_{12} \\ K_1 \\ K_2 \\ K_{12} \end{matrix} \right\} \begin{matrix} \leftarrow \text{Tensile strain} \\ \leftarrow \text{Tensile strain} \\ \leftarrow \text{Shear strain} \\ \leftarrow \text{Bending curvature} \\ \leftarrow \text{Bending curvature} \\ \leftarrow \text{Twist strain} \end{matrix} \quad [1.1]$$

$$\uparrow$$

21 elements

or

$$\text{Stress matrix} \rightarrow [\sigma] = [S][\varepsilon] \leftarrow \text{Strain matrix} \quad [1.2]$$

$$\uparrow$$

Stiffness matrix

In equation 1.1, where T_1, T_2, ε_1 and ε_2 are the tensile stresses and strains respectively in the plane of the fabric, and T_{12} and ε_{12} are the shear stress and shear strain in the fabric plane, M_1, M_2, K_1 and K_2 are the bending stresses and curvatures, M_{12} and K_{12} are twisting stress and strain, and the submatrices A_{ij} and D_{ij} represent the membrane and bending (and twisting) stiffness respectively. The B_{ij} is coupling stiffness that connects the membrane and bending modes of deformation. In short, as in equation 1.2, $[\sigma]$ is the stress matrix, $[S]$ the stiffness matrix and $[\varepsilon]$ the strain matrix. Thus, in the general case 21 stiffnesses are required to specify the elastic behaviour of an originally

flat sheet: six for membrane deformations, six for bending and twisting, and nine for coupling between the two modes.

Fabrics are usually assumed to be orthotropic, i.e. they have lines of symmetry along their two constructional directions, and the stiffness matrix [*S*] for linear elastic situation becomes

$$[S] = \begin{bmatrix} A_{11} & A_{12} & 0 & B_{14} & B_{15} & 0 \\ & A_{22} & 0 & B_{24} & B_{25} & 0 \\ & & A_{33} & 0 & 0 & B_{36} \\ & & & D_{44} & D_{45} & 0 \\ & & & & D_{55} & 0 \\ & & & & & D_{66} \end{bmatrix} \quad [1.3]$$

where directions 1 and 2 are assumed to coincide with the principal directions of orthotropy, i.e. the warp and weft directions in a woven fabric. As summarised by Lloyd, this has 13 independent stiffnesses, reducing to 12 if the coupling matrix is symmetric; to eight if the fabric is symmetric; to eight if the fabric is symmetrical about its central plane so that the B_{ij} disappears; to 6 for a square fabric such as a plain-weave with the same yarns in each direction; to four for an isotropic sheet with bending behaviour unrelated to planar behaviour; and to two plus the thickness for an isotropic solid sheet. However, if the relationship were non-linear, many of the interaction terms would reappear. The interpretation of the parameters is made by Lloyd (1980) using the special case of an orthotropic fabric, initially flat, with no elastic coupling between membrane strain and bending/twisting modes.

1.3.2.2 Extensions to basic framework

The treatment of low-strain, linear elastic deformations is unrealistic in relation to textile materials. However, the framework outlined above opens up more realistic possibilities. Lloyd (1980) discussed various modifications to deal with the non-linearities common in fabric deformations: non-linear material properties, large strains and large displacements. Particularly for non-linear material properties, if the form of non-linear stress–strain laws is already known, the tangential elasticity matrix $[S_T]$

$$[S_T] = \frac{d[\sigma]}{d[\varepsilon]} \quad [1.4]$$

can be used in the continuum analysis. Alternatively, if [*S*] is kept constant, the resulting linear elastic solution will require corrections to the stresses calculated from the previous step. If the initial stresses are zero at zero displacement, then the non-linearities can be contained in $[\sigma_0]$ and used to

apply the necessary corrections. This is known as the initial stress method in such analysis as finite element methods.

1.3.2.3 Mathematical modelling of fabric constitutive laws

As can be seen in the above treatment of non-linear fabric properties, finding non-linear stress–strain relationships of any single deformation mode is necessary for the general continuum analysis. The widespread use of computers and the development of numerical techniques such as the finite element method opens up new possibilities: attempting problems such as fitting woven fabrics to a three-dimensional surface becomes feasible; other complex fabric deformations can be predicted; and clothing CAD systems can be developed. All these need the relationships between the constitutive laws governing fabric extension, shear and bending. However, the mathematical modelling of fabric stress–strain relationships is a very tough topic. During the last 60 years, many outstanding textile scientists, including F.T. Peirce, J.W.W. Hearle, P. Grosberg and R. Postle, have devoted their talents to this field. However, their theories are self-contained, that is it is difficult to apply the results of one piece of research work to another. For example, even though there are many papers and books on fabrics, it is well known that fabrics are non-linear and elasto-plastic in nature. In the investigation of fabric complex deformations, like drape (Collier *et al*., 1991) or ballistic penetration (Lloyd, 1980), one also assumes that basic deformation behaviour, like tensile, obeys the Hookean law of solid materials. The reasons for this stem from the complex procedures of prediction or, basically, the fact that the development of mathematical models for woven fabrics is an extremely complicated and difficult task due to the large numbers of factors on which the behaviour of the fabric depends. Usually, a mathematical model is based on a large number of assumptions, covering missing knowledge or inability to express some of the relevant factors. It is not surprising that, out of the huge bulk of works published in the area, a considerable amount appears to be of theoretical interest only and largely inadequate to cope with real fabrics. Therefore, it is necessary to introduce a different approach for the mathematical modelling of fabric constitutive equations.

With fabric, fundamental distinctions may be made between three kinds of modelling, namely: predictive, descriptive and fitting or numerical models. The predictive models, as developed by Hearle *et al.* (1969) and Postle *et al.* (1988), which form most of the existing research into fabric mechanics, are based on the consideration of at least the most important of the relevant factors, while the effect of the remaining ones is covered by suitable assumptions, defining the limits of validity and the accuracy of the resulting theories. Under these restrictions, the predictive models are directly characteristic of the physics of the fabric and permit the evaluation of the

effects of the various parameters involved and the development of design procedures. Models of this form may provide a basis for evaluation of the internal state of the fabric at a microscopic level, for example, the state of stress developed between warp and weft yarns under strictly determined fabric geometries and loading conditions.

The transition from the microscopic level to the macroscopic one is usually obtained through the concept of the representative unit cell. In this way, it is possible to derive a stress–strain curve for the fabric in any of these modes of deformation and to evaluate the build-up in the level of internal forces or lateral pressures acting within the fabric as it is deformed. A detailed study of the mechanisms of fabric deformation is therefore possible, yielding relationships between the structural parameters of a woven fabric and its important mechanical properties. The number of assumptions, for models of this kind, required for an exact theory is obviously high. It is necessary to include a number of initial assumptions relating to the nature of yarn contacts and yarn cross-sectional shape within the unit cell of the fabric. Such assumptions are usually based on a great degree of simplification and they are liable to introduce large errors in any analysis of fabric mechanical or rheological properties.

However, the treatment of this relationship is usually too complicated either to understand or to apply. The increased mathematical complexity of the better solutions has made them less accessible to those who might use them, or even to other specialists. These approaches all require several pages of mathematics. Some of it is interesting, but a good deal of messy algebra has made them difficult or impossible to apply to more realistic situations.

The descriptive models (Paipetis, 1981), on the other hand, are largely empirical and reflect the need for simple mathematical relations, expressing the phenomenological behaviour of a fabric from the point of view of a particular property. For example, linear viscoelastic materials can be modelled by means of properly connected spring-and-dashpot elements. However, such models completely ignore the physics of the material, need adjustment to reality through a number of experimental values and operate within a specific range of the relevant parameters only. Still, they are undoubtedly useful, if no rigorous models are available.

In contrast to the complexity of the predictive models and the subjectivity of the descriptive models, some sort of simple mathematical equation may be used to relate stress–strain. Even if no sensible physical relationship exists between variables when introducing the function and even although the equation might be meaningless, it may nevertheless be extremely valuable for predicting the values of fabric complex deformation from the knowledge of stress or strain. Furthermore, by examining such a function we may be able to learn more about the underlying relationship and to appreciate the separate and joint effects produced by changes in certain important parameters.

These are fitting or numerical models. The modelling of this group, at the first stage, may ignore the exact mechanism taking place within the structure but emphasise the numerical relations of two variables such as stress–strain relations. This method is based on statistical considerations; it needs fewer assumptions and provides, perhaps, an approach more relevant to real situations.

There exist various methods for fitting a curve in many industrial or science fields. Constitutive laws are often estimated by using a polynomial, which contains the appropriate variables and approximates to the true function over some limited range of the variables involved. Spline, especially the cubic spline interpolation method, is also widely used for this purpose. The research work in this field, which has received comparatively little attention, can be seen in Kageyama *et al*. (1988).

1.3.3 Computational fabric mechanics

Section 1.3.2 has in fact touched on the content of computational fabric mechanics. In this section, a more specific introduction to this technique is given. Since the workshop at the NATO Advanced Study Institute (Hearle *et al*., 1980), progress in fabric mechanics has begun to slow down. The hindrance to further development of fabric mechanics stems from the complexity of the mathematical equations used to describe the complex behaviour of fabrics. The very limited solvability of these equations by traditional analytical techniques has caused much frustration among the research community, which is increasingly losing confidence in the significance of fabric mechanics in practical applications. As the mathematics becomes more complicated and less transparent, there is also a perceptible worsening of communication between theoreticians and experimentalists, leading to misunderstandings on both sides and redundancy of theoretical research. Even Hearle, who has worked in textile mechanics for about 50 years, advocated the application of advanced computational techniques as the way forward (Hearle, 1992).

Computational fabric mechanics presents a unique opportunity where cooperation between researchers with different backgrounds will be most effective. The many challenging numerical problems will be of interest to the computational mechanics community, while the participation of textile material scientists will ensure a balanced and practically useful approach. The final product should be an intelligent CAD system, the development of which relies heavily on the contribution of computer graphics experts.

1.3.3.1 General

The application of computational techniques in fabric mechanics first appeared in the late 1960s. Konopasek, Hearle and Newton at the University of

Manchester Institute of Science and Technology (UMIST) first launched a project to use computer programs to approach textile mechanics problems including fabric behaviour (Hearle *et al.*, 1972). Computational techniques have in fact gained wide application in many engineering areas: airplane designing, machine manufacturing, civil engineering, etc. One key algorithm used in computational techniques is the numerical method, particularly the finite element method, which enables the possibility of accurately predicting the behaviour of an engineering structure under a certain loading condition. Therefore, in this section, particular emphasis is put on the finite element method as well as on fabric deformation analysis.

Continuum models

As the name says, in these models, the fabric is treated as a continuum without explicit reference to its discrete microstructure. Established mathematical methods in continuum mechanics can then be applied to the analysis of fabric deformations. In the first attempt at using computers to obtain continuum solutions to fabric deformation problems, numerical solutions were adopted after differential equations had been set up. However, this approach was difficult to apply to complex non-linear deformations of fabrics as specific equations needed to be established and a computer program needed to be written for a given problem. Representative work may be found in Konopasek (1972), Lloyd *et al*., (1978), Shanahan *et al.*, (1978), Brown *et al.* (1990), Clapp and Peng (1991).

A more versatile and powerful approach is the finite element method which can be applied to predict fabric behaviour under complex conditions. The finite element method was initially developed for engineering structures made of steel and other stiff materials. It has been developed since the 1950s and is now an essential analysis tool in many engineering fields (Zienkiewicz and Taylor, 1989, 1991). In this approach, the cloth is divided into many small patches which are called the finite elements. The cloth needs to be modelled using flat or curved shell elements, as both bending and stretching are involved.

Several researchers have attempted the finite element approach with varying degrees of success. The earliest attempt was made by Lloyd (1980) who achieved some success in dealing with in-plane deformations. Collier *et al*. (1991) developed a large-deflection/small-strain analysis using a 4-noded shell element and treated the fabrics as orthotropic sheets with properties determined from KES testers. They analysed the draping of a circular piece of fabric over a pedestal as in a traditional drape test. Their numerical draping coefficients agreed reasonably well with experimentally determined values. Gan *et al.* (1991) produced a similar analysis employing a curved shell element which belongs to the degenerated isoparametric family (Surana, 1983). They presented numerical results for the draping of a circular piece of

cloth over a circular surface and a square piece over a square surface. No comparisons with results from other sources were presented. Kim (1991) also treated fabrics as orthotropic sheets in his large-deflection analysis using shell elements and presented several examples of fabric draping. He was also the only researcher to provide quantitative comparisons which demonstrated that the deformed positions of the draped fabric predicted by his analysis differ from those from physical tests by about 10 %. Another similar study is described briefly by Yu *et al.* (1993) and Kang *et al.* (1994).

The above facts show that it is possible to simulate fabric drape by non-linear finite element analysis treating fabrics as two-dimensional orthotropic sheets with both bending and membrane stiffnesses. These studies have only been able to analyse simple draping tests. Analysis of deformations is more difficult for fabrics than for other conventional engineering materials. Much work needs to be done before an accurate, reliable and efficient analysis can be developed to model all possible deformation modes in fabrics. In the immediate future, more work should be carried out to produce more precise comparisons between numerical results and physical experiments for a variety of draping cases. This will further establish the validity of the continuum approach in modelling fabric deformations.

Another area that has not been touched upon is the effect of non-linear stress–strain relationships on fabric deformations. This is partly due to the lack of explicit non-linear constitutive equations of woven fabrics in the past. Recently, Hu and Newton (1993) and Hu (1994) described a comprehensive study of the structures and mechanical properties of woven fabrics in which they established a whole set of non-linear constitutive equations for woven fabrics in tension, bending, shear and lateral compression. The inclusion of these equations in finite element simulation is expected to improve prediction accuracy in many cases and shed light on the effect of non-linear properties of fabrics on garment appearance and performance.

Discontinuum models

In contrast to the continuum model, fabrics may be modelled as an assemblage of their constituent yarns. Grosberg and his co-workers (Grosberg and Kedia, 1966; Nordy, 1968; Leaf, 1980), Hearle and Shananhan (1978), Postle *et al.* (1988) and Ghosh *et al.* (1990) adopted discrete models to predict mechanical responses of fabrics by combining yarn properties, inter-yarn interactions and fabric structures. Their work is analytical, rather than numerical, involving many pages of mathematics with the aid of personalised programs in the solution phase. In the textile literature, this work is usually referred to as structural mechanics of fabrics (Hearle *et al.*, 1969).

Viewing the yarns as curved or straight rod elements with frictional connections at the crossing points between the warp and weft yarns, the finite element method can be extended to study fabrics using discontinuum

models. Torbe (1975) defined a cruciform element with arms in the directions of the threads in woven fabrics. In the same paper, the element stiffness matrix was derived, but no example of its actual application was given. Leech and Abood (1991) dealt with the dynamic response of fabric subject to tensile and tearing loads.

A discontinuum model by itself has limited value in predicting complex fabric deformations due to the prohibitive number of yarns present, but may be useful in predicting fabric mechanical properties from yarn properties, because only a small patch of cloth needs to be modelled. The problem is thus computationally feasible. Realistic constitutive laws required for fabric deformation analysis at present are only obtainable in laboratory tests. However, such laboratory tests are not possible before a particular fabric is actually manufactured. The discontinuum method may enable the accurate modelling of fabric deformations before they are manufactured.

1.3.3.2 Other approaches

Researchers in the computer graphics community are interested in producing cloth-like behaviour for computer animation. They have produced various models based on a geometric process and/or a simplified physical model, but their purpose is not to produce accurate deformation predictions of a particular deformable material. Geometric processes, together with simple physical constraints, have also been applied successfully in the composites manufacturing field.

Breen *et al.* (1994) proposed a particle-based model to simulate the draping behaviour of woven cloth. In their physical model, the cloth is treated not as a continuous sheet but as a collection of particles that conceptually represent the crossing points of warp and weft threads in a plain weave. The various constraints and interactions between particles are represented by energy functions which are defined using KES test data. Some promising results have been obtained. This kind of model has now become almost standard for various systems of cloth simulation.

1.3.3.3 Future of computational fabric mechanics

Dictated by fashion trends, textile and clothing products move through fast cycles of renovation. Just-in-time and quick response systems are becoming increasingly important in the textiles and clothing industries. Consequently, new technologies such as automation of production processes for textiles and clothing are attracting much attention. Computational fabric mechanics and understanding of fabric structure have much to offer in realising these new technologies. This section provides a brief examination of some of these areas, particularly those related to fabric deformations and clothing CAD, where application of computational fabric mechanics should be fruitful.

Complex fabric deformation and clothing CAD

In practical use, textile fabrics are subject to a wide range of complex deformations such as drape, handle and wrinkling or buckling. If textile technologists and clothing designers are to be able to make a rational engineering design of a new fabric or garment, then these complex deformations of fabrics must first be understood. With improved understanding of the deformation characteristics of various fabrics, it is then possible to design new fabrics targeted to the needs of specific end uses.

The ultimate aim is to enable a future garment designer to carry out the whole design and simulate the final product using a computer. The computer will automatically produce completed patterns based on a vivid picture drawn freehand by the designer and a few comments on the requirements of fabrics and clothing styles. The designer can then see the garment dressed up on a body simulated using computational fabric mechanics and computer graphics. In this way, a designer or customer can survey the scene as if it were a fashion show (a virtual reality fashion show!).

Automation of clothing industry

Automation and the linking of processes are two ways to reduce labour, improve quality and increase productivity in a modern enterprise. For example, automation of the handling and transport of apparel fabrics is of vital interest to industrialised nations, where the cost of labour is a significant portion of the total product cost. However, automated handling of textile materials is a difficult task because of their unique engineering properties and the variability of these properties in diverse product applications. To automate the handling process, computer software must be developed which can predict fabric bending behaviour and other modes of deformation during the handling process based on fabric property information. Such computer software will only come with developments in computational fabric mechanics.

Other applications

Computational fabric mechanics may be interpreted to include many other aspects apart from fabric deformations, although they are the most important in developing clothing CAD systems. It may be expected that computational fabric mechanics will be equally useful in studying thermal behaviour, fatigue and wear behaviour, and air and water permeability, and dynamic problems such as the ballistic penetration behaviour of fabrics for military garments.

1.4 References

Amirbayat J (1991), The buckling of flexible sheets under tension part I: theoretical analysis, *J Text Inst*, **82**(1), 61–70.

Amirbayat J and Hearle J W S (1989), The anatomy of buckling of textile fabrics: drape and conformability, *J Text Inst*, **80**(1), 51–70.

Barker R, Ghosh T K and Batra S K (1985 May, 1986 February & 1987 March), *Reports to North Carolina State University*. Raleigh, North Carolina 27695-8301, Kawabata Consortium, School of Textiles, North Carolina State University.

Breen D E, House D H and Wozny M J (1994), A particle-based model for simulating the draping behaviour of woven cloth, *Text Res J*, **64**(11), 663–685.

Brown P R III, Buchanan D R and Clapp T G (1990), Large deflection bending of woven fabric for automated material-handling, *J Text Inst*, **81**, 1–14.

Clapp T G and Peng H (1991), A comparison of linear and nonlinear bending methods for predicting fabric deformation in automated handling, *J Text Inst*, **82**, 341–352.

Collier J R, Collier B J, Toole G O and Sargrand S M (1991), Drape prediction by means of finite element analysis, *J Text Inst*, **82**(I), 96–107.

Gan L, Steven G P and Ly N (1991), A finite element analysis of the draping of fabric, *Proc 6th Int Conf in Australia on Finite Element Methods*, University of Sydney, Australia, July 8–10, 402–414.

Ghosh T K, Batra S K and Barker R L (1990), Bending behaviour of plain-woven fabrics: a critical review, *J Text Inst*, **81**, 245–287.

Grosberg P and Kedia S (1966), The mechanical properties of woven fabrics part I: the initial load-extension modulus of woven fabrics, *Text Res J*, **38**, 71–79.

Hearle J W S (1992), *Inaugural Conference of the Chinese Students and Scholars Textile Association in UK*, Manchester, UK, unpublished presentation.

Hearle J W S and Shanahan W J (1978), An energy method for calculations in fabric mechanics, Part I: Principles of the method, *J Text Inst*, **69**, 81–91.

Hearle J W S, Grosberg P and Backer S (1969), *Structural Mechanics of Fibers, Yarns, and Fabrics Vol. 1*, New York, Wiley-Interscience.

Hearle J W S, Konopasek M and Newton A (1972), On some general features of a computer-based system for calculation of the mechanics of textile structures, *Text Res J*, **10**, 613–626.

Hearle J W S, Thwaites J J and Amirbayat J (1980), *Mechanics of Flexible Fiber Assemblies (NATO Advanced Study Institute Series: E, Applied Sciences No. 38)*, Alpen aan den Rijn, The Netherlands, Sijthoff and Noordhoff.

Hu J L (1994), *Structure and Low-stress Mechanics of Woven Fabrics* (PhD thesis, University of Manchester Institute of Science and Technology).

Hu J L and Newton A (1993), Modelling of tensile stress-strain curves of woven fabrics, *J China Text Univ*, **10**(4), 49–61.

Kageyama M, Kawabata S and Niwa M (1988), The validity of linearizing method for predicting the biaxial-extension properties of fabrics, *J Text Inst*, **79**, 543–565.

Kang T J, Lee J, Yu W R and Oh K H (1994), Prediction of woven fabric deformation using finite element method, *Proc Int Symp on Fiber Sci and Tech*, 480–481.

Kawabata S (1980), *Standardization and Analysis of Hand Evaluation*, 2nd ed, Osaka, Textile Machinery Society of Japan.

Kawabata S, Postle R and Niwa M (1982), *Objective Specification of Fabric Quality, Mechanical Properties and Performance*, Osaka, Textile Machinery Society of Japan.

Kim J H (1991), *Fabric Mechanics Analysis Using Large Deformation Orthotropic Shell Theory* (PhD thesis, North Carolina State University).

Konopasek M (1972), *Improved Procedures for Calculating the Mechanical Properties of Textile Structures*, (PhD thesis, University of Manchester Institute of Science and Technology).

Leaf G A V (1980), Woven fabric tensile mechanics, in *Mechanics of Flexible Fiber*

Assemblies, Hearle J W S, Thwaites J J and Amirbayat J (eds) Alpen aan den Rijn, The Netherlands, Sijthoff and Noordhoff, 143–157.

Leech C M and Abood S M (1991), Modelling of the dynamics of woven constructions, *Proc 1989 ASME Winter Meeting*, AMD-Vol 103, New York, ASME, 153–175.

Lloyd D W (1980), The analysis of complex fabric deformations, in *Mechanics of Flexible Fiber Assemblies*, Hearle J W S, Thwaites J J and Amirbayat J (eds), The Netherlands, Alpen aan den Rijn, Sijthoff & Noordhoff, 311–342.

Lloyd D W, Shanahan W J and Konopasek M (1978), The folding of heavy fabric sheets, *Int J Mech Sci*, **20**, 521–527.

Nordy H A (1968), *The General Model of a Fabric With Special Reference to Hysteresis*, (PhD thesis, The University of Leeds).

Paipetis S A (1981), Mathematical modelling of composites, in *Developments in Composite Material-2-stress Analysis* Holister G S (ed), London and New York, Applied Science Publishers, 1–29.

Peirce F T (1937), The geometry of cloth structure, *J Text Inst*, **28**, P45–96.

Postle R, Kawabata S and Niwa M (1983), *Objective Evaluation of Apparel Fabrics*. Osaka, Textile Machinery Society of Japan.

Postle R, Carnaby G A and Jong de S (1988), Woven fabric structure and tensile properties in *The Mechanics of Wool Structures*, Postle R, Carnaby G A and Jong de S (eds), Chichester, Ellis Horwood.

Shanahan W J, Lloyd D W and Hearle J W S (1978), Characterising the elastic behaviour of textile fabrics in complex deformations, *Text Res J*, **9,** 495–505.

Surana K S (1983), Geometrically nonlinear formulation for the curved shell elements, *Int J Numer Methods Eng*, **15**, 581–685.

Torbe I (1975), A cruciform element for the analysis of fabric structures, in *The Mathematics of Finite Elements and Applications II*: *Mafelap 1975: Proceedings the Brunel University Conference of the Institute of Mathematics*, Whiteman, J R (ed), Academic Press.

Yu W R, Kang T J and Lee J K (1993), Drape properties of woven fabrics, *Proc 2nd Asian Textile Conf*, **1**, South Korea, 20 Oct, 455–459.

Zienkiewicz O C and Taylor R L (1989, 1991), *The Finite Element Method Vols. I, II*, 4th ed, New York, McGraw-Hill.

2

Objective measurement technology of woven fabrics

2.1 Significance of Fabric Objective Measurement technology

Fabric Objective Measurement of mechanical, geometrical, surface and large deformation properties represents a very powerful tool for the quality control of fabric manufacturing, finishing and refinishing operations. It presents the possibility of an integrated computerised scientific database incorporating in objective terms the enormous wealth of experience of numerous experts who have worked in the textile and clothing industries over many years in different countries throughout the world. The application of this technology is becoming more crucial due to three important factors:

(1) the increasing level of automation in both textile and clothing manufacture;
(2) the gradual disappearance of personnel with traditional textile knowledge based on many years of experience and the simultaneous emergence within industry of conventionally trained engineers to carry out the production, research, development and quality control functions;
(3) the widespread use of the internet and all kinds of digital communication tools, as well as the large number of product varieties due to shorter terms of seasonal products and the need for quick response to maintain competitiveness in business.

The development of Fabric Objective Measurement of mechanical properties for apparel products originated with Peirce in the 1920s and 1930s (Peirce, 1930, 1937). He investigated the basic equilibrium structure of a plain-weave fabric in terms of force equilibrium and tried to build up the basic theory of fabric mechanics. His work was further developed by a number of other researchers. Grosberg and his co-workers Park and Swani at Leeds University during the 1960s pioneered the theoretical analysis of fabric mechanical properties such as tensile, bending, buckling, shear and compression (Grosberg, 1966; Grosberg and Park, 1966; Grosberg and Swani, 1966).

Their contributions led to a relatively clear picture of the physical and mechanical description of woven fabric and deformation properties.

The Swedish research team headed by Lindberg *et al*. (1960) during the late 1950s and 1960s, extensively studied the mechanical behaviour of fabrics and related the basic mechanical properties of fabric to the tailorability and appearance of manufactured clothing. Their investigations become the focus of serious work by other researchers. Experimental techniques for the measurement of these mechanical properties have been evolved over a number of years by many researchers. A variety of equipment and test methods are now available.

Although much research was aimed at developing Fabric Objective Measurement techniques and various methods for measuring these properties were developed, these techniques were practised only by academics or research institutes. Their widespread use in the textile and clothing industries was still hindered by the unavailability of a coherent system with sophisticated and sensitive instruments for measuring the low-stress mechanical properties of fabrics. In addition, without a standardised testing method, further development and applications of these low-stress mechanical properties in the apparel industry would be limited. A research leader in Fabric Objective Measurement technology was Sueo Kawabata, who developed a testing device called the Kawabata Evaluation System (KES) that, within 10 years, was to become a standard textile test facility around the world. The KES fabric evaluation system is a sophisticated computer testing facility that enables a variety of fabric tests to be carried out (Kawabata, 1982).

The KES system enables accurate and reproducible measurement of fabric low-stress mechanical properties, which facilitates the extensive comparison of experimental findings by apparel engineers and researchers all over the world and efficient communication between various manufacturing sectors, buyers and apparel designers. However, criticisms still exist due to the high cost of the instrument. The system also requires experts for the interpretation of the resulting data. These deficiencies led to the development of another testing device called the FAST (Fabric Assurance by Simple Testing) system by CSIRO in Australia. The FAST system is much cheaper and is becoming more attractive to the industry. Undoubtedly, these developments coincided with an increase in the level of automation which demanded prediction and control of fabric behaviour during production. In this chapter, the development of the principles and instrumentation of both systems will be introduced.

The Virtual Image Display System (VIDS) and more recently the intelligent Fabric Surface Analysis System (FabricEye®) are new objective measurement tools based on image analysis and artificial intelligence technologies, which have been developed specially for the analysis of fabric geometrical and surface properties. The VIDS image system is a two-dimensional image analysis system which combines the video output from a TV camera with the

graphics display of the computer so that measurements may be made directly from the TV image, but the general measurement using the VIDS image system still depends on manual mouse clicking and dragging. However, FabricEye® is an automatic three-dimensional image analysis system; it can generate a 3D profile of fabric surface and give specimens an objective grade automatically.

Other objective measurement technologies are also included in this chapter, such as Scanning Electron Microscopy (SEM) for surface effect and cantilever and drapemeter for complex deformation. It seems that the most important consequence of the introduction of fabric objective measurement technology is the promotion of technological communication between various sectors of the textile and clothing industries, research and development workers and all other areas (e.g. fibre production, retailing, merchandising) concerned with fibres, textiles and clothing. Consequently, production control and quality assurance within textile and clothing companies should become much more rational and efficient, leading to products of higher and more consistent quality. In practical terms, the fabric objective data will allow manufacturers to anticipate and overcome problems before they appear. In summary, fabric objective measurement technology provides the key for scientific and engineering as well as production principles:

(1) optimisation of fabric properties to engineer new fabrics of desirable quality and performance attributes for particular end-uses;
(2) development of new finishes, finishing agents and finishing machinery for textile materials;
(3) control of fabric finishing/refinishing to meet fabric mechanical, surface and dimensional property goals;
(4) fabric specification and process control for clothing manufacture;
(5) total fabric development from raw material to tailored garments.

2.2 Mechanical properties measurement

2.2.1 The KES system

The KES system is the first advanced and unique solution to the problem of user-friendly testing of fabric mechanical properties, and it has acquired great popularity in many countries due to the high precision and reproducibility in measurement which it offers. With the information provided by this system, it is possible to achieve effective communications and cooperation among the various sectors (e.g. researchers, industry sectors and traders) of the textile and clothing industries by specifying performance requirements and transactions based on fabric properties data. Generally speaking, the KES system has the following features:

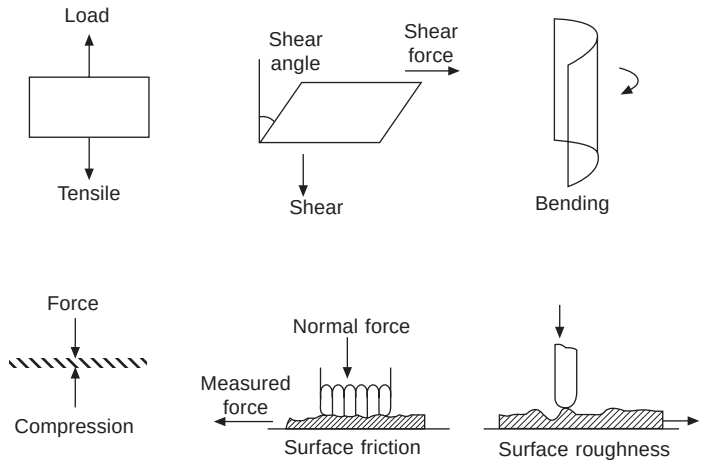

2.1 Measuring principles of the KES system.

(1) The testing is very comprehensive. Five charts and 16 parameters in the warp and weft directions can be obtained in one system, which covers almost all aspects of the physical properties of a fabric, in contrast to those testers which test single deformation modes.
(2) The tested strain regions are very similar to what happens when the fabrics are handled or when they are spread, cut, fused, sewn, or shaped and worn.
(3) A sample of the same size (20 cm × 20 cm) can be tested through the whole system. Particularly, the size of samples used for tensile testing is different from the conventional large length/width ratio such as is used on the Instron® machine.
(4) It is highly automated, and results from testing can be shown accurately on the computer attached to it, with charts and printouts of property parameters.

Detailed information on the KES instruments and the principles of measurement as shown in Fig. 2.1 can be found in KES manuals (1–4).

2.2.1.1 Configuration of the KES system

In practical terms, the extension or stress applied to woven fabrics during manufacturing, finishing, garment construction and wear is generally within the low-stress region of their characteristic stress–strain behaviour. The major stresses involved in fabric deformation under low-stress conditions are tensile, shear, bending and compression, and the KES system is a device capable of realising the testing of these low-stress deformations. It consists of four precision instruments originally designed to measure key mechanical properties related to the hand, drape and formability of fabrics, as shown in Table 2.1.

Table 2.1 The properties measured on the KES-F system

Instrument	Properties measured
KES-FB1	Tensile and shear
KES-FB2	Pure bending
KES-FB3	Compression
KES-FB4	Surface characteristics, i.e. fabric surface profile and coefficient of friction

KES-FB1 Tensile and shear tester

Just as the title suggests, this tester is for tensile and shear properties. With this tester, the tensile indices like extensibility and tensile rigidity can be obtained simply by applying a tensile strain to a sample held by two chucks. In the determination of shear property, the sample will be subjected to a preset shear deformation of ±8° shear angle under a constant tensile force.

KES-FB2 Pure bending tester

This instrument uses the principle of pure bending whereby a fabric sample is bent in an arc of constant curvature which is changed continuously. The minute bending moment of the sample is detected and the relationship between the bending moment and the curvature is recorded on an X-Y recorder.

KES-FB3 Compression tester

The instrument is designed to measure the fabric lateral compressional deformation properties which are important in the assessment of fabric handle. In the compression testing, a standard area of the fabric is subjected to a known compressive load and then the load is gradually relieved. The load is applied through a movable plunger that moves up and down and compresses the fabric on a stationary platform. Fabric compressibility can be obtained by calculating the percentage reduction in fabric thickness resulting from an increase in lateral pressure (from 50 Pa to 5 kPa). Moreover, the relationship between compressional strain and stress is automatically recorded on an X-Y recorder or computer linked with the tester.

KES-FB4 Surface tester

The instrument measures fabric surface properties which are closely related to hand feel of fabrics. The fabric frictional coefficient and the mean deviation of the coefficient of friction are detected by the friction contactor, which is directly connected to a frictional force transducer. Geometrical surface roughness is detected by the contactor for roughness. All of the measured parameters can be obtained directly from the calculation circuit of the instrument.

2.2.1.2 Information obtained from the KES-F system

A total of 16 parameters can be obtained from this system. These are:

Tensile parameters

EMT – percentage tensile elongation which is the ratio of actual extension to the original sample length, expressed as a percentage;

WT – tensile energy or work done in tensile deformation represented by area under the stress–strain curve;

RT – tensile resilience which is the ratio of work recovered to work done in tensile deformation, expressed as a percentage;

LT – tensile linearity which is a measure that defines the extent of non-linearity of the stress–strain curves. *LT* value below 1.0 indicates that the stress–strain curve rises below a 45° straight line while *LT* values greater than 1.0 indicate that the stress–strain curve falls above a 45° straight line.

Shear parameters

G – shear modulus which is the slope of the shear curve that falls between shear angles 0.5° and 5°;

2*HG* and 2*HG*5 – hysteresis width at shear angle 0.5° and 5°, respectively.

Bending parameters

B – bending stiffness which is the slope of the bending curve that lies between the radius of curvature of 0.5 cm^{-1} and 1.5 cm^{-1};

2*HB* – hysteresis width at a bending curvature of 0.1 cm^{-1}.

Compressional parameters

T_0 – fabric thickness (mm) at a very low compressive stress of 0.5 gf/cm^2;

T_m – fabric thickness (mm) at a maximum compressive stress of 50 gf/cm^2;

WC – compressional energy or work done in compression represented by the area under the compressive curve;

RC – compressive resilience which is the work recovered to the work done in compression deformation, expressed as a percentage;

LC – compression linearity which is a measure of the deviation of the deformation curve from a straight line. Higher values of *LC* imply a higher initial resistance to compression. In general, all fabrics have low values for linearity compared with tensile testing. Values range from 0.25–0.36.

Table 2.2 The parameters measured on the KES-F system

Property	Symbol	Parameter measured	Unit
Tensile	*EMT*	Extensibility, the strain at 500 gf/cm	[%]
	LT	Linearity of tensile load–extension curve	[–]
	WT	Tensile energy per unit area	[gf·cm/cm^2]
	RT	Tensile resilience, the ability of recovering from tensile deformation	[%]
Bend	*B*	Bending rigidity, the average slope of the linear regions of the bending hysteresis curve to ± 1.5 cm^{-1} curvature	[gf·cm^2/cm]
	2*HB*	Bending hysteresis, the average width of the bending hysteresis loop at ± 0.5 cm^{-1} curvature	[gf·cm/cm]
Shear	*G*	Shear rigidity, the average slope of the linear region of the shear hysteresis curve to ± 2.5° shear angle	[gf/cm·degree]
	2*HG* &	Shearing hysteresis, the average widths of the shear hysteresis loop at ± 0.5° shear angle	[gf/cm]
	2*HG*5	Shearing hysteresis, the average widths of the shear hysteresis loop at ±5° shear angle	[gf/cm]
Surface	*MIU*	Coefficient of fabric surface friction	[–]
	MMD	Mean deviation of *MIU*	[–]
	SMD	Geometrical roughness	[mm]
Compression	*LC*	Linearity of compression-thickness curve	[–]
	WC	Compressional energy per unit area	[gf·cm/cm^2]
	RC	Compressional resilience, the ability of recovering from compressional deformation	[%]
Thickness	*T*	Fabric thickness at 50 N/m^2	[mm]
Weight	*W*	Fabric weight per unit area	[mg/cm^2]

Surface parameters

MIU – coefficient of surface friction as measured over 3 cm length of fabric;

MMD – mean deviation of coefficient of friction;

SMD – surface roughness (mean deviation of surface peaks representing thick and thin places).

All mechanical properties measured on the KES system are summarised in Table 2.2.

2.2.2 The FAST system

FAST is a set of instruments and test methods developed by the CSIRO Division of Wool Technology (Australia) for measuring those properties which affect the tailoring performance of the fabric and the appearance of

the garment in wear. It consists of three simple instruments and a test method, requiring a specific sample size for both the instrumental tests and the dimensional stability test. In practice, about half a metre of fabric at full width is adequate to carry out the full range of tests.

FAST was developed to provide the industry with a simple, robust and relatively inexpensive system for the objective measurement of those fabric properties important in garment manufacture; it is thus mainly used by fabric manufacturers, finishers and garment makers. However, FAST has potential applications at all stages of fabric manufacture and use. As a result of these wide ranging applications another of the objectives of FAST can be achieved. This is to provide a language with which garment makers and fabric producers can communicate about cloth and garment properties and performance.

2.2.2.1 Configuration of the FAST system

The system comprises three simple instruments and a test method, listed as in Table 2.3.

To ensure error-free calculations, the system is connected to a computer where measurements are recorded directly and displayed on the monitor.

FAST-1 Compression meter

FAST-1 is a compression meter which can enable the measurement of fabric thickness and surface thickness at two predetermined loads. Surface thickness is defined as the difference between the values of thickness at the two predetermined loads of 0.2 kPa and 10 kPa. The measurement principle is shown in Fig. 2.2. The pressure at which thickness is measured is controlled by adding weights to the measuring cup.

FAST-2 Bending meter

FAST-2 is a bending meter which measures the bending length of the fabric. From this measurement the bending rigidity of the fabric may be calculated. The instrument uses the cantilever bending principle described in British Standard method (BS: 3356 (1990)). However, in FAST-2 the edge of the fabric is detected using a photocell, and not by eye as in some other test

Table 2.3 Configuration of the FAST system

Instrument	Properties measured
FAST-1	Compression
FAST-2	Bending
FAST-3	Extension
FAST-4 (test method)	Dimensional stability

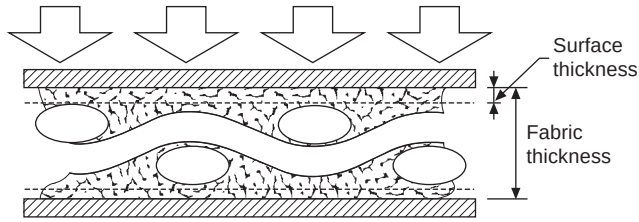

2.2 Measuring principle of the FAST-1 compression meter.

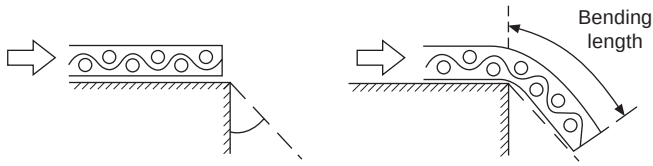

2.3 Measuring principle of the FAST-2 bending meter.

instruments. As well as making the instrument simpler to use, the elimination of this source of operator error makes FAST-2 more accurate than alternative instruments. The values of the bending length are read directly from a display on the instrument. Figure 2.3 gives the measuring principle.

FAST-3 Extension meter

FAST-3 is an extension meter which operates on a simple lever principle as shown in Fig. 2.4. By removing weights from the counterbalancing beam, the extensibility of the fabric can be measured at three different loads, thereby simulating the kind of deformation the fabric is likely to undergo during

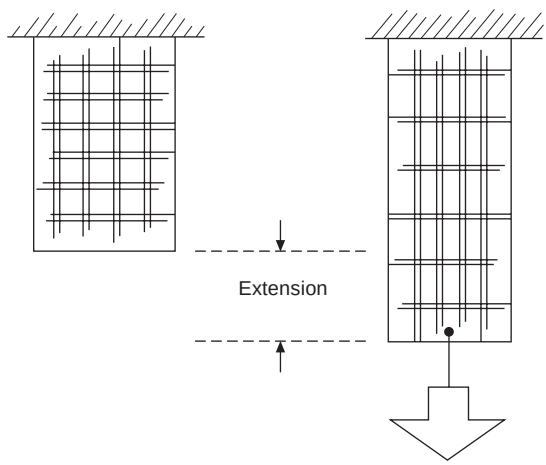

2.4 Measuring principle of the FAST-3 extension meter.

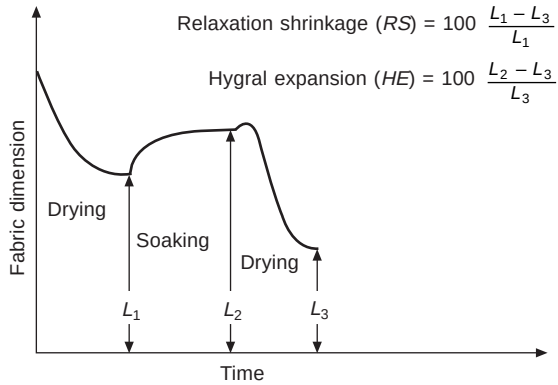

2.5 Measuring principle of the FAST-4 bending meter.

garment manufacture. The extensibility of the fabric can, in theory, be measured at any angle to the warp (or weft) threads. In practice, it is normal to measure the extensibility in only the warp, weft and bias directions.

FAST-4 Dimensional stability test

The final component of FAST is a test method which measures the changes in the dimensions of fabrics that occur when the fabric is exposed to changing environmental conditions. The test is a modification of the conventional wet–dry test. The FAST-4 test can be completed in less than two hours and does not require a conditioned atmosphere. A schematic diagram of the test procedure is shown in Fig. 2.5.

2.2.2.2 Information obtained from the FAST system

Using the FAST system, 14 parameters can be measured or calculated; these are listed in Table 2.4. The measured parameters are plotted on a control chart from which a good prediction of the performance of the fabric during garment manufacture can be derived. The importance of these parameters varies according to the end use of the fabric being tested. The system provides simple but reliable and quick response information for the control of fabric finishing and tailoring. The following section provides a detailed explanation of the properties measured by the FAST system.

Dimensional stability (FAST-4)

This term is used to describe the change in the dimensions of fabrics that occurs when the fabric is exposed to changing environmental conditions. For wool and wool-containing fabrics, there are two important components of dimensional stability.

Table 2.4 The parameters measured on the FAST system

Property	Symbol	Parameter measured	Unit
Tensile	*E*5	Extension at 5 N/m	[%]
	*E*20	Extension at 20 N/m	[%]
	*E*100	Extension at 100 N/m	[%]
	*EB*5	Bias extension	[%]
Bending	*C*	Bending length	[mm]
	B	Bending rigidity	[μN·m]
Shear	*G*	Shear rigidity	[N/m]
Compression	*T*2	Thickness at 2 gf/cm^2	[mm]
	*T*100	Thickness at 100 gf/cm^2	[mm]
	ST	Surface thickness	[mm]
	STR	Released surface thickness	[mm]
Dimensional stability	*RS*	Relaxation shrinkage	[%]
	RC	Hygral expansion	[%]
Derived parameter	*F*	Formability	%·mm^2

Relaxation shrinkage

The irreversible change in fabric dimensions (shrinkage or expansion) that occurs when the fabric is wet out or exposed to steam. Relaxation shrinkage is caused by the release of cohesively- or temporarily-set strains which are imposed on fabrics during the late stages of finishing. In the FAST system, relaxation shrinkage is defined as the percentage change in dry dimensions of the fabric measured after relaxation in water at room temperature.

Hygral expansion

Hygral expansion is the reversible change in the dimensions of the fabric that occurs when the moisture content of the wool fibres is altered. Using FAST, hygral expansion is defined as the percentage change in dimensions of the relaxed fabric from wet to dry. These two components are described mathematically as follows:

$$\text{Relaxation shrinkage} = \frac{L_1 - L_3}{L_1}$$

$$\text{Hygral expansion} = \frac{L_2 - L_3}{L_3}$$

where L_1 = length of dry, relaxed fabric, L_2 = length of wet fabric after relaxation in water and L_3 = length of dry, unrelaxed fabric.

Other measures of relaxation shrinkage are available such as the WIRA^{TM} steam cylinder or open press shrinkage test. These correlate well with the FAST wet–dry method.

Other methods of measuring dimensional stability are also available, and these include the DIN test, the HESC test and locked press shrinkage. However,

these tests do not separate the two components of dimensional stability and can give misleading results on some fabrics.

Extensibility (FAST-3)
The extensibility of a fabric measures the increase in fabric dimensions which occurs when it is subjected to an applied load. Using the FAST system, extensibility is measured as a percentage increase in length at sample loadings of 5 gf/cm, 20 gf/cm and 100 gf/cm width (98.1 N/m). The quoted value for fabric extensibility is that measured at 100 gf/cm. The extensibilities in the warp and weft directions measured at 5 gf/cm and 20 gf/cm are used to calculate fabric formability. Bias extensibility is measured only at 5 gf/cm width.

Bending rigidity (FAST-2)
The bending rigidity of a fabric is defined as the couple required to bend that fabric to unit curvature. The FAST system determines bending rigidity from the cantilever bending length of the fabric, measured using the principle described in BS: 3356 (1990), and fabric weight. Bending rigidity is given by:

$$\text{Weight} \times (\text{Bending length})^3 \times 9.807 \times 10^{-6}$$

with bending rigidity in μN·m, bending length in mm and fabric weight in g/m^2.

Shear rigidity (FAST-3)
Shear deformation of a fabric can be described as a trellising motion in which the angle between warp and weft threads is changed (from 90°) without imposing an extension on either set of threads. The shear rigidity of a fabric is a measure of the force required to deform the fabric in shear. In the FAST system, shear rigidity is calculated from the bias extensibility of the fabric under a load of 5 gf/cm and is given by:

$$\frac{123}{\text{Bias extensibility}}$$

with shear rigidity in N/m and bias extensibility in %.

Thickness/surface thickness (FAST-1)
Using the FAST system, the thickness of the fabric is measured at 2 gf/cm^2. The thickness of the fabric is also measured at 100 gf/cm^2 and the surface thickness, defined as the difference between the thicknesses at the two loads, is calculated from the measured data:

$$\text{Surface thickness} = \text{Thickness (2)} - \text{Thickness (100)}$$

Relaxed thickness/surface thickness (FAST-1)
The relaxed thickness and surface thickness of the fabric are measured after the fabric has been relaxed in steam (open press for 30 sec) or water (at 20 °C for 30 min). Naturally the samples must be reconditioned to the standard atmosphere before the fabric is retested using FAST-1.

Formability
The FAST system uses the derived parameter, formability, in the analysis of fabrics. Formability is a measure of the extent to which a fabric can be compressed in its own plane before it will buckle. This parameter, as the product of the bending rigidity and the extensibility of the fabric at low loads, is defined in the FAST system as:

$$\text{Formability} = \text{Bending rigidity} \times \frac{\text{Extension (20)} - \text{Extension (5)}}{14.7}$$

with formability in mm^2, bending rigidity in $\mu N \cdot m$ and extension in %.

2.2.3 Comparison of the two measuring systems

Both the KES-F and the FAST systems were originally designed for measuring low-stress mechanical properties in an accurate and reproducible manner, but they differ in several ways. First, the FAST system uses standard fabric strips 5 cm long whereas the KES system uses 20 cm × 20 cm strips. Second, the two systems also adopt different testing principles: the KES set of instruments measures the entire deformation-recovery behaviour while the FAST system determines the amounts of deformation to a single point on the deformation curve (Ly *et al*., 1988). For example, the KES bending tester employs the principle of pure bending in measuring the bending property. The constantly changing curvatures of the fabric specimen are recorded allowing both elastic and frictional components for the bending moment to be measured separately. The FAST bending tester, on the other hand, is based on the cantilever principle. In the case of measuring the shear property, the principle of bias extension measurement is adopted by the FAST shear tester whereas the KES-F system measures the simple shear with sides at constant length.

A number of workers also compared the results measured by both systems. Ly *et al.* (1991) found the results measured by the two systems to be highly correlated with each other, even though significant difference in values may exist between them. The approach used in the KES system seems more similar to the actual fabric deformation in shearing and bending and it allows continuous measurement of deformations. In addition, the shape of the load–extension curve, which can reveal the actual deformation characteristics of fabrics more clearly and accurately, is attainable. On the one hand the FAST

system is simpler to use and cheaper. The price of the FAST system is only about one eighth of the price for the KES-F system. Therefore, the FAST system can be more easily applied in industry. On the other hand, for more in-depth research and development work on the low-stress mechanical properties of fabrics, the KES system is preferred. Therefore, the general opinion was that FAST data could be swiftly applied to commercial production, but the KES system was said to be an ideal laboratory tool and a precise factory testing facility.

2.3 Geometrical and surface properties measurement

2.3.1 The VIDS image analysis system

Most of the geometrical parameters can be measured by the VIDS image analyser (manual for VID system). Figure 2.6 is a systematic diagram of the VIDS image analysis system. The VIDS system combines the video output from a TV camera with the graphics display of an Apple® computer so that measurements may be made directly from the TV image. A CalComp® digitising tablet allows the operator to ensure a range of feature parameters using VIDS software packages. VIDS software packages contain general measurement, area fractions measurement, four-dot measurement, two-dot measurement, linear measurement, twist angle and point count programs. The results of these measurements may be displayed on the computer screen, printed using a printer or stored on floppy disk.

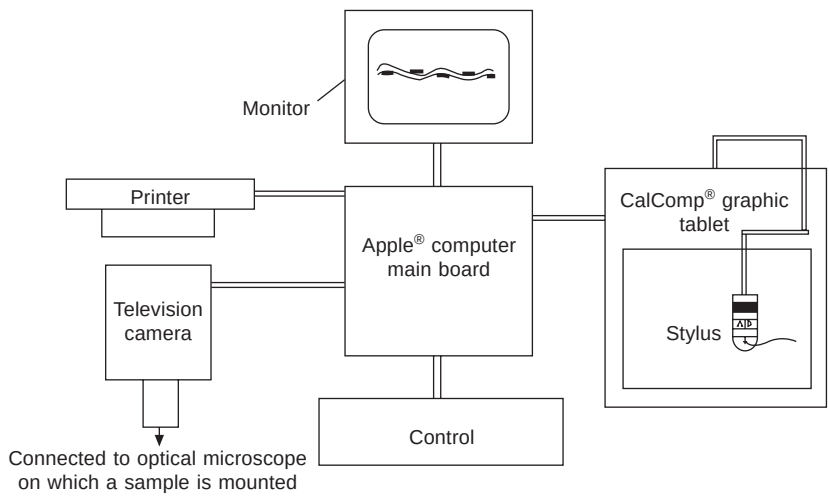

2.6 Schematic illustration of the image analysis system.

The VIDS general measurement program allows the user to draw round features displayed on the computer screen using the digitising tablet and four-button cursor. The following results may be obtained for each feature as well as the mean and the standard deviation of each:

- Area, perimeter, form factor, maximum projected horizontal and vertical lengths. This program was used to measure area of yarn cross-section and crimp height of yarns in the present case.
- The VIDS Two-Dot measurement program allows the rapid measurement of features which can be defined by two points. This program was used for measuring major and minor diameters of yarns in a fabric.
- The twist angle program allows the user to measure the angle of a feature to the horizontal line. It was employed to measure the weave angle of warp and weft yarns in a fabric.

2.3.1.1 Preparation of samples

In examining fabric structure, it is first necessary to set the fabric in resin. This is done by cutting a small piece of fabric such that its length and width are 25×25 mm, and sticking this sample on a stiff paper frame with a square hole of about 20×20 mm in the middle. The stiff paper with the sample fabric is inserted vertically into a rubber mould. A liquid mixture of epoxy resin ARALDITE MY753 and ARALDITE HARDENER HY951 (ratio 10:1) is poured into a mould. After 24 hours, the resin block is cut into very thin slices on a slow speed saw. The thickness of a slice is usually larger than Å (major diameter of thread values of 1 and 2 for warp and weft). So it is about 100–300 microns in the case of fabrics used in the present investigation. Transparent embedding agents are commercially available. The slices are then employed for the observation and measurement of various geometrical parameters and SEM.

To prepare good samples, care should be taken with the following problems:

- The solution ratio of the mixture liquid must not be less than 1:10. If it is, the sample block containing the fabric will be too soft. When cutting, it may cause distortion of the yarns in the fabric, producing incorrect data.
- Drying time of less than 24 hours or a holding force of the sample for cutting which is too large could cause the same problem.
- The thickness of a slice also must be appropriate. If the slice of a sample is too thick, the adjacent yarns may not be separated from each other; if it is too thin, the yarn may be cut into pieces.

All of these affect the measurability of a sample.

2.3.1.2 Measurement of geometrical parameters

Sett, thread-spacing

The number of warp and weft threads per centimetre was determined by using parallel-line gratings as described in British Standard BS 2862: 1984. Five readings of every sample were taken to represent the threads per unit length of one material. The average number of threads per cm and the thread-spacing were then calculated. If n stands for the threads per unit length, the spacing p can be calculated using the following formula

$$p_i = \frac{1}{n_j} \qquad i, j = 1\text{–}2 \qquad [2.1]$$

The tested sett and thread-spacing are listed in Table 2.5.

Yarn crimp

Two methods, namely the image analysis method and the tension method, were used for yarn crimp in a woven fabric.

Table 2.5 Sett and space of sample fabrics

Sample	Sett (threads/cm)		Space (mm)	
	n_1	n_2	p_1	p_2
2	58.7	28.7	0.170	0.348
3	52.8	26.8	0.189	0.373
4	57.9	27.6	0.173	0.362
5	59.5	29.5	0.168	0.339
6	52	27.2	0.192	0.368
7	66.9	34.7	0.149	0.288
9	67.7	33.5	0.148	0.299
10	72.84	37.4	0.137	0.267
11	72.84	37.4	0.137	0.267
12	71.7	37.4	0.139	0.267
13	59	28.7	0.169	0.348
14	59	29	0.169	0.345
16	19.69	13.39	0.508	0.747
18	19.69	13.39	0.508	0.747
20	21.65	13.19	0.462	0.758
21	22.64	20.08	0.442	0.498
22	23.23	16.54	0.431	0.605
23	36.22	26.77	0.276	0.374
24	28.35	20.87	0.353	0.479
25	24.8	21.65	0.403	0.462
26	31.1	21.85	0.323	0.458
27	28.74	25.98	0.348	0.385
1	51.2	41.7	0.195	0.24
8	37.8	33.86	0.265	0.295

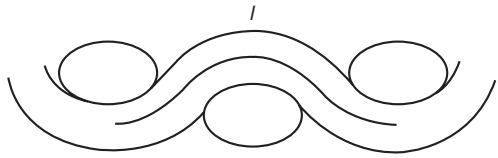

2.7 Measurement of yarn.

Tested by image analysis

The determination of 1, the yarn length per unit, is a key parameter for crimp calculation. The image of the cross-section of a yarn in a fabric is displayed on the computer screen through a magnified system. The length of the central line of a yarn was measured using the linear measurement program of a VIDS system as shown in Fig. 2.7. Then, the crimp C is calculated as equation (2.2).

$$c_i = \frac{1 - p_j}{p_j} \times 100\% \quad i, j = 1\text{–}2 \qquad [2.2]$$

Tested by tension method

Yarn crimp was also measured by applying a specified tension to a length of yarn and measuring the resultant extension, which may be dependent on the particular tension used in testing. The testing method referred to British Standard BS 2862: 1984.

The tested data for every fabric using these two methods are listed in Tables 2.6 and Table 2.7.

Crimp height

As shown in Fig. 2.8, the crimp height of yarns was measured using the general measurement program introduced above. The sample is positioned

Table 2.6 Measured crimp using image method

Sample	c_1	c_2	Sample	c_1	c_2
2	11.93	23.27	16	15.15	6.33
3	9.88	16.16	18	4.44	14.20
4	13.16	14.18	20	18.25	19.07
5	18.00	19.00	21	16.46	15.46
6	14.24	24.80	22	0.89	16.15
7	14.51	20.42	23	20.47	19.53
9	17.25	15.09	24	6.44	21.91
10	12.20	16.54	25	6.08	4.16
11	12.20	16.54	26	11.44	8.85
12	15.94	14.72	27	6.52	9.21
13	11.93	18.00	1	12.59	22.88
14	18.90	12.00	8	15.12	9.62

Table 2.7 Measured crimp using tension method

Sample	c_1	c_2	Sample	c_1	c_2
2	9.19	6.27	16	4.36	6.06
3	8.91	5.93	18	6.64	7.86
4	8.43	5.36	20	1.82	18.57
5	9.29	5.50	21	2.21	9.43
6	7.14	3.64	22	3.15	6.43
7	9.75	6.21	23	4.25	14.38
9	9.56	5.16	24	2.86	4.30
10	7.31	4.50	25	4.30	6.79
11	8.41	5.56	26	3.57	8.14
12	8.21	4.00	27	4.14	10.55
13	7.86	5.04	1	6.36	11.44
14	9.79	5.75	8	11.00	16.89

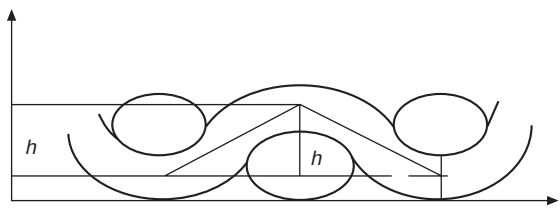

2.8 Measurement of crimp height.

to ensure that the surface of the fabric touches the horizontal line. In order to do this, peaks of the weave of the tested fabric are positioned on the horizontal line. We need only spot three places to form a close triangle. The height of the triangle is read by the maximum vertical projected length, which is the crimp height of a yarn within the fabric. The measured results are listed in Table 2.8.

Table 2.8 Measured crimp heights

Sample	h_1 (mm)	h_2 (mm)	Sample	h_1 (mm)	h_2 (mm)
2	0.144	0.081	16	0.193	0.181
3	0.144	0.089	18	0.111	0.22
4	0.154	0.086	20	0.153	0.328
5	0.151	0.079	21	0.164	0.217
6	0.167	0.082	22	0.145	0.195
7	0.15	0.068	23	0.147	0.153
8	0.131	0.074	24	0.164	0.244
10	0.118	0.061	25	0.136	0.129
11	0.107	0.064	26	0.129	0.122
12	0.106	0.064	27	0.134	0.13
13	0.134	0.07	1	0.103	0.098
14	0.159	0.081	8	0.084	0.134

Yarn diameters

Minor and major diameters of yarns, as shown in Fig. 2.9, were measured using the two-dot program. The measurements are made by positioning the screen cursor over the first point to be marked and pressing down a button on the cursor so that a dot appears on the screen in the middle of the cursor. The button on the cursor is then lifted, moved and pressed down again to give a second dot and also a beep which indicates that a complete two-dot measurement has been made. The tested minor and major diameters and flattening coefficients are shown in Table 2.9.

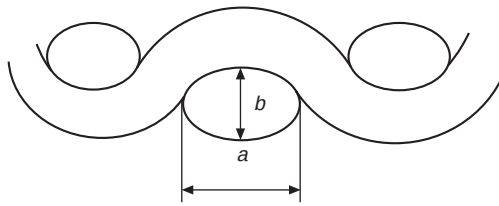

2.9 Measurement of yarn diameters in fabric.

Table 2.9 Measured diameters for samples

Sample	Major diameters		Minor diameter		Flatten coeff.	
	a_1	a_2	b_1	b_2	e_1	e_2
2	0.21	0.24	0.08	0.1	2.63	2.4
3	0.18	0.2	0.09	0.1	2	2
4	0.17	0.19	0.09	0.09	1.89	2.11
5	0.21	0.21	0.08	0.09	2.63	2.33
6	0.22	0.23	0.1	0.09	2.2	2.56
7	0.2	0.18	0.07	0.07	2.86	2.57
9	0.21	0.18	0.07	0.09	2	1.86
10	0.19	0.15	0.06	0.06	3	2
11	0.16	0.16	0.06	0.06	3.17	2.5
12	0.15	0.16	0.06	0.06	2.67	2.67
13	0.19	0.21	0.08	0.09	2.5	2.67
14	0.2	0.2	0.08	0.09	2.38	2.33
16	0.19	0.2	0.13	0.14	1.46	1.43
18	0.29	0.31	0.25	0.21	1.16	1.48
20	0.3	0.45	0.22	0.19	1.36	2.37
21	0.25	0.31	0.17	0.15	1.47	2.07
22	0.18	0.29	0.15	0.12	1.2	2.42
23	0.2	0.25	0.14	0.12	1.43	2.08
24	0.22	0.27	0.12	0.14	1.83	1.93
25	0.32	0.32	0.11	0.12	2.91	2.67
26	0.21	0.3	0.13	0.1	1.62	3
27	0.23	0.27	0.09	0.09	2.56	3
1	0.16	0.18	0.09	0.08	1.78	2.25
8	0.16	0.13	0.08	0.07	2	2.4

Table 2.10 Measured and calculated areas of yarns

Sample	Calculated	Measured		
	$A_1 = A_2 = A$	A_1	A_2	A_1/A_2
2	0.013	0.01419	0.01717	0.826
3	0.01306	0.012	0.01445	0.830
4	0.01306	0.01236	0.01517	0.815
5	0.01306	0.01395	0.01441	0.968
6	0.01628	0.01463	0.01487	0.984
7	0.01093	0.01111	0.01113	0.998
9	0.01093	0.01087	0.01474	0.737
10	0.00817	0.0084	0.00922	0.911
11	0.00818	0.0784	0.0791	0.991
12	0.00817	0.00878	0.0096	0.915
13	0.01306	0.0125	0.01406	0.889
14	0.01306	0.01434	0.01542	0.930
16	0.01628	0.0178	0.02013	0.884
18	0.0543	0.06393	0.06479	0.987
20	0.04635	0.05177	0.07174	0.722
21	0.0543	0.02719	0.04157	0.654
22	0.02163	0.02099	0.03355	0.626
23	0.02163	0.01589	0.0201	0.791
24	0.03109	0.02644	0.03355	0.788
25	0.02716	0.0229	0.02846	0.805
26	0.01862	0.01919	0.02095	0.916
27	0.02163	0.01591	0.01847	0.861
1	0.01093	0.01005	0.01038	0.968
8	0.01649	0.0078	0.01009	0.773

Area of yarn cross-section in a fabric

To measure the area of yarn cross-section, one draws round the border of the cross-section of a yarn using the general measurement program. When the beginning and the end of the borderline are overlapped, the complete measurement of area of a yarn has been made. The measured and calculated areas from calculated diameters are listed in Table 2.10.

Weave angle

The twist-angle program in the VIDS system was used for testing the weave angle of yarns in a fabric as shown in Fig. 2.10. The line formed by connecting two dots which are on the central line of the yarn has an angle with the horizontal line. This is weave angle θ. The measured results are listed in Table 2.11.

The cross-section photographs shown in this chapter were taken using a camera attached to the eyepiece of an ordinary optical microscope. Two photographs of each direction of a sample were obtained.

There are several points which need to be noted for an accurate measurement: boundary clearness in contact area of warp and weft yarns; hairiness of a

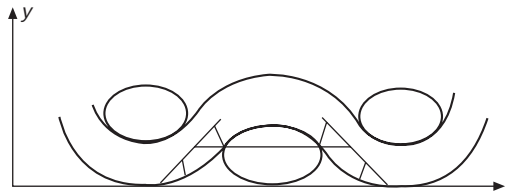

2.10 Measurement of weave angle.

Table 2.11 Measured weave angle

Sample	θ_1	θ_2	Sample	θ_1	θ_2
2	35.6	34.7	16	18.8	20
3	41.1	43.4	18	32.7	39.1
4	37.1	39.5	20	19.9	40.5
5	45.9	39.7	21	24.5	35.1
6	43	41.2	22	10.2	34.9
7	37.8	37.6	23	31.1	43
9	40.4	35	24	27.2	45.3
10	34.2	33.6	25	35.5	37.7
11	33.3	33.8	26	31.4	34.9
12	38.4	33.3	27	30.3	33.2
13	35.6	37.3	1	36.5	44.4
14	42.1	35.9	8	25.3	37.1

yarn; positioning the sample before measuring; irregularity of yarn structure; and calibration before testing.

2.3.2 Scanning electron microscope

The scanning electron microscope (SEM), as its name suggests, is an electron optical instrument: it uses a beam of electrons to illuminate the specimen. The electron beam is generated with a gun, accelerated by a high voltage, and formed into a fine probe by a series of electromagnetic lenses. The electron-optical column through which the beam passes is held under a high vacuum to allow a free path for the electrons, and to prevent a high voltage discharge. The electron beam is rastered across the surface of the specimen by means of a series of deflection coils, and this raster is synchronous with that of a cathode ray tube (CRT). The signals produced, as a result of the beam being rastered across the specimen surface, are collected by an appropriate detector, amplified and displayed upon the CRT. The magnification of the image is the relationship between the length of the scan line on the specimen and the length of the scan line CRT.

The electron beam striking a specimen surface requires a conducting path to earth in order to remove any electron charge that results. Conducting

materials do not produce problems, but non-conducting materials may need a conducting coating applied to the surface to simplify operation. This second CRT is used specifically for photography. It has a much faster image decay rate than the viewing CRT, such that only a single scan line is visible at any one time. The screen itself is photographed, using Polaroid, 35 mm, 120 or 220 films; a conventional camera is used. Each line of the image is exposed to the emulsion, the camera shutter being held open for the duration of a single frame scan.

2.3.2.1 Experiment on fabric surface image

As shown in Fig. 2.11, a sample is stuck to a metal stub, the diameter of which is 15 mm, using adhesive double-sided tapes. The specimen must be coated with gold before testing. There are two reasons why we coat specimens prior to insertion into the SEM. First, because non-conducting specimens build up a surface charge through which secondary electron information is unable to penetrate, the image we view may be distorted both in signal level, and image form. Second, it is necessary in order to provide a surface layer that produces a higher secondary electron yield than the specimen material. To make the specimen easier to handle in the microscope (less charge and distortion), a sputter coating was used. In sputter coating a gold target is bombarded with heavy gas atoms. Metal atoms ejected from the target cross the discharge to deposit onto the surface of a specimen. A low vacuum environment is used (0.1–0.05 mbar), which, with the modern low voltage sputter coaters, enables metal to be deposited at up to 1 mm/s^{-1}. A photographic image of the fabric surface was taken with the magnification around 50.

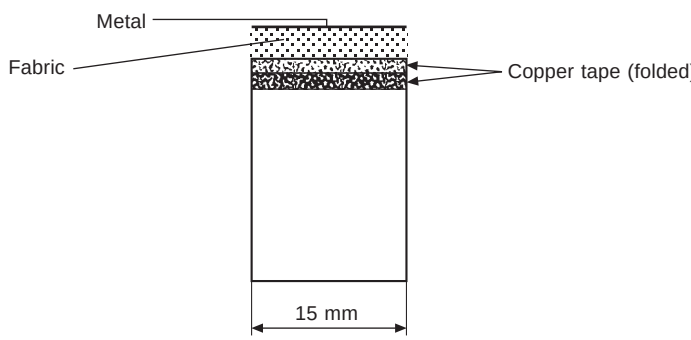

2.11 Preparation of sample for SEM.

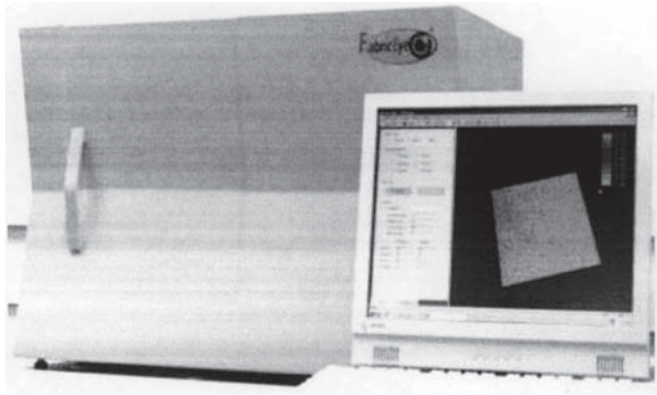

2.12 FabricEye®.

2.3.3 FabricEye®

2.3.3.1 Introduction

Pilling, wrinkle and hairiness on fabrics or garments are well-known phenomena, and these unpleasant appearance attributes can seriously compromise the fabric's acceptability. Currently, all pilling, wrinkle and hairiness testing systems available on the market are manual and subjective. These cannot provide an accurate, reliable and consistent assessment.

FabricEye® (shown in Fig. 2.12) was developed by the Institute of Textile and Clothing of the Hong Kong Polytechnic University led by Dr Jinlian Hu and Professor Edward Newton. It is an intelligent and comprehensive fabric surface inspection system which aims at tackling the inconsistency created by various subjective evaluations. The initial objective was pilling evaluation. Two patents applications have already been submitted for the mechanical design.

Quality grading standards, such as those described by AATCC and ASTM for pilling appearance evaluation, are subjective. There is always inconsistency among different experts due to different physical and psychological factors, such as fatigue and personal preference. Such evaluation is time- and money-consuming but unreliable. In today's business environment, quality is becoming more and more important; such subjective, old-fashioned, non-scientific evaluation is no longer effective and needs to be replaced.

FabricEye® is a system which was built with edge lighting capturing technology. It consists of a specially designed belt-driven machine together with intelligent software composed of several modules. Pilling, wrinkling, seam-puckering, hairiness and fuzziness were the analysis modules for objective evaluation.

2.13 Subjective evaluation of fabric appearance.

2.3.3.2 Traditional subjective assessments

Traditional assessments for fabric appearances like pilling, hairiness and wrinkle are basically subjective, with grading carried out by comparison between the fabric sample and the standard rating photographs as shown in Fig. 2.13. The process is thus rather reliant on the observers' experience. Assessment of fabric hairiness is even more arbitrary since there are no criteria which can be referred to. The process is thus rather subjective and the results generated are lacking in accuracy. The only way to improve the accuracy of the results is to have the specimen assessed by as many people as possible, and thus a fabric sample usually has to be inspected by at least three people, an evaluator, a supervisor and an approver, which means at least three times for one fabric. If a dispute arises, more people and laboratories will be involved. The process is rather time-consuming and the test results obtained are seemingly neither reliable/nor generally accepted.

Other quality standards for pilling or wrinkle evaluation, based on subjective evaluation like ASTM and AATCC, also suffer the many disadvantages listed below:

(1) **Inexperience:** people may lack the experience to appreciate and control the quality of the fabrics or garments. This will increase the incidence of rejection and the costs associated with it.
(2) **Lack of accuracy:** the evaluation will have bias and will not be accurate, due to the human factors involved.
(3) **Slow process:** humans may easily get weary after working for a long period of time and so the assessment process will be affected by human fatigue.
(4) **Inconsistency:** different people and environments will give rise to different opinions, preferences and results.
(5) **Other:** damaging and fading of the photographic standards will affect the result.

For visual assessment the data analysis confirmed that significant variations do exist within laboratories, and there are even larger variations between different laboratories. Thus, subjective evaluation does not give results which are consistent among different parties, at different places and at different times. All these factors can adjust perception and grading ability. In turn these can all affect the costs which arise from wrong decisions being made.

2.3.3.3 Overview of the FabricEye® system

Background

Since the 1950s, researchers attempted to investigate the characteristics of fabric appearance using computer and image technologies (Serra, 1982; Xu *et al*., 1998; Tsai and Hsieh, 1999; Hu, 2001; Hu *et al.*, 2001, 2002a,b. They usually processed greyscale images, which were captured using change coupled device (CCD) camera. However, anisotropic light intensity with colour-patterned fabrics presented a problem with these pictures. Thus, other researchers began to develop new approaches to capture fabric images which are not affected by fabric patterns, such as the laser technique (Xu, 1998).

By using the laser technique, the three-dimensional profile of a fabric surface could be extracted; however, its limitations in the form of difficulty in practical operation and high instrumental cost combined with low precision hindered commercial development.

Because the above three techniques – manual, image technology and laser scanner – cannot fulfil the requirements of industry, Dr Hu Jinlian in the Institute of Textiles and Clothing of the Hong Kong Polytechnic University led her team to develop a digital system for the objective evaluation of fabric appearance. They were able to prove that the digital evaluation of fabric appearance is possible and feasible based on the following points:

- image processing techniques applied to many fields
- decrease in hardware costs
- improvement in quality and reliability of cameras
- powerful and effective tools for the evaluation
- user-friendly

Configuration of the FabricEye® system

FabricEye® includes five basic components as shown in Fig. 2.14: a lighting panel which supplies a constant amount of light; a closed black box where capture takes place avoiding the interruption from external lighting; a programmed electronic component to control the signals of several pieces of hardware; a high-speed industrial type CCD camera; and a standard personal computer equipped with analysis software.

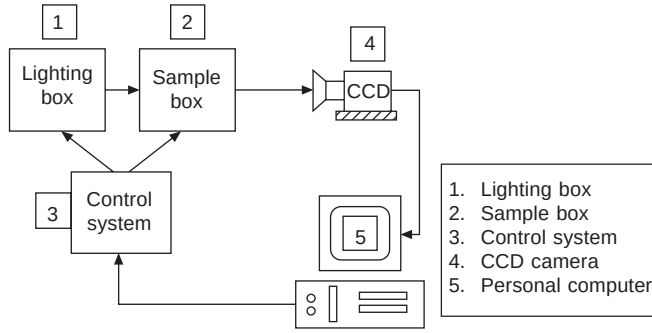

2.14 System structure of FabricEye®.

FabricEye® system specification and requirements
The Fabric Eye® system specification and requirements are shown in Table 2.12.

Information obtained from the FabricEye® system
In general, FabricEye® can provide a surface profile for the user. The surface profile can be displayed in two modes: a two-dimensional greyscale mode and a corresponding three-dimensional false-colour mode as shown in Fig. 2.15.

In the pilling evaluation modules, six features will be evaluated from the surface profile. They are the 'Average Measured Thickness', 'Average Pilling Counts', 'Pilling Size', 'Pilling Area', 'Pilling Height' and 'Pilling Circularity'.

Table 2.12 Fabric Eye® system specification and requirements

System specification	
CCD camera	Resolution: (640 × 480) pixels Shutter speed: 1/8000 seconds
Step motor	Phase number: 2
Dimension	[610 (L) × 310 (H) × 240 (W)] mm
Scanning and analysis time	~ 25 seconds and ~ 10 seconds
Computer requirements	
CPU	800 MHz
Memory	256 MB
Disk space	1 GB
Operating system	Microsoft Windows® 98/2000
Fabric sample requirements	
Dimension	[105 × 105] mm (Standard size for ASTM D3512)
Thickness	[0.2–10] mm
Type	Knitted and woven

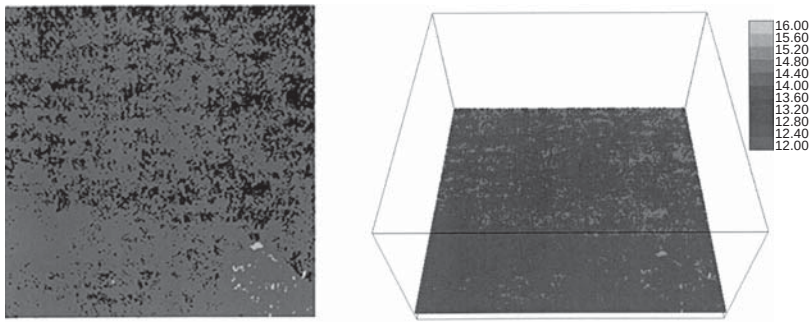

2.15 Displaying mode.

According to Xin *et al.*, (1999, 2002), these six parameters have very high correlation factors with the subjective grading and were thus the ones chosen to be summarised.

The principle of FabricEye®

The hardware of the instrument consists of lighting sources, sample mounting mechanism, sample running mechanism, high-speed CCD camera and scanner, image analysis software package, a commercial personal computer, and a specially designed control unit. Several patents and a trade mark have been registered.

In order to construct the three-dimensional profiles of fabrics, a CCD camera was used which has resolution of 640×480 pixels and took several periodically grabbed images to produce the image map.

To eliminate the effect of colour, a special lighting and sample holding system was developed, with new algorithms for the evaluation of fabric appearance attributes such as pilling, wrinkling, polar fleece fabrics, etc. Very good results have been achieved. Among them, one patent has been filed.

The software of the instrument consists of image capture, image display, image analysis and results output. The scanning time is below 25 sec and the analysis time is below 10 sec.

FabricEye® can produce a three-dimensional map of the fabric surface and extract prominent digital features to give a quantified description of fabric appearance. It can carry out grading as well as an experienced judge.

Evaluation procedure

FabricEye® was intentionally designed with the following features:

(1) automatic analysis with detailed report;
(2) ease of use so that minimum training would be required;
(3) measurement free of the effect from colours;

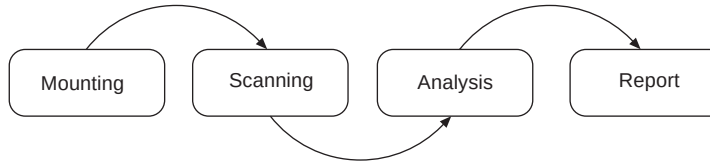

2.16 Evaluation procedure of FabricEye®.

(4) reading generated quickly but repeatable;
(5) grading decision should be compatible with standards.

Considering the five issues above, fabric analysis by FabricEye® was reduced to only four steps, simply illustrated in the flow diagram given in Fig. 2.16, and outlined below.

Step 1 – mounting sample
Mount fabric sample on the testing belt (Fig. 2.17).

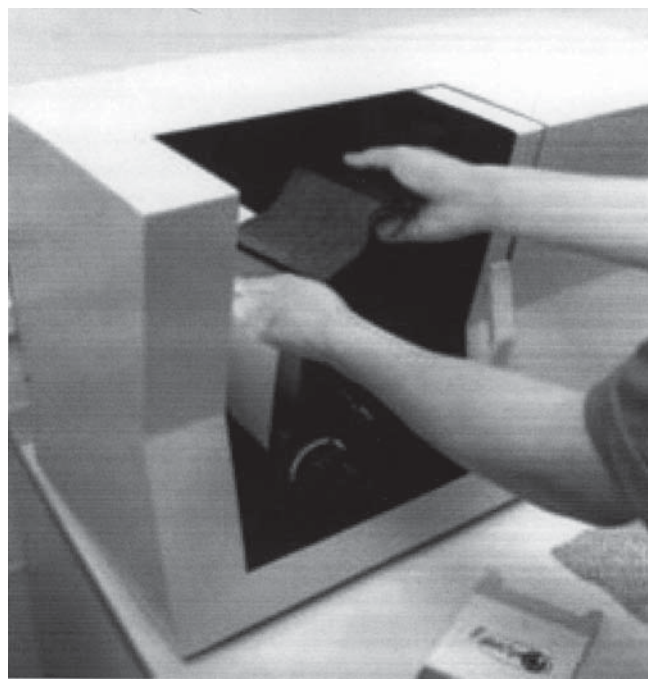

2.17 Mounting a fabric sample on the testing belt.

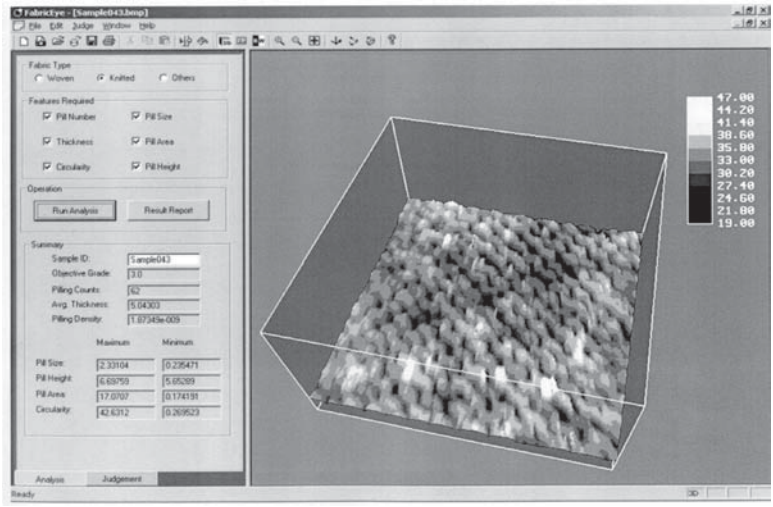

2.18 Generated fabric map.

Step 2 – 3D surface map generation
Run the step motor to move the sample and simultaneously capture the images of fabric profile. Both processes are controlled by computer. Image software will automatically generate a three-dimensional surface map of fabric sample, shown in Fig. 2.18.

Step 3 – feature analysis
Automatic background balance, automatic threshold, automatic feature extraction and related image analysis techniques are applied in this step. Features of fabric surface, for example, pill number, pill size, pill height, and so on are extracted accurately. The quality grade of the sample is intelligently determined by these features. Feature analysis is illustrated in Fig. 2.19.

Step 4 – result report
In this step, the statistical result of these features is reported automatically; the user can easily open a special database to record these features or export them into a document. Figure 2.20 shows a results report.

The analysis of thickness in FabricEye®
One of the important features provided by FabricEye® is the analysis of surface roughness. The roughness measurement on fabrics characterises the fabric's surface from its nature and properties. This is actually an effective method to study the washing effect.

The analysis includes the following parameters: (1) average thickness, (2) relative smoothness, (3) surface skewness, and (4) relative flatness. These parameters will be illustrated in the following sections.

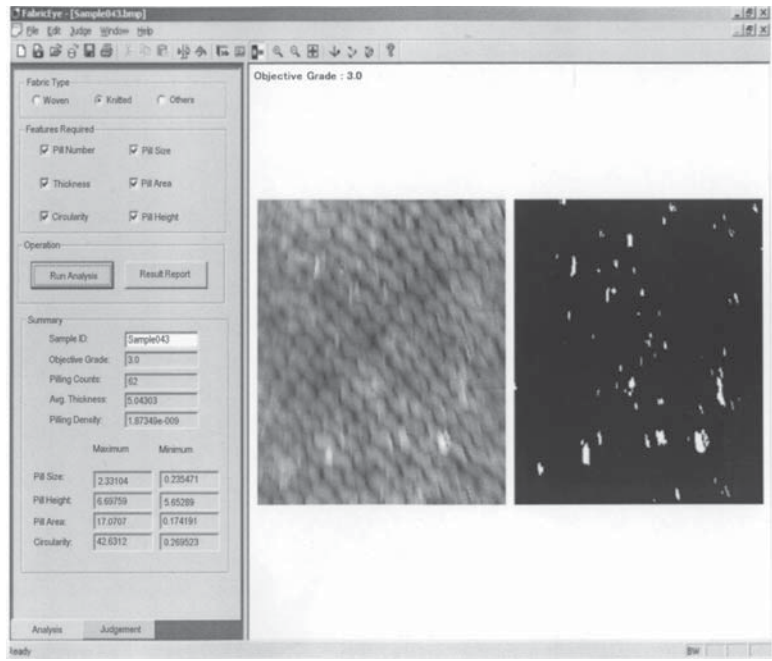

2.19 Feature analysis.

Fabric pilling evaluation report
Sample ID: sample 001
Objective grade: 1.0

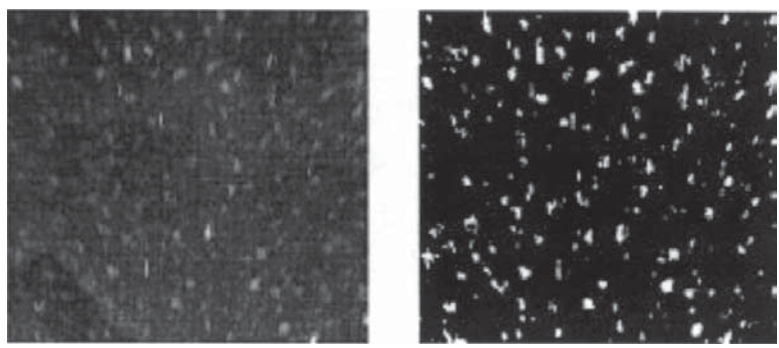

Statistics
(All dimensions in mm)
Average pilling count: 4.2813
Average thickness: 3.85
Pilling density: 1.33e–008

	Maximum	Minimum	Average
Pill size:	1.49	0.16	0.52
Pill height:	4.76	3.97	4.23
Pill area:	7.01	0.08	1.23
Pill circ.:	53.53	0.02	8.69

2.20 Result report.

Average thickness

The traditional method using a clamping device is a kind of compressive measurement taken over a relatively large area. FabricEye® takes more than 2 million uncompressed measurements over the entire sample surface:

$$\text{thickness} = \Sigma \frac{n}{N}, \qquad [2.3]$$

where n is the value of sampling points and N the total number of sampling points over the surface.

The difference between measurements obtained manually and those obtained using FabricEye® can be used to describe the hairiness and fuzziness of fabrics.

Suppose that *TF* is the average thickness measurement by FabricEye® and *TM* is the average thickness measurement by manual device. There are three possible situations:

- **Situation 1 (*TF* > *TM*):** The measurement by FabricEye® is greater than by manual. This is the most frequently observed situation. For most of the common fabrics, hairiness and fuzziness exist. Since the reading from FabricEye® is non-compressive, the hairiness and fuzziness contributed to the height. The clamping device pressed down the hairs and thus the reading taken from it is lower than from FabricEye®.

  In other words, in studying the washing effect, the value of the difference is meaningful. The more the difference, the more hairy and fuzzy the fabric is. The washing effect is relatively effective.
- **Situation 2 (*TF* = *TM*):** The measurements from FabricEye® and manual are equal or almost the same. This indicates that the fabric is quite flat. It could be either a woven fabric or an unwashed fabric in which the celluloses have not yet been digested. It implies that the washing method is ineffective and should be revised.
- **Situation 3 (*TF* < *TM*):** The situation in which the FabricEye® reading is smaller than the manual measurement rarely occurs. It has nothing to do with the washing, but is probably due to the physical structure and components of the fabric. It is usually a knitted fabric with large loop. The yarn loop density is comparatively low. Figure 2.21 could explain the phenomenon.

  The contact area of the clamp of the thickness measuring device is usually relatively large and the force from the device is not sufficient to press the loop structure but only the hairiness and fuzziness. The relatively harder loop structure blocks the in-depth measurement. However, FabricEye® takes numerous sample readings over the entire surface. The thickness is an averaged height value from the sampling points. Therefore, the measurement from FabricEye® would be lower than the manual one in this case.

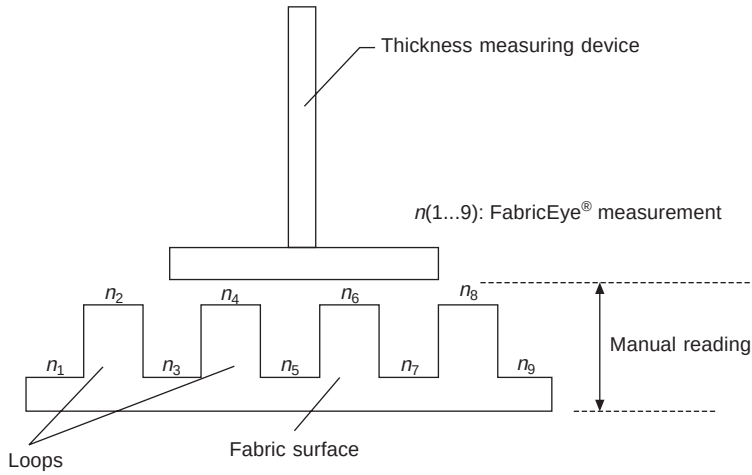

2.21 Difference of measurement between manual and FabricEye®.

Relative smoothness

The relative smoothness is a global analysis of the surface roughness, as shown in Fig. 2.22. It provides an overall idea of how much variation there is on the surface. More rough or strongly patterned fabrics will give a greater value. The value is useful in comparative studies between fabrics. Equation 2.4 governs the relative smoothness:

$$\text{relative smoothness} = 1 - \frac{1}{1 + \sigma^2} \qquad [2.4]$$

where σ^2 is the variance of the height of sampling points.

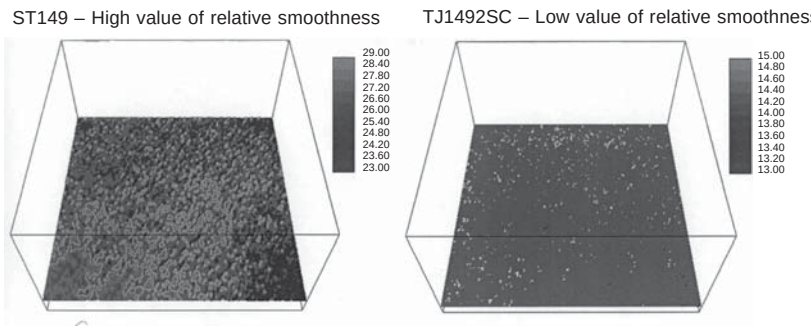

2.22 Relative smoothness demos. Left: sample showing high degree of relative smoothness. Right: sample showing low degree of relative smoothness.

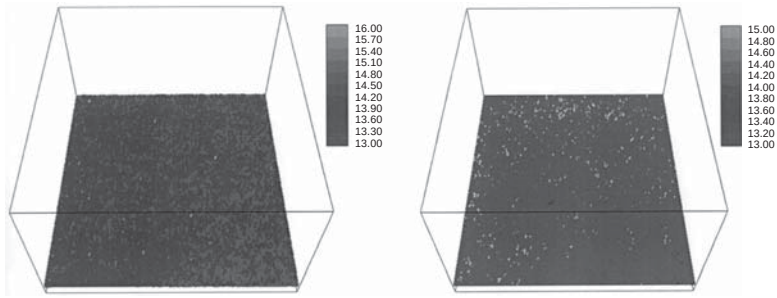

2.23 Surface skewness demos. Left: (negative value) few raised peaks appear in light grey. Right: (positive value) few sunken zones appear in dark grey.

Surface skewness

Surface skewness is a study of the third degree of the height response as shown in Fig. 2.23. Its value indicates if any extrema exist on the surface. A positive value indicates the presence of some sunken zone, while a negative value indicates a raised zone. Equation 2.5 governs surface skewness:

$$\text{skewness} = \frac{E(n - \bar{n})}{\sigma^3}, \qquad [2.5]$$

where E is the expected value, $\bar{n}$ is the average value of sampling points and σ is the standard deviation of the height of sampling points.

Relative flatness

Relative flatness is a localised study of the amount of extrema as shown in Fig. 2.24. It is actually a fourth degree of the height response. Its value indicates if the amount of extrema present is serious. The greater the value, the more corresponding extrema would be observed. Equation 2.6 governs relative flatness:

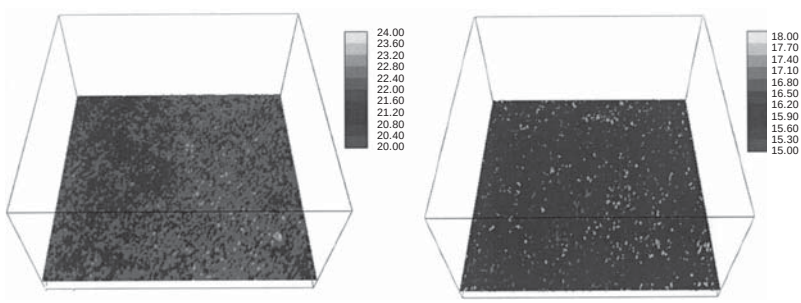

2.24 Relative flatness demos. Left: (lower value) fewer extrema (in white) could be observed. Right: (higher value) more extrema (in white) could be observed.

$$\text{relative flatness} = \frac{E(n - \bar{n})}{\sigma^4}, \qquad [2.6]$$

where E is the expected value and σ is the standard deviation of the height of sampling points.

Applications

FabricEye® further summarised the evaluation process by giving the specimens an objective grade. The rapid results from the equipment allow the fabric buyers to make decisions quickly. Furthermore, quality evaluation laboratories can release manpower to carry out other experiments with a higher requirement for technical input. Manufacturers can further utilise the other data obtained for product development and characterisation.

With future integrated modules, FabricEye® can be applied to the fashion and textile industry, laundry services, and custom inspection for the different appearance evaluation of pilling, wrinkling, surface hairiness, texture/density, seam puckering and polar fleece fabrics and garments.

To summarise, FabricEye® brings many benefits to the industry in terms of better quality management, with quick response and lower production costs, as well as quality production, with efficient quality control and informative and objective statistics. It can also eliminate arguments due to different subjective judgments from different inspectors.

2.4 Complex deformation measurement

2.4.1 Introduction

The drape of a fabric in a broader sense refers to the manner in which the fabric hangs, shapes and flows on the model form, such as on the body and furniture, by gravity when only part of it is directly supported. In some literature, wrinkling, buckling, handle and bending may mean drape. In the present context, the dominant role played by the gravity of the fabric in drape is emphasised. The folding from fabric drape which takes up a complex three-dimensional form with double curvature is unique for drape, but single curvature of fabric deformation, such as the cantilever test, is also included in the present review, as long as fabric deformation results from its own weight.

Research into this theoretically complicated and practically important topic originated with Peirce in 1930. For several decades, this paper has been regarded as a benchmark and a source of investigation for many researchers. Particularly since the year 2000, the investigation of fabric drape has attracted the attention of many researchers, partly because of the attempt to realise the clothing CAD system by introducing fabric properties in which the fabric drape is the key element. The intention here is to make a comprehensive

survey of the existing research into fabric drape and its application to the textiles and clothing industries since Peirce. The contents consist of: experimental study and evaluation methods; empirical study of the relationship between fabric drape and mechanical properties; assembling methods, theoretical investigation, analytical and numerical prediction; current status and future trends of research in this area are also included. It consists of two parts. The first part of this review deals with test and evaluation of drape, and empirical study carried out by textile specialists. The second part will discuss theoretical aspects and numerical simulation as well as its applications.

2.4.2 Cantilever methods

In the past, the cantilever test was mainly used to determine fabric stiffness, e.g. bending rigidity (constant and whole bending curve) and/or possibly frictional couple. Its association with fabric drape and extensive discussion here are due to the following reasons: first, the cantilever test utilises the response of a fabric under its own weight, which is essentially the drape behaviour of a fabric, but in only two dimensions; second, bending properties obtained for this test are the key element for predicting fabric drape generally; third, many numerical or theoretical investigations into fabric drape used the standard fabric cantilever test to verify their mechanics models and/or the accuracy of their software programmes. Finally, some investigations for fabric handling related to fabric drape are based on Peirce's cantilever theory (Postle and Postle, 1992).

Cantilever methods for the evaluation of fabric drape were first introduced to textile specialists by Peirce (1930), based on the recognition that stiffness has a large effect on drapeability. In his original paper, nine types of cantilever were proposed for different types of fabrics.

The standard tester, called a flexometer, which has now become the standard Shirley Stiffness Tester, was described in detail by Peirce (1930). On this tester, the angle through which a specimen of cloth droops when a definite length is held out over an edge can be measured. The specimen is a rectangle with a large length to width ratio (6:1). By means of a mathematical formula, this angle is converted into a term called 'bending length', which is a measure of fabric drapeability in two dimensions; Peirce even called it 'drape stiffness'.

Peirce mentioned in the same paper another eight types of fabric cantilevers to compensate for the shortness of the rectangle cantilever. Various modifications of the method had been worked out to deal with those fabrics which were unsuitable for the standard method. For example, for very stiff such as starched and ironed fabric, a weight can be added to the free-end of the specimen, called a weighted rectangle. For a very flimsy fabric, a triangle cantilever may be used. A material too stiff, but curling badly when tested as a weighted rectangle, may be better dealt with as a triangle weighted at the

tip. Because the curling is not so pronounced in a broader strip, Peirce also suggested another cantilever with a wider (6 in) strip. With the broader instrument, it is also possible to test a specimen cut in circular form. For fabrics where the tendency to curl is so pronounced that the strip takes a complete twist, a long specimen of 20 cm is cut, with the middle marking a dot, and the two ends placed together to form a pear- or ring-shaped loop. The depression of the middle point is much the same as for a strip of the same length.

F.R.L. Testing Machines Inc. (1980) reported that the F.R.L. Cantilever Bending Tester is capable of testing thin sheet material, textiles and other flexible materials, including carpets. After Peirce and F.R.L. Cantilever, several versions of the tester were designed. Some improvements in this test were made, particularly in terms of automation.

Kalyanaraman and Siveramakrishnan (1984) designed an electronic cantilever meter based on optoelectronic principles. Their instrument has the same accuracy as the Shirley Stiffness Meter and works on the same principle, but the measurement is objective and could easily be automated.

The FAST system developed by CSIRO in 1993 consists of a cantilever bending meter. The principle for FAST-2 is very similar to that of the Shirley Stiffness Tester in which the fabric bends under its own weight until its leading edge intercepts a plane at an angle of 41.5° from the horizontal. Compared with the Shirley Stiffness tester, the FAST-2 was designed to test a wider specimen (50 mm), even though any sample width from the standard 2.45 cm up to 50 mm can be employed. In addition, this instrument encloses totally the electronics and detection apparatus. The fabric leading edge is detected, as it is moved across to the measurement cavity, initiating the length measurement, then as it cuts a light beam inclined at 41.5° to the horizontal. After a settling and adjustment period the bending length is displayed digitally.

Russell (1994) reported an alternative instrument for the measurement of fabric bending length in contrast with the commercial Shirley Stiffness Tester and the FAST-2 bending meter. He pointed out that both instruments use a sliding bar and encounter problems with some fabrics, such as pile fabrics or those made of filament yarns. For these slippery or easily deformed fabrics, with this simultaneous weighting and sliding procedure, the slider can slip over the surface of filament fabrics and cause the fabric to cockle as it is slid along the platform, leading to wrong bending lengths. In addition, they cannot be used at all on slivers, rovings or yarns. For this purpose, he developed a testing instrument that combines the principles of the Shirley and FAST-2 testers with elements of a comb sorter apparatus used for fibre distribution.

Clapp *et al.*, developed an indirect method of measuring the moment–curvature relationship for fabrics (Clapp *et al*., 1990; Clapp and Peng, 1991). At the same time, they developed a method to measure the draped profile of

the cantilever. Deformed co-ordinates were recorded as a fabric sample was cantilevered under its own weight from a fixed support. The advantage of this method is that fabric non-linear bending behaviour, inherent in most fabrics, is readily obtained, unlike in the traditional cantilever beam test. Moreover, the draped image obtained by using a laser sensor can be used for the verification of the numerical simulation results.

Potluri *et al*. (1996) also developed an experimental technique to verify their numerical method for the capability to compute for general situations. A laser triangulation sensor, attached to a robot arm, was used for measuring the cantilever profile of the fabric samples. A manipulating device positions the fabric sample as a cantilever of specified length. The laser scans along the centre line of the fabric cantilever. The *x* co-ordinates are obtained from the robot position and the *y* co-ordinates are obtained from the output signal of the triangulation sensor.

2.4.3 Drapemeter

Cusick (1961) and Chu *et al*. (1950) made a great contribution to the practical measurement of fabric drape. The current standard so-called drapemeter is the result of their effort, in which the drape coefficient, the ratio of projected area to specimen's original area, is determined. The drape coefficient can provide an objective description of the deformation, although it is not a complete description. A low drape coefficient indicates easy deformation of a fabric. The advantage of this method over the cantilever is its capability to test the three-dimensional drape feature, and it can thus differentiate between the paper and a textile fabric. Further investigations or changes on this type of drapemeter are limited, but advances in this method can also be traced.

Vangheluwe and Kiekens (1993) measured the drape coefficient using image analysis. A CCD camera is mounted centrally above the drapemeter. This camera sends the image to a monitor and a frame grabber in a personal computer. The frame grabber digitises the image. The drape coefficient is calculated using a ratio not of masses but of areas. Calibration is carried out by recording the image of the drape tester without a test sample. The image analysis system presents a number of advantages, which makes it preferable to the traditional measuring method. A test using the suggested method will take no more than 10 sec, whereas the cut-and-weigh method easily requires more than 5 min. Moreover, the results obtained when using the cut-and-weigh method are subjective because the drawing and cutting are influenced by the laboratory assistant. By using this system, the authors investigated the time dependence of drape coefficient at 10 min intervals.

Collier *et al*. designed a digital drapemeter to measure fabric drape coefficient by using photovoltaic cells (Collier and Collier, 1990; Collier, 1991; Collier *et al*., 1991a, b). This drapemeter utilises the principle of the standard

experimental drapemeter and applies a bottom surface of photovoltaic cells to determine the amount of light blocked by a fabric specimen draped on a pedestal. A digital display gives the amount of light being absorbed by the photovoltaic cells, which is related to the amount of drape of the fabric specimen. This principle was quickly adapted by textile researchers in China.

Stylios *et al*. (1996) developed a new drapemeter, which measures the drape of any fabric both statically and dynamically, in true three-dimensions, by using a CCD camera as a vision sensor. This system, called the Marilyn Monroe Meter (M3), has been used to measure real fabric drape behaviour, and is being used to verify their theoretical prediction model. The draped profile of the specimen can be taken and presented on a computer.

2.5 References

AATCC, *Technical Manual of the American Association of Textile Chemists and Colorists*, http://www.aatcc.org.

ASTM-D3511 (2002), Standard test method for pilling resistance and other related surface changes of textile fabrics: brush pilling tester, New York, ANS I.

ASTM-D3512 (2002), Standard test method for pilling resistance and other related surface changes of textile fabrics: random tumble pilling tester, New York, ANS I.

ASTM-D3514 (2002), Standard test method for pilling resistance and other related surface changes of textile fabrics: elastomeric pad, New York, ANS I.

ASTM-D4970 (2002), Standard test method for pilling resistance and other related surface changes of textiles fabrics: martindale tester, New York, ANS I.

BS3356 (1990), Method for determination of bending length and flexural rigidity of fabrics.

BS2862: (1984), ISO 7211/2 Methods for determination of number of threads per unit length (withdrawn, superseded)

Chu C C, Cummings C L and Teixeira N A (1950), Mechanics of elastic performance of textile materials, part V: A study of the factors affecting the drape of fabrics – the development of a drape meter, *Text Res J*, **20**, 539–548.

Clapp T G and Peng H (1991), A comparison of linear and nonlinear bending methods for predicting fabric deformation in automated handling, *J Text Inst*, **82**, 341.

Clapp T G, Peng H, Ghosh T K and Eischen J W (1990), Indirect measurement of the moment-curvature relationship for fabrics, *Text Res J*, **60**(9), 525–533.

Collier B J (1991, Fall), Measurement of fabric drape and its relation to fabric mechanical properties and subjective evaluation, *Clothing and Textiles Research Journal*, **10**, 46–52.

Collier B J and Collier J R (1990), CAD/CAM in the textile and apparel industry, *Clothing and Textiles Journal*, **8**(3), 7–13.

Collier J R, Collier B J, Gina O'tool and Sargand S M (1991a), Drape prediction by means of finite element analysis *J Text Inst*, **82**, 96–107.

Collier J R, Collier B J, Gina O'tool and Sargand S M (1991b), Development of a digital drape tester, *ACPTC combined proceedings*, 35.

Cusick G E (1961), *The Measurement of Fabric Drape*, (PhD thesis, University of Manchester Institute of Science and Technology).

F R L Cantilever bending tester (1980 Aug), New York 11701, Testing machines Inc 400 Bayview Ave, Amityville, 1 p News release literature.

Grosberg P (1966), The mechanical properties of woven fabrics part II: the bending of woven fabrics, *Text Res J*, **36**, 205–210.

Grosberg P and Park B J (1966), The mechanical properties of woven fabrics part V: the initial modulus and the frictional restraint in shearing of plain weave fabrics, *Text Res J*, **36**, 420–431.

Grosberg P and Swani N M (1966), The mechanical properties of woven fabrics part IV: determination of the bending rigidity and frictional restraint in woven fabrics, *Text Res J*, **36**, 338–45.

Hu J L (2001), Digital system for the objective evaluation of fabric appearance, *Proc 6th Asian Textile Conference – Innovation & Globalization* Aug. 22–24, Hong Kong Polytechnic University, Hong Kong.

Hu J L, Xin B J and Yan H J (2001), Subjective and objective evaluation of polar fleece fabric appearance after abrasion, *Proc Technitex 2001 – the 1st Autex Conference*, June 26–29, Povoa de Varzim, Portugal.

Hu J, Xin B and Yan H (2002a), Measurement and modeling of 3D wrinkes in fabrics, *Text Res J*, **72**, 863–870.

Hu J, Xin B and Yan H (2002b), Classifying fleece fabric appearance by extended morphological fractal analysis, *Textile Res J*, **72**, 879–885.

Kalyanaraman A R and Siveramakrishnan A (1984), Electronic fabrics stiffness meter – performance evaluation with the known instruments, *Text Res J*, **54**(7), 479–484.

Kawabata S (1982), The development of the objective measurement of fabric handle, *Proc First Japan-Australia joint symposium on objective specification of fabric quality, mechanical properties and performance*, Kyoto, Textile Machinery Society, Japan, 31–59.

Lindberg J, Waesterberg and Svenson R (1960), Wool fabrics as garment construction materials, *J Text Inst*, **51**, T1475–1493.

Ly N G, Tester D H, Buckenham P, Roczniok A F, Brothers M and de Jong S (1988), *ITO Report No 11*, Paris Meeting.

Ly N G, Tester D H. Buckenham P, Roczniok A F, Adriaansen A L, Scaysbrook F and De Jong S (1991), Simple instruments for quality control by finishers and tailors, *Text Res J*, **61**(7), P402–406.

Manual for KES-FB, 1–4

Manual For VID system, UMIST

Peirce F T (1930), The handle of cloth as a measurable quality, *J Text Inst*, **21**, 337–416.

Peirce F T (1937), The geometry of cloth structure, *J Text Inst*, **28**, P45–96.

Postle J R and Postle R (1992), Fabric bending and drape based on objective measurement, *Clothing Sci & Tech*, **4**(5), 7–15.

Potluri P, Atkinson J and Porat I (1996), Departments of textiles and mechanical engineering, large deformation modelling of flexible materials, *J Text Inst*, **87**(1), 129–151.

Russell S J (1994), Alternative instrument for the measurement of fabric bending length (Univ of Leeds); (Letter to Editor), *J Text Inst*, **85**(1), 82–83.

Serra J (1982), *Image Analysis and Mathematical Morphology, Vol I*, New York, Academic Press.

Stylios G K, Wan T R and Powell N J (1996), Modelling the Dynamic Drape of Fabrics on Synthetic Humans in a Virtual Fashion Show, *Int J Clothing Sci & Tech*, **8**(3), 95–122.

Tsai D M and Hsieh C Y (1999), Automated surface inspection for directional textures, *Image and Vision Computing*, **18**, 49–62.

Vangheluwe L and Kiekens (1993), Time dependence of the drape coefficient of fabrics, *Int J Clothing Sci & Tech*, **5**, 5–8.

Xin B J and Yu X F (1999), Automatic measurement of the yarn density of woven fabric, *J China Text Univ*, **25**, 34–37.

Xin B, Hu J and Yan H (2002), Objective evaluation of fabric pilling using image analysis techniques, *Textile Res J*, **72**, 1057–1064.

Xu B, Cuminao D F and Keyes N M (1998), Evaluating fabric smoothness appearance with a laser profilometer, *Text Res J*, **68**, 900–906.

3

Structural properties of fabric

3.1 Theories of woven fabric structure

3.1.1 Introduction

The geometry of fabrics has considerable effects on their behaviour. For example, the weft dimension decreases and weft crimp increases when the cloth is stretched in the warp direction; cloth shrinks when the fibres swell on wetting. Therefore, studies of fabric geometry have played an important role in the following areas:

(1) prediction of the maximum sett of fabric which should be woven, and fabric dimensional properties;
(2) derivation of relationship between geometrical parameters, such as crimp and weave angle;
(3) prediction of mechanical properties by combining fabric geometry with yarn properties such as Young's modulus, bending rigidity and torsional rigidity;
(4) help in understanding fabric performance, such as in handle and surface effects.

3.1.2 Geometry theories

3.1.2.1 Yarn configuration in plain-weave fabrics

As we know, fabrics are not regular structures capable of description in mathematical forms based on geometry; but many believe that we can idealise the general characters of the materials into simple geometrical forms and physical parameters in order to arrive at mathematical deductions. To represent the configuration of threads in woven fabrics, many different forms of geometry have been put forward by textile researchers.

In conventional approaches, the general character of fabrics was idealised into simple geometrical forms. These studies were often based on the

assumption of arbitrary geometrical models for the weave crimp and yarn cross-sectional shapes. They treated the micromechanics of fabrics on the basis of the unit-cell approach, i.e. fabrics are considered as a repeating network of identical unit cells in the form of crimp waves and constant yarn cross-section in the woven structure. By combining this kind of geometry with or without physical parameters, mathematical deductions could be obtained. The yarn configuration in fabric is mainly determined by the form of crimp waves and the cross-sectional shape of yarns in a given position. The cross-sectional shape of yarns in four existing models is reviewed below.

For convenience, the symbols used throughout are listed as follows:

d – free circular-thread diameter
D – sum of circular diameters ($d_1 + d_2$)
a – major diameter of flattened thread
b – minor diameter of flattened thread
e – thread flattening coefficient (a/b)
h – height of crimp wave
T – fabric thickness ($h_1 + b_1$ or $h_2 + b_2$, whichever is greater)
p – average thread spacing for the fabric as a whole
n – average number of threads per unit length ($n = 1/p$)
c – thread crimp
K – cover factor
θ – maximum angle of the thread axis to plane of cloth in radius
l – length of thread axis between planes containing the axes of consecutive cross threads
l_c – contact length of yarn
N – cotton count of yarn

Subscripts 1 and 2 are used to denote warp and weft. If in any relation no subscript is used it is to be understood that either 1 or 2 may be inserted throughout.

The systematic study of woven fabric geometry was started in 1937 when Peirce's paper (Peirce, 1937) was published. Notable examples of geometrical models include Peirce's model of plain-weave fabrics (Peirce, 1937) as shown in Fig. 3.1.

In this model, a two-dimensional unit cell (or repeat) of fabric was built up by superimposing linear and circular yarn segments to produce the desired shape. His model of plain-weave fabrics could be obtained if the yarns were assumed to be circular in cross-section and highly incompressible, but at the same time perfectly flexible so that each set of yarns had a uniform curvature imposed upon it by the circular cross-sectional shape of the interlacing yarns. Derivation of the relationships between the geometrical parameters and such parameters as thread-spacing, weave crimp, weave angle and fabric thickness forms the basis of the analysis. This model is convenient for calculation, and

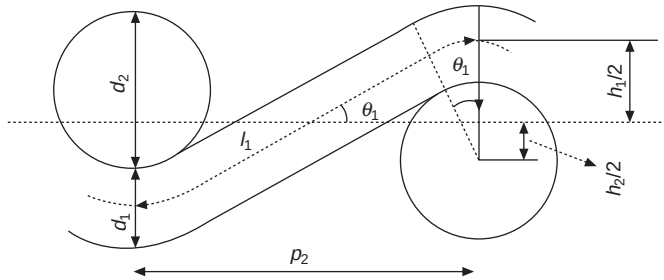

3.1 Peirce's circular cross-section geometry of plain-weave fabrics.

has been found useful in the ordering and interpretation of observation; it is especially valid in very open structures. But the assumptions of circular cross-section, uniform structure along the longitudinal direction, perfect flexibility, and incompressibility are all unrealistic, which leads to the limitations on the application of this model.

In more tightly woven fabrics, however, the inter-thread pressures set up during weaving cause considerable thread flattening normal to the plane of the cloth. Peirce recognised this and proposed an elliptic section theory as shown in Fig. 3.2. Because such geometry would be too complex and laborious in operation, he adopted an approximate treatment, which involved merely replacing the circular thread diameter in his circular-thread geometry with the minor diameter of the appropriate elliptic section as shown in Fig. 3.3.

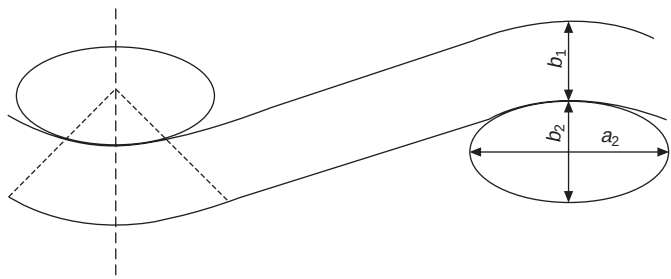

3.2 Peirce's elliptic cross-section geometry of plain-weave fabrics.

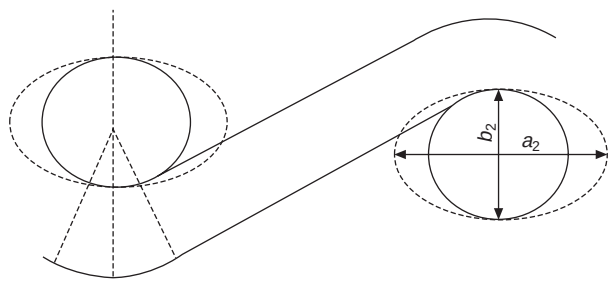

3.3 Peirce's approximate treatment of flattened yarn geometry of plain-weave fabrics.

This treatment was adequate for reasonably open fabrics, but it still does not permit of application to jammed structure. To overcome this difficulty, Kemp (1958) proposed a racetrack section as shown in Fig. 3.4 to modify cross-sectional shape; this consisted of a rectangle enclosed by two semi-circular ends and had the considerable advantage that it allowed the relatively simple relations of circular-thread geometry, already worked out and tabulated by Peirce, to be applied to a comprehensive treatment of flattened threads. In the paper on 'An energy method for calculations in fabric mechanics', a lenticular geometry was proposed by Hearle and Shanahan (1978) as shown in Fig. 3.5.

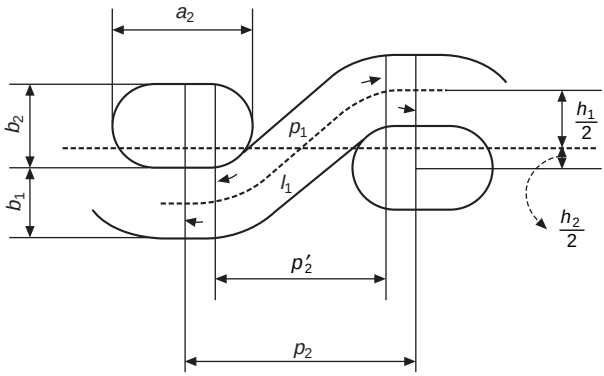

3.4 Kemp's racetrack section geometry of plain-weave fabrics.

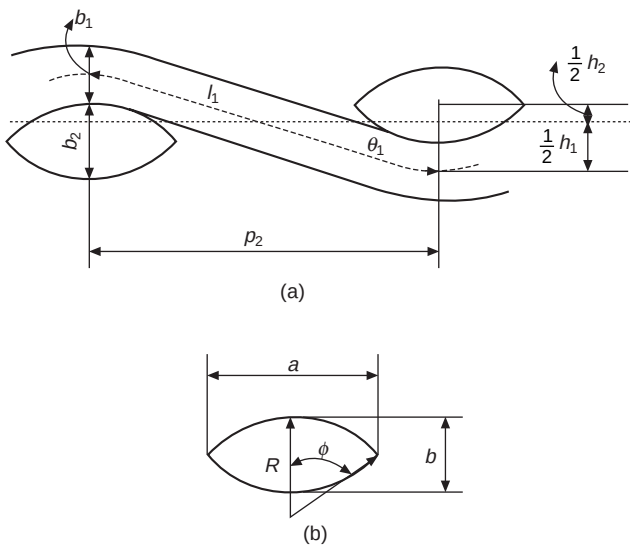

3.5 Hearle's lenticular section geometry of plain-weave fabrics.

3.1.2.2 Mathematical description of the models

Among the four models mentioned above, it was found by the author that lenticular geometry developed by Hearle *et al*. and illustrated in Fig. 3.5 is the most general model mathematically. We can establish equations for this model and derive equations for other ones.

The equations for lenticular geometry established by Hearle *et al*. are:

$$\left.\begin{aligned} p_i &= (l_j - D_j\theta_j)\cos\theta_j + D_j \sin\theta_j \\ h_{ii} &= (l_i - D_i\theta_i)\sin\theta_i(1 - \cos\theta_i) \\ D_i &= 2R_j + b_i \\ a_{ii} &= 2R_j \sin\theta_i \\ b_{ii} &= 2T_i \cos\theta_i \\ e_i &= a_i/b_i \\ \sin\phi_i &= 2e_i/(1 + e_i^2) \\ h_1 + h_2 &= b_1 + b_2 \\ l_{cj} &= D_i\theta_i \end{aligned}\right\} \quad [3.1]$$

where R_j, is the lenticular radius and θ_i is the lenticular angle.

By substituting $\phi = 90°$, $a_i = b_i = 2R_i = d_i$, $D_1 = D_2 = d_1 + d_2 = D$ into the above equations, the Peirce's geometry as shown in Fig. 3.1 can be obtained. The equations are as follows:

$$\left.\begin{aligned} p_1 &= (l_2 - D\theta_2)\cos\theta_2 + D\sin\theta_2 \\ p_2 &= (l_1 - D\theta_1)\cos\theta_1 + D\sin\theta_1 \\ h_1 &= (l_1 - D\theta_1)\sin\theta_1 + D(1 - \cos\theta_1) \\ h_2 &= (l_2 - D\theta_2)\sin\theta_2 + D(1 - \cos\theta_2) \\ h_1 + h_2 &= d_1 + d_2 = D \\ l_{c2} &= D_1\theta_1 \le l_1 \\ l_{c1} &= D_2\theta_2 \le l_2 \end{aligned}\right\} \quad [3.2]$$

Therefore, Peirce's geometry can be regarded as a special case of Hearle's lenticular one. And race-track geometry as shown in Fig. 3.4 as a modification of this model, gives the following equations:

$$\left.\begin{aligned} p_i &= a_i - b_i + (l_j' - D\theta_j + D\sin\theta_j) \\ h_i &= (l_i' - D\theta_i)\sin\theta_i + D(1 - \cos\theta_i) \\ l_i' &= l_i - a_i + b_i \\ h_1 + h_2 &= b_1 + b_2 = D \\ l_{cj} &= D_i\theta_i + a_i - b_i \\ e_i &= a_i/b_i \end{aligned}\right\} \quad [3.3]$$

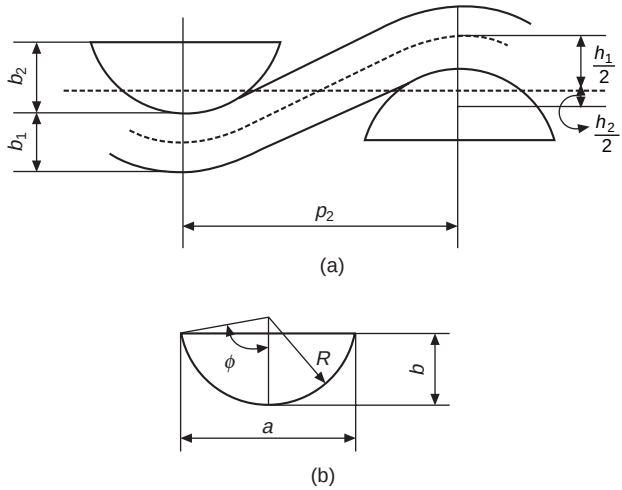

3.6 Bowshaped geometry of plain-weave fabrics.

Including elliptic geometry, the four kinds of geometry are symmetrical ones.

As can be seen in Fig. 3.6, a horizontally asymmetrical geometry which is called bowshaped geometry is also observed frequently. Its geometrical parameters can also be formulated according to the principles of lenticular geometry (Newton and Hu, 1992; Hu and Newton 1993; Hu, 1994) as shown in equation 3.4. The basic equations are identical to those in lenticular geometry except for the two in the square brackets.

$$\left.\begin{aligned}
&p_i = (l_j - D_j\theta_j)\cos\theta_j + D_j \sin\theta_j \\
&h_i = (l_i - D_i\theta_i)\sin\theta_i\,(1 - \cos\theta_i) \\
&D_i = 2R_j + b_i \\
&a_i = 2R_i \sin\phi_i \\
&[b_i = R_i \cos\phi_i] \\
&e_i = a_i/b_i \\
&[\sin\phi_i = 4e_i/(4 + e_i^2)] \\
&h_1 + h_2 = b_1 + b_2 \\
&l_{cj} = D_i\theta_i
\end{aligned}\right\} \qquad [3.4]$$

3.2 Structural parameters of woven fabrics

From the previous research on the geometric theories introduced above, several parameters could be extracted to characterise the fabric geometry. In this section, a general description of every parameter will be given. Some of them need not be calculated but can only be measured.

3.2.1 Yarn diameter

According to the Peirce's (1937) circular yarn section, $1/d$, and the number of diameters per inch in the cotton system:

$$\frac{1}{d} = \frac{29 \cdot 3\sqrt{N}}{v} \qquad [3.5]$$

$$\frac{1}{d} = 28\sqrt{N} \qquad [3.6]$$

and

$$d = \frac{1}{28\sqrt{N}} = \frac{0.0357}{\sqrt{N}} \text{ (inch)} = \frac{36}{\sqrt{N}} \text{ (mils)} = \frac{0.91}{\sqrt{N}} \text{ (mm)} \qquad [3.7]$$

where v, the specific volume, is the ratio of the volume occupied by a material to that of the same weight of water under compression. Of the woven structure, $v = 1.1$ for cotton yarn.

3.2.2 Thickness

Fabric thickness is given by t_1 or t_2 whichever is greater, where $t_1 = h_1 + d_1$, $t_2 = h_2 + d_2$. When yarn diameters are assumed to be circular:

$$t = \max(t_1, t_2) \qquad [3.8]$$

For flattening section yarns, fabric thickness

$$t_1 = h_1 + b_1 \qquad t_2 = h_2 + b_2 \qquad [3.9]$$

The condition that the two threads project equally produces a smooth surface and gives the minimum thickness, t_{min}

$$t_{min} = h_1 + d_1 = h_2 + d_2 = \frac{1}{2}(h_1 + h_2 + d_1 + d_2) = D \qquad [3.10]$$

where $h_1 = D - d_1$. So the minimum thickness is the sum of the thread diameters.

The maximum thickness is attained when one or other of the threads is straightened as far as possible. In an open cloth, where either may be straightened to zero crimp, this thickness should be

$$t_{max} = D + d_{max} \qquad [3.11]$$

d_{max} is the diameter of the thicker thread, and it is attained by straightening the thinner threads. If $d_1 = d_2 = d$:

$$t_{min} = 2d = D$$

$$t_{max} = 3d \qquad [3.12]$$

3.2.3 Cover factor

Fabric cover is defined by Hamilton (1964) geometrically as the proportion of fabric area covered by actual yarns. In practice, cover factors are normally calculated for warp and weft independently. For example, a fabric having 50 warp threads per centimetre, each 0.01 cm in major diameter, would have a warp cover factor (K_1) of 0.5 or 50 %. In the case of circular section threads, warp and weft cover factors are given by

$$K_1 = n_1 d_1 \qquad K_2 = n_2 d_2 \qquad [3.13]$$

For flattened threads, warp and cover factors for plain weave are thus given by

$$K_1 = n_1 a_1 \qquad K_2 = n_2 a_2 \qquad [3.14]$$

And overall cover factor K is calculated from K_1 and K_2 as follows:

$$K = K_1 + K_2 - K_1 K_2 \qquad [3.15]$$

The cover factor thus indicates the degree of closing or cover. Increasing the projection of the area covered by threads through using yarn with greater 'ooziness', or by flattening in finishing and more regularity will improve the cover of cloth.

3.2.4 Crimp

Crimp is the percentage of excess of length of the yarn axis over the cloth length:

$$c_1 = \left(\frac{l_1}{p_2} - 1 \right) \times 100\ \% \qquad c_2 = \left(\frac{l_2}{p_1} - 1 \right) \times 100\ \% \qquad [3.16]$$

The primary geometrical parameter is the crimp magnitude. It provides a good basis for investigating many complicated phenomena, such as stress–strain relations, hand and creasing. And, in particular, crimp has been used as a fundamental parameter for calculating other geometrical parameters such as crimp height or weave angle which are not easy to measure. Therefore, to study fabric structure or related problems, measuring yarn crimp in fabric is essential. But the actual difficulty in measuring this parameter is not entirely solved or recognised, perhaps, by many researchers.

3.2.5 General problems

In previous research, much effort has been devoted to the geometry of woven fabrics and related problems under the assumption of constant yarn configuration in fabric. For example, since Peirce, the inter-thread pressure

set up during weaving, which causes considerable thread compression, has been recognised as only uniform flattening normal to the fabric plane. His elliptic cross-section model has been regarded as a little bit closer to the actual structure than the circular cross-section due to compressibility. However, the other factors were still not given proper consideration, especially in that it does not permit of any variation along both lateral and longitudinal directions. Adding other models such as Kemp's race-track cross-section and Hearle's lenticular one, the principles on which all these models are based remain unaltered. In particular, it is always assumed either explicitly or implicitly that geometric shape is constant for each model of the unit cell, that is, the variation of the fabric structure was considered insignificant in the analysis. It may not be justified to look only at constant structure and ignore investigation of variation in the structure in the study in fabric geometry.

Firstly, it is a fact that fabrics are extremely complicated materials that do not conform even approximately to any of the ideal features normally assumed in engineering structural analysis and mechanics. Secondly, the measurement of geometrical parameters is not easy in practice. Nobody has measured the full set of geometrical parameters so far, but many rely on the calculations of some formula derived from the geometrical model, mainly from Peirce's model. As we know, there are problems in the model itself. So we have a right to doubt the validity of simplified formulae derived from this model. Therefore, the measurement techniques need to be developed.

Thirdly, a thorough and precise understanding of the effects of fabric geometry on fabric mechanical properties is a precondition for the development of total fabric engineering which will enable a fabric with the right combination of performance characteristics for a particular end use to be designed and manufactured without lengthy and costly trials. But these important effects of fabric construction on fabric mechanical properties tested on the KES system remain almost unexplored.

3.3 Twist redistribution of folded yarns in woven fabrics

Figure 3.7 shows the surface images of several woven fabrics made of folded yarns. From Fig. 3.7a, which represents a very open woven fabric, it can be seen that the length of a folded yarn in one twist is inserted into one repeat of plain weave fabric. Other samples shown in Figs 3.7b and c exhibit a similar effect. For very close fabrics with few turns of twists, one turn of twist may be inserted into one and a half or two repeats of a plain-weave fabric. There is no literature reporting that a designer would match sett and twists exactly in this way. The phenomenon is here called 'twist redistribution' in a woven fabric because twists of a folded yarn are subjected to adjustment when a woven fabric is formed. It may suggest the contraction of folded

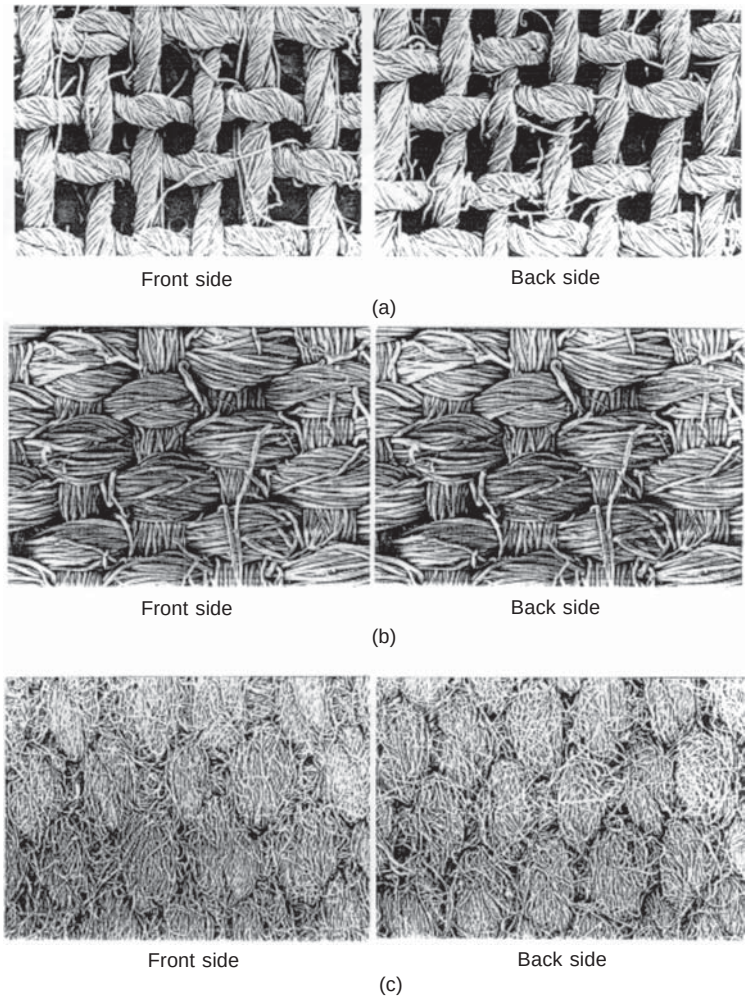

3.7 Surface images of woven fabrics with folded yarns: (a) surface image of an open fabric with folded yarns; (b) surface image of a poplin fabric with folded yarns; (c) surface image of a canvas fabric with folded yarns.

yarns in the longitudinal direction and expansion in the diametrical direction in a woven fabric in most cases. It can be explained in the following ways.

From the above figures, it is also very clear that the two folds of a yarn become parallel with each other and to the fabric plane at the contact region of the two yarn systems of a woven fabric in most cases. This can be explained by the principle of minimum energy when a system reaches an equilibrium state. Figure 3.8 shows a two-cylinder system with the constraints of walls, in which the equilibrium state must be the (b) state.

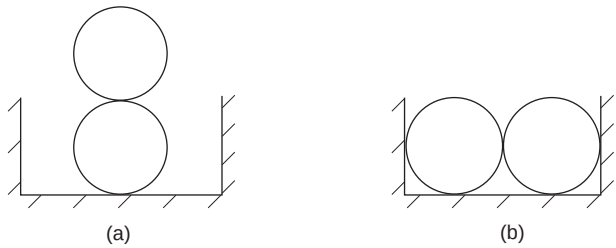

3.8 Equilibrium condition of two cylinder system.

There may be many states between (a) and (b); whatever the state of the two-cylinder system at the beginning, eventually they will reach the (b) state if there is little friction present. In the case of a folded yarn in a woven fabric, which is constrained by the twists and the adjacent yarns, the parallel state of two folds is enforced by the compression force between warp and weft yarns, and this will increase the twist angle of the folded yarn; thus it contracts the folded yarns per centimetre length of fabric, and the measurement in the diametrical direction will increase if the density of yarns remains the same as that before weaving. Therefore more yarns are contained in 1 cm length of fabric when folded yarns are used. We may think it is similar to the increase of yarn twists.

Figure 3.9 shows the dimensional changes of folded yarns in a certain section of a woven fabric: (a) represents the length of folded yarns before weaving, in which γ is the twist angle of the two folds; (b) represents the length of yarns within a fabric with the assumption that no twist redistribution happens, in which case the twist angle and the width of yarns remain the same as before weaving; (c) describes the actual length of a folded yarn due to the twist redistribution, in which the length of the folded yarn becomes shorter and thicker than before weaving because twist angle γ is increased by σ.

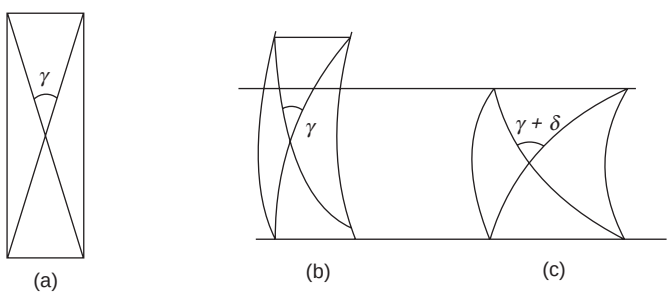

3.9 Dimensional changes of folded yarn in a woven fabric with twist redistribution.

In addition, the twist redistribution might affect the sett of a woven fabric, or make the spacing smaller than designed. But the tested geometrical and mechanical data listed later suggest that while this possibility may exist, it is not very large. In addition, the rule of twist redistribution described above is the general trend; it is not necessarily always exactly true in any segment of yarn because the actual twists may not be exactly matched with the sett even after twist redistribution. This finding, with the other phenomena discussed in other sections, may be useful for understanding the geometrical, mechanical and quality differences between two fabrics, for example two poplin fabrics of which one is made of folded yarns and the other of single yarns, other industrial specifications being similar.

3.4 Relationship between fabric structure and surface properties

3.4.1 Introduction

The properties of a fabric surface are very important in terms of both psychological and physical effects on the human being's appreciation of that fabric. For example, the sensations perceived from the contact of clothing with the skin can greatly influence our overall feeling of comfort. The KES system has a testing machine especially designed for assessing fabric surface properties.

The KES instrument measures the height of a surface of a fabric over a 2 cm length (forwards and backwards) along principal directions. This gives two values for geometrical roughness, *SMD*1 and *SMD*2. The geometrical roughness (*SMD*) is a measure of the surface contour of the fabric, an increase in *SMD* suggests an increase in surface variation of a fabric. Figure 3.10 shows the principles of the measurement process.

Interest in studying the geometry of fabric surfaces by objective means goes back to 1955, when Butler *et al.* (1955) reported the design and implementation of their instrument known as the cloth profile recorder. The main objective of the design was the assessment of fabric faults such as repping and the differences in pick spacing along the warp direction. Since this early work, there has been no reported work that describes the objective measurement of surface roughness until the KES system was introduced by Kawabata (1980). Later in 1985, an instrument was introduced which moves the fabric by means of a turnable in order to measure the heights around a 360° rotation. At the same time, a multi-purpose tester was designed by Amirbayat which, in addition to measuring the drape or bending stiffness of fabrics, measures the surface properties and their variation during wear (Hearle and Amirbayat, 1988, Amirbayat and Cooke, 1989). Having realised that there is a force imposed when testing, which affects the measurement of the

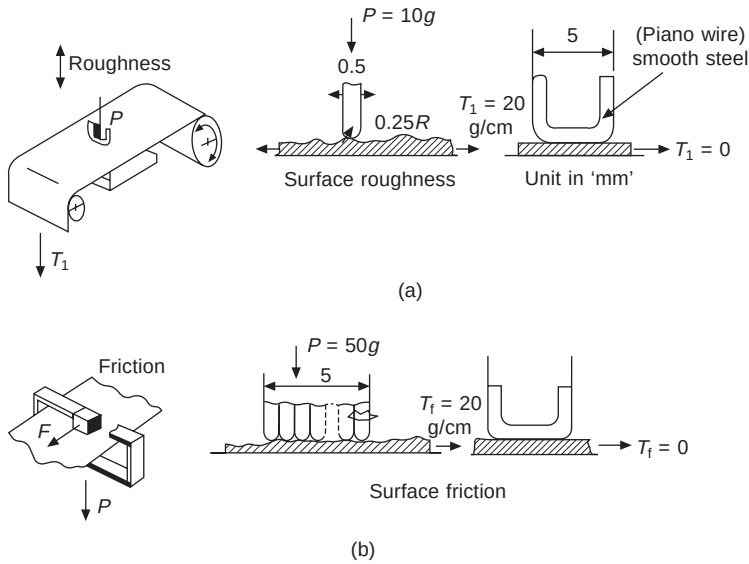

3.10 (a) Principles for the measurement of geometrical roughness *SMD;* (b) principles for the measurement of fabric friction coefficient *MIU.*

roughness in the KES surface tester, Ramgulam reported a non-contact method of surface assessment using laser triangulation techniques in 1990 (Ramgulam *et al.*, 1993).

The friction coefficient (*MIU*) is another property measured by the KES surface tester; it is accompanied by its deviation (*MMD*). Kawabata and Mooroka (Barker *et al*., 1985–1987) separated the coefficient of surface friction into two parts: the first part is associated with the friction between the fabric and the surface of a rigid body. The second component comes from other sources. It is assumed to be related to energy losses caused by inter-fibre friction from compressional deformations occurring when a fabric is subjected to rubbing, denting and crushing. The relative importance of these two terms varies with the type of the surface contact and with the applied load. The deviation of the coefficient of friction (*MMD*) is a measure of slip stick behaviour. The principles involved are shown in Figs 3.10a and b. As the probe sticks and binds on the irregular fabric surface the frictional force changes, giving deviations from the mean friction value.

Except for some qualitative explanations as above, existing research on surface properties is generally concerned with the three parameters related with fabric hand or tailorability (Kawabata, 1980; Barker *et al.*, 1985–1987). To the best of the author's knowledge, there exists little investigation of the charts from the KES surface testing and the quantitative relationship between surface properties and fabric geometry.

An investigation will be presented of the characteristics of the geometrical roughness and friction properties of woven fabrics tested by the KES surface tester together with theoretical explanations for these phenomena. A brief discussion will also be provided about the effects of the warp yarn hardening, indicated in Chapter 4, on the surface properties through the comparison of the warp and the weft direction values. Models for the prediction of geometrical roughness and friction properties of woven fabrics will also be developed.

3.4.2 Characteristics of surface geometrical roughness curves

Figure 3.11 is an example of the charts from the KES surface roughness testing. In this figure, the troughs represent the lowest places on the fabric surface, and the peaks the crowns of the yarns in a fabric. The waves on the chart are not very regular, but it was found that the number of the waves generally equals the sett of fabric in the cross direction. The definition of the geometrical roughness in the KES system is included in equation 3.17 and shown in Fig. 3.12.

$$SMD = \frac{1}{X}\int_0^x |\, T - \bar{T} \,|\, \mathrm{d}x \qquad [3.17]$$

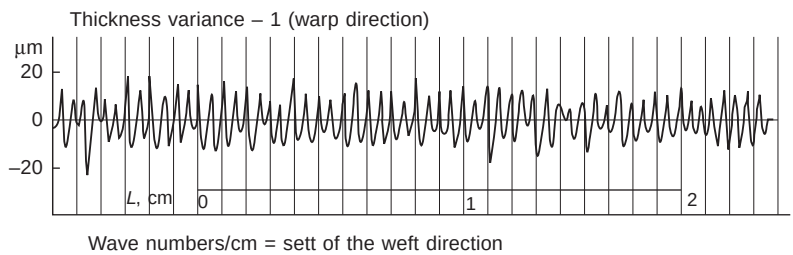

3.11 Surface roughness chart measured by the KES system.

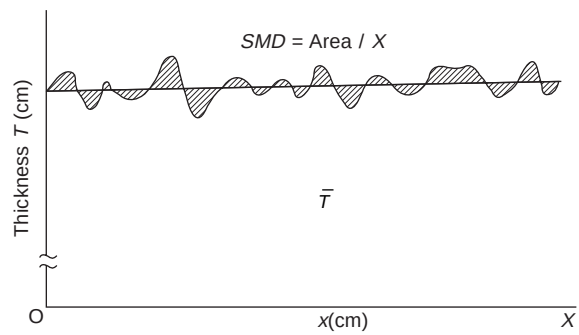

3.12 The definition of geometrical roughness (*SMD*).

3.13 Cross-section image of plain-weave fabric containing two consecutive yarns.

3.4.3 Modelling of fabric geometrical roughness

One of the cross-sectional images of fabric containing two consecutive yarns can be seen from Fig. 3.13. The fabric roughness depends on yarn spacings, irregularity, fabric design and other fabric geometrical factors. If the irregularity of yarns and hairiness are not considered, the geometrical roughness of a woven fabric can be simplified into what is shown in Fig. 3.14, where y is the distance between the lowest places and the highest places on the fabric surface on the tested side. The average thickness of the fabric is located at the centre of y; the geometrical roughness is a measure of the variation of fabric thickness around the central point of y. From the definition of the KES parameter, *SMD*, it is obvious that the roughness measured is the average height of the area constructed by the average line and the zigzag curves.

If the same principle is used, and the simplified regular roughness change is introduced as in Fig. 3.15, the relationship between fabric roughness and geometrical parameters is as in equations 3.18 and 3.19, where the symbols are the same as in Fig. 3.15; R_t is the theoretical roughness. The average height of the isosceles triangle is:

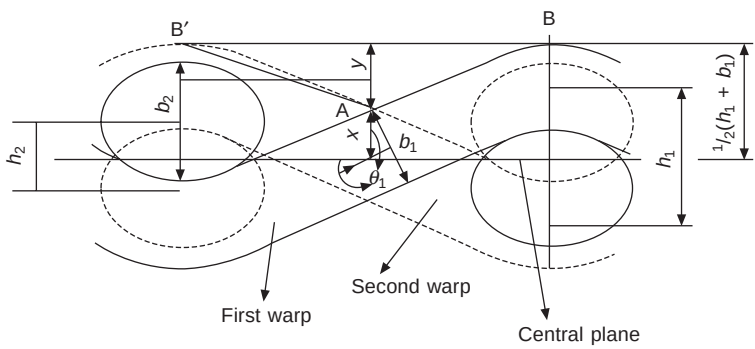

3.14 Geometrical roughness of woven fabrics.

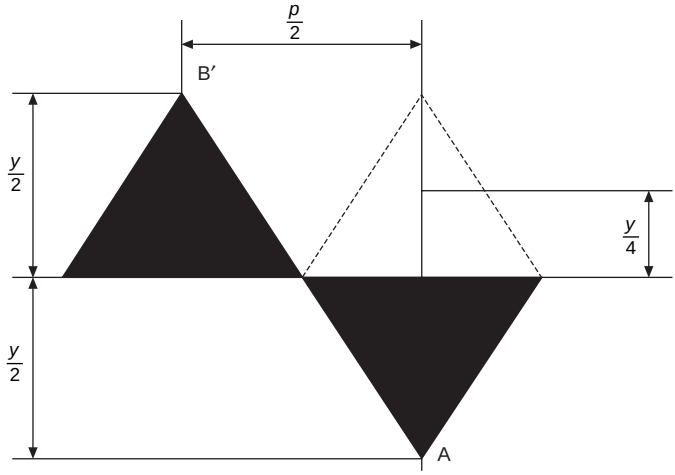

3.15 Simplified geometrical roughness cycle of woven fabrics.

$$\frac{\frac{1}{2}\left(\frac{1}{2}y \cdot \frac{1}{2}p\right)}{\frac{1}{2}p} = \frac{1}{4}y \qquad [3.18]$$

and

$$R_{ti} = \frac{y}{4} = \frac{1}{4}\left(\frac{h_i + b_i}{2} - x\right) = \frac{1}{4}\left(\frac{h_i + b_i}{2} - \frac{b_i}{2\cos\theta}\right) \qquad [3.19]$$

$$= \frac{1}{8}\{h_i + b_i(1 - \cos^{-1}\theta_i)\}$$

where $i = 1$ and 2.

3.4.4 Theoretical and measured fabric geometrical roughness

The data obtained from the KES surface testing is called measured roughness to distinguish it from the theoretical roughness as described in equation 3.19. It is found that the theoretical values are always smaller than the measured values and the difference is quite large in some cases. An explanation for this phenomenon is given as follows:

(1) the simplification of the model is the main reason leading to the smaller calculated values – as can be seen from Figs 3.14 and 3.15, the straight line B′A simply includes a smaller area than the curved line B′A;
(2) lack of knowledge of the hairiness of yarns and the variation of the fabric structure;

(3) difficulty in measuring the geometrical parameters may also be responsible for this difference.

3.4.5 Friction properties of woven fabrics

It is interesting to note that, for many fabrics, their friction property charts are closely related to their roughness charts. It can be clearly seen as shown in Fig. 3.16 that they consist of waves, whose number is equal to the sett of the cross-section. Furthermore, the correlation coefficient for the deviation of friction coefficient (*MMD*) and the measured geometrical roughness (*SMD*) is always high. This may suggest that the geometrical roughness contributes to the measured fabric frictional coefficient. We may make use of Fig. 3.14 again to give a description of this relationship.

In Fig. 3.17, we assume the slip stick of the KES surface tester is at different places at different times. B′, O′, A, O, B are several representative positions. Figure 3.18 is the force analysis which takes the position of O′ as an example to derive the relationship between the fabric friction properties and the positions.

The coefficient of the friction between fabric surface and the slip stick is defined as the ratio of the sliding force to the compressional load. The mathematical definition of the *MMD* is as follows:

$$MMD = \frac{1}{X}\int_0^x |\mu - \bar{\mu}|\,\mathrm{d}X \qquad [3.20]$$

where X is the testing difference and $\bar{\mu}$ the average function coefficient.

The equilibrium conditions in the x and y axes give the following equations:

$$\left.\begin{aligned} f &= F\cos\alpha + P\sin\alpha \\ N &= P\cos\alpha - F\sin\alpha \end{aligned}\right\} \qquad [3.21]$$

and

$$\mu_y = \frac{f}{N} = \frac{F\cos\alpha + P\sin\alpha}{P\cos\alpha - F\sin\alpha} \qquad [3.22]$$

Thus we have

$$\mu_f = \frac{F}{P} = \frac{\mu_y\cos\alpha - \sin\alpha}{\cos\alpha + \mu_y\sin\alpha} = \frac{\mu_y - \mathrm{tg}\alpha}{1 + \mu_y\mathrm{tg}\alpha} \qquad [3.23]$$

where P is a predetermined constant pressure, F the sliding force along the fabric plane, which can be sensed as friction force in the KES surface tester, N reacting perpendicular to the actual fabric surface, μ_y is the friction coefficient of yarns with the solid stick or the fabric friction coefficient when the

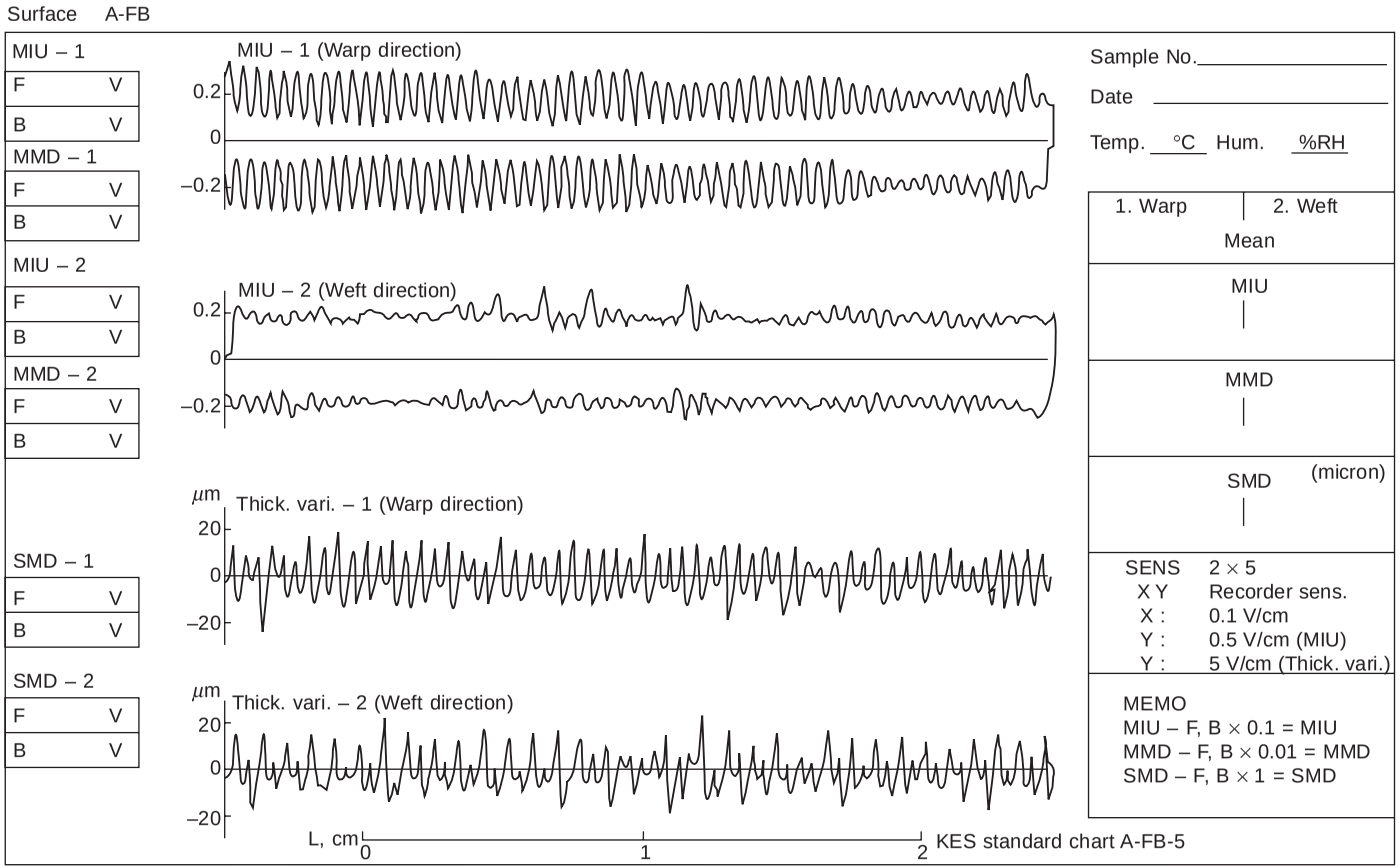

3.16 Comparison of characteristics of friction and surface roughness.

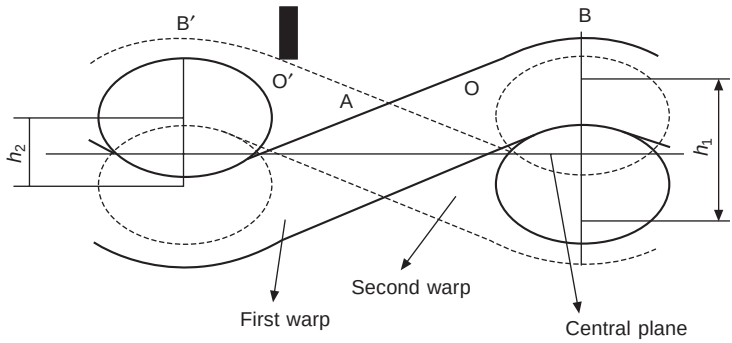

3.17 Positions of friction stick on the fabric surface.

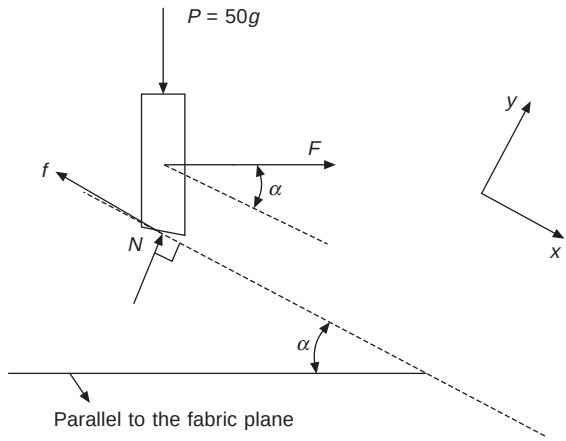

3.18 Force analysis of slip stick.

geometrical roughness is assumed to be zero; and f is the friction force along the actual fabric surface, α the angle of actual fabric surface with the horizontal plane at the position O′ in Fig. 3.17. μ_f is the fabric friction coefficient which is equivalent to MIU measured on the KES system. If $\alpha < 0$, the slip stick is in the AOB section, μ_f increases with the increase of $|\alpha|$; if $\alpha > 0$, the stick in the B′O′A section, μ_f decreases with the increase of α; if $\alpha = 0$, the stick is at the crown of the yarn wave, the friction coefficient is equal to μ_y ($\mu_f = \mu_y$).

Table 3.1 shows an example of the application of equation 3.23. It is assumed that $\mu_y = 0.2$, the maximum value of α is 8°. From this table we can find that the average fabric friction coefficient μ_f is 0.201448, which is equivalent to definition of *MIU* measured on the KES system, the deviation of μ_f is 0.073029, which may be regarded as *MMD*. In addition, Fig. 3.19 indicates that the variation of the friction coefficient is a periodic function. It needs to be noticed that the values of α are very small in this example,

Table 3.1 Predicted friction variation when $\mu_y = 0.2$

Position	α (degree)	α (radian)	μ_f	$\mu_f - \bar{\mu}$
B′	0	0	0.2	0.001448
	1	0.017444	0.181919	0.019529
	2	0.034889	0.163952	0.037496
	3	0.052333	0.146088	0.055360
	4	0.069778	0.128315	0.073133
	5	0.087222	0.110621	0.090827
	6	0.104667	0.092996	0.108452
	7	0.122111	0.075427	0.126021
Both sides of A	8	0.139556	0.057905	0.143543
	–8	–0.139556	0.350310	0.148862
	–7	–0.12211	0.330842	0.129394
	–6	–0.10467	0.311597	0.110149
	–5	–0.08722	0.292561	0.091113
	–4	–0.06978	0.273717	0.072269
	–3	–0.05233	0.255053	0.053605
	–2	–0.03489	0.236554	0.035106
	–1	–0.01744	0.218208	0.016760
B	0	0	0.2	0.001448
Averages			0.201448	0.073029

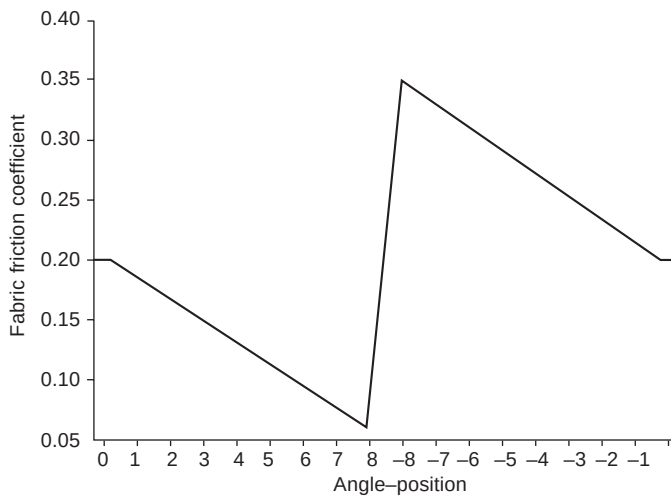

3.19 Predicted friction variation when $\mu_y = 0.2$.

only 8°. If we increase α, the calculated results are usually larger than the measured ones. Meanwhile, if the average value of μ_y is small, say 0.15, the calculated fabric friction variation tends to be larger than the measured one, as shown in Table 3.2. In a word, the calculated *MMD* will be far larger than the measured one when the value of *MIU* is around 0.15 since the usual

values of *MMD* are generally less than 0.02. In addition, if we increase the value of α, the values of μ_f are even less than zero. Of course this will never be reflected in the actual charts. The reasons for this discrepancy may be caused by the fact that the width of the slip stick is larger (0.5 mm) than we assumed (< $1/2p$ = 0.1 mm–0.15 mm), which means that the slip stick need not go through every point as we described in Fig. 3.17.

Table 3.2 Predicted friction variation when $\mu_y = 0.15$

Position	α (degree)	α (radian)	μ_f	$\mu_f - \bar{\mu}$
B′	0	0	0.15	0.001068
	1	0.017444	0.132208	0.018860
	2	0.034889	0.114498	0.036570
	3	0.052333	0.096858	0.054210
	4	0.069778	0.079278	0.071790
	5	0.087222	0.061746	0.089322
	6	0.104667	0.044252	0.106816
	7	0.122111	0.026785	0.124283
Both sides of A	8	0.139556	0.009335	0.141733
	–8	–0.139556	0.296721	0.145653
	–7	–0.12211	0.277836	0.126768
	–6	–0.10467	0.259134	0.108066
	–5	–0.08722	0.240600	0.089532
	–4	–0.06978	0.222221	0.071153
	–3	–0.05233	0.203984	0.052916
	–2	–0.03489	0.185876	0.034808
	–1	–0.01744	0.167886	0.016818
B	0	0	0.15	0.001068
Averages			0.151068	0.071746

3.4.6 Comparison between warp and weft surface properties

The comparison between the warp and weft direction surface properties suggests that the warp values of the measured geometrical roughness are likely to be larger than the weft ones; and the warp values of measured friction coefficient, *MIU*, seem to be smaller than those of the weft ones. This may indicate that the strain hardening of the warp direction affects the surface properties of a woven fabric. It can be explained as follows.

The surface test on the KES system involves a compression load; the work-hardened warp yarns may have higher resistance to compression than the non-hardened weft yarns. Thus, the measured geometrical roughness in the warp direction is likely to be higher than in the weft one. As for the difference in *MIU*, the plastic strain of warp yarns in the longitudinal direction increases the orientation of fibres in a yarn; thus it reduces the denting and crushing effect when friction occurs.

3.5 Relationship between compression behaviour and fabric structure

The low-load compression behaviour of woven fabrics is very important in terms of hand and comfort. It is also useful for fabric handling during garment manufacturing. In addition, it is found that the analysis of the pressure–thickness relationship may shed light on the structure of fabrics, which may be useful for automatic inspection and image analysis of woven fabrics.

3.5.1 Compression behaviour of fibrous assemblies

Before we deal with fabrics, it is necessary to have a look at the compression behaviour of fibrous assemblies. If a loose sample of wool fibres is compressed, the pressure P exerted on the sample is generally inversely proportional to the cube of the volume v of the sample:

$$P = \frac{\lambda}{v^3} \qquad [3.24]$$

where λ is a constant of proportionality (Postle *et al*., 1988).

Research on the mechanics of the compression of fibre assemblies was initiated by Van Wyk (1946) and reviewed by Carnaby (1980). The compression curve of pressure versus specific volume was derived in his review paper, and the exact relationship describing the compression behaviour of the fibrous mass is

$$P = \lambda\left(\frac{1}{v^3} - \frac{1}{v_0^3}\right) \qquad [3.25]$$

where v is the volume of the mass, and v_0 is the value of v when pressure $P = 0$.

In addition to the above relationship for the load–compression of fibrous assemblies, Van Wyk (1946) also suggested a correction to it for assemblies which have been compressed to a volume small enough for the incompressible volume of the fibres to become significant, and for assemblies at zero pressure. The corrected relationship is described in equation 3.26:

$$P = \lambda\left(\frac{1}{(v - v')^3} - \frac{1}{(v_0 - v')^3}\right) \qquad [3.26]$$

where v' represents its limiting volume at large pressure. For very loose structure, v' may be negligible and the equation taken the form of equation 3.25.

For over 50 years, this relationship has been examined both experimentally and theoretically for fibrous masses. Despite its shortcomings, Van Wyk's original model has not been superseded. A number of developments have

been reported, which extend its application to assemblies in which the fibres have particular orientations, and finally to fabrics (De Jong *et al.*, 1986; Postle *et al.*, 1988).

3.5.2 Compression behaviour of woven fabrics

3.5.2.1 Application of Van Wyk's law

The process of applying Van Wyk's law to woven fabrics is actually the modelling of pressure–thickness curves. In equation 3.26, if the value of P represents the pressure on a unit area of a fabric, v is equal to the fabric thickness t. With this fact, Postle *et al*. (1988) applied the relationship defined by equation 3.26 and its simplified form to the fabric pressure–thickness curves as a particular case of the fibrous assembly problem.

They began by using the three-parameter equation 3.26 to fit the compression curves of wool fabrics tested on the KES-F compression tester. The fitted curves were in many cases very close to the measured pressure–thickness curves. The incompressible thickness of the fabrics t' is generally between 0.5 and 0.9 of the fabric thickness t at a pressure of 50 gf/cm^2. They concluded that, in contrast to the application of equation 3.26 to loose wool or silk, the value of t' is not negligible. They also reported that the value of $\lambda(v_0 - v')^3$ in equation 3.26 was small in relation to the maximum pressure $P = 50$ gf/cm^2 employed in the test. By using this finding and neglecting the last term, they employed a simplified equation:

$$P = \frac{\lambda}{(t - t')^3} \qquad [3.27]$$

where the thickness t or volume per unit area of fabric is large and undefined at zero pressure.

Furthermore, by utilising the measured thickness T_m of the fabric at a pressure of 50 gf/cm^2 and the energy WC underneath the pressure–thickness curve between 0.5 and 50 gf/cm^2; it was found that the two parameters in equation 3.27 may be calculated:

$$t' = t_m - \frac{2E}{P}, \quad \lambda = \frac{8E^3}{P^2} \qquad [3.28]$$

It is assumed that the energy E absorbed by the fabric with the pressure between 0 and 50 gf/cm^2 equals WC. Thus, on substitution of the measured values of WC for E, and the thickness at 50 gf/cm^2 for t_m in equation 3.27, the limiting fabric thickness t' and the parameter λ may be determined.

The application of this method to wool fabrics (Postle *et al.*, 1988) showed that the fitted values for λ and t' are in many cases close to the measured KES curves, with some deviation at pressures less than 20 gf/cm^2. In addition, the measured thickness of a range of fabrics at 1000 gf/cm^2 and the thickness

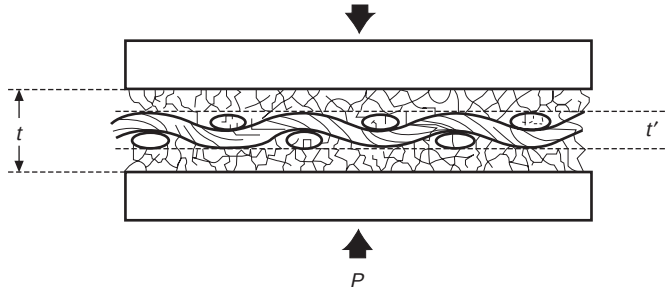

3.20 The proposed model of a woven fabric under lateral compression.

extrapolated from equation 3.24, fitted over the range from 0.5–50 gf/cm^2, correlating well (r = 0.99) with slope 1 and an intercept of 0.

3.5.2.2 Interpretation for fabric structure

de Jong *et al*. (1986) also used equation 3.27 to analyse the mechanics of wool fabric compression in order to interpret the results obtained on wool during finishing. In return, the feedback information could be used for the maintenance of consistent quality in finished fabrics due to the fact that the lateral compression properties of some fabric groups (e.g. wool fabrics) are generally altered by the finishing procedure.

In their analysis, a model, as shown in Fig. 3.20 considers the fabric to consist of three layers: a relatively incompressible core layer in contact with much more compressible surface layers on either side. These two surface layers (the face and back of the fabric) follow Van Wyk's law. As indicated above, the value of λ for these layers is negligibly small. The value of constant t' therefore represents the thickness of the incompressible core of the fabric.

3.5.3 Statement of the problems

Figure 3.21 shows a typical compression curve recorded on the KES system, according to which we may find a close-to-linear relationship between pressure and thickness at the latter part of the curve under a pressure larger than 20 gf/cm^2. This section of curve is also characterised by a very steep slope which indicates that fabrics are extremely incompressible. Thus the general shape of the curve is largely governed by pressure in the range from 0–20 gf/cm^2. The values of t_m and *WC* provided by the KES system are not very reliable for predicting the whole curve because they do not usually match the data read off the curves. Therefore, the universality of the model used by De Jong needs to be proved and its accuracy improved.

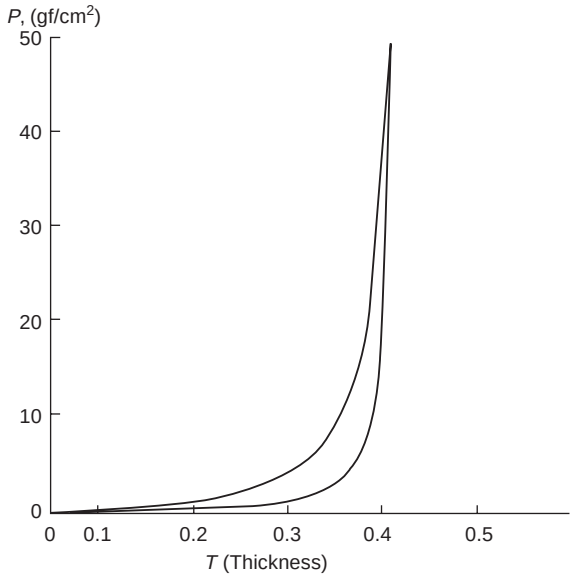

3.21 Typical compression (pressure–thickness) curve of woven fabrics.

In the following section, equation 3.27 will be extended to cotton fabrics. As we all know, wool fabric is very different from cotton fabric in structure. As shown in Fig. 3.12, cotton poplin fabrics have very few protruding fibres on their surface while wool fabrics are apparently very hairy. Therefore, although equation 3.27 can be successfully applied to wool fabrics, its applicability to cotton fabrics still awaits confirmation. The method we used is again non-linear regression. Moreover, an alternative method is also introduced to make equation 3.27 easier to use.

In addition, an analysis of equation 3.27 will be given together with a comparison with the measured geometrical thickness. This analysis reveals a clearer picture of fabric structure in which a five-layer structure is suggested.

3.5.4 Fitting of compression curves for cotton fabrics

Inspired by the success of tensile modelling and the comparison of the two kinds of curves (tensile and compression), an attempt was made to use an exponential function to model the pressure–thickness curves. The proposed function is as follows:

$$P = e^{\alpha t - \beta} - 1 \qquad [3.29]$$

where P is pressure and t thickness; two constants α and β need to be estimated.

However, the results fitted by equation 3.29 were not very successful. Therefore, equation 3.27 used by De Jong *et al.* was adopted. We first used two parameters, obtained on the KES system, namely T_m and WC, to fit the

curves. Similar results to wool fabrics can be observed, i.e. good agreement with measured results when the pressure is larger than 20 gf/cm^2 with deviations under pressure less than 20 gf/cm^2. In other cases, there exist large deviations between the predicted data and the tested results, due to the original deviations of WC and T_m from the data read off the curves or for other unknown reasons.

Therefore, a non-linear regression method was employed to improve the goodness of fit of equation 3.27. Three approaches, namely exponential function, power function with two estimations using T_m and WC, and a power function with non-linear regression, are compared. The representative results are shown in Fig. 3.22 together with a comparison of using WC and

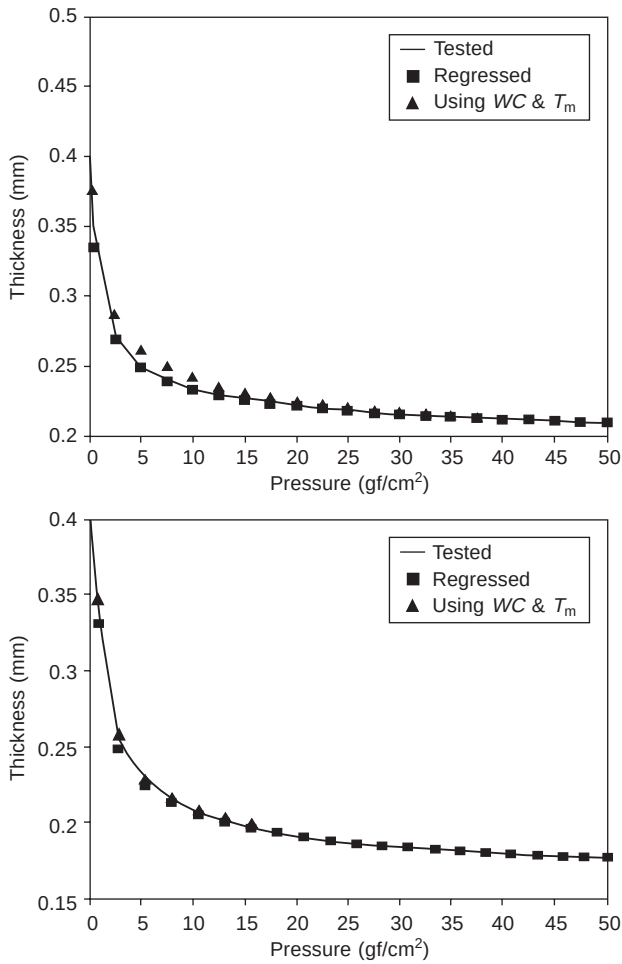

3.22 Comparison of compression curve fitted by non-linear regression method and using WC and T_m.

T_m. Sometimes the results fitted using *WC* and T_m are close to those regressed but, in most cases, the regressed results are much better than those using *WC* and T_m. Figure 3.23 shows two other examples of comparisons of the results using the three methods, in which cases the results using *WC* and T_m are comparatively good. However, even here, it is clear that the regression method is more accurate. The residuals or deviations produced by the non-linear regression method are very small, on average only about 1/4 and 1/5 of those produced by using *WC* and T_m.

From these figures, one can see that the goodness of fit of equation 3.27 to the tested curves may be improved considerably by the non-linear regression

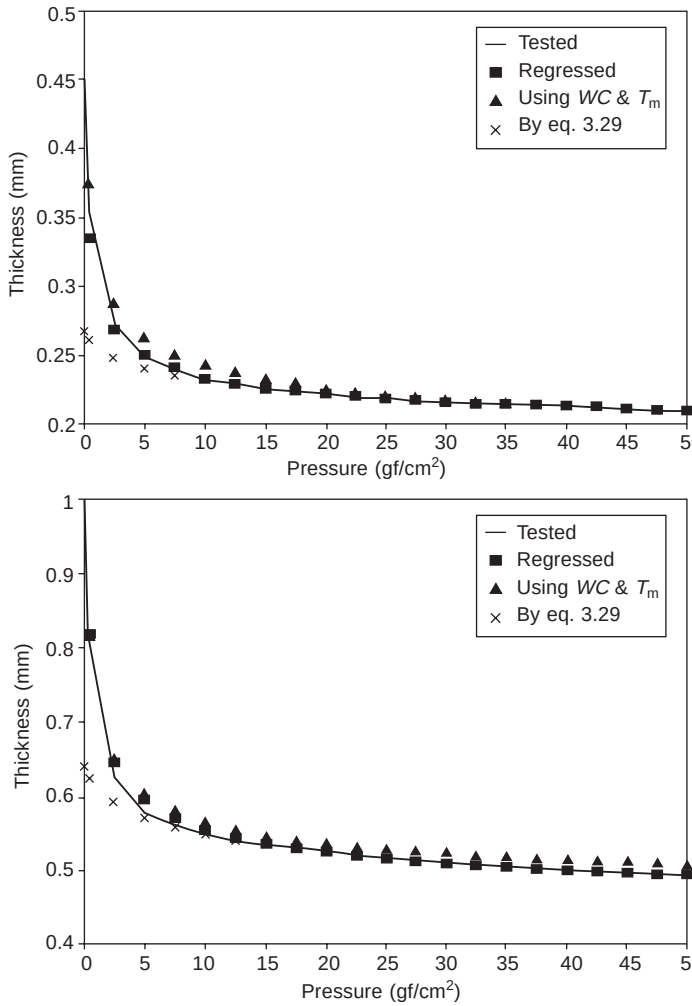

3.23 Comparison of compression curve fitted by three methods.

method. By contrast, the data predicted using WC and T_m demonstrate various degrees of deviation from the tested results.

3.5.5 Mechanical and geometrical thickness

According to equations 3.8 and 3.9 above, the fabric thickness with no external pressure, t, may be calculated from the measured geometrical parameters, namely, crimp height h and minor diameter b of yarn. We call this the geometrical thickness. At the same time, one can obtain the fabric thickness from the KES system T_0, when pressure is at 0.5 gf/cm^2; and the thickness T_m when pressure equals 50 gf/cm^2; these are called mechanical thicknesses. In addition, from equations 3.8 and 3.9, incompressible thickness t' is also introduced. The comparisons of these thicknesses may be very interesting; in fact, they provide a deeper insight into the fabric structure.

Generally, the geometrical thickness of all woven fabrics lies between T_0 and T_m, or T_0 and t'. The geometrical thickness is actually much smaller than T_0. This is beyond expectation because the geometrical thickness was measured principally under zero pressure, but T_0 was measured under a pressure of 0.5 gf/cm^2. Therefore, theoretically, T_0 should be smaller than the geometrical thickness t.

The underlying mechanism for this phenomenon might lie in the fact that during geometrical measurement, crimp height h and minor diameter b were determined by excluding protruding fibres of the yarn surface. Thus the geometrical thickness excludes the hairs on the yarn surface and the crimp crowns above the average thickness. However, the KES compression tester can output everything it can sense, including the hairs and the crimp crowns above the average height of woven fabrics. Therefore, the difference between T_0 and t results from this, and the actual structure of woven fabrics, as shown in Fig. 3.24, is revealed. In it a five-layer structure is still valid but the two outlayers consist of crimp crowns and not only protruding hairs.

In this structure, the furthest outlayers on either side of a fabric contain hairy fibres and crowns above the average geometrical thickness; the secondary

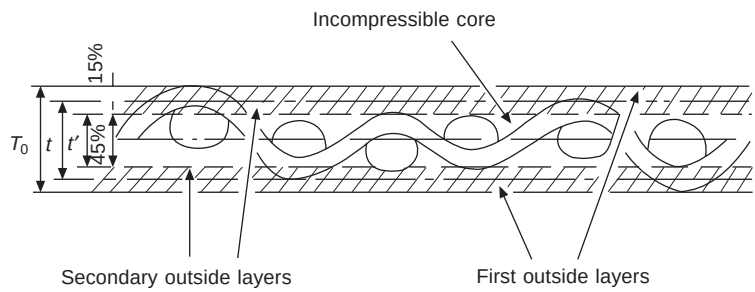

3.24 Five-layer structure of woven fabrics.

layers on either side on a fabric represent another two compressible layers which form the firm structure of the fabric; the t' represents the incompressible core of a fabric. The outlayers and secondary layers of this structure obey Van Wyk's law. The incompressible core layer possesses about 40 % of the whole fabric thickness, which indicates that fabrics are highly incompressible; the two secondary layers have more than 20 %; the first layer about 40 %, which shows that the irregularity of the fabric surface is very large.

3.5.6 Conclusions

Generally speaking, the two-parameter function described by equation 3.27 can quite accurately describe pressure–thickness curves for cotton fabrics provided that the estimation methods are appropriate. It is suggested that the incompressible thickness t' and the parameter λ in equation 3.27 be evaluated or modified by a non-linear regression method. This improves the predictability of the proposed model to a considerable extent. Or, alternatively, in a similar way to what will be described in Chapter 6, they can be evaluated by solving the following two simultaneous equations:

$$\lambda = \sum_{i=1}^{n} \left(\frac{P_i}{(t_i - t')^4} \right) \cdot \sum_{i=1}^{n} \left(\frac{1}{(t_i - t')^7} \right) \qquad [3.30]$$

and

$$\lambda = \sum_{i=1}^{n} \left(\frac{P_i}{(t_i - t')^3} \right) \cdot \sum_{i=1}^{n} \left(\frac{1}{(t_i - t')^6} \right) \qquad [3.31]$$

In addition, the relationship between the mechanical and geometrical thickness is found. Comparison of the fabric geometrical and mechanical thickness not only supports the layers theory of fabrics proposed by De Jong, *et al.* but also allows the derivation of a five-layer fabric structure.

3.6 References

Amirbayat J and Cooke W D (1989), Change in surface properties of fabrics, *Text Res J*, **59**, 469.

Barker R *et al.* (3/1987, 2/1986, 5/1985), *Reports to North Carolina State University*, Raleigh, North Carolina 27695-8301, Kawabata Consortium, School of Textiles, North Carolina State University.

Butler K J, Cowhig W T and Michie N A (1955), *Skinner's Silk and Rayon Rec*, **29**, 732.

Carnaby G (1980), The compression of fibrous assemblies, with applications to yarns and cables, in *Mechanics of Flexible Fibre Assemblies*, Hearle J W S, Thwaites J J and Amirbayat J (eds), Sijthoff and Noordhoff, 99.

De Jong S, Snath J W and Michie N A (1986), A mechanical model for the lateral compression of woven fabrics, *Text Res J*, **57**, 759.

Hamilton (1964), A general system of woven fabric geometry, *J Text Inst*, T79.

Hearle J W S and Amirbayat J (1988), The design of a multipurpose fabric tester, *J Text Inst*, **79**, 588.

Hearle J W S and Shanahan J W (1978), An energy method for calculations in fabric mechanics, part I: principles of the method, *J Text Inst*, **69**, 81–89.

Hu J L (1994), *The Structure and Low-stress Mechanics of Woven Fabrics* (PhD thesis, University of Manchester Institute of Science and Technology.

Hu J L and Newton A (1993), Modelling of tensile stress–strain curves of woven fabrics, *J China Text Univ.*, **10**(4), 49–61.

Kawabata S (1980), Examination of effect of basic mechanical properties of fabric hand, in *Mechanics of Flexible Fibre Assemblies* (*NATO Advanced Study Institute Sciences; E, Applied Sciences No. 38*), Hearle, J W S, Thwaites J J and Amirbayat J (eds), Alpen aan den Rijn, The Netherlands, Sijthoff and Noordhoff, 405.

Kemp A (1958), An extension of Peirce's cloth geometry to the treatment of nonlinear threads, *J Text Inst*, **49**, T44–48.

Newton A and Hu J (1992), The geometry of cloth structure, *Proc Inaugural Conference of the Chinese Students and Scholars Textile Association in UK*, Manchester 23.

Peirce F T (1937), The geometry of cloth structure, *J Text Inst*, **28**, P45–96.

Postle R, Carnaby G A, and de Jong S (1988), Surface of woven fabrics, in *The Mechanics of Wool Structures*, Poster R, Carnaby G A and de Jang S (Eds), Chichester, Ellis Horwood Ltd, 387.

Ramgulam R B, Amirbayat J and Porat I (1993), Measurement of fabric roughness by a non-contact method, *J Text Inst*, **84**, 99.

Van Wyk C M (1946), Note on the compressibility of wool, *J Text Inst*, **37**, T285.

4

The tensile properties of woven fabrics

4.1 General tensile behaviour of woven fabrics

4.1.1 Introduction

Tensile properties are one of the most important characteristics governing fabric performance in use. Their study involves many difficulties due to the great degree of bulkiness in fabric structure and the strain variation during deformation. In particular, each piece of fabric consists of a large quantity of constituent fibres and yarns and hence any slight deformation of the fabric will give rise subsequently to a chain of complex movements of these. This makes the situation more complicated since both fibres and yarns behave in a non-Hookean way during deformation and present hysteresis with time effect (Konopasek, 1970).

4.1.2 Tensile stress–strain curve of woven fabrics

Figure 4.1 illustrates a typical tensile stress–strain curve of a woven fabric derived on the KES-F apparatus. For this curve, the initial region demonstrates

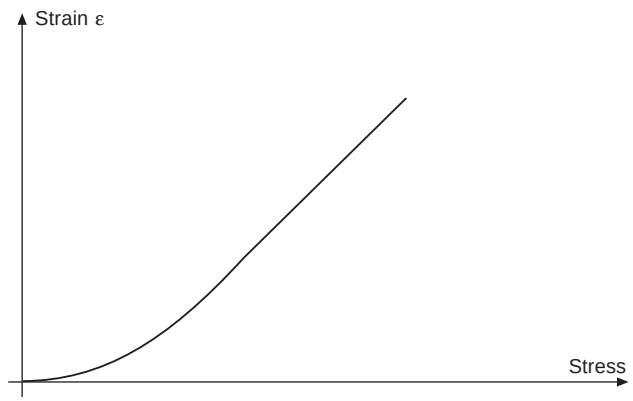

4.1 Tensile stress–strain curves.

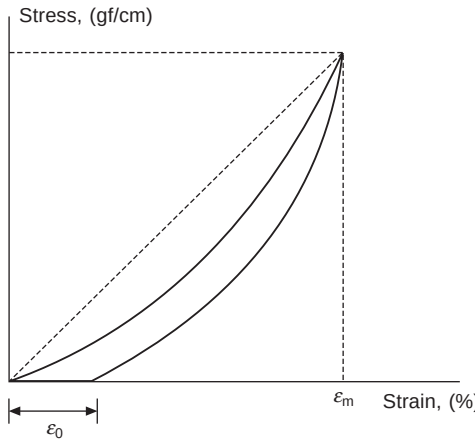

4.2 Loading and unloading cycle in the tensile stress–strain curve.

a low slope due to decrimping and crimp-interchange. After that, the slope of the stress–strain curve rises steeply until its summit is reached, an effect which can be assumed to stem from the induced fibre extension. In addition, the magnitude of the summit of the stress–strain curve is governed by the level of yarn crimp and the relative ease of distortion of the yarn *per se*.

If what the fabric undergoes is a cyclic loading process, i.e. the fabric was first stretched from zero stress to a maximum and then the stress was fully released, then an unloading process will follow the loading process. As a result, a residual strain, ε_0, will be observed since textile materials are viscoelastic in nature. Due to the existence of residual strain, the recovery curve will never return to the origin, as shown in Fig. 4.2. This is the hysteresis effect, which denotes the energy lost during the loading and unloading cycle. Due to the existence of hysteresis, a deformed fabric cannot resume its original geometrical state. In Fig. 4.2, the shift to the right from the origin of the unloading curve depicts the magnitude of the hysteresis effect and indicates the amount of permanent set resulting from the loading history.

4.1.3 Extension in the principal directions

Usually, when a plain woven fabric is extended in either of the principal directions, a straightening of the crimped yarns will also occur in the direction of force. The interaction between the two sets of yarns must therefore be considered. A drop in the yarn amplitude and the weave angle will thus be found when the contact of two sets of yarns in the warp and weft directions grows. During tensioning, these yarns appear to become less flattened due to their consolidation into a rounder or more circular cross-section (Hearle *et al*., 1969). In addition, the crimp-interchange will take place at the crossover point, i.e. one set of yarns increases in crimp level, while the other decreases.

When the fabric is further extended by an applied force, yarn and fibre extensions will occur, but the yarn extension only accounts for a small portion of the total extension as compared with the effect of decrimping. Individual fibre movement within the yarns also occurs at the contact point of two sets of yarns. This movement allows the fibre to avoid the high strains that might be induced by extension. Energy loss will also take place during tensioning due to the restriction of fibre movement posed by inter-fibre strains.

Regarding the uniaxial tensile properties of plain woven fabrics, De Jong and Postle (1977a,b) stated that there are six independent dimensionless parameters to be considered in the case of a balanced woven fabric (produced from identical warp and weft yarns). The six parameters include: (a) the ratio of warp to weft yarn length per crossing yarn; (b) the ratio of yarn diameter to yarn modular length; (c) the ratio of yarn compression rigidity to bending rigidity; (d) the yarn compression index; (e) the ratio of yarn extension rigidity to bending rigidity; and (f) the degree of set. They also stated that the effect of the ratio of yarn compression rigidity to bending rigidity on the relative fabric extension can be accounted for by the yarn extension. Thus, a large part of the fabric extension can be explained by yarn extension when this ratio is lower. In addition, the average of Poisson's ratios can be explained in the selected range where the inter-yarn distance can increase to allow the yarns to turn into a rounder or more circular cross-section during tensioning.

4.1.4 Extension in bias directions

When a plain woven fabric is extended to its final state in bias direction, it can be seen from Fig. 4.3 that the warp yarn will rotate which brings the maximum elongation close to the direction of force (F). There is a deviation

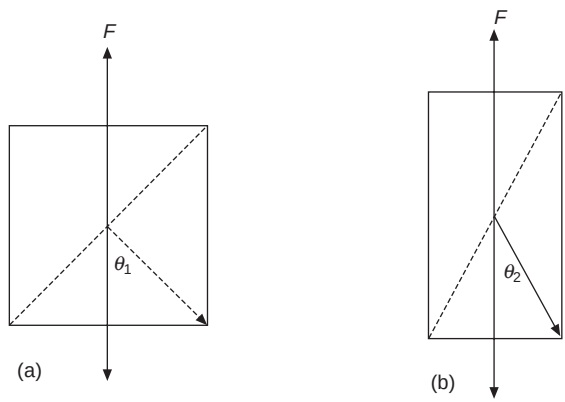

4.3 Fabric extension in bias directions (arrow within square indicating the warp direction): (a) initial position before extension; (b) final position after extension.

in the direction ($\theta_1 > \theta_2$) at the final position. If a force is applied, the fabric will suffer a strain to reach its final position. The magnitude of the strain is governed by the deviation of the angle to the warp direction, and the diagonal direction (± 45°) presents the maximum changes in length. As a result, the maximum elongation will occur at one diagonal and the other diagonal direction demonstrates the maximum contraction. Thus the characteristics of the Poisson effect should be identified by the changes in length parallel and perpendicular to the direction of force.

If stress is applied at an angle to the warp or weft direction, the mode of deformation will become rather complicated, presented as a combination of extension and shear. If the unit cell of the plain woven fabric is regarded as a trellis, it will be extended by rotating the numbers of the trellis relative to each other in bias directions (Weissenberg, 1949).

During KES-F tensile and shear testing, if a fabric is prepared in bias directions, for some yarns, only one or neither of their ends will be clamped. As a result, three cases need to be considered in this event:

(1) both ends of the yarns are held between two clamps for the extension of the warp or weft direction;
(2) only one end of the yarns is held for the extension from ± 15° to ± 75° (bias directions) to the warp direction;
(3) both ends of yarns are free for the extension of 0° or 90° to the warp direction corresponding to the warp or weft direction.

When deformation takes place in bias directions, little tension will exist in the yarns. However, due the existence of the frictional restraint between the interlaced yarns at their contact points, there is still some tension in the yarns between two neighbouring crossovers and a bending couple in deforming the crossed yarns (Spivak and Treloar, 1968). In addition, shear properties will lead to an increase in the tension of individual yarns between the contact points.

Due to the above reasons, a higher magnitude of tensile properties will be recorded in the bias directions than in the warp and weft directions. As higher crimp is usually obtained in the warp yarns, the values of tensile properties in the warp direction are comparatively higher than those in the weft direction. All these observations are discussed with reference to the experimental findings in the following sections.

4.2 Modelling of tensile behaviour of woven fabrics

4.2.1 Introduction

The pioneer in the investigation of tensile deformation of woven fabrics is Peirce (1937). His model assumed that the cross-section of the yarns in the

fabrics is circular, but this assumption of circular yarn cross-section in the fabric is highly theoretical. Therefore, many researchers modified his geometrical model to analyse tensile behaviour. Based on Peirce's rigid thread model (1937), Grosberg and Kedia (1966) analysed the small strain within the initial load–extension curve. Three approaches are reported by Leaf (1980) in order to analyse the tensile behaviour of plain woven fabrics. His first approach is based on Gastigliano's theorem for small deformation only. A force equilibrium method and an energy approach are used for the analysis of large deformation.

In an attempt to define theoretically the planar stress–strain relationships of woven fabric, Weissenberg (1949) introduced the trellis model. He treated the yarns as rods which are inextensible and inflexible. The yarns are pinpointed at their nodal points with lines of zero elongation in the pattern by offering no resistance to the allowed changes in the orientation of the lines. With these assumptions, the theory of strain, stress and the relationship between them is clearly defined. He also stated that the Poisson effect and evading action are observed when external forces are applied. Textile material in its nature and applied state is anisotropic, and the orientation of the framework of the trellis to the direction of the pull would vary with the direction of pull in the material. The Poisson's ratio could be found from a given lengthwise extension and a given widthwise contraction. He indicated that the experiments made on the model would predict a modified Poisson effect with maximum elongations and contractions occurring not parallel and perpendicular to the direction of the pull but along the bisectrices. In addition, there would be a rotation of the directions of maximum elongation and contraction, which would bring, in the terminal position, the direction of maximum elongation nearer to that of the pull. He described the material as taking an 'evading action' by rotating round and having its maximum extension in a direction different from that of the pull.

Chadwick *et al.* (1949) investigated the bias deformation of a woven fabric with the application of the trellis model under a simple pull. They showed that the warp and weft yarns underwent changes not only in length and spacing under bias extension, but also in their orientation to one another and to the direction of pull. In their experimental work, rectangular specimens are cut out in various directions. Each specimen is subjected to a series of simple pulls of increasing amount in a direction lengthwise to the rectangle. In the experiments, the behaviour of the model showed directly the various characteristics of the strains from the initial to the terminal position. They found good agreement between the mode of deformation of the trellis model and the fabrics in bias directions.

Cooper (1963) investigated the relationship between bias extension and bias shear. Kilby (1963) examined the planar stress–strain relationships of a simple trellis which is different from that discussed by Weissenberg (1949).

He suggested that a fabric might be regarded as being equivalent to an anisotropic lamina which shows the Poisson effect and has two planes of symmetry at right angles to one another. Kilby was the first to derive the fabric tensile modulus in any direction other than the warp and weft directions. He indicated that the bias extension involved the shear modulus.

Later, an analysis of the geometrically similar tests of bias extension and simple shear for plain woven fabrics was carried out by Spivak and Treloar (1968). They showed that the bias extension test involved a reduction in area and hence did not correspond to pure shear; on the contrary, simple shear had a constant-area deformation. They concluded that it is impossible to predict the complete stress–strain properties of a fabric in simple shear from measurements of bias extension.

De Jong and Postle applied an energy analysis to the woven fabric structure to investigate deformation (De Jong and Postle, 1977a,b). The independence of the fabric construction is advantageous in using energy analysis of fabric behaviour. They observed that there are some difficulties encountered when applying a generalised force analysis to fabric structure. Thus, when using force analysis, it is found necessary to divide the unit cell of the structure into segments, at the ends of which forces and/or couples might act. The length of each segment had to be varied because the point of action of the internal forces is not fixed. In their study, the fabric load–extension curves and yarn-decrimping curves for the plain-weave construction are computed for a realistic range of input parameters. They tested the tensile properties of plain woven fabrics in both the grey and the finished state, and the computed results are employed to explain the behaviour of yarns during fabric extension.

Skelton (1971) compared the mechanical properties of triaxial and orthogonal fabrics. He found that the tensile strength of the triaxial fabric is dependent upon the amount of shear distortion sustained by the fabric at rupture, but it seemed probable that the variation of strength with direction would be less than the variation found in orthogonal fabrics. More recently, Anandjiwala and Leaf (1991a,b) studied large-scale tensile deformation of plain woven fabrics. Their investigation used the approximation of non-linear yarn bending behaviour for both the undeformed fabric state and the stress analysis. They found that the agreement between experiment and theory is sometimes reasonable, but it is better during extension than during recovery.

Anandijawala and Leaf mainly concentrated on the tensile and shear modulus of plain woven fabrics. No numerical models are found to predict the anisotropy of fabric tensile properties, such as tensile work (*WT*), tensile elongation (*EMT*), tensile linearity (*LT*) and tensile resilience (*RT*), measured using Kawabata's system (KES-F).

The majority of previous research into the tensile behaviour of woven fabrics concentrated on predictive modelling, which always involved very complicated mathematical relations between stresses and strains (Grosberg

and Kedia, 1966; Shanahan *et al*., 1978; Anandjiwala and Leaf, 1991a,b). In addition, the predictability of these models is not always satisfactory.

In particular, Kawabata and Bassett used numerical modelling methods for fitting the tested tensile curves. Kawabata *et al*. reported a linearisation method to model the biaxial tensile stress–strain relation of fabrics, and verified its validity in a paper by Kageyama *et al*. (1988).

In Bassett's Ph.D thesis (1988), the determination of constitutive laws of fabrics and the use of these properties in calculating stress–strain in fabric in garment-like systems were studied. For this purpose, the least squares method was used to fit multivariate polynomial curves to experimental data from woven worsted fabrics.

From the work of both Kawabata and Bassett it is clear that very complicated procedures were still involved for obtaining the constants and strain transformation. Thus, to date, there exists no practical explicit function between stress and strain for tensile deformation of woven fabrics. Therefore, better models for tensile stress–strain relations are needed in terms of both accuracy and practicality.

What is presented here is an attempt to establish an equation for the tensile stress–strain relationship for woven fabrics. An exponential function with two parameters was selected to describe tensile stress–strain curves. A non-linear regression technique was first used to estimate the unknown parameters in the proposed function. Using the proposed function, the predicted results of tensile stress–strain relationships show excellent agreement with experimental data. In addition, several methods which may be used to estimate the unknown parameters in the proposed function are suggested.

4.2.2 Modelling of tensile loading curves

To obtain a satisfactory model for the tensile stress–strain relationship of a fabric, some principles must be followed:

(1) The proposed function should belong to the correct function group, for example exponential or power function.
(2) It should have a format which is easy to compute or interpret. Usually a function with more than four parameters can rarely be evaluated satisfactorily using the non-linear regression method.
(3) It should satisfy the initial conditions of a physical process, e.g. when force equals zero, strain equals zero.
(4) Hopefully, the parameters in the selected function will be related, especially to the yarn physical properties and fabric structure for the intended purpose.

An exponential function with two parameters is chosen to depict the tensile curve of a woven fabric:

$$f = \frac{e^{\alpha\varepsilon} - 1}{\beta} + e_r \qquad [4.1]$$

where f is stress and ε strain, α and β are unknown parameters, e_r the error term.

The SPSS non-linear regression programme can be used to fit the tested tensile curve with the proposed model, in which f and ε can be read off tensile stress–strain curves tested on the KES system while α and β are unknowns to be estimated.

4.2.3 Estimates of the two constants

The two unknown parameters in the chosen function can be estimated in a non-linear regression technique using data read off the tested curves of woven fabrics on the KES tensile tester. The determined values are very useful for the estimation of initial values. Another three methods of estimating the two parameters follow.

4.2.3.1 Estimation of α and β using WT and EMT

From tensile testing of a fabric on the KES tensile tester, there are two parameters extracted from the chart which are *WT* – work done during tension – and *EMT* – strain when stress is equal to 500 gf/cm. We can use these to construct two equations which can be solved for α and β:

$$500 = \frac{e^{\alpha \cdot EMT} - 1}{\beta} \qquad [4.2]$$

and

$$WT = \frac{1}{100}\int_0^{EMT} f\,d\varepsilon = \frac{e^{\alpha \cdot EMT} - 1 - \alpha \cdot EMT}{100\alpha\beta} \qquad [4.3]$$

4.2.3.2 Estimation of α and β taking two points

If the error term in equation (4.1) is ignored and two sets of test data can be obtained, say (ε_1, f_1) and (ε_2, f_2), the following simultaneous system of equations can be solved for α and β:

$$f_1 = \frac{e^{\alpha\varepsilon_1} - 1}{\beta} \qquad [4.4]$$

and

$$f_2 = \frac{e^{\alpha\varepsilon_2} - 1}{\beta} \qquad [4.5]$$

4.2.3.3 *Estimation of α and β by the least squares method (more points method)*

Another method for the estimation of α and β is the more points method. This is in fact the least squares as in linear regression. Suppose we have n sets of data from a tensile curve of a fabric (ε_1, f_1), (ε_2, f_2), . . . (ε_n, f_n), then we can write

$$f_i = \frac{e^{\alpha\varepsilon_i} - 1}{\beta} + e_{ri} \qquad [4.6]$$

so that the sum of squares of deviation from the true line is

$$s = \sum_{i=1}^{n} e_{ri} = \sum_{i=1}^{n}\left(f_i - \frac{e^{\alpha\varepsilon_i} - 1}{\beta} \right)^2 \qquad [4.7]$$

We can differentiate the above equation first with respect to α and then β, setting the results equal to zero, and hence we get two normal equations:

$$\frac{\partial S}{\partial \alpha} = \frac{2\alpha}{\beta} \sum_{i=1}^{n}\left(f_i - \frac{e^{\alpha\varepsilon_i} - 1}{\beta} \right) e^{\alpha\varepsilon_i} = 0 \qquad [4.8]$$

and

$$\frac{\partial S}{\partial \beta} = \frac{2}{\beta^2} \sum_{i=1}^{n}\left(f_i - \frac{e^{\alpha\varepsilon_i} - 1}{\beta} \right) (e^{\alpha\varepsilon_i} - 1) = 0 \qquad [4.9]$$

The solution of α and β can thus be given by:

$$\alpha = \frac{\sum_{i=1}^{n} (e^{\alpha\varepsilon_i} - 1)^2}{\sum_{i=1}^{n} (f_i (e^{\alpha\varepsilon_i} - 1))} \qquad [4.10]$$

and

$$\beta = \frac{\sum_{i=1}^{n} (e^{\alpha\varepsilon_i} (e^{\alpha\varepsilon_i} - 1))^2}{\sum_{i=1}^{n} (f_i \cdot e^{\alpha\varepsilon_i})} \qquad [4.11]$$

If $n = 2$, the results are equal to the two equations used in the two-point method. Theoretically, more data would provide more accurate estimates. However, this is not always true because it may cause a big residual due to the difficulty of reading data off a curve, in which case more data can result in a more biased subjective measurement. Therefore, n is not necessarily very big. It is found that $n = 13$ is big enough for good results; $n = 4$ or 5 may

result in accurate estimates of parameters. When n is not very big, say 5, it can be calculated on a package like TK Solver as long as initial guesses are not far beyond the expected results.

4.2.4 Interpretation of the selected function

4.2.4.1 Young's modulus

A particularly important part of the stress–strain curve is the initial portion; starting at zero stress in most cases it could be seen that the first portion of the curve is fairly straight, indicating a linear relationship between the stress and the strain. The tangent of the angle between the initial part of the curve and the horizontal axis is the stress/strain ratio, which is termed initial Young's modulus E_0. It describes the initial resistance to extension of a textile material. From equation 4.1, the derivative of f with respect to ε yields the modulus curve of tensile deformation:

$$E = \frac{\mathrm{d}f}{\mathrm{d}\varepsilon} = \frac{\alpha}{\beta}\,\mathrm{e}^{\alpha\varepsilon} \qquad [4.12]$$

when $\varepsilon = 0$, $E = E_0 = \alpha/\beta$. Thus α/β is the initial Young's modulus. The above equation can be written as follows:

$$E = E_0 \cdot \mathrm{e}^{\alpha\varepsilon} \qquad [4.13]$$

Because the tangent of the angle between the initial part of the curve and the horizontal axis is the stress/strain ratio, E carries a unit of gf/cm in the case of the KES system. Again from equation 4.1, β carries a unit of cm/gf while α is a dimensionless quantity. We can use the Maclaurin expansion formula:

$$f(\varepsilon) = \frac{1}{\beta}\left(\frac{\alpha\varepsilon}{1!} + \frac{\alpha^2 X^2}{2!} + \ldots + \frac{\alpha^n X^n}{n!} + R_n(\varepsilon)\right) \qquad [4.14]$$

where $R_n\varepsilon$ is the remainder.

If ε is infinitesimal,

$$f(\varepsilon) = \frac{\alpha}{\beta}\varepsilon \qquad [4.15]$$

which is a straight line with residual of

$$R_1(\varepsilon) = \alpha^2 \mathrm{e}^{\alpha\theta\varepsilon}(1-\theta)\varepsilon^2 \quad (0 < \theta < 1) \qquad [4.16]$$

This indicates that the initial portion of the stress–strain curve starting at zero stress is close to a linear line. Besides, if we further differentiate E with respect to ε, the following equation can be obtained:

$$\frac{\mathrm{d}E}{\mathrm{d}\varepsilon} = \alpha E \quad \text{or} \quad \frac{\mathrm{d}E}{E} = \alpha\mathrm{d}\varepsilon \qquad [4.17]$$

From this equation, it appears that α is a reinforcing factor for the increase of Young's modulus E. This relation is frequently found in many physical phenomena.

The initial region of very low slope for the fabric tensile stress–strain curves represents the region of decrimping and crimp-interchange in woven fabrics for which only very small fibre stresses are developed within the fabric when the weave crimp has been fully extended. This means that further extension of the fabric is possible by extension of fibres with the interlaced yarns.

4.2.4.2 Relationship of α with crimp

According to equation 4.1, it may be assumed that there exist two different groups of factors which affect the stress–strain relation. One group affects α while the other influences β.

First it was hypothesised that the larger the yarn crimp the higher the value of β since larger β denotes larger stress induced for a given strain. The analysis, however, reveals that parameter α is correlated with crimp reversely and β has no obvious relation with crimp c. In fact, it is found that an obvious linear relationship exists between α and crimp c. This linear relationship between α and c agrees with the existing recognition that the larger the crimp, the more extensible a fabric. Moreover, this relationship is also consistent with the above interpretation of the selected function, in which α is a dimensionless factor.

In addition, it is also demonstrated that the tangents of stress–strain curves differ with the direction even for the same woven fabric. This fact indicates that there exists an anisotropy for the tensile properties of woven fabrics, as reported in the next section. Another focus of this chapter, the strain hardening effect, can also provide a strong explanation.

4.3 Anisotropy of woven fabric tensile properties

4.3.1 Introduction

One of the difficulties in analysing the tensile behaviour of woven fabrics lies in the fact that any extension occurring at an angle to the warp or weft direction usually involves a different mechanism of deformation. For example, in the 45° direction to the warp and weft, the modulus is almost completely determined by the shear behaviour of the fabric, while if it is extended in the warp or weft direction, the shear behaviour has no part to play (Hearle *et al*., 1969). Therefore, the tensile performance of a fabric is apparently an integration of a multi-directional effect. We term this phenomenon the 'anisotropy' of tensile properties of woven fabrics and it becomes the subject of the following

section. This topic is very meaningful in that little literature about the anisotropy phenomenon can be found despite the fact that there is already a sea of publications dealing with fabric tensile properties; but most of these have concentrated on what happens to the warp and weft directions.

As the term indicates, the word 'anisotropy' means that there is great variation in fabric tensile properties with changes in direction. Firstly, this is because a woven fabric is highly anisotropic in nature. Secondly, most fabric structures are asymmetrical, like twill and satin woven fabrics, and thus the force needed to stretch fabrics in different directions will vary a lot from one to another. This is basically a reflection of the different underlying deformation mechanism. For example, when a woven fabric is under bias extension, shear deformation will occur and thus shear property comes into play to influence the tensile behaviour of a fabric. In this case, the tensile behaviour of a fabric will apparently differ from what occurs when the extension happens merely in two principal directions (Hearle and Amirbayat, 1986a,b).

The work covers all the four parameters measured on Kawabata's system (KES-F): tensile work (*WT*), tensile elongation (*EMT*), tensile linearity (*LT*) and tensile resilience (*RT*) based on Kilby's Young's Modulus model (1963).

4.3.2 Modelling the anisotropy of tensile properties

4.3.2.1 Tensile work (WT)

Kilby (1963) firstly introduced the Young's modulus in any direction other than warp and weft as follows:

$$\frac{1}{E_\theta} = \frac{\cos^4\theta}{E_1} + \left[\frac{1}{G} - \frac{2\sigma_{pt}}{E}\right]\sin^2\theta\cos^2\theta + \frac{\sin^4\theta}{E_2} \qquad [4.18]$$

where E_1, E_2 and E_θ are the Young's moduli to the warp, weft and θ directions respectively, G denotes the shear modulus, and σ_{pt} indicates the Poisson's ratio relating the contraction in the weft direction to the strain in the warp direction. In order to simplify the calculation, he rearranged the above equation into:

$$\frac{1}{E_\theta} = \frac{\cos^4\theta}{E_1} + \left[\frac{3}{E_{45}} - \frac{1}{E_1} - \frac{1}{E_2}\right]\cos^2\theta\sin^2\theta + \frac{\sin^4\theta}{E_2}$$

or

$$\frac{1}{E_\theta} = \frac{\cos^4\theta}{E_1} + \frac{\cos^2\theta\sin^2\theta}{G'} + \frac{\sin^4\theta}{E_2} \qquad [4.19]$$

where

$$\frac{1}{G'} = \frac{4}{E_{45}} - \frac{1}{E_1} - \frac{1}{E_2}$$

Equation (4.19) is very useful for predicting the full form of the polar diagram of modulus against angle, when values of the parameters in only warp, weft and θ directions are known. Rearranging equation 4.1, the following relation is obtained:

$$\varepsilon = \frac{\ln(\beta F + 1)}{\alpha} \quad \Rightarrow \quad E = \frac{\mathrm{d}F}{\mathrm{d}\varepsilon} = \frac{\alpha}{\beta} \mathrm{e}^{\alpha\varepsilon} \qquad [4.20]$$

The tensile work, *WT*, is thus

$$WT = \int_0^{\varepsilon_m} F(\varepsilon)\, \mathrm{d}\varepsilon \qquad [4.21]$$

where ε_m is the strain at the upper-limit load F_m = 500 gf/cm, and *F* denotes the tensile load, a function of strain. Combining equations (4.20) and (4.21), we have

$$WT = \frac{E}{\alpha^2} - \left[\frac{\ln(\beta F_m + 1) + 1}{\alpha\beta}\right] \qquad [4.22]$$

F_m is a constant (= 500 gf/cm) which is directly obtained from the stress–strain curve on the KES-F apparatus. α and β are variables and will have different values in different directions. To simplify the procedure, the term $[\ln(\beta F + 1) + 1]/\alpha\beta$ is set to be *K*. Then *WT* may be written, and if *E* varies with angle θ, *WT* will also vary with θ and the above equation becomes

$$WT = \frac{E}{\alpha^2} - K \quad \Rightarrow \quad E_\theta = (WT_\theta + K)\alpha^2 \qquad [4.23]$$

Putting $E_\theta = (WT_\theta + K)\alpha^2$ into equation (4.19) gives

$$\frac{1}{\alpha^2(WT_\theta + K)} = \frac{\cos^4\theta}{\alpha^2(WT_1 + K)} + \frac{\cos^2\theta \sin^2\theta}{G'} + \frac{\sin^4\theta}{\alpha^2(WT_2 + K)} \qquad [4.24]$$

where

$$\frac{1}{G'} = \frac{4}{\alpha^2(WT_{45} + K)} - \frac{1}{\alpha^2(WT_1 + K)} - \frac{1}{\alpha^2(WT_2 + K)}$$

$$= \frac{1}{\alpha^2}\left[\frac{4}{(WT_{45} + K)} - \frac{1}{(WT_1 + K)} - \frac{1}{(WT_2 + K)}\right]$$

$$= \frac{1}{\alpha^2}\left(\frac{1}{G''}\right)$$

Substituting $1/G' = 1/\alpha^2\,(1/G'')$ into equation (4.24), the tensile energy (*WT*) of the tensile parameters is derived as follows:

$$\frac{1}{(WT_\theta + K)} = \frac{\cos^4\theta}{(WT_1 + K)} + \frac{\cos^2\theta \sin^2\theta}{G''} + \frac{\sin^4\theta}{(WT_2 + K)} \qquad [4.25]$$

Principally, K varies with α and β which are different values in various directions. K is taken as a constant, due to the linear relationship found in its numerator and the denominator in various directions. In order to simplify the calculation of tensile energy (WT), α and β can be recorded directly from the warp direction. Thus, the tensile work in any direction can be obtained using equation (4.25) when values of the tensile work at the warp, weft and 45° directions are known.

4.3.2.2 Tensile elongation (EMT)

EMT reflects the extensibility of a fabric. It is a measure of a fabric's ability to be stretched under tensile load. The larger the *EMT* value, the more extensible the fabric. A similar approach to that of tensile work (WT) is adopted in the derivation of a tensile elongation (EMT) model. The model for the prediction of Young's modulus in any direction other than the warp and weft directions is derived by Kilby (1963), and a mathematical rearrangement is made to form equation (4.26):

$$\frac{1}{E_\theta} = \frac{\cos^4\theta}{E_1} + \left[\frac{1}{G} - \frac{2\sigma_{pt}}{E}\right]\cos^2\theta \sin^2\theta + \frac{\sin^4\theta}{E_2}$$

$$\Rightarrow \quad \frac{1}{E_\theta} = \frac{\cos^4\theta}{E_1} + \left[\frac{4}{E_{45}} - \frac{1}{E_1} - \frac{1}{E_2}\right]\cos^2\theta \sin^2\theta + \frac{\sin^4\theta}{E_2} \qquad [4.26]$$

where E_1, E_2 and E_θ are the Young's moduli to the warp, weft and θ directions respectively, G is the shear modulus, σ_{pt} the Poisson ratio. Equation (4.26) is useful for predicting the full form of the polar diagram of modulus against angle, when values of the parameters in the warp, weft and 45° directions are known.

In general, the tensile stress–strain relationship for textile materials is non-linear and characterised by a simple concave shape. However, in order to simplify the analysis, the author assumed that a tensile curve is linear to derive a model for *EMT* in different directions relative to its warp or weft direction. With this assumption, *EMT* of a woven fabric may be derived very conveniently from the simple relation as $E = F/\varepsilon$.

Since F is kept constant at 500 gf/cm during experiments, tensile modulus is inversely proportional to extension when the tensile curve is assumed to be linear. Then we can write $E_\theta = F_\theta/\varepsilon_\theta$ in terms of θ and substitute into equation (4.26). Thus:

$$\frac{\varepsilon_\theta}{F} = \frac{\varepsilon_1 \cos^4\theta}{F} + \left[\frac{4\varepsilon_{45}}{F} - \frac{\varepsilon_1}{F} - \frac{\varepsilon_2}{F}\right]\cos^2\theta \sin^2\theta + \frac{\varepsilon_2 \sin^4\theta}{F} \qquad [4.27]$$

where

$$G' = \frac{1}{F}\,(4\varepsilon_{45} - \varepsilon_1 - \varepsilon_2)$$

ε_{45} is the mean value of ε_θ of ± 45° and G' is a constant. After rewriting equation (4.27),

$$\varepsilon_\theta = \varepsilon_1 \cos^4\theta + \frac{\cos^2\theta \sin^2\theta}{G'} + \varepsilon_2 \sin^4\theta \qquad [4.28]$$

Replacing ε by *EMT*, the tensile strain of the tensile parameters is derived as follows:

$$EMT_\theta = EMT_1 \cos^4\theta + \frac{\cos^2\theta \sin^2\theta}{G'} + EMT_2 \sin^4\theta \qquad [4.29]$$

where

$$G' = \frac{4}{EMT_{45}} - \frac{1}{EMT_1} - \frac{1}{EMT_2}$$

In the previous case, E is considered to vary linearly with ε and EMT_θ is derived based on this linear relationship. In this case, however, a more precise model for *EMT* is derived based on the non-linear relationship from Hu (1994). Her model described the tensile stress–strain curve with an exponential function with two parameters shown as follows.

$$F = \frac{e^{\alpha\varepsilon} - 1}{\beta} \qquad [4.30]$$

where F is stress, ε is strain, α and β are unknown parameters. The unknown parameters α and β can be solved by using the SPSS non-linear regression method or TK Solver. F and ε are read off from tensile stress–strain curves tested on a particular fabric on the KES-F apparatus. α and β are obtained from the warp direction. Now, E is treated as the derivative of F with respect to ε:

$$\frac{1}{E} = \frac{\beta}{\alpha}\frac{1}{e^{\alpha\varepsilon}} \qquad [4.31]$$

α and β are taken as constant regardless of the different directions so that they are obtained from the warp direction. When E changes with angle, and this is the case for ε, then $1/E_\theta = (\beta/\alpha)(1/e^{\alpha\varepsilon_\theta})$ and substituting it into equation (4.26) yields equation (4.32).

$$\frac{\beta}{\alpha}\left(\frac{1}{e^{\alpha\varepsilon_\theta}}\right) = \frac{\beta}{\alpha}\left(\frac{\cos^4\theta}{e^{\alpha\varepsilon_p}}\right) + \frac{\cos^2\theta \sin^2\theta}{G} + \frac{\beta}{\alpha}\left(\frac{\sin^4\theta}{e^{\alpha\varepsilon_t}}\right) \qquad [4.32]$$

Hence

$$\frac{1}{G} = \frac{\beta}{\alpha}\left(\frac{4}{e^{\alpha\varepsilon_{45}}} - \frac{1}{e^{\alpha\varepsilon_p}} - \frac{1}{e^{\alpha\varepsilon_t}}\right) = \frac{\beta}{\alpha}\frac{1}{G''}$$

Substituting $1/G = (\beta/\alpha)\,(1/G'')$ into equation (4.26) gives

$$\frac{1}{e^{\alpha\varepsilon_\theta}} = \left(\frac{\cos^4\theta}{e^{\alpha\varepsilon_p}}\right) + \frac{\cos^2\theta\sin^2\theta}{G''} + \left(\frac{\sin^4\theta}{e^{\alpha\varepsilon_t}}\right)$$

$$e^{-\alpha\varepsilon_\theta} = e^{-\alpha\varepsilon_p}\cos^4\theta + \frac{\cos^2\theta\sin^2\theta}{G''} + e^{-\alpha\varepsilon_t}\sin^4\theta$$

and

$$\varepsilon_\theta = -\frac{1}{\alpha}\left(e^{-\alpha\varepsilon_p}\cos^4\theta + \frac{\cos^2\theta\sin^2\theta}{G''} + e^{-\alpha\varepsilon_t}\sin^4\theta\right) \qquad [4.33]$$

Replacing ε by *EMT*,

$$EMT_\theta = -\frac{1}{\alpha}\left(e^{-\alpha EMT_p}\cos^4\theta + \frac{\cos^2\theta\sin^2\theta}{G''} + e^{-\alpha EMT_t}\sin^4\theta\right) \qquad [4.34]$$

The tensile strain (*EMT*) in any direction can be obtained by using the above models (equations 4.22 and 4.24) when values of the tensile strains at warp, weft and 45° directions are known. The polar diagram of *EMT* of different woven fabrics can also be predicted by this model (Lo and Tsang, 1999).

4.3.2.3 Linearity (LT)

Linearity is a measure of the extent of non-linearity of the tensile stress–strain curve. It depends on the ratio between tensile work (*WT*) and tensile elongation (*EMT*) from the stress–strain curve. The model of tensile linearity (*LT*) can thus be denoted as follows:

$$LT_\theta = \frac{WT_\theta}{cons\tan t^* EMT_\theta} \qquad [4.35]$$

4.3.2.4 Tensile resilience (RT)

Tensile resilience (*RT*), which is the ratio of work recovered to the work done in tensile deformation, is expressed as a percentage ($RT = WT'/WT$). Work recovery (WT') is the tensile force at the recovery process while tensile energy (WT) in tensile deformation is represented by the area under the stress–strain curve in the loading process. And thus the existing *WT* model and the proposed WT' model for the loading and unloading processes respectively can be used to predict the tensile resilience (*RT*) of woven fabrics.

For the loading process of the tensile stress–strain curve, a model is derived by Hu and Newton (1993) for the loading stress–strain curve. Their approach is to establish a model with an exponential function, in which two parameters are derived by using a non-linear regression method.

As the tensile recovery curve is followed by a very rapid decrease in the fabric stress in the unloading process, function 4.36 is thus established:

$$F' = ae^{b\varepsilon} - c \qquad [4.36]$$

where F' is stress, ε is strain, a, b and c are unknown parameters.

Work recovery model (WT')

The work recovery (WT') of the tensile stress–strain curve could also be described with the proposed exponential function with two unknown parameters. The unknown parameters a, b and c in function 4.36 can be solved using the SPSS non-linear regression program and F' and ε can be directly recorded from tensile stress–strain curves tested on the KES system. The derivative of F' with respect to ε yields tensile modulus,

$$E' = \frac{\mathrm{d}F'}{\mathrm{d}\varepsilon} = abe^{b\varepsilon} \quad \Rightarrow \quad \varepsilon = \frac{\ln(E'/ab)}{b} \qquad [4.37]$$

Tensile recovery (WT') as defined in the KES system is work recovery in tensile deformation represented by the area under the stress–strain curve. Combining equations 4.36 and 4.37, we get

$$\begin{aligned} WT' &= \int_{\varepsilon_0}^{\varepsilon_\mathrm{m}} F'(\varepsilon)\mathrm{d}\varepsilon \\ &= \int_{\varepsilon_0}^{\varepsilon_m} (ae^{b\varepsilon} - c)\mathrm{d}\varepsilon \\ &= \left| \frac{ae^{b\varepsilon}}{b} - c\varepsilon \right|_{\varepsilon_0}^{\varepsilon_\mathrm{m}} \\ &= \frac{E'_\mathrm{m} - E'_0}{b^2} - \frac{c}{b}\left(\ln \frac{E'_\mathrm{m}}{E'_0}\right) \end{aligned} \qquad [4.38]$$

If E' varies with an angle θ, WT' will also vary with θ and the above equation becomes

$$WT'_\theta = \frac{(E'_\mathrm{m})_\theta - (E'_0)_\theta}{b^2} - \frac{c}{b}\left[\ln \frac{(E'_\mathrm{m})_0}{(E'_0)_\theta}\right] \qquad [4.39]$$

where $(E'_\mathrm{m})_\theta$ and $(E'_0)_\theta$ are the Young's moduli of the tensile recovery curve in various directions. All can be calculated from the Kilby Young's modulus model (equation 4.18). As the two parameters b and c vary with angle θ, they will give different values in various directions. To simplify the calculation of WT' by statistical mean of least squares analysis, b and c take their average in the warp, weft and ± 45° directions rather than the value of their corresponding individual direction (Lo *et al*., 1999a,b).

Tensile resilience model (*RT*)

With the work recovery model (WT'), tensile resilience (*RT*) of woven fabrics could be easily predicted from the work recovery (WT') and tensile work (WT) models. Tensile resilience (*RT*) is the ratio of work recovered to work done in tensile deformation expressed as a percentage:

$$RT = \frac{WT'}{WT} \times 100\ \% \qquad [4.40]$$

If *RT* varies with angle θ, equation 4.40 becomes

$$RT_\theta = \frac{WT'_\theta}{WT_\theta} \times 100\ \% \qquad [4.41]$$

4.3.3 Polar diagrams of the tensile model

4.3.3.1 General features

The values of tensile parameters (*WT*, *EMT*, *LT* and *RT*) usually differ in direction; thus some points in the polar diagram have to be normalised in the warp direction to simplify the comparison and analysis. When the value of these parameters in the warp direction is fixed, changes in the bias directions can be easily observed from the polar diagram. The normalised tensile parameters can be obtained by dividing each parameter by their averaged value.

As shown by Figs 4.4–4.7, many similarities can be found in the polar diagrams of different tensile parameters:

(1) The pattern is symmetrical to the warp and weft directions.
(2) The value of each parameter differs with the angle and the maximum happens exactly at either the warp (*WT* of satin, *LT*) or weft directions

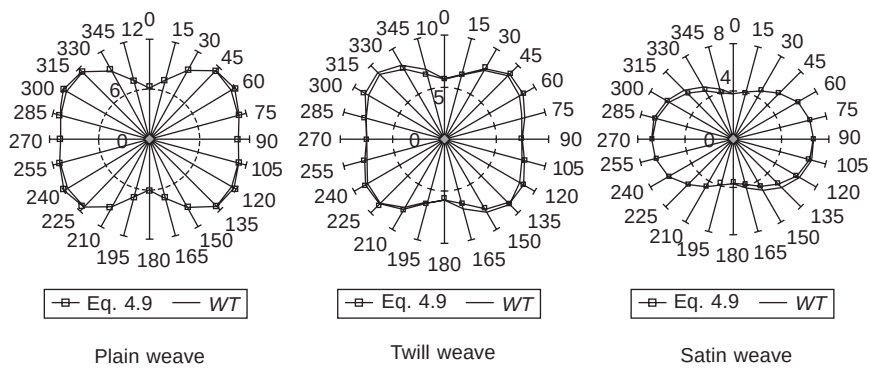

4.4 Typical polar diagram of tensile work (*WT*).

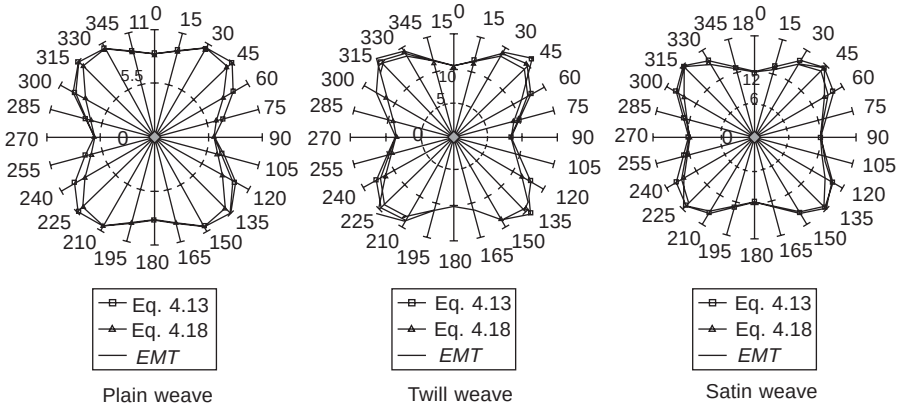

4.5 Typical polar diagram of tensile extension (*EMT*).

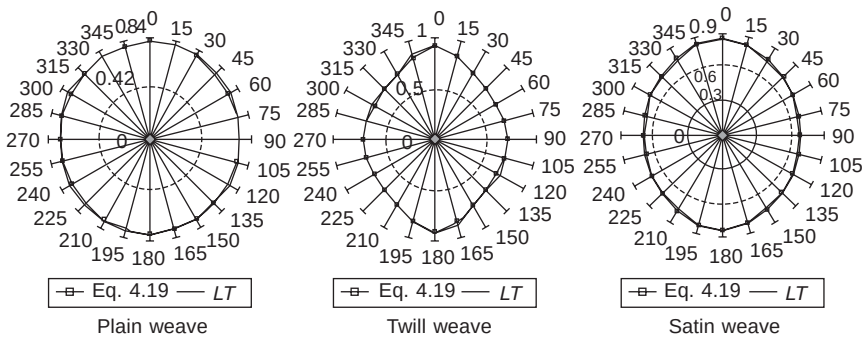

4.6 Typical polar diagram of tensile linearity (*LT*).

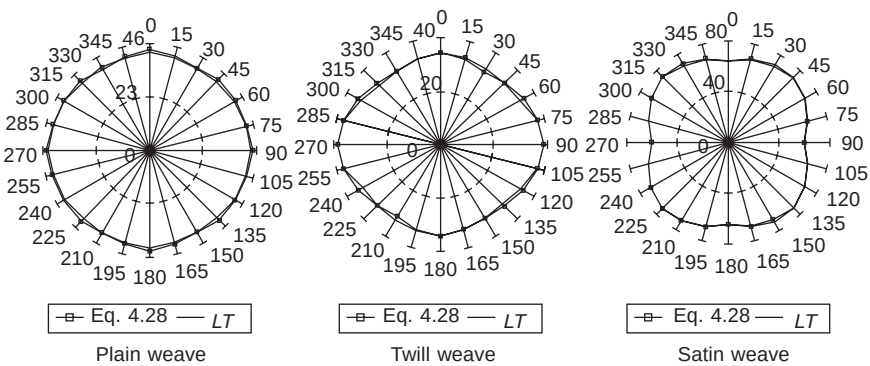

4.7 Typical polar diagram of the tensile resilience model (*RT*).

Table 4.1 Classification of polar diagrams of tensile parameters

Types	Conditions	Shape of polar diagram
1	$WT_1 \approx WT_2 \approx WT_\theta$	Circular shape (isotropic)
	$(WT_1 \approx WT_2) > WT_\theta$	Butterfly or Hexagonal Shape
	$(WT_1 \approx WT_2) < WT_\theta$	Rhombus shape
2	$WT_1 > WT_\theta > WT_2$	Gourd or elliptic shape (maximum value in warp direction)
	$WT_1 < WT_\theta < WT_2$	Gourd or elliptic shape (maximum value in weft direction)

or at ± 45° angle (*WT*, *EMT*) corresponding to the warp and weft directions.

(3) For some tensile parameters, the polar diagram generated from satin woven fabrics might differ somewhat from that of plain and twill woven fabrics due to its long floats, examples of which include the *WT* polar diagram.

(4) The polar diagrams of each parameter can be classified into two types on the basis of their general shapes. If the value of the parameter between the warp and weft directions is similar, the polar diagram will display a circular, rhombus or butterfly shape. We name this pattern Type 1. Type 2 refers to those featuring a gourd shape with their maximum value either in the warp or in the weft direction, as shown in Table 4.1.

4.3.3.2 Factors influencing tensile parameters

Influence of fabric weaves on *WT*

Twill and satin woven fabrics usually demonstrate lower tensile work (*WT*) as compared with plain woven fabrics, due to the presence of floats, but no apparent difference can be observed in the *WT* values of plain, 2/2 twill and 3/3 twill woven fabrics in the warp direction if their warp densities are kept constant. In addition, the value of *WT* will increase with the rise in weft densities, indicating that more work is needed to extend the fabric with high weft density.

Due to the frictional force between the contact points of the warp and weft yarns, several factors will contribute to the amount of energy loss, including the ratio of the yarn counts in the warp and weft yarns, the ratio of the yarn spacing, the average yarn spacing, the type of weaves, the direction of force applied to the fabrics, etc. The experimental data of *WT* indicates that the tensile work of plain woven fabrics is generally higher than that of the twill and satin woven fabrics. As the ratio of yarn spacing and the average yarn spacing of plain woven fabrics are comparatively smaller than those of twill and satin woven fabrics, greater energy is needed to overcome the frictional

restraint existing at the interlacing points of the warp and weft yarns. As neighbouring yarns cross over interlacing points, the yarns are prevented from moving, especially when extension occurs in bias directions. In such a case, the yarns are extended by rotating the unit cell in the direction of the pull. Thus, larger energy consumption results in the extension of plain woven fabric in bias directions.

In contrast with this, lower yarn crimp is exhibited in the looser weave construction of twill and satin woven fabrics, especially in the weft direction. Consequently, yarn extension is no longer the main factor affecting fabric deformation, viz. fibre extension also comes into play. As a result, an increase in the work in bias directions occurs due to the addition of fibre extension. This also explains why the tensile work in the weft direction is found to be higher than that in the warp direction.

Influence of weft density on *EMT*

Weft density is an important factor governing *EMT* values. With the increase in weft density for any fabric type, a rise in the magnitude of *EMT* in all directions will be observed. A direct image of this is an outward spreading along any direction for all woven fabrics. As the width of a fabric is usually fixed, the yarns will jam and come into contact when the weft density has reached its limit. Hence, an increase in the inter-yarn friction will be found when the weft yarns are closely packed together.

For a unit cell of a plain woven fabric, the warp and weft yarns interlace with each other in a format of one up and the other down. Thus, when a fabric is under tension, the yarn bending rigidity in this lattice structure will restrict yarn movement by producing frictional force. Generally, this restriction will increase with the rise in the weave density. In addition, the yarn crimp will also grow with the increase in weave density and, in the meantime, a reduction in the modular length will be found. Therefore, more energy is needed to extend a fabric with high density.

A twill woven fabric usually exhibits larger elongation than plain woven fabrics due to its loose structure, despite its low yarn crimp. In addition, the extension of a loose-structured fabric usually involves yarn slippage or even fibre extension when large tension is applied. Thus, a broadening effect can also be found in the contour of its polar diagram when the weft density is increased.

Influence of Poisson's ratio on *EMT*

When a fabric is extended lengthwise in one direction, widthwise contraction will be found in the other as revealed by our experiments, made on the KES-F apparatus using all specimens. Poisson's ratio is such a measure of the relative changes in length in the directions of the pull to that in a direction perpendicular to it (Chadwick *et al*., 1949). Therefore, it can be predicted

that a relationship exists between the Poisson effect and the anisotropy of tensile elongation (*EMT*) and tensile work (*WT*) of woven fabrics.

For a woven fabric, it seems that its Poisson's ratio differs considerably from one direction to another. In addition, the maximum elongation can be experimentally proven at ± 45° directions as discussed in the previous section. It is also evident that maximum widthwise contraction and evading action happen at ± 45° directions. These maxima at ± 45° might be attributable to the increased internal friction in the perpendicular direction and maximum pressure existing at the warp and weft interlacing points. Also observed in tensile testing is a necking effect, which might stem from yarn migration towards both ends of the clamps.

For a clear picture of the Poisson effect on widthwise contraction, the lengthwise extension is kept constant. Consequently, in common with the situation with *EMT* and *WT*, a similar effect is found in the Poisson's ratio of woven fabrics. For woven fabrics, their Poisson's ratios in the two principal directions are very close to each other. However, an apparent difference exists in the Poisson's ratios of twill and satin woven fabrics. This indicates that a lower crimp interchange effect appears in loose fabric structures.

During uniaxial extension, only one set of yarns is firmly held at both ends, while both ends of the other set of yarn are free of tension; this leads to the great similarity in its Poisson's ratios in the two principal directions. However, in the bias directions, only one end of the yarns will be clipped during extension. The yarns can thus easily move along each other, especially in a loose structure such as in twill and satin weaves. These yarns also present a tendency to move towards the clamps due to the lack of pinpointing effect. Also proved is a higher ratio of lengthwise elongation to widthwise contraction in bias directions.

Figure 4.8 shows the unit cell of a uniaxially stretched plain woven fabric. It is quite clear that the lengthwise extension in ± 45° direction (length y' in Fig. 4.8b) is larger than that in either of the two principal directions (length y in Fig. 4.8a). If the lengthwise extension is kept constant, a higher widthwise contraction of woven fabric will also be observed in the ± 45° direction as indicated by x'.

Although the above results were developed on apparel fabrics, it has been experimentally confirmed that their validity can also be extended to industrial woven fabrics.

4.4 Strain-hardening of warp yarns in woven fabrics

4.4.1 Introduction

From intuition, it would be expected that a square plain woven fabric should exhibit similar extensibility in its two principal directions. For poplin fabrics,

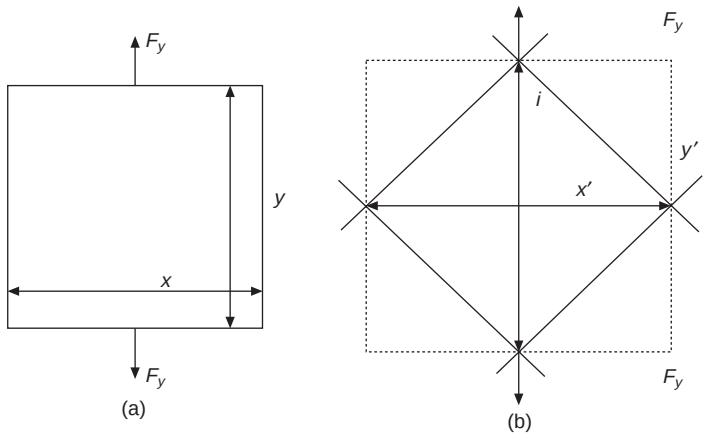

4.8 Unit cell of plain woven fabric after uniaxial tension: (a) Extension in the warp or weft direction; (b) Extension in 45° direction.

a fabric type with prominent larger crimp level in warp yarns, the extensibility of warp yarn should be far superior to that of weft yarns. However, KES testing reveals that against our expectation, the square fabric possesses greater variation in extension in its two principal directions than the poplin. In addition, tensile resilience, *RT*, seems to have a larger value in the warp direction than that in the weft for many fabrics while *WT*, the tensile energy, always exhibits a lower value in the warp. These facts reveal that a woven fabric is more extensible in the weft direction. A direct image of this phenomenon is that the shape of the tensile stress–strain curve of a woven fabric is usually steeper in the warp direction than that in the weft, as shown in Fig. 4.9. This phenomenon is apparently due to the repeated loading and unloading a woven fabric experiences during manufacturing and processing.

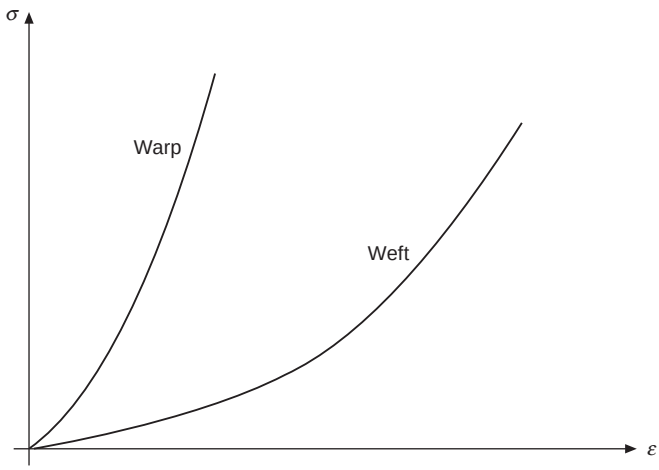

4.9 Comparison of the tensile stress–strain curves in principle directions of woven fabrics.

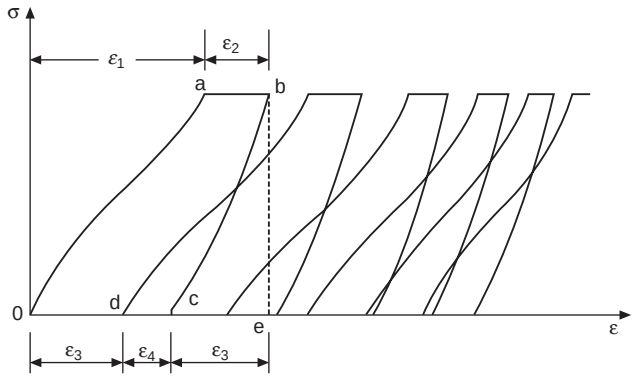

4.10 Cyclic tensile stress–strain curves of textile materials.

4.4.2 Theory of plasticity

4.4.2.1 Work-hardening

Figure 4.10 shows the cyclic tensile stress–strain curves of textile materials. It is obvious that when an inelastic material like a yarn or a fabric is subjected to cyclic loading, the loops will get narrower and narrower as cyclic loading and unloading goes on. As a result, the energy needed to stretch the material gets less and less while the strain becomes smaller and smaller at the same maximum strain.

In Fig. 4.11, the tensile curve of a general engineering material is presented. If at any point between the elastic limit B and the maximum load point C the

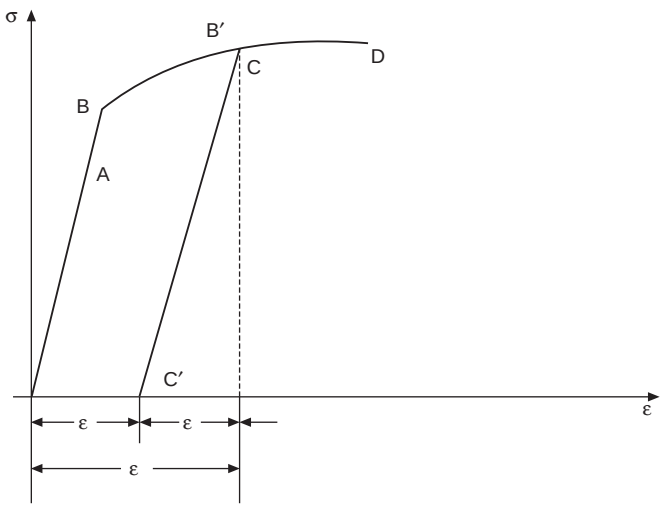

4.11 Stress–strain curve for a conventional engineering material.

tensile stress in the material is removed, unloading will take place along a line parallel to the elastic line, as shown in the figure by B′C′. Part of the strain is thus recovered and part remains permanently. Upon reloading, the unloading line B′C′ is retracted with very minor deviations. Actually a very thin hysteresis loop is formed, which is usually neglected. Plastic flow does not start again until the point B′ is reached. With further loading, the stress–strain curve is continued along B′C′ as if no unloading had occurred. Point B′ can thus be considered as a new yield point for this material. From this. fact, it appears that the Young's modulus in this second cycle would be equal to or larger than that of the first cycle. Three conclusions follow from this, Firstly we can infer that the modulus at any point is the smallest in the first loading cycle. The modulus of a later cycle is generally larger than that of the immediately previous cycle, or the extension of the material in the first cycle is the largest among all cycles for a given cyclic stress. For example, the Young's modulus of the third cycle is larger than that of the second cycle; in turn, the modulus of the fifth cycle may be larger than that of the fourth cycle … Secondly, when a constant stress is given for two cycles, for example at B′, we can see that the energy to extend the material during the first cycle is much larger than that in the second cycle, which is only a part of that in the first cycle; in turn, energy in the first cycle will be larger than that in the second one. Thirdly, if we release the loading at B′ it is obvious that the tensile resilience of the second cycle is 100 %, but the first cycle has only a fraction of it; that is, the tensile resilience of the second cycle will be larger than that of the first cycle and consequently the energy resilience in the later cycle may be larger than in all the previous ones. This is caused by plastic strain in the previous steps. The effect of this strain is called work–hardening or strain-hardening.

In plasticity theory, when a real material is deformed plastically, it 'work-hardens'. That is, as the material deforms, its resistance to further deformation increases. The degree of hardening is a function of the total plastic work and is otherwise independent of the strain path. This is sometimes known as the equivalence of plastic work. In other words, the resistance to further distortion depends on the amount of the work. The effect of different discontinuous processing procedures of woven fabrics, namely the extension stresses in the warp direction, can be simulated at irregular cyclic loading. They produce accumulated plastic strains in yarns of woven fabrics. The effect of plasticity is a permanent deformation. Even though a fabric is fully relaxed, the deformation caused by processing cannot be removed entirely.

Thus when a final product, a fabric, is tested on a tensile tester in a laboratory, this causes the *EMT* difference between warp direction and weft direction, even though the other conditions are the same for warp and weft yarns; *WT* in the weft direction is larger than that in the warp direction; the recovered energy is larger in the warp direction; and it can be observed that

the warp yarns in a woven fabric are harder to extend than those in the weft direction.

4.4.2.2 Plastic strains

From the above section, plastic strain in woven fabrics before tensile testing is recognised by the comparison of the warp and weft tensile properties of a woven fabric and it is suggested by comparing cross-sectional areas of warp and weft yarns.

If it is assumed that yarn density remains unchanged before and after fabric manufacturing and processing, the difference in the yarn areas between warp and weft directions in a fabric can be attributed as a warp yarn extension along its axis direction.

The value of warp yarn extension may be calculated using a plastic deformation principle, assuming that plastic strain involves no volume change, thus:

$$e_{xp} + e_{yp} + e_{zp} = 0 \qquad [4.42]$$

where e_{xp}, e_{yp}, e_{zp} are logarithmic plastic strain changes in the x, y, z direction respectively.

The logarithmic strain is defined as:

$$e = \ln \frac{l}{l_0} \qquad [4.43]$$

In the case of the KES system, we use engineering strain $\varepsilon \times 100$ %:

$$\varepsilon = \frac{l - l_0}{l_0} \qquad [4.44]$$

These two strains have the following relation:

$$e = \ln (1 + \varepsilon) \qquad [4.45]$$

The definition of logarithmic strain was suggested by Ludwik. For small extensions, the engineering strain, ε (first defined by Cauchy), is approximately equal to the logarithmic strain e.

Under the condition of volume constancy, the relationship of three principal engineering strains can be expressed:

$$(1 + \varepsilon_x)(1 + \varepsilon_y)(1 + \varepsilon_z) = 1 \qquad [4.46]$$

For infinitesimal strains, we may neglect the products of the strains and equation 4.46 reduces to

$$\varepsilon_x + \varepsilon_y + \varepsilon_z = 0 \qquad [4.47]$$

In the case of yarns in woven fabrics, for elliptic yarn cross-section, the z

axis represents yarn axial direction, the *x* axis the major diameter direction and the *y* axis the minor diameter direction. Then equation 4.42 can be written as:

$$\ln\left(\frac{a}{d_0}\right) + \ln\left(\frac{b}{d_0}\right) + e_{zp} = 0 \qquad [4.48]$$

where a and b are major and minor diameters of yarn in a woven fabric, d_0 is the original diameter of the yarn.

If the cross-sections of yarn are regarded as circular and the equivalent diameter, d, is calculated using measured yarn area, the relation can be expressed:

$$2\ln\left(\frac{d}{d_0}\right) + e_{zp} = 0 \qquad [4.49]$$

One piece of evidence of the effects of the plastic strain on different directions of a woven fabric is that the cross-sectional areas of warp yarns are generally smaller than those of weft when made of the same yarns, as shown in Fig. 4.12. Statistical calculations of the plastic strains in the longitudinal direction of yarns in a fabric show that the warp yarns in a woven fabric have a positive or extended plastic strain before testing and the weft yarns a negative one, which makes warp yarns in a woven fabric harder to stretch than weft yarns. The difference of plastic strains in warp and weft directions is shown to have linear relationships with *EMT*, *WT* and *RT*.

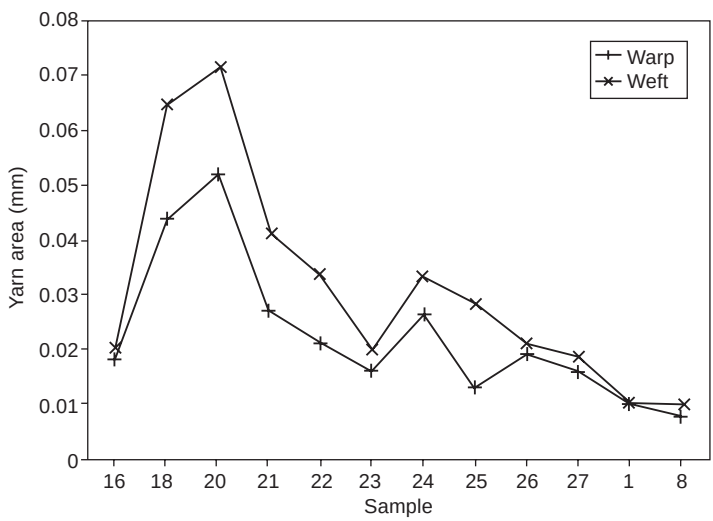

4.12 Comparison of yarn cross-section areas of warp and weft yarns.

4.4.3 Relationship between plastic strain and tensile properties

It has been shown qualitatively that the tensile properties of a woven fabric are closely related to the strain-hardening effect. In this section, the quantitative relations between them will be provided.

Figure 4.13 shows the relationship between the *EMT* difference and the plastic strain difference of warp and weft yarns in woven fabrics. From Fig.

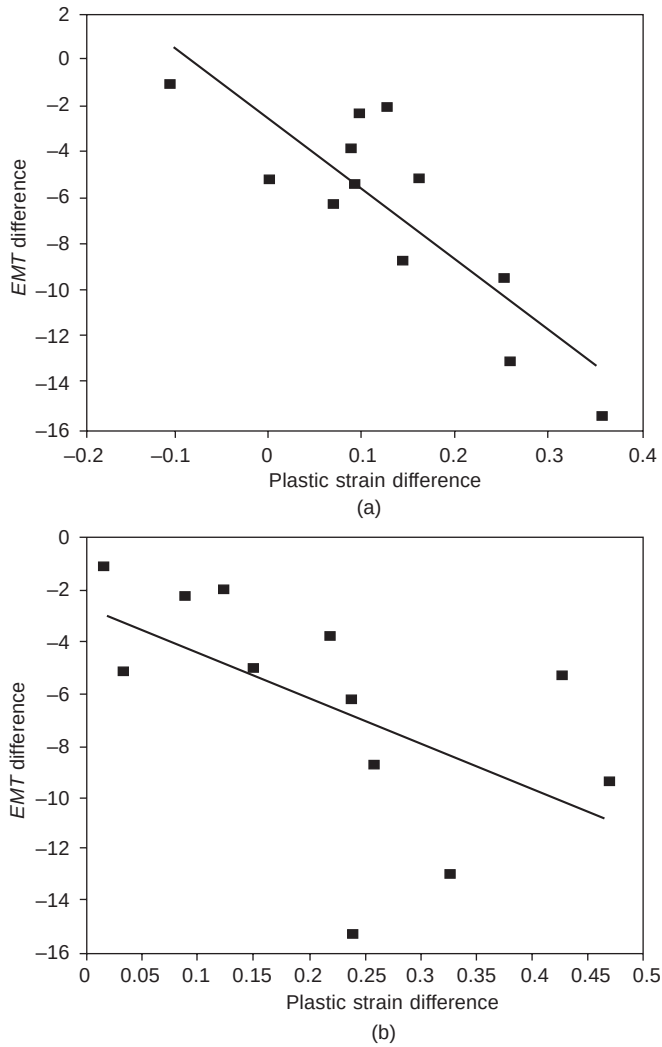

4.13 Relationship between ΔEMT and Δe for (a) circular cross-section and (b) elliptic cross-section.

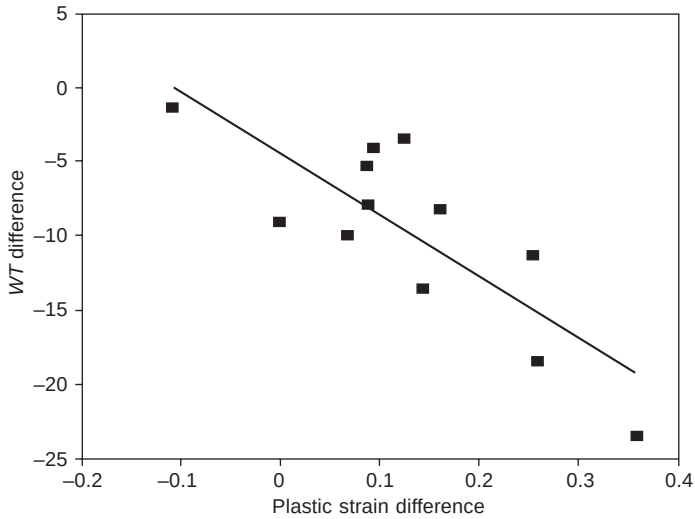

4.14 Relationship between ΔWT and Δe.

4.13a, whose plastic strain is calculated using equation 4.49 for the equivalent circular cross-sectional diameter of measured yarn area, it appears that a good linear relationship exists. Figure 4.13b, whose calculation is based on elliptic cross-section, shows similar trends.

Figure 4.14 plots the relationships between *WT* difference and plastic strain difference of warp and weft yarns in woven fabrics. It is clear that a good linear relationship also holds. Figure 4.15 depicts the relationships between *RT* difference and plastic strain difference of warp and weft yarns in woven fabrics. It is apparent that the larger *e* produces the larger *RT*.

4.5 Summary

This chapter introduces the author's contribution to the study of the tensile properties of woven fabrics. It starts with an introduction of the general concept of tensile properties with the focus placed on the features of tensile stress–strain curves of woven fabrics as well as the complexity of the deformation of woven fabrics under tensile load. This is followed by modelling the tensile behaviour of woven fabrics. Also presented is a study of the anisotropy of the tensile properties of woven fabrics together with an in-depth investigation of the strain-hardening effect observed from tensile stress–strain curves. The conclusions reached include:

(1) A woven fabric's tensile property is very difficult to study due to the great bulkiness in fabric structure in addition to the complexity in the structure and strain distribution of its constituent fibres and yarns and of the fabric itself as well as the strain variation during deformation. A

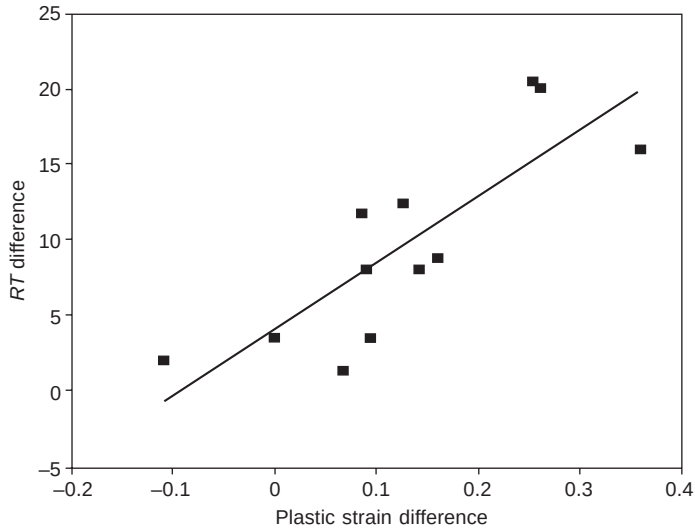

4.15 Relationship between ΔRT and Δe.

deformed fabric cannot resume its original geometrical state due to the existence of hysteresis. This is inherent since textile material is viscoelastic.

(2) The tensile stress–strain relationship of a woven fabric can be successfully described by an exponential function, $f = [(e^{\alpha\varepsilon} - 1)/\beta] + e_r$, in which α is a reinforcing factor for the increase of Young's modulus E. There is also found an obvious linear relationship between α with the crimp level c of the fabric.

(3) Regarding the various tensile parameters (*WT*, *EMT*, *LT*, *RT*), a great deal of similarity is found in their polar diagrams: their shapes are all symmetrical to the warp and weft directions; the value of each parameter differs with the angle; and the maximum happens exactly at either the warp (*WT* of satin, *LT*) or weft directions or at ± 45° angle (*WT*, *EMT*) corresponding to the warp and weft directions. The polar diagram of each parameter can be classified into two similar groups depending on the relationship of parameter values between the warp and weft directions.

(4) The strain-hardening phenomenon is found in woven fabrics. This phenomenon has a significant effect on the tensile properties of a woven fabric, as reflected by the variation in the Young's modulus value between warp and weft directions. It is believed that this phenomenon could be associated with the repeated loading and unloading a woven fabric experiences during manufacturing and processing.

4.6 References

Anandjiwala R D and Leaf G A V (1991a), Large-scale extension and recovery of plain woven fabrics, part I: theoretical, *Text Res J*, **61**, 619–634.

Anandjiwala R D and Leaf G A V (1991b), Large-scale extension and recovery of plain woven fabrics, part II: experimental and discussion, *Text Res J*, **61**, 743–755.

Basset (1988), The biaxial tensile and shear properties of textile fabrics and their application to the study of fabric tailorability, *PhD thesis*, The University of New South Wales.

Chadwick G E, Shorter S A and Weissenberg K A (1949), A trellis model for the application and study of simple pulls in textile materials, *J Text Inst*, **40**, T111–160.

Cooper D N E (1963), A bias extension test, *Text Res J*, **33**, T315–317.

De Jong S and Postle R (1977a), An energy analysis of woven-fabric mechanics by means of optimal-control theory, *Text Res J*, **48**, 127–135.

De Jong S and Postle R (1977b), An energy analysis of woven-fabric mechanics by means of optimal-control theory part I: tensile properties, *J Text Inst*, **68**(11), 350–361.

Grosberg P and Kedia S (1966), The mechanical properties of woven fabrics part I: the initial load-extension modulus of woven fabrics, *Text Res J*, **36**, 71–79.

Hearle J W S and Amirbayat J (1986a), Analysis of drape by means of dimensional groups, *Text Res J*, **56**, 727–733.

Hearle J W S and Amirbayat J (1986b), The complex buckling of flexible sheet materials part I: theoretical approach, *Int J Mech Sci*, **28**(6), 339–358.

Hearle J W S, Grosberg P and Backer S (1969), *Structural Mechanics of Fibres, Yarns, and Fabrics vol 1*, New York, Wiley-Interscience.

Hu J L (1994), *Structure and Low Stress Mechanics of Woven Fabrics* (PhD thesis, University of Manchester Institute of Science and Technology).

Hu J L and Newton A (1993), Modeling of Tensile Stress-strain Curve of Woven Fabrics, *J China Text Univ*, **4**, 49–61.

Kageyama M, Kawabata S, Niwa M (1988), The validity of a linearizing method for predicting the biaxial-extension properties of fabrics, *J Text Inst*, **79**, 543–565.

Kilby W F (1963), Planar stress-strain relationships in woven fabrics, *J Text Inst*, T9–27.

Konopasek M (1970), *Improved Procedures for Calculating the Mechanical Properties of Textile Structures* PhD thesis, University of Manchester Institute of Science and Technology.

Leaf G A V (1980), Woven fabric tensile mechanics, in *Mechanics of Flexible Fibre Assemblies (NATO Advanced Study Institute Series; E, Applied Sciences No. 38)*, Hearle J W S, Thwaites J J and Amirbayat J (eds), The Netherlands, Alpen aan den Rijn, Sijthoff and Noordhoff, 143–157, 647.

Lo W M and Tsang Y Y (1999), Anisotropy of tensile strain of balance twill woven fabrics, 2nd *International Textile and Apparel Conference*, SENA 1/CETIQT Rio de Janeiro, Brazil, July, 1999, CD ROM.

Lo W M, Hu J L and Lo M (1999a), Bending hysteresis of twill woven fabrics in various directions, *J China Text Univ*, **16**(3), 37–41.

Lo W M, Hu J L and Lo M T (1999b), Tensile resilience of cotton woven fabrics, *Proc* 5th *Asian Textile Conference*, Kyoto, Sept 30–Oct 2, **1**, 623–626.

Peirce F T (1937), The geometry of cloth structure, *J Text Inst*, **28**, T45–96.

Shanahan W J, Lloyd D W and Hearle J W S (1978), Characterizing the elastic behavior of textile fabrics in complex deformations, *Text Res J*, **48**(15), 495.

Skelton J (1971), Triaxially woven fabrics: their structure and properties, *Text Res J*, **14**(8), PP637–647.

Spivak S M and Treloar L R G (1968), The behavior of fabrics in shear, part III: the relation between bias extension and simple shear, *Text Res J*, *Sept*, 963–971.

Weissenberg K (1949), The use of a Trellis model in the mechanics of homogenous materials, *J Text Inst*, **40**, T89–110.

5

The bending properties of woven fabrics

5.1 General bending behaviour of woven fabrics

5.1.1 Introduction

The bending properties of fabrics govern many aspects of fabric performance, such as hand and drape, and they are an essential part of the complex fabric deformation analysis. Thus, the bending of woven fabrics has received considerable attention in the literature. Computational models for solving large-deflection elastic problems from theoretical models have been applied to specific fabric engineering and apparel industry problems, for example, the prediction of the robotic path for controlling the laying of fabric onto a work surface (Brown *et al.*, 1990, Clapp and Peng, 1991).

The most detailed analyses of the bending behaviour of plain-weave fabrics were given by Abbott *et al*. (1973), de Jong and Postle (1977), Ghosh *et al.* (1990a,b,c), Lloyd *et al*. (1978) and Hu *et al*. (1999, 2000). Modelling the bending of a woven fabric requires knowledge of the relationship between fabric bending rigidity, the structural features of the fabric, and the tensile/bending properties of the constituent yarns, measured empirically or determined through the properties of its constituent fibres and the yarn structure. It requires a large number of parameters and is very difficult to express in a closed form. Thus, the applicability of such models is very limited. Konopasek (1980a) proposed a cubic-spline-interpolation technique to represent the fabric moment–curvature relationship.

5.1.2 Moment–curvature curve of bending behaviour

Fabrics are very easy to bend. Their rigidity is usually less than 1/10 000 that of metal materials and about 1/100 that of tensile deformation. Bending properties of a fabric are determined by the yarn-bending behaviour, the weave of the fabric and the finishing treatments applied. Yarn-bending behaviour, in turn, is determined by the mechanical properties of the constituent

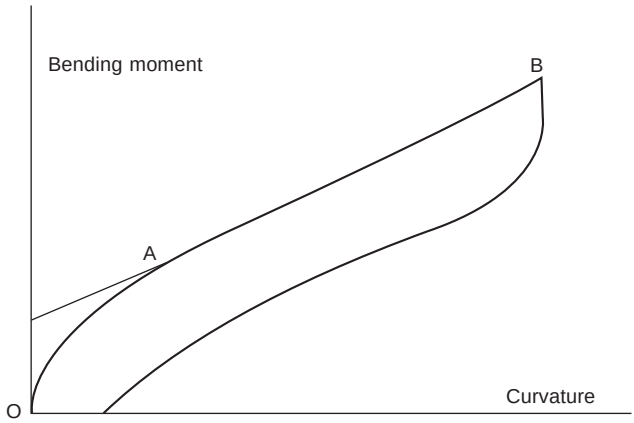

5.1 Typical bending curve of woven fabrics.

fibres and the structure of the yarn. The relationships among them are highly complex. Figure 5.1 illustrates a typical bending curve of woven fabrics.

For this curve, it is normally thought that there is a two-stage behaviour with a hysteresis loop within low-stress deformation: (a) an initial higher stiffness non-linear region, OA; within this region the curve shows that the effective stiffness of the fabric decreases with increasing curvature from the zero-motion position, as more and more of the constituent fibres are set in motion at the contact points; (b) a close-to-linear region, AB; since all the contact points are set in motion, the stiffness of the fabric seems to be close-to-constant.

It should be noted that when a woven fabric is bent in the warp or weft direction, the curvature imposed on the individual fibres in the fabric is almost the same as the curvature imposed on the fabric as a whole. As high curvatures meet when fabrics are wrinkled, the coercive couple or hysteresis is affected by viscoelastic decay of stress in the fibre during the bending cycle (Postle *et al.*, 1988). However, in applications where the fabric is subjected to low-curvature bending, such as in drapes, the frictional component dominates the hysteresis. Thus, if the strain in the individual fibres is sufficiently small that viscoelastic deformation within the fibres can be neglected, the hysteresis in Fig. 5.1 is attributed to non-recoverable work done in overcoming the frictional forces. The effect of the fibre's viscoelasticity in this section will not be considered because the bending of fabrics on the KES tester is within low-stress regions.

5.1.3 Bending stiffness

The primary concern with the conventional research in fabric bending is the bending stiffness. Bending stiffness is one of the main properties that control

fabric bending. It should be defined as the first derivative of the moment–curvature (M–ρ) curve. If the structure of the bending curve is linear, M is directly proportional to the curvature produced. Some studies have been conducted to predict fabric bending stiffness. It has proved very difficult to calculate bending stiffness explicitly, due to the numerous factors that affect its value if the stiffness of the whole bending process is considered. In reality, the bending stiffness of fabrics is usually approximated to a constant which can be considered as steady-state-average-stiffness and the initial non-linear region is ignored. This is a low-order approximation to the actual non-linear bending properties present in most fabrics. Clapp and Peng (1991) have shown that the approximation to a constant stiffness may yield inaccurate values when calculating the fabric-buckling force in the initial buckling stage (Brown, 1998). As we can see in Fig. 5.1, the actual experimental M–ρ curves are non-linear, at least in the initial region in which the slope of the M–ρ curve for small values of ρ is greater than that for larger values of ρ. Thus, the bending-stiffness, B, should be a non-linear, continuous function of curvature.

5.1.4 Relationship between bending stiffness and bending hysteresis

The effect of friction on the steady-state-stiffness, known as ‘elastic stiffness’ in the literature, of fabric bending is well known to us and has been studied by a number of workers, including Peirce, Platt, Kleine and Hamburger, and Cooper before Liversey and Owen. But different researchers have different views on the manner and extent of this effect. Peirce suggested that a theoretical minimum warpway or weftway stiffness for a fabric might be calculated by summing the bending stiffness of the yarns; this was examined more fully by Cooper who found that friction or binding between the fibres causes the observed stiffness to exceed this minimum. The contribution of inter-fibre friction to the stiffness of a fabric has usually been studied by subjecting the specimen to a bending cycle and examining the resulting hysteresis curves. Liversey and Owen (1964) derived a mathematical formula for the minimum fabric bending stiffness, neglecting interactions between the fibres; this formula took account of the twist and crimp in the yarns. An instrument was described in their classical paper titled ‘Cloth stiffness and hysteresis in bending’ to assist in determining the nature of the interactions between fibres which cause the observed fabric bending stiffness to exceed the theoretical minimum.

In Grosberg’s conclusion (1980), however, there is no friction present in the region of the close-to-linear portion of the bending curves; friction only affects the coercive moment. Postle *el al*. (1988) also thought that the internal friction has no effect on elastic bending or shear stiffness but did not mention whether friction exists during this period of deformation. Skelton (1974 and

1976) thought internal friction is always present during deformation but is independent of elastic stiffness. They all agreed that hysteresis is a measure of internal friction.

5.2 Modelling the bending behaviour of woven fabrics

5.2.1 Modelling the bending curves using non-linear regression

The modelling of the bending (moment–curvature) curve of woven fabrics started with the work of Peirce (1930). The theoretical modelling can be divided into three categories: predictive modelling, descriptive modelling and numerical modelling. The majority of the existing research work has been in the area of predictive modelling, in which the analytical relationship between fabric bending properties, yarn-bending behaviour and constituent-fibre behaviour, on the assumption of a given geometrical disposition of fibres or yarns in the fabric, is obtained. This kind of model was very difficult to solve in a closed form and thus very difficult to apply. A review of the research in this field was carried out by Ghosh *et al.* (1990a,b,c). It is not intended to re-review here due to its limited relevance.

Many numerical modelling methods are used in mechanical engineering, and they are useful for the stress–strain analysis of a structure. Konopasek (1980) proposed the use of the cubic-spline-interpolation technique to represent the stress–strain relationship of fabric bending. The cubic-spline-interpolation technique is useful when the mathematical relationship between moment and curvature is not available, but it is rather cumbersome in computation and application. When the relationship of moment–curvature of fabric bending is available, a non-linear regression method may be used to estimate constants in the equation. The following introduces the descriptive model established by Oloffson (1967). It is expected that this model can be fitted using the non-linear regression technique.

There are examples scattered through the literature of rheological studies, or descriptive modelling, including sliding elements that are in accordance with Oloffson's study, in which a simple non-viscous combination consists of a sliding element (f_N) in parallel with an elastic element (E_N) in Fig. 5.2 or a block connected by a spring to a wall.

If the initial strain is equal to zero and $\sigma \geq \sigma_N$, the conditions exist for the displacement $\varepsilon_N|$ as a function of the external stress σ. If a series of coupled elements of the type is considered arranged in the sequence:

$$\sigma_{f1} < \sigma_{f2} < \sigma_{f3} < \ldots < \sigma_{fN} < \ldots \qquad [5.1]$$

the force on all the elements is then the same:

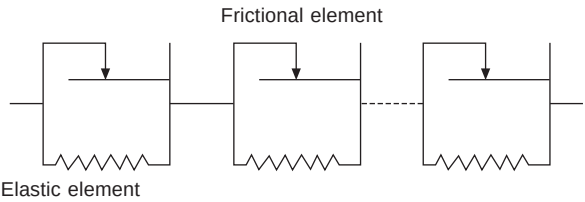

5.2 Assembly of frictional and elastic elements.

$$\sigma_1 = \sigma_2 = \sigma_3 \ldots \sigma_N = \sigma \qquad [5.2]$$

and the total deformation can be found by summing:

$$\varepsilon_1 + \varepsilon_2 + \varepsilon_3 + \ldots \varepsilon_N + \ldots = \varepsilon \qquad [5.3]$$

$$\varepsilon = \sum_{N=1}^{N-1} \varepsilon_n = \sigma \sum_{N=1}^{N-1} \frac{1}{E_N} - \sum_{N=1}^{N-1} \frac{\sigma_{fN}}{E_N} \qquad [5.4]$$

If a continuous model considered by changing the step function

$$\sigma_{f1} < \sigma_{f2}\sigma_{f3} < \ldots < \sigma_{fN} < \ldots \qquad [5.5]$$

corresponding to finite elements of Fig. 5.2 into a continuous function σ which increase with F (differential elements), then a continuous function for E_N can we expressed as a function of σ:

$$\frac{1}{E_N} = k\sigma^m \mathrm{d}\sigma \qquad [5.6]$$

where the infinitesimal range $\mathrm{d}\sigma$ is introduced and β is the curvature of the fabric. The equation can thus be obtained:

$$\varepsilon = \sum_{N=1}^{N-1} \frac{(\sigma - \sigma_{fN})}{E_N} = \int_0^{\sigma} (\sigma - \sigma_f)\, \varphi(\sigma_f)\, \mathrm{d}\sigma_f \qquad [5.7]$$

$$\varphi(\sigma_f) = k\sigma_f^m \qquad [5.8]$$

and

$$\varepsilon = k \int_0^{\sigma} (\sigma - \sigma_f)\sigma^m \mathrm{d}\sigma = \frac{k}{(m+1)(m+2)}\, \sigma^{m+2} \qquad [5.9]$$

where m is the conditional coefficient.

For an assembly of identical or nearly identical elements $m = 0$, hence a stress–strain relationship of the form:

$$\varepsilon = A\sigma^2 \qquad [5.10]$$

or

$$\sigma = B\varepsilon^{\frac{1}{2}} \qquad [5.11]$$

where A and B are two arbitrary constants. Equation (5.11) has been used in several cases for bending and shear initial behaviour. From the derivation conditions, this equation could be valid for the whole range of the deformation. But in practice, we can see that only the initial part was thought to obey this law. The principal range of m for fabric bending was reported to be $-0.1 > m > -0.9$.

In conventional studies, the Oloffson's model has only been applied when $m = 0$ and been used in the initial region of the moment–curvature curve; the latter stage has been considered as a linear relationship and even independent of the frictional element. The present work makes an attempt to modify equation 5.11 into a two-parameter function and to extend it to fit to the whole curve of experimental results using a non-linear regression method. The modified function including two constants α and β is as follows:

$$M = \alpha\rho^{\beta} \qquad [5.12]$$

where M is the bending moment and ρ the curvature.

5.2.2 Bending stiffness

Considering bending stiffness as a constant, the bending curve of fabrics can be described using equation 5.12. If the B–K (bending stiffness, B, versus curvature, K) curve is defined as the first derivative of the M–K curve,

$$B = \alpha\beta\rho^{(\beta-1)} \qquad [5.13]$$

the simulated bending stiffness now is a continuous, non-linear function of the curvature.

5.2.3 Estimation of two constants

Similar to the methods in Chapter 4, there are several ways to estimate the two constants α and β, but the most reliable one should be the non-linear regression method. The second choice may be the application of a general least squares method using more than two points. Suppose there are n sets of data from a bending curve of a woven fabric $(\rho_1, M_1), (\rho_2, M_2), \ldots, (\rho_n, M_n)$, then we have:

$$M_i = \alpha\rho_i^{\beta} \qquad [5.14]$$

So the sum of the squares of deviation from the true line is

$$S = \sum_{i=1}^{n} (M_i - \alpha\rho_i^{\beta})^2 \qquad [5.15]$$

By mathematical operation using the least squares principle, the following two equations can be obtained:

$$\alpha = \frac{\sum_{i=1}^{n} M_i \rho_i^{\beta-1}}{\sum_{i=1}^{n} \rho_i^{\beta}}, \quad \alpha = \frac{\sum_{i=1}^{n} M_i \rho_i^{\beta}}{\sum_{i=1}^{n} \rho_i^{\beta}} \qquad [5.16]$$

5.3 Modelling the bending properties of woven fabrics using viscoelasticity

5.3.1 Introduction

The bending performance of fabrics is characterised through parameters such as bending rigidity and hysteresis. However, the problem of how to separate the viscoelastic and frictional components in hysteresis remains unsolved. A detailed investigation of the bending of woven fabrics that determines the frictional couple through the cyclic bending curve of the fabric is needed. Hence, a theoretical model composed of a standard-solid model in parallel with a sliding element is proposed. The bending properties of woven fabrics are quantitatively studied.

Linear viscoelasticity is in fact applicable to many viscoelastic materials like wool, polyester, nylon and so on. In the study of fabric rheology from the phenomenological viewpoint, two simple rheological models consisting of linearly elastic and frictional elements, proposed by Oloffson (1967), are most popular in the textile literature (Grosberg 1966; Hamilton and Postle, 1974; Gibson and Postle, 1978; Hu, 1996). These models do not account for fibre viscoelastic processes which occur during fabric deformation and recovery. Chapman proposed a theoretical model in which the material is termed as 'generalized linear viscoelastic' and showed that the result fits single wool and nylon fibres at low strains (1 %) under changing temperature and relative humidity (Chapman, 1973; 1974a, 1975). The fabric has been shown to behave as a GLVE sheet in bending with an internal frictional moment (Chapman, 1974b). The frictional couple associated with each fibre in bending is principally considered as a function of strain and absolute time (Chapman, 1974c, 1980; Grey and Leaf, 1975, 1985; Ly, 1985). One of the fundamental ways to characterise the rheology of viscoelastic material is to bend the sample to a designated curvature and observe its transient behaviour. The recovery of fabrics from bending (Chapman, 1976), shear (Asvadi and Postle, 1994), creasing (Chapman, 1974d; Shi *et al*., 2000a,b,c) and wrinkling (Denby, 1974a,b; Denby, 1980; Postle *et al*., 1988) can be calculated through the knowledge of stress relaxation.

5.3.2 The linear viscoelasticity theory in the modelling of bending behaviour

Deformation, stress relaxation and subsequent recovery of fabrics can be studied quantitatively using the rheological model of linear viscoelasticity. Linear viscoelasticity is applicable for many viscoelastic materials when they are deformed to low strain (Postle *et al*., 1988). Modelling the viscoelastic behaviour of materials may involve using simple multiple-element models or generalised integrated forms.

In order to simplify the calculation, the fibre is assumed to be linearly viscoelastic and its bending behaviour can be described by the standard solid model. The fabric is considered to be a viscoelastic sheet with internal frictional constraint. Its bending behaviour can be described by a three-element linear viscoelastic model in parallel with a frictional element, as shown in Fig. 5.2. The model is governed by the following equation (Chapman, 1974a):

$$M(k) = M_{\mathrm{v}}(k) + \dot{k}/|\dot{k}| \times M_{\mathrm{f}} \qquad [5.17]$$

In equation (5.17), $M(k)$ is the bending moment of the fabric, k is the curvature of the fabric at time t, M_{f} is the frictional constraint and m_{v} is the viscoelastic bending moment of the fabric. $\dot{k}$ is the rate of change of curvature (cm/s). The factor $\dot{k}/|\dot{k}|$ is the sign of the curvature change, which means that any curvature change of the fabric is opposed by the frictional constraint M_{f}. The frictional constraint interacts with the viscoelastic behaviour of single fibres to impose a limit on the recovery a fabric may eventually attain.

Frictional constraint restricts free movement of the fibres in fabric during bending. It is supposed that the fabric in bending acts like a linear spring in parallel with a frictional element and the frictional constraint is assumed to be a constant M_0 (Grosberg, 1966; Oloffson, 1967). The couple of the frictional sliding element is termed the 'coercive couple'. The coercive couple for fabrics in bending is half the distance between the cut-offs on the vertical or moment axis of the cyclic bending curve.

The intercept has been interpreted as being entirely due to the frictional moment and equal to $2M_0$ in the past (Grosberg, 1966). However, the frictional moment, in fact, only accounts for a portion of this intercept. Another portion of the intercept will be due to viscoelastic effects because the fibres are viscoelastic in nature (Konopasek, 1980b). In fact, the frictional constant varies with the maximum curvature imposed on the fabric (Ly, 1985). Since constant frictional constraint will lead to greater error and reduce the applicability of the model and the intercept on the bending moment axis made by the hysteresis loop is smaller than the $2HB$ from the Pure Bending Tester in Kawabata's Evaluation System, we assume that the frictional constraint is proportional to the curvature imposed on the fabric, as depicted in Fig. 5.3.

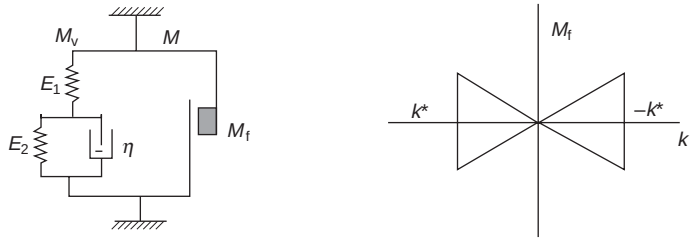

5.3 A three-element-plus-frictional viscoelastic model for bending of fabric.

If a fabric is bent at a constant rate of change of curvature ρ, the viscoelastic bending moment of the fabric of unit length can be expressed as

$$M_v(t) = \rho \int_0^t B(\tau)\,d\tau \qquad [5.18]$$

where $B(\tau)$ is relaxation modulus of the fabric. For a standard solid model, $B(\tau)$ is given by

$$B(\tau) = E_1 e^{-t/T} + \frac{E_1 E_2}{E_1 + E_2}(1 - e^{-t/T}) \qquad [5.19]$$

where the constant $T = \eta/(E_1 + E_2)$ is the relaxation time of the model, E_1 and E_2 are elasticity moduli of the springs, η is the viscosity coefficient of the damper. Substituting equation (5.19) into equation (5.18), the viscoelastic bending moment of the fabric can be written as follows:

$$M_v(t) = \frac{E_1 E_2}{E_1 + E_2}\rho t + \frac{E_1^2}{(E_1 + E_2)^2}\rho\eta(1 - e^{-t/T}) \qquad [5.20]$$

$$= at + b(1 - e^{-t/T})$$

In equation (5.20),

$$a = \frac{E_1 E_2}{E_1 + E_2}\rho, \quad b = \frac{E_1^2}{(E_1 + E_2)^2}\rho\eta$$

When the fabric is cycled between curvature k^* and $-k^*$, a typical hysteresis curve for bending deformation is as shown in Fig. 5.4. The cyclic bending curve can be separated into regions where alternate positive and negative rates of change of curvature are inserted. By applying equation (5.20) the complete bending hysteresis cycle due to the viscoelasticity of the sample can be calculated. Using the Boltzman superposition principle to add the effects caused by the component strain rate for each portion of the hysteresis curve of the viscoelastic component, we can calculate the moment at points 1, 2, 3 and 4 in Fig. 5.4. For bending at a constant rate of ρ and limiting curvature k^*, $k = \rho t$, $t^* = k^*/\rho$, the viscoelastic bending moment at time t^*, $2t^*$, $3t^*$ and $4t^*$, is respectively obtained as

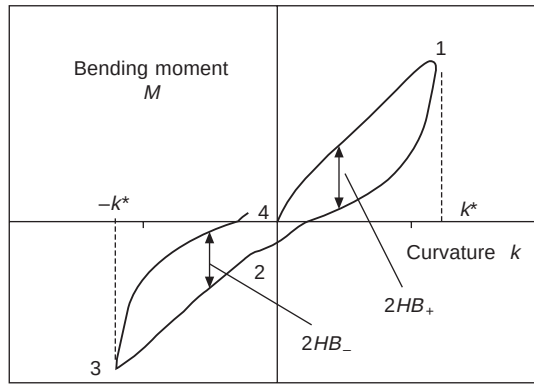

5.4 An idealised hysteresis loop for fabric bending.

$$M_{v1} = M_v(t^*) \qquad (t = t^*) \qquad [5.21]$$

$$M_{v2} = M_v(2t^*) - 2M_v(t^*) \qquad (t = 2t^*) \qquad [5.22]$$

$$M_{v3} = M_v(3t^*) - 2M_v(2t^*) \qquad (t = 3t^*) \qquad [5.23]$$

$$M_{v4} = M_v(4t^*) - 2M_v(3t^*) + 2M_v(t^*) \qquad (t = 4t^*) \qquad [5.24]$$

where M_{v1}, M_{v2}, M_{v3} and M_{v4} are viscoelastic components of the bending moment at points 1, 2, 3 and 4 in Fig. 5.4. Substituting equation (5.22) into equation (5.23), the viscoelastic moments at time t^*, $2t^*$, $3t^*$ and $4t^*$ can be expressed as, respectively

$$M_{v1} = at^* + b(1 - \gamma) \qquad (t = t^*) \qquad [5.25]$$

$$M_{v2} = -b(1 - \gamma)^2 \qquad (t = 2t^*) \qquad [5.26]$$

$$M_{v3} = -at^* - b(1 - 2\gamma^2 + \gamma^3) = -M_{v1} + \gamma M_{v2} \qquad (t = 3t^*) \qquad [5.27]$$

$$M_{v4} = b(1 - \gamma^2)(1 - \gamma)^2 \qquad (t = 4t^*) \qquad [5.28]$$

where

$$\gamma = e^{-t^*/T} = e^{-(E_1+E_2)t^*/\eta} \qquad [5.29]$$

For cyclic bending between curvature k^* and $-k^*$, as depicted in Fig. 5.4, the frictional constraint at points 1, 2, 3 and 4 varies and the total moments at each point can be defined in the following manner:

$$M_1 = M_v + \mu k^* = at^* + b(1 - \gamma) + \mu k^* \qquad (t = t^*) \qquad [5.30]$$

$$M_2 = M_{v2} = -b(1 - \gamma)^2 \qquad (t = 2t^*) \qquad [5.31]$$

$$M_3 = M_{v3} - \mu k^* = -M_{v1} + \gamma M_{v2} - \mu k^* \qquad (t = 3t^*) \qquad [5.32]$$

$$M_4 = M_{v4} = b(1 - \gamma^2)(1 - \gamma)^2 \qquad (t = 4t^*) \qquad [5.33]$$

However, there are only three independent equations in equations (5.30–5.33). Another equation must be established in order to find the solution to

the other two unknown variables. One of the parameters used to characterise the bending properties of the fabric in the KES-FB-2 Bending Tester is 2*HB*, as depicted in Fig. 5.4, which is independent of equation (5.33) and is given by:

$$2HB_{+} = M_{+}(k) - M_{-}(k) = M_{v+}(k) - M_{v-}(k) + 2M_{f}(k)$$
$$= b\left(2 - e^{\frac{k}{\rho T}} - 2e^{\frac{k^{*}-k}{\rho T}} + e^{\frac{2k^{*}-k}{\rho T}}\right) + 2\mu k \qquad [5.34a]$$

and

$$2HB_{-} = M_{+}(-k) - M_{-}(-k) = M_{v+}(-k) - M_{v-}(-k) + 2M_{f}(-k)$$
$$= b\left(2 - e^{-\frac{4k^{*}-k}{\rho T}} + 2e^{-\frac{3k^{*}-k}{\rho T}} + e^{-\frac{2k^{*}+k}{\rho T}} - 2e^{-\frac{k^{*}-k}{\rho T}} - 2e^{-\frac{k^{*}+k}{\rho T}}\right)$$
$$+ 2\mu k \qquad [5.34b]$$

where, the subscript $_{+}$ means the fabric is bent forward and the subscript $_{-}$ means the fabric is bent backwards. $2HB_{+}$ and $2HB_{-}$ are the width of the hysteresis loop at a specific curvature $\pm k$. In the KES-FB Pure Bending Tester, it is defined at curvature ± 1 cm^{-1}. Their average can be obtained as

$$2HB = (2HB_{+} + 2HB_{-})/2 = bQ + 2\mu k \qquad [5.35a]$$

where

$$Q = 0.5\left(4 - e^{-\frac{4k^{*}-k}{\rho T}} + 2e^{-\frac{3k^{*}-k}{\rho T}} + e^{-\frac{2k^{*}+k}{\rho T}} - 2e^{-\frac{k^{*}-k}{\rho T}} + e^{-\frac{2k^{*}-k}{\rho T}}\right.$$
$$\left. - 2e^{-\frac{k^{*}+k}{\rho T}} - 2e^{-\frac{k^{*}-k}{\rho T}} - e^{-\frac{k}{\rho T}}\right) + 2\mu k \qquad [5.35b]$$

Equation (5.33) can be merged as

$$\left.\begin{aligned} M_1 &= M_{v1} + \mu k^{*} = at^{*} + b(1-\gamma) + \mu k^{*} \\ M_2 &= -b(1-\gamma)^2 \\ M_1 + M_3 &= -b\gamma(1-\gamma)^2 \end{aligned}\right\} \qquad [5.36]$$

Solving simultaneous equations (5.35) and (5.36), the parameters are given by

$$\left.\begin{aligned} \gamma &= \frac{M_1 + M_3}{M_2} \\ b &= -\frac{M_1 + M_3}{\gamma(1-\gamma)^2} \\ \mu &= \frac{2HB - bQ}{2k} \\ a &= \frac{M_1 - b(1-\gamma) - \mu k^{*}}{t^{*}} \\ T &= -t^{*}/\ln\gamma \end{aligned}\right\} \qquad [5.37]$$

Then, three parameters of the standard solid model can be obtained as follows:

$$\left.\begin{aligned} E_1 &= \frac{aT + b}{T\rho} \\ E_2 &= \frac{a(aT + b)}{b\rho} \\ \eta &= -T(E_1 + E_2) = -\frac{(aT + b)^2}{b\rho} \end{aligned}\right\} \quad [5.38]$$

Thus, the proposed bending model for a fabric can be established through three points in the moment–curvature curve and a hysteresis parameter.

5.4 Modelling the wrinkling properties with viscoelasticity theory

5.4.1 Introduction

When a fabric is creased and then released, the residual forces in the fibres enable the fabric to unfold or recover. Wrinkle recovery is thus defined as the property of a fabric that enables it to recover from folding deformations. The most common method of testing crease recovery (ISO 2313, IWTO Drift TM 42) and wrinkle recovery (AATCC 66-1990) is to bend a strip of fabric by heavy loading at controlled time and air conditions and measure the angle of recovery after releasing the load.

During wrinkling deformation, all fabrics show a varying degree of inelasticity, such as viscoelasticity and inter-fibre friction, because of the viscoelastic nature of the constituent fibres and the rearrangement within the fibre assembly. Their responses to applied loads are rate- or time-dependent. At any time, the state of stress within a fabric depends on the entire loading history. The viscoelastic nature of the constituent fibre is responsible for the phenomenon of stress relaxation, and the inter-fibre friction provides the fabric frictional stress during deformation and is responsible for the irreversible deformation. Studying these inelastic effects in fabrics enables us to understand and eventually predict important performance characteristics.

In this section the modelling of wrinkling, wrinkle recovery and set of fabrics are established using the rheological model of linear viscoelasticity based on the bending model developed in Section 5.3. The recovery of the fabrics after release from wrinkling is analysed and the wrinkle recovery angle of the fabrics is calculated using the model parameters derived from pure bending test.

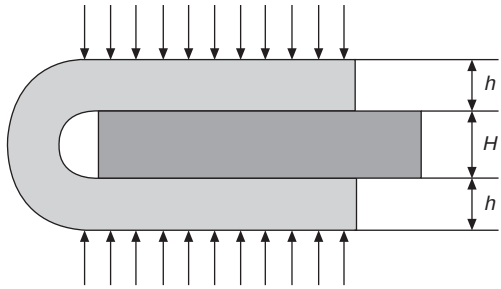

5.5 Wrinkling of a fabric for testing of wrinkle recovery angle.

5.4.2 Modelling the wrinkle recovery angle of woven fabrics

Assume that a woven fabric is simply folded in the warp or weft direction and pressed together by a uniform pressure normal to the surface of the fabric, as shown diagrammatically in Fig. 5.5.

When a fabric is held at a fixed curvature k_0 for a period of time t, and if the fabric is considered as viscoelastic sheets with internal constraints, which follow the three-element model in parallel with a sliding element and the frictional constraint is considered to be proportional to the curvature of the fabric as shown in Figs 5.1 and 5.2, the relaxation stress for the standard solid model may expressed as (Creus, 1986; Yan, 1990)

$$M_v(t) = E_1 k_0 e^{-t/T} + \frac{E_1 E_2}{E_1 + E_2} k_0 (1 - e^{-t/T}) \qquad [5.39]$$

It can be found that the relaxation moment decreases progressively when the fabric is held at a constant curvature. That is to say, the residual moment in the fibre drops with time or the moment needed to maintain the fabric at a constant curvature reduces gradually as indicated in Fig. 5.6(a).

The fabric is creased for a length of time w and then released against a restraining couple M_f. Based on the Boltzmann superimposition principle, removing the applied force that maintains constant curvature k_0 is equivalent to a $-M_r$ being exerted in the opposite direction on the fabric, that is, $M_r(t)$ ($t > w$) equal to $M_v(t)$ ($t > w$) in magnitude, but opposite in direction, as shown in Fig. 5.6(b). M_r acts on the fabric and makes it recover from wrinkling or creasing deformation. M_r can be divided into two portions. One portion, M_{rv} acts on the standard solid element. Another portion, M_{rf} is assumed in the frictional element. The frictional constraining couple is directly proportional to the curvature of the fabric according to the assumption above. If the fabric has a curvature k_r from curvature k_0 under the action of M_r, then the frictional constraining couple is equal to μk_r.

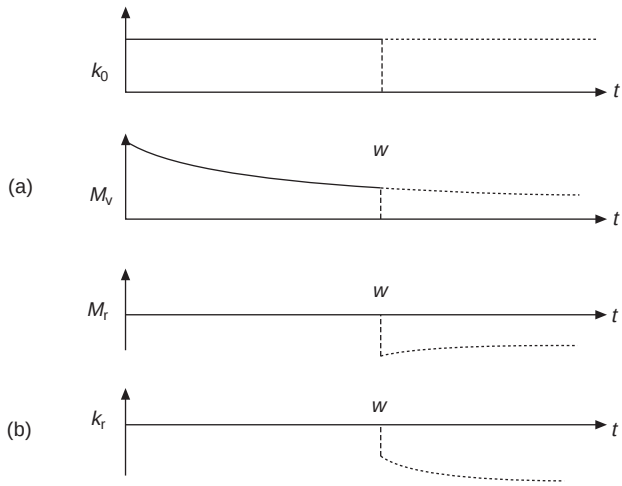

5.6 Stress and strain relation of the model during insertion of wrinkles and wrinkle recovery (a) step curvature applied during insertion of wrinkles and stress relaxation; (b) residual stress and curvature recovery of the fabric after releasing.

At instant t after the fabric is released, the moment can be expressed as

$$M_r(w + \tau) = M'_v(\tau) + \mu k_r \qquad [5.40]$$

where k_r is the curvature of the fabric produced by M_r. To calculate wrinkle recovery of the fabric after release from a fixed curvature, we consider now the curvature change of the fabric under a stress $-M_r$. The constitutive equations for the standard solid element can be established as follows:

$$M'_{rv} + \frac{\eta}{E_1 + E_2}\dot{M}'_{rv} = \frac{E_1 E_2}{E_1 + E_2}k_r + \frac{E_1}{E_1 + E_2}\eta\dot{k}_r \qquad [5.41]$$

Substituting equation (5.40) into and rearranging equation (5.41) gives

$$\dot{k}_r + \left(\frac{E_1 + E_2}{E_1\eta}\mu + \frac{E_2}{\eta}\right)k_r = \frac{E_2}{\eta}k_0 - \frac{\mu}{E_1} \qquad [5.42]$$

Solving equation (5.42), the recovery deformation of the fabric is given by

$$k_r(\tau) = \frac{E_1 k_0}{(E_1 + E_2)(\mu + E_1)}(E_1 e^{-w/T} + E_2)e^{-\left(\frac{E_1+E_2}{E_1\eta} + \frac{E_2}{\eta}\right)\tau} + \frac{E_1 E_2 k_0 - \mu\eta}{(E_1 + E_2)\mu + E_1 E_2}\left[1 - e^{-\left(\frac{E_1+E_2}{E_1\eta} + \frac{E_2}{\eta}\right)\tau}\right] \qquad [5.43]$$

The remnant curvature of the fabric at moment τ after the applied force is removed can be expressed as

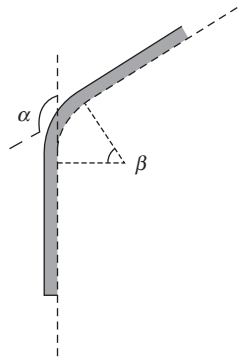

5.7 The proposed model for the wrinkle recovery angle of a fabric.

$$k(\tau) = k_0 - k_r(\tau) \quad [5.44]$$

We assume that the bent portion of the fabric takes a semi-circular profile during the insertion of wrinkles and a circular arc profile during recovery from wrinkles, as shown in Fig. 5.7. If the length of the circular arc is constant and equal to that of the semi-circle, that is

$$\frac{\pi}{k_0} = \frac{\pi - \alpha}{k} \quad [5.45]$$

then, the wrinkle recovery angle of the fabric can be expressed as

$$\alpha = \pi\left(1 - \frac{k}{k_0}\right) = \pi\frac{k_r}{k_0} \quad [5.46]$$

The instantaneous wrinkle recovery angle α_0 and the maximum wrinkle recovery angle α_∞ at time $\tau = 0$ and $\tau = \infty$ can be derived respectively as follows:

$$\alpha_0 = \frac{E_1}{(E_1 + E_2)(\mu + E_1)}(E_1 e^{-w/T} + E_2) \times 180° \quad [5.47]$$

$$\alpha_\infty = \frac{E_1E_2k_0 - \mu\eta}{(E_1 + E_2)\mu + E_1E_2}\frac{180°}{k_0} \quad [5.48]$$

It can be seen that the wrinkle recovery angle is completely determined once we know the values of k_0, w, τ and the parameters of the elements in the model. Thus, the wrinkle recovery angle of the fabric can be predicted using the model parameters derived from the pure bending test.

5.5 Anisotropy of woven fabric bending properties

5.5.1 Introduction

Bending behaviour of a woven fabric can be characterised by bending rigidity (B) and bending hysteresis ($2HB$). Bending rigidity is the resistance of a

fabric to bending, which can be defined as the first derivative of the moment–curvature curve. Bending hysteresis is the energy loss within a bending cycle when a fabric is deformed and allowed to recover, denoting the difference in bending moment between the loading and the unloading curves when the bending curvature is fixed.

Postle *et al.* and Hu have proved the close relationship between bending rigidity and bending hysteresis. In particular, Postle *et al*. reported very good correlation between the bending and the hysteresis parameters measured from fabric bending deformation recovery curves (1988). Moreover, the research done by Chung and co-workers (Chung *et al*., 1990; Chung and Hu, 2000) indicates that the correlation coefficient of bending stiffness and bending hysteresis is quite high, 0.9333 for cotton fabric. For worsted and Schengen woven fabrics, B and $2HB$ are also very high, 0.7872 and 0.7596 respectively. This implies that bending stiffness and bending hysteresis are not independent, but have a linear relationship (Hu, 1994).

There may be some differences in the mechanism operating in bending rigidity and bending hysteresis of woven fabrics but, based on the above findings, it is assumed that they have similar mechanisms. Thus this section discusses an attempt to apply the existing models for bending rigidity to bending hysteresis of plain woven fabrics. Also presented is an attempt to examine which of the existing models is the best for predicting bending hysteresis.

5.5.2 Directionality of fabric bending rigidity

Peirce (1930) produced a formula for calculating the stiffness of a fabric in any direction in terms of the stiffness in the warp and weft direction. This was derived from the theory for homogenous elastic material and it was found to be empirically satisfactory. It is suggested that the reason for this is that most of the fabrics which Peirce tested were made from cotton. In addition, he also reported a formula to predict the bending stiffness in various directions, in which the values in the warp and weft directions were known.

Go *et al.* (1958) measured the bending stiffness of fabrics using the heart loop method. They indicated that the bending stiffness of the fabric is dependent on the bending model of the test piece. The bending stiffness of fabric having long floats on its surface was smaller in face-to-face bending than back-to-back. The effect of the crimp of the component yarn of fabric on the fabric bending stiffness was generally small. Later, Go and Shinohara (1962) reported that on the polar diagram of bending stiffness there was minimum presented at 45° to the warp when the fabric was bent. Their formula neglected the restriction at the interaction of the warp and weft directions. They concluded that the stiffness of textile fabrics depended upon their bending directions and that, in general, the stiffness in bias directions was relatively small.

Cooper (1960) used cantilever methods to determine fabric stiffness and stated that there was no evidence to suggest that there was any appreciable shearing of the fabric caused by its own weight. He concluded that the stiffness of a fabric may vary with direction of bending in different ways, but for most practical purposes measurement along warp, weft and one other direction was sufficient to describe it.

Cooper conducted a detailed study of the stiffness of fabrics in various directions and has produced polar diagrams of bending stiffness. He found that some fabrics had a distinct minimum value at an angle between the warp and weft direction while others had similar values between the warp and weft. In general, viscose rayon fabrics provided an example of the former and cotton fabrics an example of the latter.

These effect were explained in terms of the fabric bending stiffness in the warp and weft direction and the resistance offered by the yarns to the torsional effects which are inseparable from bending at an angle to warp and weft (Cooper, 1960). He concluded that the resistance offered by the yarns to the torsional deformation is low when the interaction between the yarns is low and vice versa.

Shinohara *et al*. (1980) derived an equation empirically which is similar to the equation introduced by Peirce and analysed the problems using three-dimensional elasticas. They assumed the constituent yarns of woven fabrics to be perfectly elastic, isotropic, uncrimped and circular in cross-section, and to behave in a manner free from inter-fibre friction. In addition, they also presented another equation containing a parameter n which was related to V introduced by Cooper (1960) in order to predict the shape of a polar diagram.

5.5.3 Theoretical study of fabric bending properties

Peirce first introduced the bending rigidity of a fabric by applying an equation in his classical paper as follows:

$$B = wc^3 \qquad [5.49]$$

where B is the bending rigidity, w is the weight of the fabric in grams per square cm and c is the bending length. He also introduced another equation for bending rigidity in various directions. This formula enabled the value for any direction to be obtained when the values in the warp and weft directions were known:

$$B_\theta = \left[\frac{\cos^2\theta}{\sqrt{B_1}} + \frac{\sin^2\theta}{\sqrt{B_2}} \right]^{-2} \qquad [5.50]$$

where B_1, B_2 and B_θ are bending rigidities in warp, weft and θ directions, respectively.

A similar equation could also be considered empirically by Shinohara *et al.* (1980):

$$B_\theta = (\sqrt{B_1}\cos^2\theta + \sqrt{B_2}\sin^2\theta)^2 \quad [5.51]$$

Go *et al.* also reported an equation which was theoretically derived by neglecting twist and frictional effects from equation (5.50):

$$B_\theta = B_1\cos^4\theta + B_2\sin^4\theta \quad [5.52]$$

(Go *et al.* 1958; Go and Shinohara 1962).

Later, Cooper (1960) presented an equation including twist effect. The results of the twisting effect were found to be valuable in practical applications and so equation (5.53) was derived:

$$B_\theta = B_1\cos^4\theta + B_2\sin^4\theta + (J_1 + J_2)\cos^2\theta\sin^2\theta \quad [5.53]$$

where J_1 and J_2 are constants due to torsional moment.

Chapman and Hearle (1972) also derived a similar equation by energy analysis of helical yarns as follows:

$$\begin{aligned} B_T &= n_1 v_1 \sin^2\theta(B\sin^2\theta + J_y\cos^2\theta) \\ &\quad + n_2 v_2\cos^2\theta(B\cos^2\theta + J_y\sin^2\theta) \\ B_T &= n_1\theta + \eta\cos^2\theta + n_2 v_2\cos^2\theta(B\cos^2\theta + J) \end{aligned} \quad [5.54]$$

where B_T is an expression for the bending rigidity per unit width of a thin fibre web of linearly elastic fibres and there are n_1 yarns per unit length in the warp direction, each containing v_1 number of fibres, and n_2 yarns per unit length in the weft direction, each containing v_2 number of fibres. They assume that they have a two-dimensional assembly of very long straight fibres of the same type, with bending rigidity B and torsional rigidity J_y. Their approach utilises energy considerations instead of the 'force method'. Chapman and Hearle's model involves many variables which will complicate the mathematical calculation. Their approach is, in fact, very similar to Cooper's so Cooper's model is chosen for the study.

From equation (5.53), B_1 and B_2 may be obtained directly by experimental work while J_1 and J_2 cannot. The theoretical treatment suggests that measurements of stiffness in two directions are insufficient to define a fabric's bending properties, since different types of variation with direction are still possible for fabrics with similar B_1 and B_2. An investigation into a third direction is therefore necessary, and the most convenient in practice is at bias direction (45°). In this direction, twisting effects are small provided that B_1 and B_2 are similar in magnitude. Nevertheless, the sum $(J_1 + J_2)$ may be deduced from measurements in three different directions by considering specimens cut along the warp, weft and 45° directions. Therefore, when considering $\theta = 45°$,

$$B_{45} = B_1 \cos^4 45° + B_2 \sin^4 45° + (J_1 + J_2) \cos^2 45° \sin^2 45°$$

$$= B_1\left(\frac{1}{\sqrt{2}}\right)^4 + B_2\left(\frac{1}{\sqrt{2}}\right)^4 + (J_1 + J_2)\left(\frac{1}{\sqrt{2}}\right)^2\left(\frac{1}{\sqrt{2}}\right)^2 \quad [5.55]$$

$$= \frac{1}{4}(B_1 + B_2 + J_1 + J_2)$$

where

$$J_1 + J_2 = 4B_{45} - (B_1 + B_2)$$

The term $(J_1 + J_2)$ is replaced by the stiffness value at the warp, weft and 45° directions. We may use this result to calculate other bending rigidities over all possible directions as in equation (5.56):

$$B_\theta = B_1 \cos^4 \theta + B_2 \sin^4 \theta + [4B_{45} - (B_1 + B_2)] \cos^2 \theta \sin^2 \theta \quad [5.56]$$

In Cooper's paper, he argued that the shape of polar diagrams of bending rigidity B may show three types of variation between fabrics. The ratio $(J_1 + J_2)/(B_1 + B_2) = V$ is introduced to predict the trends in polar diagrams. When the term $(J_1 + J_2)$ is replaced by the stiffness values of warp, weft and 45° directions, the equation for the ratio V will change as follows:

$$V = \frac{4B_{45} - (B_1 + B_2)}{B_1 + B_2} \quad [5.57]$$

Cooper's model for calculation of ratio V is dependent on bending rigidity (B_1 and B_2) and torsional rigidity (J_1 and J_2). This leads to different shaped polar diagrams. Furthermore, different ratios of bending rigidity in warp and weft directions can also contribute different shapes of polar diagrams. When the torsional rigidity is replaced by the bending rigidity of warp, weft and 45° directions, the calculation of ratio V is simplified.

From the results provided by Cooper (1960), it may be seen that the range of ratio V is between 0 and 1. He found that some fabrics with very open structure had a distinct minimum value at an angle between warp and weft direction when $V = 0$. In this case, the model is identical to that derived by Go *et al.* (1958). When $V = 1$, these minima are absent and the model is qualitatively similar to that described by Peirce (1937) and Shinohara *et al.* (1980).

In Cooper's model (1960), the coefficient of $\cos^2\theta \sin^2\theta$ was related to the torsional rigidities of the yarn. It was found that the polar diagram of fabric bending rigidity fitted reasonably with other models. However, there is a limitation, which relates to ratio V (equation 5.57) introduced by Cooper (1960). Since fibres display marked non-linear viscoelasticity, and this is superimposed on a complicated yarn and fabric geometry, this also gives rise to frictional restraints between fibres and between yarns. If the fabric is bent

in the bias direction, high inter-yarn friction arises due to the relative movement of the yarns (Chapman *et al.*, 1972); it is, therefore, impossible to obtain $V = 0$.

On Cooper's theoretical polar diagram (1960), distinct minima are presented in the polar diagram of fabric bending rigidity between the two principal directions when a very open plain fabric is examined. Go *et al.*'s (1958) model may be applicable to a very open structure fabric as the twist and frictional effect in this type of fabric is small. However, their model cannot be applied in the prediction of fabric bending rigidity of other types of fabrics.

Since observed values do not always agree with the theoretical model (equation 5.51) derived by Shinohara *et al.* (1972), they presented another model containing a parameter n which relates to V introduced by Cooper (1960) as follows:

$$B_\theta = B_1 \cos^4 \theta + B_2 \sin^4 \theta + 2n\sqrt{B_1 B_2} \cos^2 \theta \sin^2 \theta \qquad [5.58]$$

and

$$\frac{V}{n} = \frac{2\sqrt{B_1 B_2}}{B_1 + B_2} \qquad [5.59]$$

where V/n is a ratio of geometrical mean to arithmetical mean of B_1 and B_2. From experimental results on commercially available fabrics, Shinohara *et al.* found that the values of n are in the range from 0 to 1 and minimum values exist in 45° directions for certain types of fabrics. The term n presented by Shinohara *et al.* (1980) is also used to predict the trends in polar diagrams, and similar trends are observed in Cooper's ratio V. They reported that tight fabrics generally have larger values of n, and sleazy fabrics have a smaller value of n.

5.5.4 Polar diagrams of the bending model

5.5.4.1 General features of the polar diagrams

Similar polar diagrams are observed from three of the existing models (Peirce's model, Shinohara *et al.*'s model, and Cooper's model). These polar diagrams and the diagram produced from Go *et al.*'s model can be classified generally into two types according to their shape. The polar diagrams of various values of B_1/B_2 in Types 1 and 2 models are shown in Fig. 5.8, which demonstrates the theoretical polar diagrams of fabric bending rigidity in various directions.

It can easily be observed from Fig. 5.8 that the anisotropy of Type 2 omits the resistance at the intersection of warp and weft. Therefore, distinct minima are present between the warp and weft directions. However, a circular shaped polar diagram is obtained when B_1 equals B_2 in anisotropy of Type 1. If the

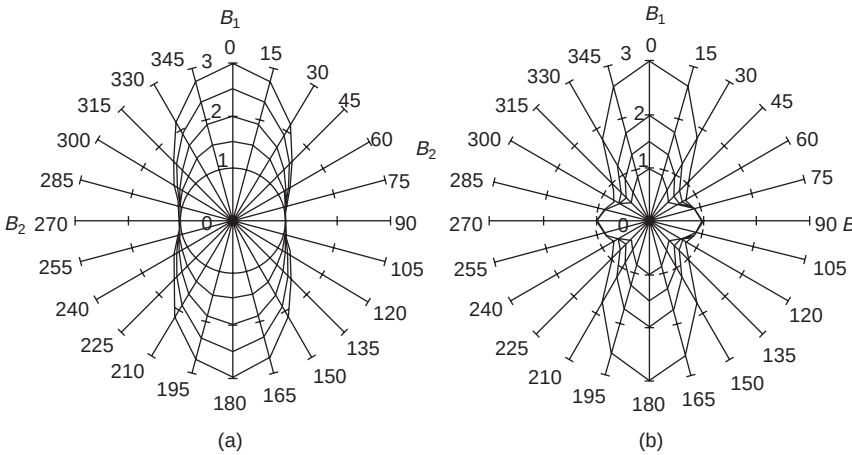

5.8 Theoretical curves of bending rigidity of fabric anisotropy; (a) type 1: by Peirce, Shinohara *et al.* and Cooper; (b) type 2: by *Go et al.*

difference between the bending rigidity B_1 and B_2 becomes larger, an ellipse or gourd shape is illustrated in the polar diagram of fabric bending rigidity.

5.5.4.2 Comparison of four models

In this section, the predictability of the four models (Go *et al.*, Peirce, Shinohara *et al.* and Cooper) discussed above will be compared. Additionally, the effect of ratio *V* on plain woven fabrics in different weave densities will be investigated as will the shapes of the polar diagrams of bending hysteresis from different values of ratio *V* on cotton plain woven fabrics.

For ease of comparison it is convenient to fix the bending hysteresis in the warp direction so that changes occurring along any other directions can be easily observed from the polar diagrams. This fixed bending hysteresis can be obtained by averaging all results recorded in the warp direction, and then multiplying or dividing the bending hysteresis of each fabric by this average value. In this way, the points in the warp direction can be fixed and any differences other than warp direction can be seen in the polar diagrams of different fabrics. Trends in the ratio *V* can also be observed with different types of plain woven fabrics.

Figure 5.9 illustrates the bending hysteresis of lighter (loose) and heavier (tight) plain fabrics produced from the outputs of four models against the experimental result. As Go *et al.*'s model neglects the twist and frictional effect, the polar diagram of this model exhibits a cross shape with minima around the 45° direction. Peirce's, Shinohara *et al.*'s and Cooper's models show elliptic shapes.

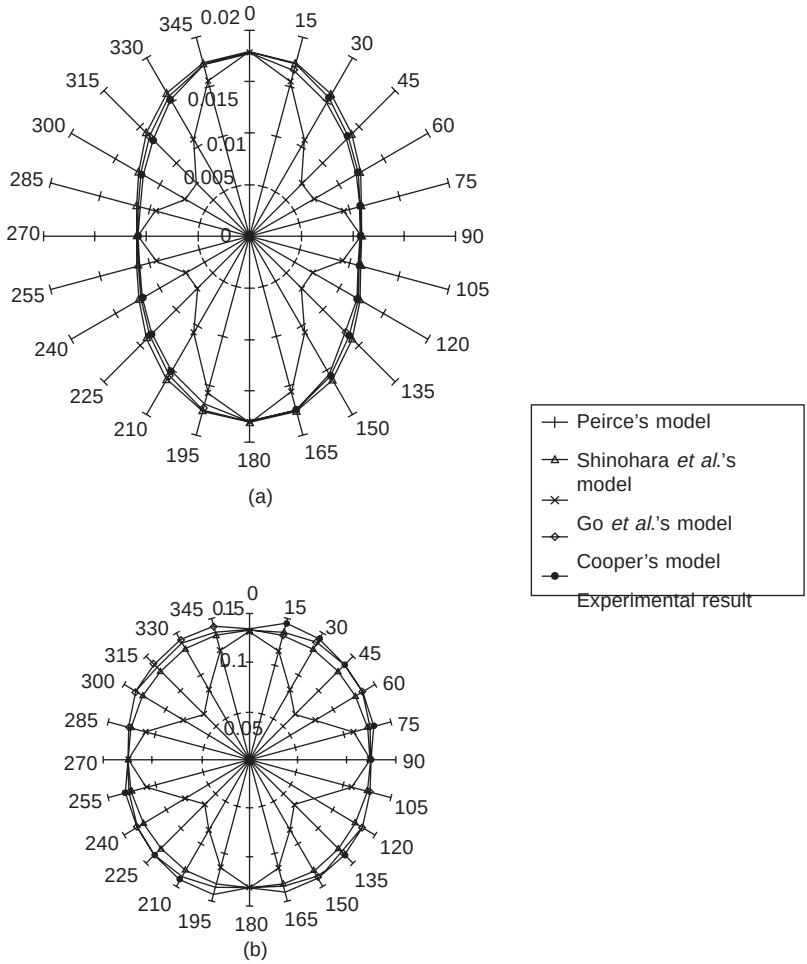

5.9 Comparison of four models with the experimental result of bending hysteresis: (a) light plain woven fabric; (b) heavy plain woven fabric.

All experimental results on plain woven fabrics are close to values calculated from Peirce's, Shinohara *et al.*'s and Cooper's models. It is also found that the average deviation between Go *et al.*'s model and the experimental result is the largest when compared with other models, which indicates that Go *et al.*'s model cannot be applied to the prediction of polar diagrams of bending hysteresis. Therefore, the twisting and frictional effects play significant roles in the calculation of bending properties.

From Cooper's theoretical polar diagram (Cooper, 1960), there are distinct minima in the polar diagram of bending rigidity between warp and weft directions when a very open plain light woven fabric is examined. Go *et al.*'s model may also be applicable to loose fabrics as the twist and frictional

effect in a very open plain fabric is small. In contrast, these minima are absent in the polar diagrams of bending hysteresis. Bending hysteresis is a measurement of inter-yarn friction. When the fabric is bent on the bias, relative movement of the yarns occurs and is maintained by high inter-yarn friction. Therefore, there are no minima present on the bias directions. In Fig. 5.9(a), it is found that Peirce's, Shinohara *et al.*'s and Cooper's models are well fitted to the polar diagrams of bending hysteresis of loose fabrics. However, Go *et al.*'s model should not be applied to the prediction of the shape of a polar diagram of bending hysteresis in loose fabric.

Another fact is that each model produces larger deviation on heavy fabrics than on light fabrics. Besides, it is not difficult to see from Fig. 5.9(b) that the highest value of the bending hysteresis of heavy fabrics is observed around 15° to the warp. It also reveals that the component around this angle contributes the highest bending hysteresis. However, beyond 15°, the bending hysteresis of these fabrics decreases with the increase in angle.

In addition, although Peirce's, Shinohara *et al.*'s and Cooper's models can all be applied to the prediction of polar diagrams of bending hysteresis for loose to tight plain woven fabrics, of the three, Cooper's model presents the lowest deviation from the experimental results. Therefore, it can be seen that the twist and frictional effects in Cooper's model play an important role in the prediction of bending hysteresis on either loose or tight plain woven fabrics. Moreover, when comparing the bending hysteresis of loose and tight plain woven fabrics, the deviation in loose plain fabric is smaller than that in tight plain fabric.

From the above analysis, we may conclude that Cooper's model is the most reliable in the prediction of bending hysteresis in both loose and tight plain woven fabrics.

5.5.4.3 Effect of ratio V on bending hysteresis

Figure 5.10 illustrates the *HB* polar diagrams of eight different types of plain cotton fabrics, from which we can see that the trends are spreading outwards along the weft direction with the increase in ratio *V*. If the ratio *V* is larger than 1.10, the maximum value of bending hysteresis will be observed at around 15° to the warp.

The loose structure allows the movement of yarns along the warp and weft directions. The floating yarns present in this structure may lead to lower inter-yarn friction. As a result, the lowest bending hysteresis is obtained from the loose fabrics. On the contrary, the tight structure avoids yarn movement and this will increase the bending hysteresis of the fabrics. Therefore, larger bending hysteresis leads to the expansion of the polar diagram along the weft direction. The predicted shapes of the polar diagrams of bending hysteresis from ratio *V* of cotton plain woven fabrics are given in Fig. 5.11.

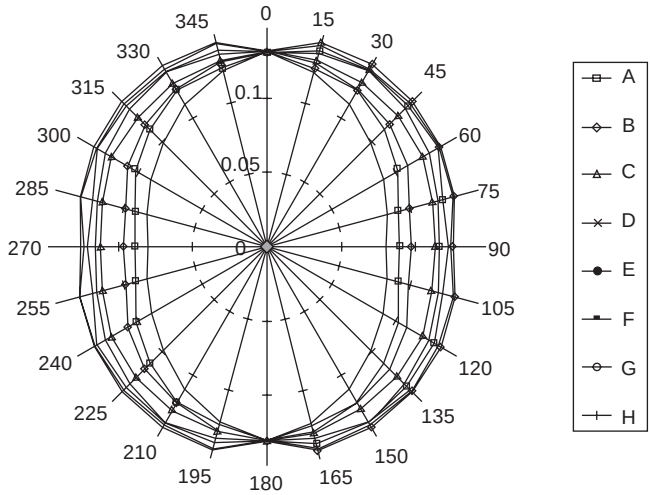

5.10 Effect of ratio *V* on bending hysteresis of plain woven fabrics.

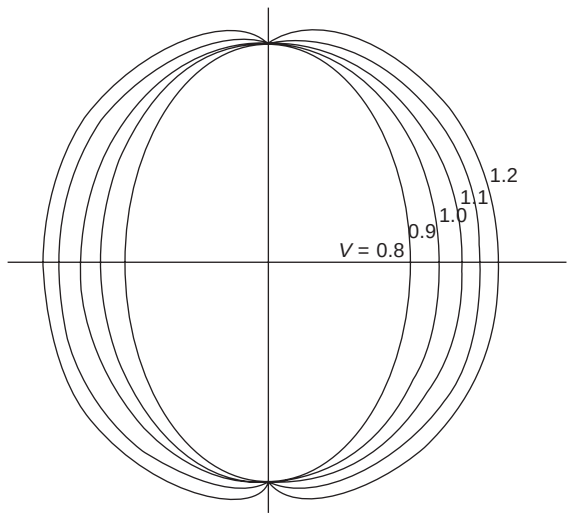

5.11 The relationship between ratio *V* and bending hysteresis of cotton plain woven fabrics.

5.5.4.4 Effect of weft density on polar diagram

Similar to the effect of ratio *V*, with the increase in weft density, the *HB* polar diagrams also exhibit a tendency to spread outwards, as shown in Fig. 5.12.

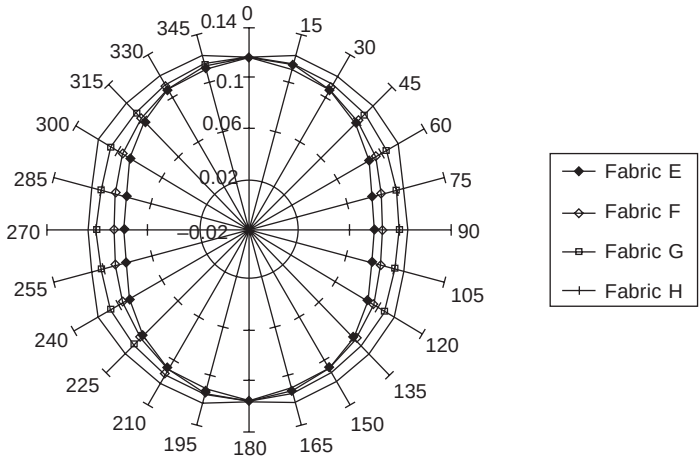

5.12 Effect of weft density of plain woven fabrics. Ranking of weft density: $E < F < G < H$.

5.6 Summary

This chapter presents a comprehensive study of the bending properties of woven fabrics. After an explanation of the general concept of bending properties, two different methods, non-linear regression technique and viscoelasticity theory, are introduced to model the bending behaviour of woven fabrics. Finally, as in Chapter 4, a study of the anisotropy of the bending properties of woven fabrics is also provided. We may draw the following conclusions from this chapter:

(1) Non-linear regression techniques can be successfully used to model the bending curves of woven fabrics based on Oloffson's rheological model. The estimates obtained using non-linear regression seem to be different from those used in the existing research. In addition, bending stiffness is thought to be continuous and can be obtained by the differentiation of the moment–curvature curve with respect to curvature.

(2) The inelastic bending behaviour of woven fabrics can be quantitatively analysed using linear viscoelasticity theory. With the rheological model developed, it is found that the bending properties of the fabric under low curvature can be characterised using a standard solid element in parallel with a frictional element. Element parameters of the model can be determined through three points in the bending curve and the bending hysterisis. The difference between $2HB+$ and $2HB-$ and the intercept of the curve at moment axis should be attributed to friction between the fibres.

(3) Based on Chapman's assumption of a semi-circular form for a fabric

bend, a simple rheological model consisting of a linearly elastic element and a frictional element is successfully used to study creasing of the fabric strips and the compression of the fabric loops. The relationship between the creasing behaviour and deformation is established and solutions are given for a linearly elastic material with constant internal frictional constraint. In addition, the formula deduced by the authors can provide a better fit than the formula given by Chapman.

(4) An extensive study of the existing bending hysteresis models reveals that Peirce's, Shinohara *et al.*'s and Cooper's models can be applied to predict the bending hysteresis anisotropy of various apparel woven fabrics, but Go *et al.*'s model can be applied only to fabrics with very open structure. This finding confirms the statement that the twisting and frictional effects have a significant role in bending properties. Moreover, all the four models are better used to predict light fabrics. In particular, Cooper's model is found to be the best one to predict the anisotropy of bending rigidity and it is also the only one that can be extended to industrial woven fabrics.

5.7 References

AATCC Test Method 66 (1990), *Wrinkle Recovery of Fabrics: Recovery Angle Method*, Research Triangle Park, NC, AATCC.

Abbott G M, Grosberg P and Leaf, G A V (1973), The elastic resistance to bending of plain-woven fabrics, *J Text Inst*, **64**, 346–362.

Asvadi S and Postle R (1994), An analysis of fabric large strain shear behaviour using linear viscoelasticity theory, *Text Res J*, **64**(4), 208–214.

Brown P R (1998), *Large Deflection Bending of Woven Fabric for Automated Material Handling* Master's thesis, NC, North Carolina State University, Raleigh.

Brown III P R, Buchanan D R and Clapp T G (1990), Large deflection bending of woven fabric for automated material handling, *J Text Inst*, **81**, 1.

Chapman B M (1973), Bending stress relaxation and recovery of wool, nylon 66, and terylene fibers, *J App Polym Sci*, **17**, 1693–1713.

Chapman B M (1974a), A model for crease recovery of fabrics, *Text Res J*, **44**, 531–538.

Chapman B M (1974b), Determination of the rheological parameters of fabric in bending, *Text Res J*, **45**, 137–144.

Chapman B M (1974c), Linear superposition of viscoelastic responses in non-equilibrium system, *J App Polym Sci*, **18**, 3523–3526.

Chapman B M (1974d), The importance of inter-fibre friction in wrinkling, *Text Res J*, **45**, 531–538.

Chapman B M (1975), The rheological behaviour of keratin during the aging process, *Rheol Acta*, **14**, 466–470.

Chapman B M (1976), Bending and recovery of fabrics under conditions of changing temperature and relative humidity, *Text Res J*, **46**, 113–122.

Chapman B M (1980), Viscoelastic, frictional and structural effects in fabric wrinkling, in *Mechanics of Flexible Fibre Assemblies* (*NATO Advanced Study Institute Series: E*

Applied Sciences No. 38) Hearle J W S, Thwaites J J and Amirbayat J (eds), The Netherlands, Alpen aan den Rijn, Sijhoff and Noordhoff.

Chapman B M and Hearle J W S (1972), The bending and creasing of multicomponent visco-elastic fibre assemblies part I: general consideration of the problem, *J Text Inst*, **63**, 385–403.

Chung S P and Hu J L (2000), Bending behaviour of woven fabrics with a vertical seam, *Text Res J*, **70**(2), 48–53.

Chung S P, Hu J L and Lo M T (1999), Effect on seam allowance of a plain seam on bending of woven fabrics, *Res J Text Appl*, **3**(1), 45–64.

Clapp T G and Peng H (1991), A comparison of linear and non-linear bending methods for predicting fabric deformation in automated handling, *J Text Inst*, **82**, 341.

Cooper D N E (1960), The stiffness of woven textiles, *J Text Inst*, **51**, T317–335.

Creus G J (1986), Viscoelasticity-basic theory and applications to concrete structure, in *Lecture Notes in Engineering 16*, C A Brebbia and S A Orszag (eds), Heidelberg, Springer-Verlag, Berlin.

De Jong S and R Postle (1977), An energy anlysis of woven-fabric mechanics by means of optical-control theory part II: pure-bending properties, *J Text Inst*, **68**, 62–369.

Denby E F (1974a), The wrinkling of wool worsted fabrics part I: fibre and yarn deformation in bending, *J Text Inst*, **65**, 239–245.

Denby E F (1974b), The wrinkling of wool worsted fabrics part II: bending set in single fibres and fabric and the effect of ageing, *J Text Inst*, **65**, 246–249.

Denby E F (1980), The interconversion of stress-relaxation and recovery: some applications, *J Text Inst*, **71**, 201–209.

Ghosh T K, Batra S K and Barker R L (1990a), The bending behaviour of plain-woven fabrics part I: a critical review, *J Text Inst*, **81**(3), 245–255.

Ghosh T K, Batra S K and Barker R L (1990b), The bending behaviour of plain-woven fabrics part II: the case of bilinear thread-bending behaviour and the effect of fabric set, *J Text Inst*, **81**, 255–271.

Ghosh T K, Batra S K and Barker R L (1990c), The bending behaviour of plain-woven fabrics part III: the case of linear thread-bending behaviour, *J Text Inst*, **81**, 273–287.

Gibson V L and Postle R (1978), An analysis of the bending and shear properties of woven, double-knitted outerwear fabrics, *Text Res J*, **48**, 14–27.

Go Y and Shinohara A (1962), Anisotropy of the crease recovery of textile fabrics, *J Text Mach Soc Japan*, **8**, 33–38.

Go Y, Shinohara A and Matsuhashi F (1958), Viscoelastic studies of textile fabrics part VI: anisotropy of the stiffness of textile fabrics, *J Text Mach Soc Japan*, **14**, 170–174.

Grey S J and Leaf G A V (1975), The nature of inter-fibre frictional effects in woven-fabric bending, *Text Res J*, **45**, 137–144.

Grey S J and Leaf G A V (1985), The nature of inter-fibre frictional effects in woven-fabric bending, *J Text Inst*, **76**, 314–322.

Grosberg P (1966), The mechanical properties of woven fabrics part II: the bending of woven fabrics, *Text Res J*, **36**, 205–211.

Grosberg P (1980), The bending of yarns and plain woven fabrics, in *Mechanics of Flexible Fibre Assemblies* (*NATO Advanced Study Institute Series: E Applied Sciences No. 38*), Hearle J W S, Thwaites J J and Amirbayat J (eds), The Netherlands, Alpen aan den Rijn, Sijthoff and Noordhoff, 197–209.

Hamilton R J and Postle R (1974), Bending and recovery properties of wool plain knitted fabrics, *Text Res J*, **44**, 336–343.

Hu J L (1994), *Structure and Low-stress Mechanics of Woven Fabrics* (PhD thesis, University of Manchester Institute of Science and Technology).

Hu J L (1996), Modelling of bending behaviour of woven fabric, *J China Text Univ (Eng Ed)*, **13**, 1–6.

Hu J L, Lo W and Lo M T (2000), Bending hysteresis of plain woven fabrics in various directions, *Text Res J*, **17**(3), 20–36.

Hu J L, Shi F J and Yu T X (1999), Investigation on bending and creasing of woven fabrics under low curvature, *J China Text Univ*, **16**(2), 26–31.

Hu J L, Xin B J and Yan H J (2002), Measuring and modelling 3D wrinkles in fabrics, *Text Res J*, **72**(10), 863–869.

ISO 2313-1972 (E) textile fabrics, *Determination of the recovery from creasing of a horizontally folded specimen by measuring the angle of recovery*, Geneva, ISO.

IWTO Drift TM 42 crease pressing performance test.

Konopasek M (1970), *Improved Procedures for Calculating the Mechanical Properties of Textile Structures*, PhD thesis, University of Manchester Institute of Science and Technology.

Konopasek M (1980a), Computational aspects of large deflection analysis of slender bodies, in *Mechanics of Flexible Fibre Assemblies' NATO Advanced Study Institute Series: E Applied Sciences No. 38*, Hearle J W S, Thwaites J J and Amirbayat J (eds), The Netherlands, Alpen aan den Rijn, Sijthoff and Noordhoff, 275–292.

Konopasek M (1980b), Textile application of slender body mechanics, in *Mechanics of Flexible Fibre Assemblies NATO Advanced Study Institute Series: E Applied Sciences No. 38*, Hearle J W S, Thwaites J J and Amirbayat J (eds), The Netherlands, Alpen aan den Rijn, Sijthoff and Noordhoff, 293–310.

Liversey R G and Owen J D (1964), Cloth stiffness and hysteresis in bending, *J Text Inst*, **55**, T516–529.

Lloyd D W, Shanahan W J and Konopasek M (1978), The bending of heavy fabric sheets, *Int J Mech Sci*, **20**, 521–527.

Ly N G (1983), Bending strain in a sharp fabric crease, *Text Res J*, **53**, 571–573.

Ly N G (1985), The role of friction in fabric bending, in *Objective Measurement: Application to Product Design and Process Control*. Kawabata S, Postle R and Niwa M (eds), Osaka, Textile Machinery Society of Japan, 481–488.

Oloffson B (1967), A study of inelastic deformations of textile fabrics, *J Text Inst*, **58**, 221–241.

Peirce F T (1930), The handle of cloth as a measurable quantity, *J Text Inst*, **21**, P377–416.

Postle R, Carnaby G A and de Jong S (1988), *The Mechanics of Wool Structures*, Chichester, Ellis Horwood.

Shi F J, Hu J L and Yu T X (2000a), Modelling of creasing properties of woven fabrics, *Text Res J*. **70**(2), 247–255.

Shi F J, Hu J L and Yu T X (2000b), Modelling of viscoelastic bending properties of woven fabrics, *J China Text Univ*, **17**(1), 51–56.

Shi F J, Hu J L and Yu T X (2000c), Study of creasing in woven fabrics, *J Text Res*, **1**(21), 11–17.

Shinohara A, Shinohara F and Sakaebara K (1972), Theoretical study on anisotropy of bending rigidity of woven fabrics, *J Text Mach Soc Japan*, **26**, 75–79.

Skelton, J. (1974) The fundamentals of fabric shear, *Textile Research Journal*, **4**(12), 862–869.

Yan H J (1990), *Manual of Textile Fibres*, Beijing, China Textile Press, 280–296.

6

The shear properties of woven fabrics

6.1 General shearing behaviour of woven fabrics

6.1.1 Introduction

Textile fabrics in practical use are subjected to a wide range of complex deformations. The shear properties of woven fabrics are of importance in many applications. To understand the mechanisms of fabric shear behaviour, Dreby (1941), Go *et al*. (1957), Morner and Eeg-Oloffson (1957), Kawabata (1972, 1980) and Kawabata *et al.* (1972) introduced their shear apparatus to measure fabric shear properties. Later, Cusick (1961), Lindberg *et al*. (1961) and Grosberg and Park (1966) found a qualitative means of describing shear properties using a model. They indicated that the hysteresis produced during shearing is determined wholly by the frictional restraints arising during rotation of the yarn from the intersecting points in the fabric. In addition, the existing literature proved that shear mechanism is one of the important properties influencing the draping, pliability and handle qualities of woven fabrics (Kawabata, 1980; Oloffson, 1967; Lloyd *et al*., 1978). Shear deformation of woven fabrics also affects the bending and tensile properties of woven fabrics in various directions rather than in the warp and weft directions only (Chapman, 1980; Skelton, 1976).

6.1.2 Shear stress–strain curve

Shear behaviour of woven fabrics has received wide attention. Up to now general stress–strain curve in shear has been considered as showing the characteristics that are illustrated in Fig. 6.1. If a fabric is deformed at low levels of strain, the OA region, the shear stiffness is initially large, and decreases with increasing strain. In this region, the shear behaviour is dominated by frictional mechanisms and the decreasing incremental stiffness is generally attributed to the sequential movement of frictional elements. As soon as the stress is large enough to overcome the smallest of the frictional restraints

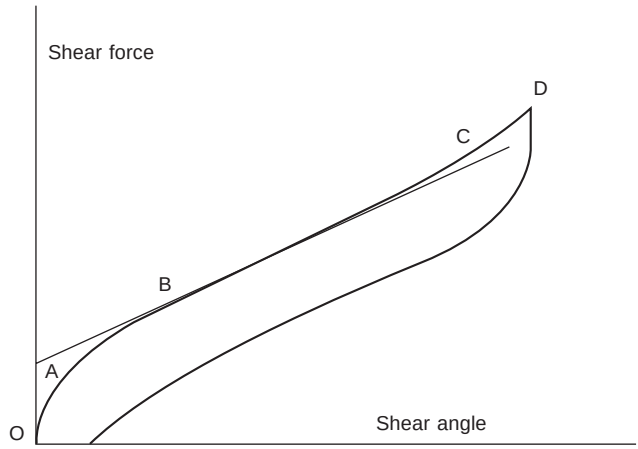

6.1 Stress–strain curve of woven fabrics during shear deformation.

that are acting at the intersection regions, the system starts to slip, and the incremental stiffness falls – this is the AB region. At a particular amplitude of stress, the incremental stiffness reaches a minimum level, point B, and remains almost linear over a range of amplitudes with slopes that are thought to be controlled by the deformation of the so-called 'elastic elements' in the fabric. It is a commonly observed fact that above a relatively low level of shear strain (5–10°), the shear stiffness increases with increasing strain. At amplitudes greater than a certain amount, point C, the incremental stiffness again begins to rise, and the closed curves increase in width with increasing amplitudes of shear angle. It seems that this is due to steric hindrance between the two bent intersectioning yarns, leading to transverse distortion of the yarns, or riding up of the intersection, or both.

There are two parameters used in most of the literature (three in the KES system) which control the extent of the non-linear region and characterise the general nature of fabric shear. These are the slope of the stress–strain curve where it attains its minimum value, and the hysteresis. The minimum slope of the curve represents the contribution of the so-called 'purely elastic elements' of the assembly and, when this value is achieved, it is assumed that all the frictional contact points are in motion. The decreasing stiffness region of the curve is of interest since it is here that the hysteresis loss in the cyclic deformation is determined.

6.1.3 Relationship between shear and bending deformations

Some authors have reported that the shear and bending of woven fabrics have a strong relationship. For example, it has been suggested that the shear

energy loss is a good guide to the kind of behaviour that can be expected in bending. Skelton thought that the shear and bending are not merely related but essentially identical (Skelton, 1980).

In a paper by Dawes and Owen (1971), the correlation between the two measurements of shear stiffness and bending stiffness is found to be quite good and the overall changes in mechanical properties as the environmental conditions change are very similar in the two modes of deformation. Thus it was believed that they share a common origin.

Skelton further argued that, for instance, for a shear angle of a few degrees (5°), and a fabric with 20 threads/cm, the effective curvature in the yarn is:

$$\frac{5 \times 20}{57} \approx 2 \text{ cm}^{-1} \qquad [6.1]$$

This is typical of the curvature levels that have been investigated in studies of fabric bending behaviour. Thus the magnitude and distribution of the curvature in the yarns in the bent state are almost identical to those in the sheared state.

6.2 Modelling of shearing behaviour of woven fabrics

6.2.1 Theory

Several authors have attempted a structural analysis to predict shear properties, but the conclusions reached differ in some respects and in addition the calculations are not presented in a form that can be readily put to practical use (Mark and Taylor, 1956; Morner and Eeg-Olofsson, 1957; Lo, 2001; Lo and Hu, 2002; Behre, 1961; Cusick, 1961; Postle *et al.*, 1976; Skelton, 1976). It is recognised that the detailed mechanisms which are operating are extremely complex and it is difficult to devise a convincing model that is adequate to explain them. However, the shear behaviour, especially in the initial region, is thought by some authors to be controlled by elastic and frictional elements simultaneously. In a general sense the behaviour of an array of elastic and frictional components has been studied by Oloffson (1967), and by Skelton (1976) and Skelton and Schoppee (1976). As discussed in the previous chapter, some of the existing literature put forward the belief that the stress–strain behaviour of a series of assemblies similar to frictional–elastic units can be reasonably represented in the initial, non-linear region of shear by an expression of the form:

$$\sigma = K\varepsilon^{1/2} \qquad [6.2]$$

where σ and ε are the shear stress and strain respectively and k is the material constant. This is the simplified Oloffson formula which is the same as the bending deformation.

6.2.2 Relationship between shear stiffness and hysteresis of woven fabrics

Figure 6.2 gives an example of the tested relationships between shear stiffness G and shear hysteresis $2HG$ and $2HG5$. It can be seen that, as in bending deformation, their relations are linear. The correlation coefficients can be as high as 0.9507 for G and $2HG$, and 0.9683 for G and $2HG5$. This may indicate, as discussed in Chapter 5 on bending properties, that friction exists during the whole shear process and not only in the initial region, because the hysteresis is mainly caused by the frictional element, especially $2HG$. In addition, friction and elastic elements always exist simultaneously. Thus it

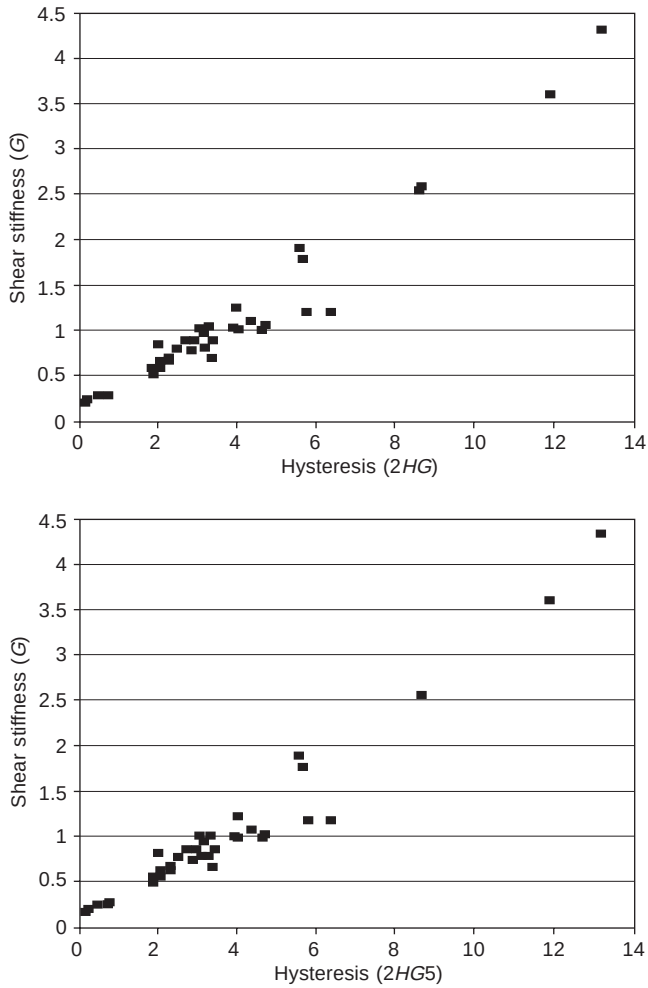

6.2 Shear stiffness vs shear hysteresis.

may not be appropriate to say that there is a pure elastic region, but the frictional effect is continuous throughout the entire shear process. The decreased value of shear stiffness after the initial region is attributable to the value of the dynamic friction coefficient being smaller than that of the static friction one.

6.2.3 Fitting of shear curves using non-linear regression

Since the friction and elastic elements exist simultaneously in the whole shear process before the steric hindrance occurs or in the earlier stage of shear, the stress–strain curves are assumed to be controlled by the combination of friction and elastic elements. As we saw Chapter 5, the application of the Oloffson model, in which the friction and elastic elements are considered simultaneously, is quite successful. In addition, in shear as in bending, it is also observed that shear stiffness and shear hysteresis are very closely related. This leads to the present attempt to extend the stress–strain relationship described in equation 6.2 to the following for shear deformation before steric hindrance occurs:

$$\sigma = \alpha \varepsilon^{\beta} \qquad [6.3]$$

where α and β are non-linear regression constants. The non-linear regression method is again used for estimating the constants in the equation.

Some of the shear stress–strain curves tested on the KES system, which are thought to be within the friction and elastic operating region or not involved in steric hindrance, are chosen for fitting the model; their fitted curves are given in Fig. 6.3, which shows that the tested and the calculated data are in reasonably good agreement with each other. A typical plot of tested stress and calculated stress is shown in Fig. 6.4, which indicates clearly a straight line between them.

The correlation coefficients are close to 1; but it should be noted that residuals from them are still larger than those we observed in the modelling of bending curves. Equation 6.3 is good enough to model the initial part of the shear curve of woven fabrics. In addition, shear angle also plays a part in the modelling effect of equation 6.3. For example, equation 6.3 is better used to model a KES shear curve with a maximum shear angle of 1° than 8°.

However, in practice, in many cases, this initial region is so short that it may be unnecessary to give an exact mathematical description. Thus, from the above, the modelling of shear curves using equation 6.3 cannot be described as a success. As a result, different methods for modelling a shear curve should be adopted to meet different needs. For example, if an analysis is confined to the small strain range, say, < 8°, i.e. the tested shear curve of a fabric within this is generally in the initial non-linear region or the maximum stress is smaller than or close to the minimum stiffness point, it can be

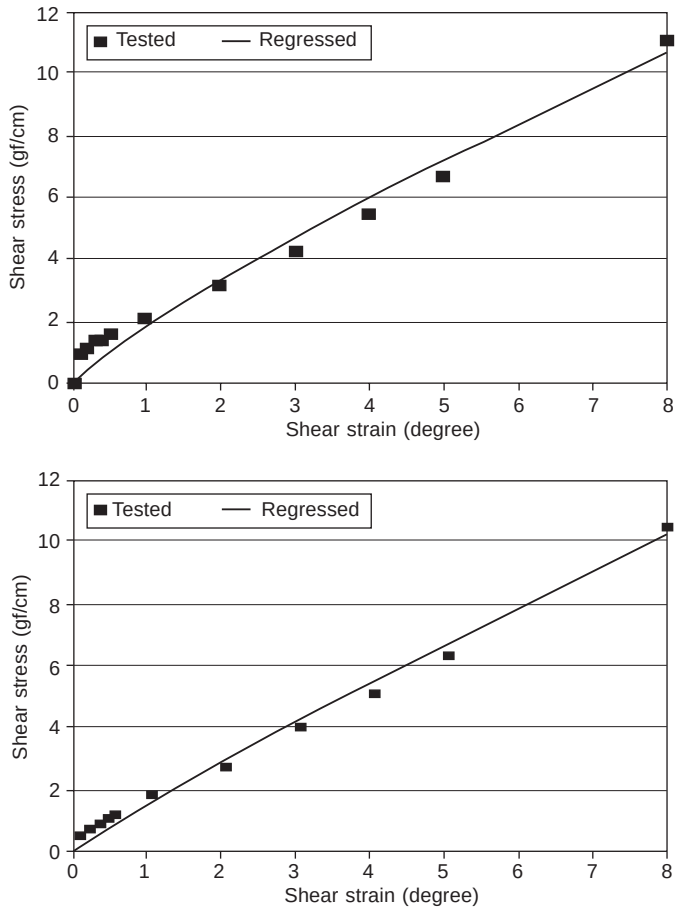

6.3 Tested and regressed shear curves.

modelled using equation 6.3; if the shear stress–strain curve is much beyond this minimum stiffness point, the curve cannot be modelled in this way, but a numerical method such as cubic-spline-interpolation may be more applicable; if the curve has a long close-to-linear range and the initial non-linear range is difficult to define or the maximum shear angle for minimum stiffness point is close to 0, it may be convenient to use the constant G provided by the KES system in which a straight line can be found.

6.2.4 Shear stiffness

In view of the complexity of the observed shear behaviour it is perhaps unreasonable to speak of shear stiffness as a single entity. We are concerned rather with the overall stress–strain characteristic of the fabric, and with an

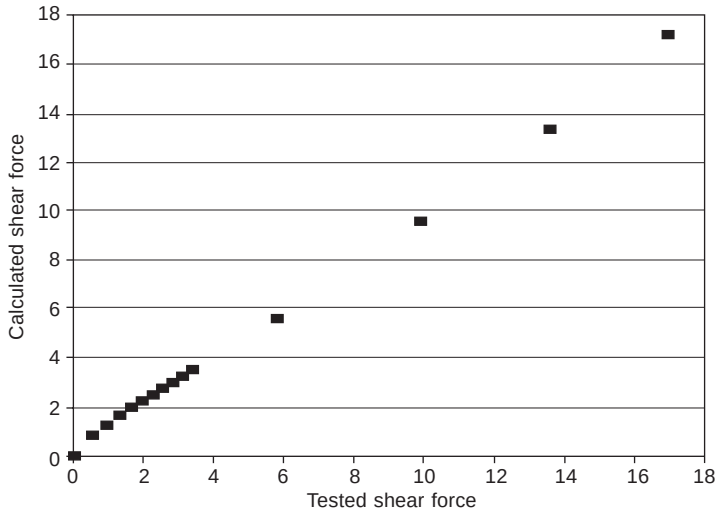

6.4 Tested and calculated shear stress.

understanding of the mechanisms operating when a fabric undergoes shear deformation. However, for a fabric like sample 18, if the shear condition is limited within 8° strain, the stress–strain curve may be modelled using the power function proposed by Oloffson, equation 6.3. Thus the shear stiffness may be found by differentiating the stress–strain function with respect to strain as shown in Fig. 6.5. It should be noted that the stiffness calculated is usually larger than that of the tested *G*. Therefore if the application needs high accuracy and continuous shear stiffness, it may be reasonable to use other numerical methods such as cubic-spline-interpolation to model it. In

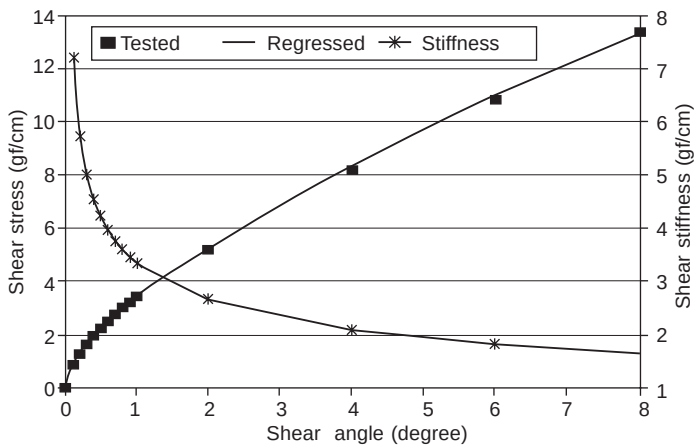

6.5 Comparison of fitted curves and KES tested data.

some cases, if a continuous stiffness is not strictly required, it may be convenient to use the KES constant shear stiffness *G*.

Generally speaking, the initial part of the shear curve can be modelled with a power function like equation 6.3. If continuous shear stiffness is required in some cases in the initial region, the equation is still accurate enough to be used for finding shear stiffness.

6.2.5 Comparison of warp and weft direction properties

The warp values of the shear properties, *G*, 2*HG* and 2*HG*5, can be compared with those in the weft. The results indicate that the values of the warp and weft 2*HG* and 2*HG*5 have no obvious differences if the warp and weft direction have similar yarns and similar cover factors, but *G* has marginally larger warp values. At the same time, the results also show that the larger the cover factor the larger the values of *G*, 2*HG* and 2*HG*5. Unlike the situation in bending, the hardening in the warp direction of woven fabrics seems to have little effect on the shear properties. This contradicts the argument that shear behaviour is identical in nature to bending properties. Perhaps a reasonable explanation may be jamming in the warp direction for high-density fabrics. That is, the larger values of *G*, 2*HG* and 2*HG*5 in the warp direction for the high-cover-factor fabrics are caused by the jamming effect. However, this jamming effect is not so prominent in fabrics with low-cover-factor or similar cover factors in the two principal directions. This suggests that the jamming effect may happen at a much earlier stage than the usually stated shear angle of 5–8°. The friction in shear exists mainly at the interface of the two systems of yarns, but inter-fibre friction within a yarn occurs in bending. This can be seen from the relationship between shear properties and cover factor.

6.2.6 Relationship between cover factor and shear properties

Figure 6.6 shows the general relationship between cover factor and the shear parameters *G*, 2*HG* and 2*HG*5, which is obtained from Fig. 6.7. According to this figure, we may find that when the ratio of warp and weft cover factor is smaller than 1.4, the increase in the ratio of cover factor causes an increase in the ratio of shear hysteresis 2*HG*; when the ratio of cover factor is greater than 1.5, the ratio of 2*HG* is almost certain to remain constant. This is because when the actual cover factor is larger than 100 %, further increase of the cover factor in most cases does not increase the actual contact area between the two systems of yarns. Another factor is that the relation of *G* and 2*HG* to the cover factor is similar to that of 2*HG*.

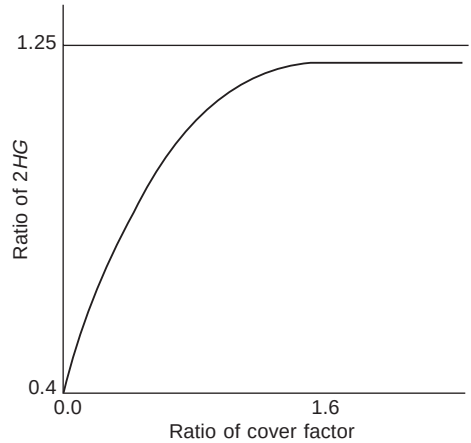

6.6 Generalised relationship of shear property and cover factor.

6.2.7 Relationship between bending and shear behaviour

Figure 6.8 illustrates the plots of bending properties against shear properties for cotton fabrics. It is clear that the dots have some trends, but these trends seem rather obscure. All this may indicate that they do have some relationship in some cases but not in all.

The comparison of warp and weft direction properties in Chapter 4 reveals that strain-hardening in the warp direction in woven fabrics hardens the bending behaviour as well; but it seems to have little significance for shear behaviour because there are no trends showing that the warp values of G, $2HG$ and $2HG5$ are larger than those of the weft when the cover factors and the yarn properties are similar. This suggests that the mechanisms operating in bending and shear may be different.

The results analysed above suggest that bending and shear may have some relationship, but that this relationship is not always as strong as described in some of the existing literature and that, in some cases, they are different in nature. Mechanically speaking, the two deformation modes both involve the friction and bending of yarns, but these two mechanisms are operating in different ways, especially the frictional effect. The inter-fibre friction in shear seems to be less important than it is in bending; thus the hardening of warp yarns of woven fabrics, which affects the internal friction, has little effect on shear behaviour.

6.3 Testing of shear properties

6.3.1 Introduction

The appearance of garments on human bodies has always been the prime concern of both fabric and garment designers. Up to now, design of fabric

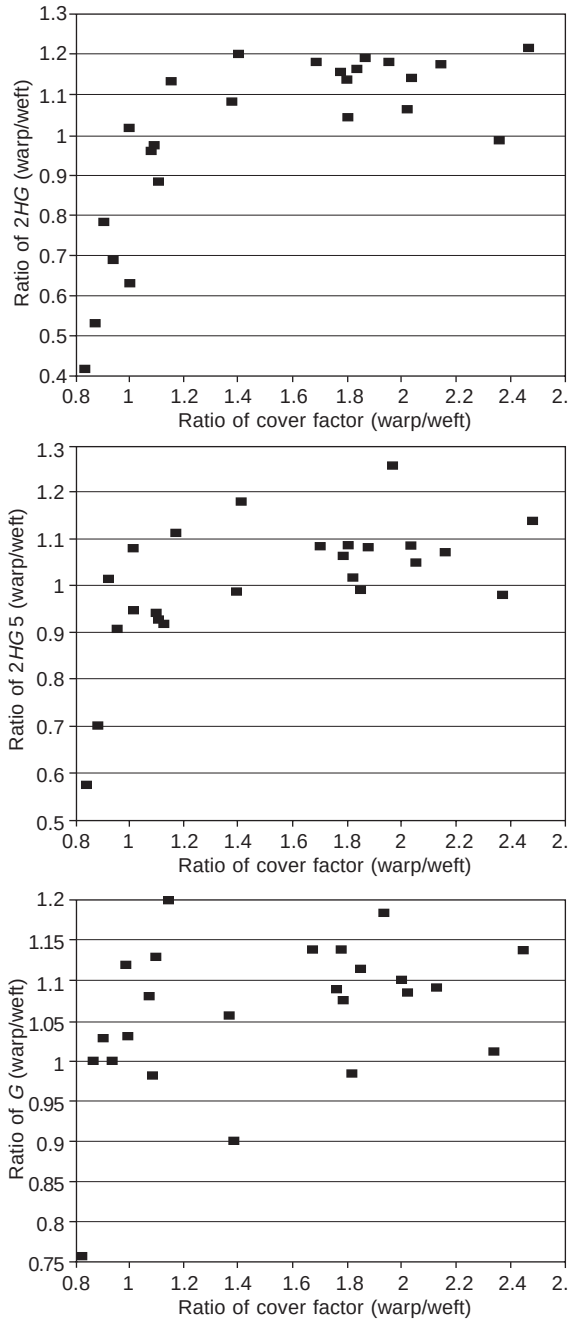

6.7 Relationship between cover factor and shear parameters.

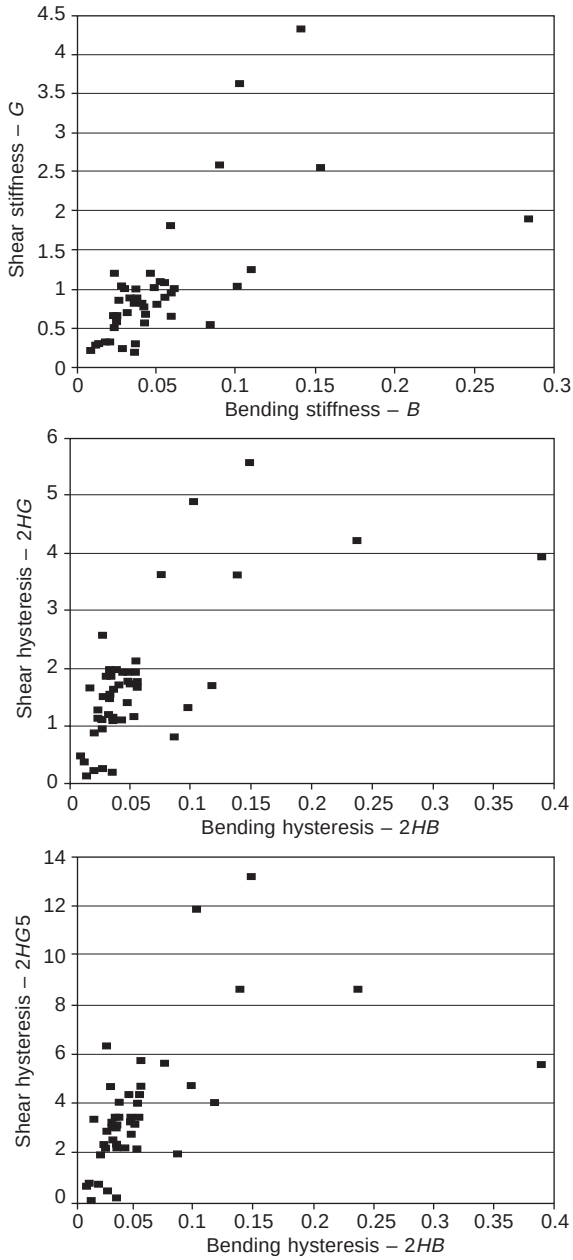

6.8 Relationship between shear and bending properties.

and garments has relied heavily on past experience and trial-and-error. As textiles and clothing products, dictated by modern fashion trends, move through ever faster cycles of renewal, just-in-time and quick response are becoming ever more important in the textiles and clothing industries. Consequently, modern technologies such as computer-aided design (CAD) are attracting increasing attention. The development of advanced CAD systems capable of simulating complex fabric deformations on human bodies will have great benefits for the textiles and clothing industries: faster industry responses to market demands, higher product quality, more variety, and reduced production costs.

While there have been a significant number of attempts to develop clothing CAD systems (Okabe and Akami, 1984; Collier *et al.*, 1991; Gan *et al.*, 1991; Kang *et al.*, 1994), progress has been hindered by the lack of ability to simulate the true appearance of fabrics on computers. No reliable and efficient technique currently exists for the numerical prediction of complex fabric deformations, which generally involve buckling and post-buckling large deformations, large rotations, material non-linearities, and complex interactions between the fabric and the human body. In this section, an attempt will be reported to establish an appropriate non-linear constitutive model for fabric materials in the analysis of fabric complex deformations, an area in which several difficulties currently exist.

Fabrics are generally treated as orthotropic thin sheets in a numerical model (e.g. finite-element shell model). The tensile membrane and bending properties determined by existing test procedures, e.g. the KES system (Kawabata, 1980), are suitable for direct use in constitutive models, but there are difficulties in translating the shear modulus obtained from the KES shear tester into a sensible figure for the true shear modulus.

Because fabrics are susceptible to buckling under external forces, it is very difficult to design perfect shear test equipment. The KES shear tester is the only commercialised one for fabrics so far, and it is widely used for various applications, such as fabric hand and tailorability evaluation. This existing test procedure for fabric shear modulus involves a piece of rectangular cloth clamped along two opposite edges and free on the other two edges. During the test, the cloth is pre-tensioned and then subjected to shear forces on the clamped edges which undergo relative displacements as a result of the applied shear forces as shown in Fig. 6.9. The deformations and forces in the cloth so loaded do not correspond to a pure shear state as achieved in a conventional shear test for other engineering materials in Fig. 6.10. Therefore, the test result cannot lead directly to the determination of the fabric shear modulus, particularly in the non-linear range of stress–strain relationship.

It is desirable to obtain an analytical solution for the problems advanced above. In applied mechanics, there exists an analytical solution to the shear stress or strain distribution on the specimen used, as shown in Fig. 6.9 for

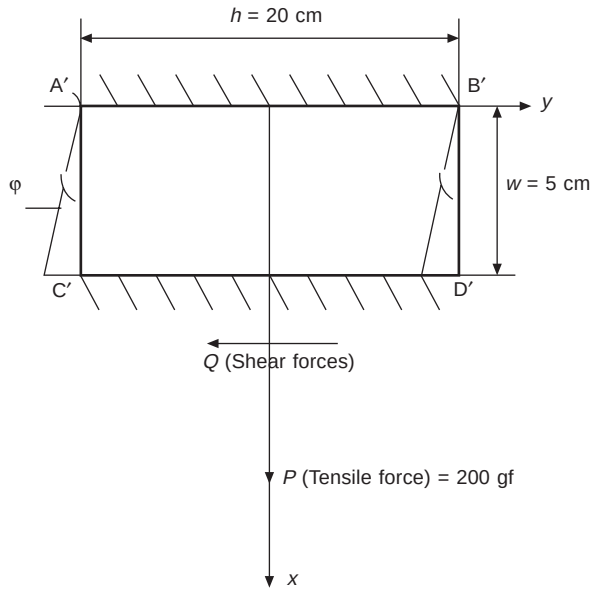

6.9 The KES shear testing apparatus.

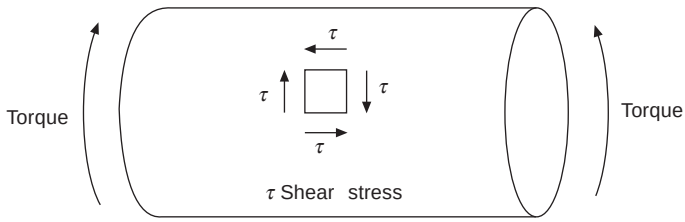

6.10 Conventional test to determine the shear modulus of a stiff material.

homogenous isotropic materials. However, no existing analytical solution for orthotropic materials can be found in the literature. Textile fabrics are not homogeneous isotropic materials, and no analytical solution has been presented for the fabric specimen in the KES shear tester.

6.3.2 The KES shear test

A schematic diagram for a specimen under KES shear test has been shown in Fig. 6.9. The size of the fabric specimen is 20 cm × 20 cm and the tested area is 20 cm × 5 cm. On this specimen, a tension of 10 gf/cm is imposed along the clamped sides of the fabric in the *x* direction to avoid buckling of the fabric. During the test, the cloth is subjected to shear forces on the clamped edges which undergo relative displacements along the *y* axis as a

result of the applied shear forces. The angle φ represents the rotation of a point on the moving edge of the tested specimen, but not the shearing strain. The maximum angle of rotation in this test is 8° which corresponds to the wearing condition of fabrics. It is possible to find the forces exerted on the specimen, although the general loading condition and shear stress distribution of the specimen are complicated.

According to the equilibrium conditions in the *X–Y* plane in Fig. 6.9, the following equations can be obtained:

$$\sum X_i = 0 \qquad [6.4]$$

$$\sum Y_i = 0 \qquad [6.5]$$

and

$$\sum M_i = 0 \qquad [6.6]$$

where X_i represents a force in the *x* direction, Y_i a force in the *y* direction and M_i a moment in the *X–Y* plane. From these relations, it is clear that the specimen is subject to a tensile force of *P*, a pair of shear forces *Q* and moments $M_1 = M_2 = Q_w$. The forces and moments exerted on the specimen in the KES shear tester are shown in Fig. 6.11.

From the above loading condition, shear stress distribution on the specimen is not uniform. It is obvious that the shear stresses at the points on the left and right edges of the specimen are always zero in the whole loading process. Thus infinitesimal element B in Fig. 6.11 has only tensile stress, but element *A* has shear stress τ, and tensile stress σ.

The conventional test to determine shear modulus for stiff engineering materials is shown in Fig. 6.10, in which a circular rod is subject to torsional deformations. Thus, the element in the circular rod is subjected to pure shear deformation. By contrast, the KES shear tester does not produce a pure shear state in the tested specimen.

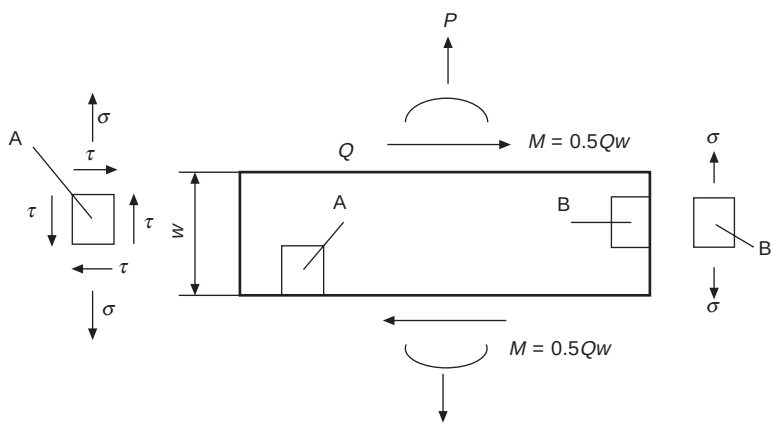

6.11 Forces exerted on fabric specimen under KES shear test.

There are two ways in which fabric mechanics researchers obtain shear modulus. One is the average slope of the shear curve when the shear angle is from 0.5–5° and the shear stress–strain relationship is simplified as linear. The other method is to find the derivative of the stress–strain curve when the shear stress–strain relation is considered as non-linear. Because the data obtained from the KES test does not correspond to pure shear, the force–rotation relationship and shear modulus derived are not applicable for numerical computation in the analysis of fabric complex deformations.

6.3.3 Finite-element analysis

From Fig. 6.11, it is clear that the shear stress distribution on the tested specimen is not uniform. In order to find out the general pattern of the shear stress (therefore strain) distribution, a finite-element analysis has been applied. To examine the typical distribution of shear stress in a KES test specimen, a finite-element analysis using 8-nodal plane-stress elements of the LUSAS finite-element package was carried out (Lucas, 1994). A linear elastic orthotropic material sheet was assumed and the constitutive law of orthotropic materials is:

$$\begin{Bmatrix} \sigma_x \\ \sigma_y \\ \tau_{xy} \end{Bmatrix} = \begin{bmatrix} c_{11} & c_{12} & 0 \\ c_{12} & c_{22} & 0 \\ 0 & 0 & c_{33} \end{bmatrix} \begin{Bmatrix} \varepsilon_x \\ \varepsilon_y \\ \gamma_{xy} \end{Bmatrix} \qquad [6.7]$$

where γ is shear strain, c_{11} and c_{22} are related to the tensile moduli E_1 and E_2 in the x and y directions respectively, c_{33} is the shear modulus and c_{12} is related to the Poisson's ratio. In finite element analysis, the material properties used are E_1 = 0.1096 MPa, E_2 = 0.0505 MPa, shear modulus C_{33} = 0.38 and Poisson's ratio ν = 0.1. The shear force applied on the specimen is 0.1 N/mm, which correspond to the properties of an ordinary fabric and loading condition in the KES shear test. The deformed shape of the specimen is shown in Fig. 6.12. In this figure, the coarsely meshed area simulates the clamping of the jaw of the KES shear tester in the longer direction, while the finer mesh area simulates the fabric specimen. The stress distribution in the x and y directions are shown in Figs 6.13 and 6.14. It can be seen from these figures that the stress is close to constant along the shorter direction while assuming a symmetrical curve in the longer direction.

6.3.4 Theory

6.3.4.1 Shear deformation of the specimen

The above finite-element analysis provides the general picture for the stress distribution in the specimen. It is desirable to obtain an analytical solution

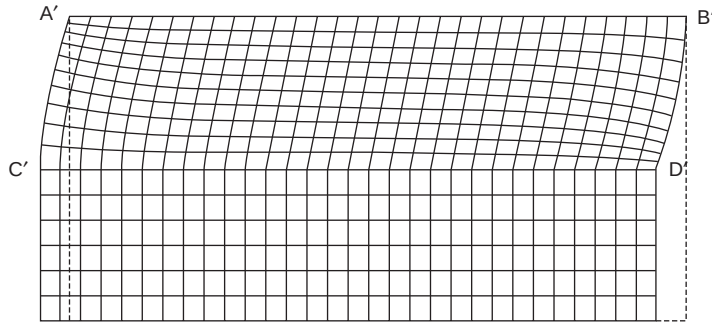

6.12 Deformed fabric specimen calculated by finite-element analysis.

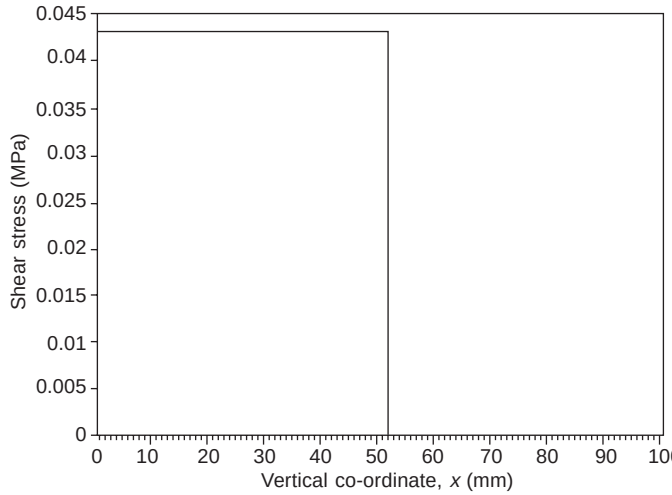

6.13 Shear stress variation along the shorter direction of the specimen.

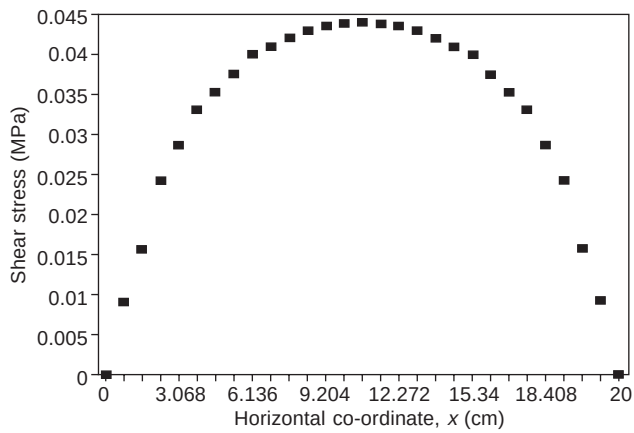

6.14 Shear stress variation along the longer direction of the specimen.

for the problem so that the exact relationship between test data and those for pure shear deformation can be obtained. The present study started with the application of the virtual work principle.

Fabric shear stress–strain relationship is usually non-linear. In order to simplify the equations, fabric material is considered to be linear and orthotropic, within a small incremental loading range from Q_n to Q_{n+1}, or Q. In this way, the results are applicable for non-linear material in the whole deformation process, during which many incremental steps for loading are taken. According to the principle of virtual work, the governing equations for plane stresses must satisfy the condition:

$$\int\int_{v} \int(\sigma_x \delta\varepsilon_x + \sigma_y \delta\varepsilon_y + \tau_{xy}\delta\gamma_{xy})\mathrm{d}V - \int_{S_1} \int(F_{nx}\delta u + F_{ny}\delta v)\mathrm{d}s = 0 \quad [6.8]$$

In this equation, σ_x, σ_y are the stresses in the x and y directions respectively, and τ_{xy} the shear stress. $\delta\varepsilon_x$, $\delta\varepsilon_y$ and $\delta\gamma_{xy}$ are virtual strains. δu and δv are the virtual displacements along the x and y directions. F_{nx}, and F_{ny} are external distributed forces on the force boundaries. The first integral in the equation is with respect to the whole volume, while the other one for the integration on the force boundaries, ds, is related to fabric width and length.

In the case of a non-linear material, all stresses represent the values within an infinitesimal range of $Q(Q_n, Q_{n+1})$, within which the stress–strain relationship can be considered as linear.

6.3.4.2 Shear strain distribution

In order to apply the above governing equations to obtain the stress distribution in the test specimen, it is necessary to set up the displacement field which should satisfy the displacement boundary conditions and agree with the results obtained from the finite-element analysis. u and v in the following two equations form the displacement field in the x and y directions:

$$u = u_0 + \sum_{i=1}^{n} a_i u_i \quad [6.9]$$

and

$$v = v_0 + \sum_{i=1}^{n} b_i v_i \quad [6.10]$$

where u_0 and v_0 are the displacements on the prescribed displacement boundary, and θ_i and b_i are the projection values in the x and y directions, respectively. In the present case, on boundary A′B′ in Fig. 6.9, u_0 and v_0 are zero because

the fabric edge is fixed during testing. In addition, because the two edges of the fabric are clamped, the partial derivatives of the displacements on A′B′ are also zero. Thus: $u_0 = v_0 = 0$. In order to facilitate the computation, the following series are selected for trial functions:

$$u = u_0 + a_1 u_1 \quad [6.11]$$

and

$$v = v_0 + b_1 v_1 \quad [6.12]$$

where

$$u_1 = x \quad [6.13]$$

and

$$v_1 = x\cos\left(\frac{\pi}{h}y\right) \quad [6.14]$$

Therefore, the corresponding strains in the *x*–*y* plane can be expressed as equations 6.15–6.17:

$$\varepsilon_x = \frac{\partial u}{\partial x} = a_1 \quad [6.15]$$

$$\varepsilon_y = \frac{\partial v}{\partial y} = -b_1 \frac{\pi}{h} x \sin\left(\frac{\pi}{h}y\right) \quad [6.16]$$

and

$$\gamma_{xy} = \frac{\partial u}{\partial y} + \frac{\partial v}{\partial x} = b_1 \cos\left(\frac{\pi}{h}y\right) \quad [6.17]$$

Shear strain distribution follows the pattern described in equation 6.17. That is, the shear strain along *x* axis is constant, in other words, there is no strain variation along the *x* axis, while a cosine relation of strain holds along the *y* axis.

6.3.4.3 Shear stress distribution

According to equation 6.7, plane stresses can be obtained as the following:

$$\sigma_x = c_{11}\varepsilon_x + c_{12}\varepsilon_y = c_{11}a_1 - c_{12}b_1 \frac{\pi}{h} x \sin\left(\frac{\pi}{h}y\right) \quad [6.18]$$

$$\sigma_y = c_{12}\varepsilon_x + c_{22}\varepsilon_y = c_{12}a_1 - c_{22}b_1 \frac{\pi}{h} x \sin\left(\frac{\pi}{h}y\right) \quad [6.19]$$

and

$$\tau_{xy} = c_{33}\gamma_{xy} = c_{33}b_1 \cos\left(\frac{\pi}{h}y\right) \quad [6.20]$$

From equation 6.20, the shear stress along the x axis is constant, or there is no stress variation along the x axis, while a cosine relation holds along the y axis. This agrees with the numerical results shown in Figs 6.13 and 6.14 from the above finite-element analysis.

6.3.4.4 *Constants in the equation*

The constants a_1 and b_1 in the above equations are unknown so far. They can be obtained from the following analysis. According to the virtual displacement principle represented in equation 6.8, the following equations can be obtained:

$$\int\int_V \int \left(\sigma_x \frac{\partial u_1}{\partial x} + \tau_{xy} \frac{\partial u_1}{\partial y} \right) \mathrm{d}V - \int_S \int F_{nx} u_1 \mathrm{d}s = 0 \qquad [6.21]$$

and

$$\int\int_V \int \left(\tau_{xy} \frac{\partial v_1}{\partial x} + \sigma_y \frac{\partial v_1}{\partial y} \right) \mathrm{d}V - \int_S \int F_{ny} v_1 \mathrm{d}s = 0 \qquad [6.22]$$

Substituting equations 6.13–6.20 into equations 6.21 and 6.22, we get

$$a_1 = \frac{\Delta P}{c_{11} h t} \qquad [6.23]$$

and

$$b_1 = -\frac{3\pi h \Delta Q}{2(3c_{33} t h^3 + c_{22} \pi^2 t w^2)} \qquad [6.24]$$

where h is the width of the specimen, t the thickness of the fabric. P is the amount of the increment of tensile force which corresponds to the pretension applied to the specimen. Q is the shear force increment from (Q_n, Q_{n+1}), and c_{11} and c_{22} can be tested from the KES tensile tester. However, c_{33}, the shear modulus cannot be determined directly from the KES shear tester, but needs to be modified.

6.3.4.5 *Shear modulus*

The following procedure is used to find c_{33}. The calculation of c_{33} needs the values of the displacement increment v of the specimen corresponding to the force increment Q. According to equations 6.12 and 6.14, the displacement of the specimen is not uniform along the y axis; it is necessary to find out the equivalent average displacement. This requires the unit force on the specimen edge. If the total force applied on the specimen edge is Q, it can be found that the distribution of unit force on the edge where $x = w$ is

$$\frac{\pi}{2h}\cos\left(\frac{\pi}{h}y\right) \qquad [6.25]$$

According to the equivalency principle, the equivalent displacement increment, v, of the points at $x = w$ should be determined by

$$1^* \ \Delta v = \int_{\frac{h}{2}}^{\frac{h}{2}} \frac{\pi}{2h}\cos\left(\frac{\pi}{h}y\right)\cdot b_1 w\cos\left(\frac{\pi}{h}y\right)\mathrm{d}y = \frac{\pi}{4}b_1 w \qquad [6.26]$$

According to equation 6.12, $b_1 w$ is the displacement in the middle point of the specimen where $y = 0$. Thus the equivalent v is $\pi/4$ times the displacement of the middle point along the moving edge of the specimen.

The value of v so obtained is usually smaller than the actual one, thus a factor is required to modify it. The average value is taken between the maximum and the minimum:

$$k = \frac{\pi}{4} + 0.5\cdot\left(1 - \frac{\pi}{4}\right) \qquad [6.27]$$

so

$$\Delta v = kb_1 w \qquad [6.28]$$

Substituting equation 6.24 into 6.28, c_{33} can be obtained:

$$c_{33} = \frac{3\pi\Delta Qhwk - 2\Delta v c_{22}\pi^2 tw^2}{6\Delta v t h^2} \qquad [6.29]$$

where v and Q can be obtained from the tested shear force–rotation relationship. If v and Q are from the shear force–rotation curve of fabric in the warp direction, c_{22} is the tensile modulus of fabric in the weft direction. Or if v and Q are from the weft direction, c_{22} must be the tensile modulus of fabric in the warp direction when stress is equal to $P/20 = 10$ gf/cm.

6.3.5 Numerical results

The above analysis has provided a picture of shear stress/strain distribution in the test specimen and a close form solution for the calculation of shear modulus of a fabric in terms of the data obtained from the KES tester. This section will deal with numerical results calculated from this solution and the accuracy and validity of the analytical solution will also be discussed.

6.3.5.1 Computation of c_{33}

c_{33} is the main focus of this study and its relation with the KES test data has been derived in equation 6.29. From equation 6.29, the computation of c_{33}

requires the value of c_{22} which is related to the tensile modulus. The tensile modulus is the value when stress = 10 gf/cm in the *y* direction, which can be obtained from the tensile curve. When the Poisson's ratio is equal to zero, c_{22} can be found from the following relationship:

$$c_{22} = \frac{E_2}{1 - \nu_{12}\nu_{21}} = E_2 = \frac{\alpha}{\beta} e^{\alpha\varepsilon} \qquad [6.30]$$

and

$$\sigma = \frac{e^{\alpha\varepsilon} - 1}{\beta} \qquad [6.31]$$

where σ is the tensile stress in gf/cm and ε the tensile strain expressed as a percentage. α and β are two constants which can be determined by the non-linear regression technique (Hu, 1994). When σ is equal to 10 gf/cm, c_{22} can be obtained from the following equation;

$$c_{22} = \frac{\alpha}{\beta}[(10 \times \beta) + 1](\text{gf/cm}) = 0.00098\frac{\alpha}{\beta}[(10 \times \beta) + 1](\text{MPa}) \qquad [6.32]$$

Or, alternatively, it can be measured on the tensile stress–strain curve when stress = 10 gf/cm. In the following section, c_{22} is calculated from equation 6.32.

6.3.5.2 Modified shear modulus from tested shear curve

In equation 6.29, *w*, *h* and *k* are known. As shown in Fig. 6.9, *h* = 20 cm = 200 mm, *w* = 5 cm = 50 mm. If the material is considered as non-linear, the modulus curve of c_{33} can be calculated from input data of *v*, *Q*, c_{22} and *t* (fabric thickness). Also, in the following computation, two fabrics are used. The values of *v* and *Q* can be obtained from the curves tested on the KES tester. The loading process is divided into 140 steps; during each step, the stress–strain relationship is assumed to be linear. When *Q* is given, ϕ can be read from the curve. From ϕ, the value of *v* can be determined from Fig. 6.15. Figure 6.16 shows the shear force–rotation curves obtained from the KES shear tester for one fabric in the warp and weft directions respectively. c_{33} can be calculated from the tested curve for warp direction or for weft direction. If the fabric is orthotropic as assumed, the modified moduli of warp and weft directions should be the same.

Figure 6.17 shows the modified shear modulus curves from the calculation. From this figure, the values from the warp and weft directions for shear modulus vary with shear strain. When the shear strain is smaller than 0.01 rad, the values of shear moduli from the warp and weft directions are very

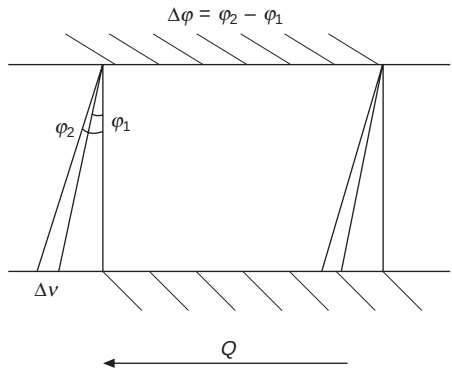

6.15 Determination of Δv.

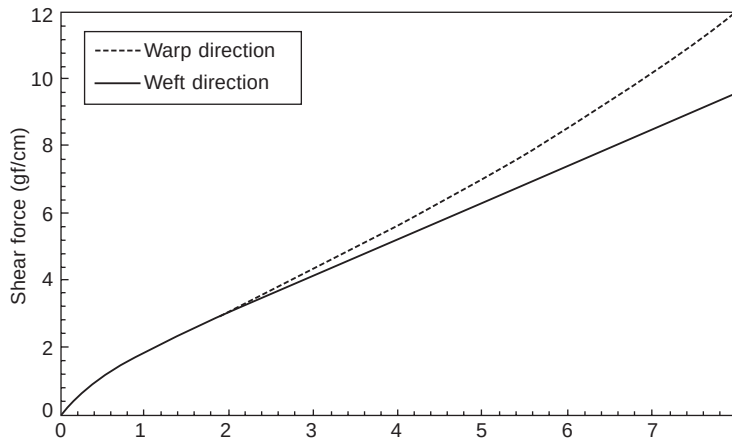

6.16 Shear force-rotation curves of KES test.

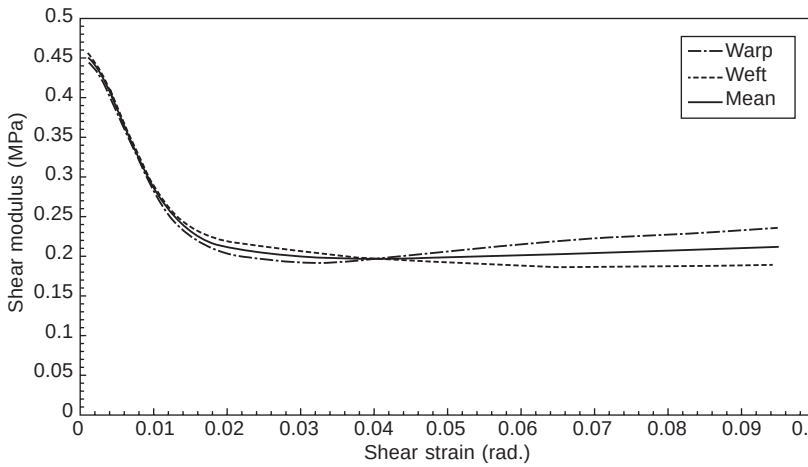

6.17 Modified shear moduli.

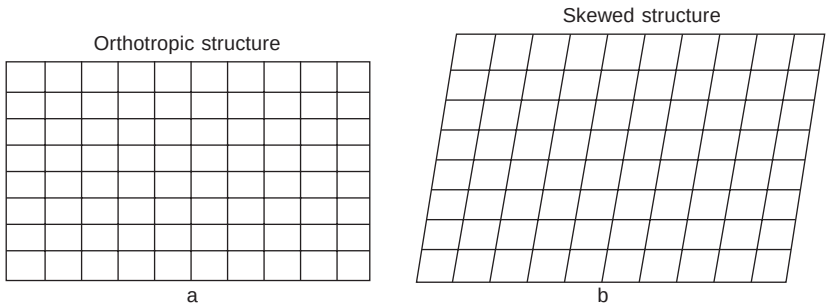

6.18 Change of orthotropic structure.

close. However, at the later stage, the difference between the warp and weft values becomes large when the strain increases. This may be due to the fact that the orthotropic assumption is inapplicable during this later stage, but valid when shear strain is very small in the initial stage.

This can be explained by Fig. 6.18. When the fabric specimen is subjected to the deformation imposed by the KES shear tester, in the initial stage, warp and weft yarns are perpendicular to each other and their rotation relative to each other is limited by internal friction between warp and weft. By contrast, in the later stage, the fabric structure is changed from state (a) to state (b), at which the warp and weft yarns are no longer perpendicular to each other. Thus the orthotropy is not held during this stage.

Therefore, the results from the present research are more accurate in the initial part of the shear deformation. In the later part, the difference between warp and weft becomes increasingly large as the shear strain increases. In view of the complexity of the later stage, it is suggested that the average c_{33} of the warp and weft values is used for representing the shear modulus of fabric sheet as shown in Fig. 6.17. Table 6.1 shows the deviations (d_1 and d_2) of warp and weft values from their averages for the fabric. The largest deviation when shear strain is 8° is around 10 % and 18 %.

6.3.5.3 Comparison of modified and tested shear moduli

From the force–rotation curve, the tangent modulus can also be derived by differentiation of force with respect to rotation angle using spline fitting. This is regarded as the tested shear modulus and represented by G, which is frequently adapted in many computations. As discussed for modified shear moduli from the warp and weft directions, tangent shear moduli directly from tested curves for the warp and weft directions are also different, thus the average values of warp and weft are used for comparison. c_{33} and G are the averages of the warp and weft directions in Fig. 6.19. The differences between the modified and tested shear moduli are listed in Table 6.2.

Table 6.1 Shear moduli of woven fabric (MPa)

γ, (rad)	c_{33}, weft	c_{33}, warp	c_{33}, average	d_1, %	d_2, %
–.0010	.4572	.4462	.4517	1.2	1.2
–.0060	.3750	.3629	.3689	1.63	1.63
–.0010	.2794	.2678	.2736	2.13	2.13
–.0160	.2335	.2214	.2274	2.68	2.68
–.0210	.2193	.2044	.2119	3.50	3.50
–.0260	.2128	.1970	.2049	3.87	3.87
–.0310	.2068	.1939	.2004	3.21	3.21
–.0360	.2026	.1942	.1984	2.11	2.11
–.0410	.1985	.1980	.1982	0.12	0.12
–.0460	.1952	.2033	.1992	2.03	2.03
–.0510	.1923	.2082	.2003	3.97	3.97
–.0560	.1904	.2130	.2017	5.61	5.61
–.0610	.1889	.2173	.2031	7.01	7.01
–.0660	.1882	.2211	.2046	8.05	8.05
–.0710	.1877	.2243	.2060	8.89	8.89
–.0760	.1882	.2272	.2077	9.41	9.41
–.0810	.1889	.2293	.2091	9.65	9.65
–.0860	.1900	.2319	.2109	9.94	9.94
–.0910	.1907	.2350	.2128	10.41	10.41
–.0960	.1913	.2387	.2150	11.02	11.02

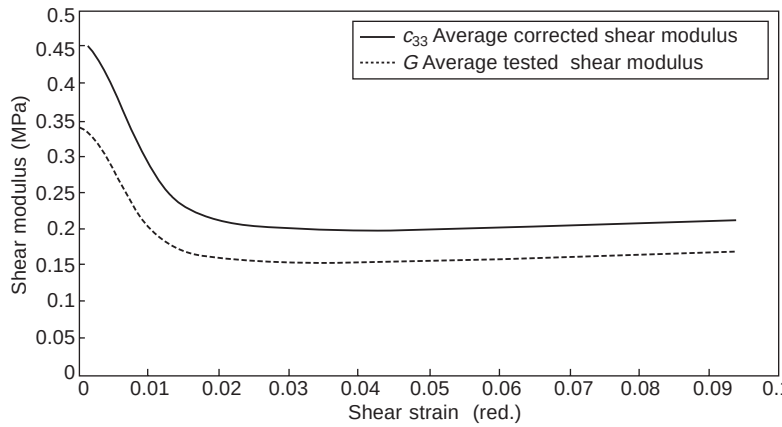

6.19 Comparison of simple and modified shear moduli.

From these two figures, the modified modulus c_{33} is consistently larger than the one derived from the tested data which corresponds to the conventional shear stiffness G. In other words, from Fig. 6.19, the shear modulus derived from the test is always smaller than the modified ones. More than 25 % and up to 32 % of error can be found in the later stage. Thus the error of the tested shear modulus is very significant.

Table 6.2 Comparison of shear moduli for woven fabric

γ (rad)	c_{33} average (MPa)	G, average (MPa)	Difference, % $(G - c_{33})/c_{33}$
.0010	.4517	.3361	–25.8
.0060	.3689	.2625	–28.8
.0110	.2736	.1932	–29.4
.0160	.2274	.1673	–26.5
.0210	.2119	.1600	–24.5
.0260	.2049	.1557	–24.0
.0310	.2004	.1536	–23.3
.0360	.1984	.1535	–22.6
.0410	.1982	.1543	–22.2
.0460	.1992	.1552	–22.1
.0510	.2003	.1562	–22.0
.0560	.2017	.1574	–22.0
.0610	.2031	.1585	–22.0
.0660	.2046	.1597	–22.0
.0710	.2060	.1609	–21.9
.0760	.2077	.1622	–21.9
.0810	.2091	.1637	–21.7
.0860	.2109	.1654	–21.6
.0910	.2128	.1674	–21.3
.0960	.2150	.1697	–21.1

6.3.5.4 *Modified shear modulus calculated from the tested parameter G*

From the KES shear test, a single value of G is given for the shear stiffness, which is the slope between shear angle of 0.5–5° as shown in Fig. 6.20. This is equivalent to considering that the shear deformation of the fabric is linear

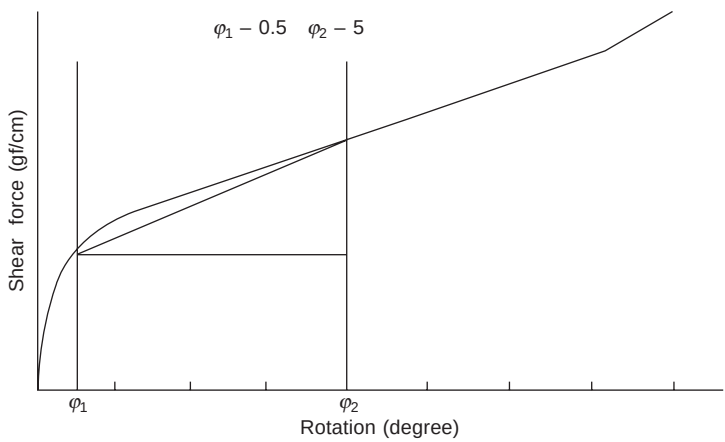

6.20 Determination of G on the KES shear tester.

Table 6.3 c_{33} calculated from G and related parameters

Sample	Direction	α	β	$0.2\times c_{22}$	G	t	c_{33}	$(0.2\times c_{22})/c_{33}$	c_{33}/G
2	weft	0.258	0.006	0.009	0.253	0.222	0.314	2.89	1.24
	warp	0.451	0.034	0.003	0.223		0.296	1.18	1.33
3	weft	0.304	0.011	0.006	0.212	0.233	0.272	2.16	1.28
	warp	0.526	0.040	0.004	0.195		0.258	1.40	1.32
4	weft	0.366	0.013	0.006	0.154	0.240	0.190	3.32	1.23
	warp	0.435	0.027	0.004	0.136		0.173	2.28	1.28
5	weft	0.271	0.008	0.007	0.220	0.230	0.277	2.55	1.26
	warp	0.474	0.035	0.004	0.200		0.265	1.35	1.32
6	weft	0.302	0.003	0.024	0.571	0.249	0.204	3.38	1.23
	warp	0.715	0.006	0.026	0.580		0.708	3.66	1.22
7	weft	0.227	0.004	0.011	0.247	0.218	0.297	3.64	1.20
	warp	0.450	0.030	0.004	0.227		0.300	1.27	1.32
9	weft	0.288	0.007	0.009	0.280	0.205	0.346	2.66	1.24
	warp	0.404	0.038	0.003	0.277		0.373	0.76	1.35
10	weft	0.290	0.006	0.009	0.210	0.179	0.242	3.92	1.15
	warp	0.556	0.033	0.004	0.185		0.235	1.87	1.37
11	weft	0.338	0.008	0.009	0.256	0.171	0.306	2.97	1.19
	warp	0.485	0.033	0.004	0.217		0.281	1.37	1.30
12	weft	0.313	0.008	0.009	0.235	0.170	0.278	3.10	1.18
	warp	0.483	0.026	0.005	0.218		0.278	1.64	1.28
13	weft	0.232	0.006	0.008	0.245	0.204	0.302	2.76	1.23
	warp	0.604	0.077	0.003	0.220		0.295	0.92	1.34
14	weft	0.296	0.006	0.011	0.208	0.240	0.247	4.32	1.19
	warp	0.509	0.047	0.003	0.192		0.255	1.22	

after the initial stage. For simplification, in many applications, the value of G is used for shear stiffness in place of c_{33}.

As mentioned earlier, this is not the correct value for pure shear deformation. It is desirable that an analytical solution can be used for calculating the shear modulus from the value of G. According to the definition of G from KES testing, equation 6.29 becomes:

$$c_{33} = 1.4\frac{f_2 - f_1}{\varphi_2 - \varphi_1} \cdot \frac{1}{t} - 0.2c_{22} = 1.4\frac{G}{t} - 0.2c_{22} \qquad [6.33]$$

Data for G from 24 fabrics were used for the calculation of c_{33}. The results are shown in Table 6.3.

It can be seen from this table that the difference between tested and modified moduli is also very large, about 25–30 %. The effect of c_{22} is not very significant. From this table and equation 6.33, the error caused by ignoring c_{22} is about 2 %. If the term containing c_{22} is ignored, the ratio of the modified and tested shear moduli is equal to 1.4 which is also applicable for continuous non-linear shear stiffness.

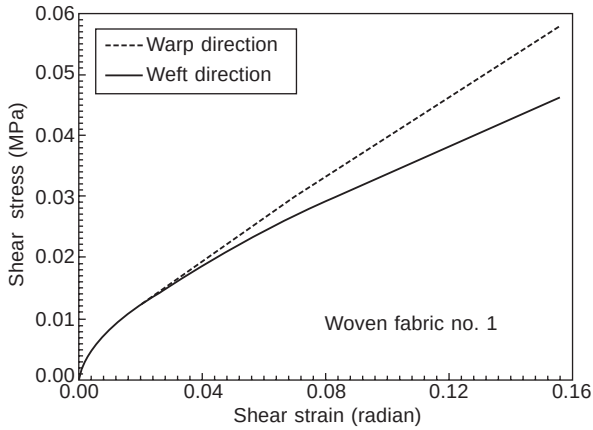

6.21 Modified shear stress–strain curve.

6.3.5.5 Stress–strain relationship

Because the shear force–rotation curve from the KES tester does not correspond to the pure shear state, it needs to be modified. The modified version can be obtained from the analytical solution for c_{33}. Within the small range of force increment, the shear stress and strain relationship is linear. Two fabrics were examined as above. The whole loading process is also divided into 140 steps, thus non-linear stress–strain curves are obtained. The shear stress–strain curves are shown in Fig. 6.21.

6.4 Shear properties of woven fabrics in various directions

6.4.1 Introduction

Shear behaviour of woven fabrics in both principal directions has received wide attention as it affects many types of fabric behaviour, but little attention is paid to the shear properties in other directions, which is no less important than that in the principal directions since garments in practical use deform in various directions. Therefore, a quantitative knowledge of the shear properties in bias directions becomes a must for garment design and new fabric development, and this is the main topic of this section.

As we all know, the shear behaviour of a woven fabric can be characterised by two shear parameters, i.e. shear rigidity (G) and shear hysteresis ($2HG$ and $2HG5$). Shear rigidity is the resistance of a fabric to shear while shear hysteresis is the energy loss within a shear deformation cycle. Existing literature has suggested a strong relationship between shear rigidity and shear hysteresis (Collier, 1991; Hu and Newton 1993; Hu, 1994; Jeong and Phillips, 1998). The results obtained from Collier, Jeong and Phillips and Hu indicated that

the correlation coefficients of shear rigidity and shear hysteresis can be as high as 0.90 or more. Based on the assumption that shear rigidity and shear hysteresis share a similar mechanism, a *G*-predicting model can be developed through the KES data collected from a wide range of woven fabrics. Furthermore, the proposed model can be further applied to predict shear hysteresis. The validity of the model for shear hysteresis, which has been visualised in the form of polar diagrams, will be confirmed, and the results also indicate a linear relationship between shear rigidity and shear hysteresis which not only holds in the principal directions, but is also present in bias directions.

6.4.2 Modelling of the anisotropy of shear properties

The classical elasticity theory is developed by Kilby (1961, 1963) based on the assumption that a fabric is an anisotropic lamina possessing a Poisson effect and with two planes of symmetry at right angles to one another. According to the elasticity theory (Hu, 1994), the behaviour of tensile and shear properties from the theoretical transformation of various compliances in the principal and bias directions can be used to yield the following equations:

$$\frac{1}{E'_X} = \frac{\cos^4\theta}{E_1} + \left(\frac{1}{G} - \frac{2\nu_{12}}{E_1}\right)\cos^2\theta\sin^2\theta + \frac{\sin^4\theta}{E_2} \qquad [6.34]$$

$$\frac{1}{E'_Y} = \frac{\sin^4\theta}{E_1} + \left(\frac{1}{G} - \frac{2\nu_{12}}{E_1}\right)\cos^2\theta\sin^2\theta + \frac{\cos^4\theta}{E_2} \qquad [6.35]$$

and

$$\frac{1}{G'_{XY}} = 4\left(\frac{1}{E_1} + \frac{1}{E_2} + \frac{2\nu_{12}}{E_1}\right)\cos^2\theta\sin^2\theta + \frac{1}{G}(\cos^2\theta - \sin^2\theta)^2 \qquad [6.36]$$

where E'_X, E'_Y and G'_{XY} denote the tensile modulus in the X' and Y' axes and shear rigidity between both principal directions respectively with an angle θ.

With equation 6.32, the shear rigidity in the X' and Y' axes can be obtained directly from experimental tensile modulus, while ν_{12} cannot. The theoretical treatment suggests that measurements of modulus in two directions are insufficient to define a fabric's shear rigidity, since variations with direction are still possible for fabrics with similar E_1 and E_2. An investigation of the third direction is therefore necessary, and the most convenient direction is the 45°. Thus, the sum $(1/E_1 + 1/E_2 + 2\nu_{12}/E_1)$ may be deduced from measurements in three directions by considering specimens cut along the warp, weft and 45° directions. Therefore, when considering $\theta = 45°$ values, equation 6.32 gives

$$\frac{1}{G_{45}} = 4\left(\frac{1}{E_1} + \frac{1}{E_2} + \frac{2\nu_{12}}{E_1}\right)\left(\frac{1}{\sqrt{2}}\right)^2\left(\frac{1}{\sqrt{2}}\right)^2 \quad [6.37]$$

and

$$\frac{2\nu_{12}}{E_1} = \frac{1}{G_{45}} - \frac{1}{E_1} - \frac{1}{E_2} \quad [6.38]$$

Substituting equation 6.37 into equation 6.32, we get

$$\frac{1}{G_\theta} = \left(\frac{1}{G_{45}}\right)\cos^2\theta\sin^2\theta + \frac{1}{G}(\cos^2\theta - \sin^2\theta)^2 \quad [6.39]$$

Thus fabric shear rigidity in various directions can be predicted from equation 6.39 when its values in the warp and ± 45° directions are measured. As shear rigidity provides a measure of the resistance to the rotational movements between the warp and weft yarns at the intersecting points when the fabric is subjected to a small shear deformation, its relationship between both principal directions should be determined. That is, a strong linear relationship is obtained in the two principal directions by Mahar *et al*. (1989, 1990) and it is elucidated that the measurement on fabric shear properties can be simplified and is necessary in only one principal direction. It is further proved from equation 6.39 that the shear rigidity in either the warp or weft direction with ± 45° directions gives a very satisfactory result in various directions. However, if the differences in the values of shear rigidity between the warp and weft directions are large, the average value will be taken in both principal directions in the calculation of shear rigidity in various directions given in equation 6.39.

Shear hysteresis of the fabric can be defined as the energy loss within the shear cycle when the fabric is deformed and allowed to recover to its original position. Since strong linear relationship between shear rigidity (G) and shear hysteresis ($2HG$ and $2HG5$) has been proved by several researchers (Collier, 1991; Hu, 1994; Jeong and Phillips, 1998), the proposed G-predicting model in different directions can be applied to shear hysteresis ($2HG$ and $2HG5$) of different fabrics.

6.4.3 Polar diagrams of the shear model

6.4.3.1 General features

As shown by Figs 6.22 and 6.23, the shear parameters, i.e. shear rigidity G and shear hystereses, $2HG$ and $2HG5$, exhibit great similarities. First, the shapes of their polar diagrams are all symmetrical to the warp and weft directions. Second, the values of these parameters change with the angle with their maxima exactly at ± 45° to the warp or weft direction. Therefore,

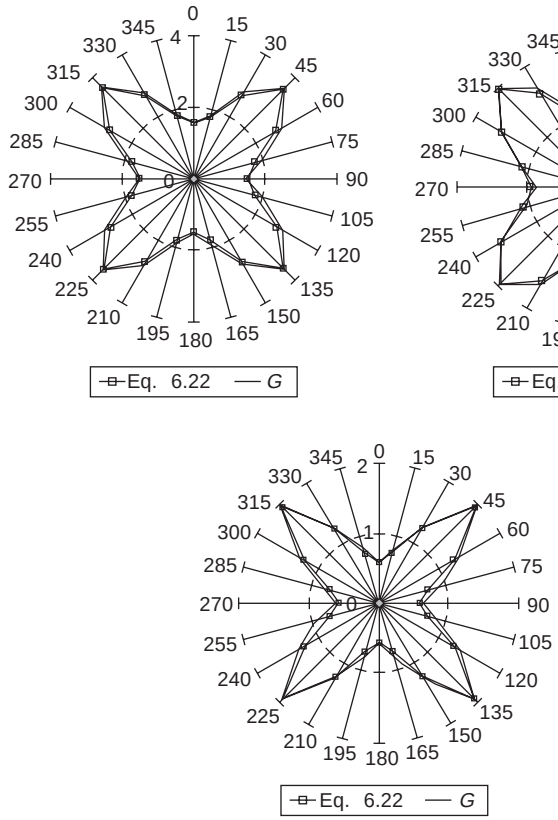

6.22 Typical polar diagram of shear rigidity (*G*).

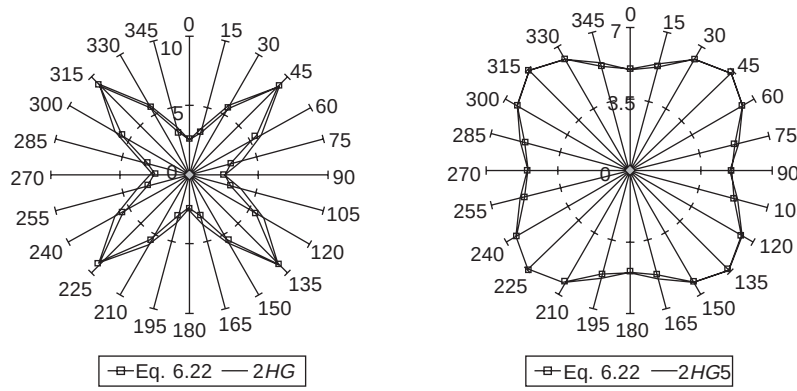

6.23 Typical polar diagram of shear hysteresis (2*HG*, 2*HG*5).

the shape of these polar diagrams is mainly governed by their values at ± 45°. Presumably, the anisotropy of the shear rigidity should be due to some inherent difference in their physical behaviour, the types of finishes undergone and the stiffness of the constituent yarns or fibres, the contact area at the intersecting points of two sets of yarns, the fibre packing density in the yarns, and so on. As a result, any combination of these factors can confer different shear characteristics in woven fabrics even when produced in the same material.

From fabric geometry, there is a normal pressure acting at each intersecting point of two sets of yarns in the unset fabric. As the shear force is applied to the fabric and usually has a larger magnitude than the frictional restraint at the intersecting point of yarns, the fabric will deform with hysteresis effect. In this case, the fabrics woven with natural fibres will have larger value of shear hysteresis than those with synthetic fibres due to the relatively low contact area of synthetic fibres at each yarn intersecting point.

The values of shear properties will be decreased after the finishing process. It is a fact that the residual bending stress existing in the yarns is released with the drop of the normal reaction acting on the crossing over regions. Thus commercially available woven fabrics usually have lower values of shear properties than laboratory-produced woven fabrics.

As the shear deformation depends upon the frictional and elastic forces within a fabric, elastic force will be built up rapidly if tightly woven fabric is sheared where limited sliding of yarns over each other is allowed in their crossing over points. On the contrary, the frictional forces will be very low if the fabric is loosely constructed and produced in weaves such as twill and satin.

6.4.3.2 Effect of weave density on fabric shear

In this section, our discussion is based on the analysis of plain and twill fabrics. Because the warp densities of these fabrics are kept constant, any changes in the trends of polar diagrams of shear properties can be considered to be due to the different weft densities of these fabrics. The polar diagrams of shear rigidity and shear hysteresis with different weft densities are plotted in Fig. 6.24.

The highest shear rigidity and shear hysteresis are observed from the plain fabrics while the lowest is found from the 3/3 twill fabrics shown in Fig. 6.23. For different weft densities, the results obtained from Fig. 6.24 show that the values of shear rigidity and shear hysteresis increase with the increase in the weft density of woven fabrics. From all experimental results, the shape of the polar diagrams moves inward to outward when the fabric weave density increases. This is because a loose structure has lower inter-yarn friction and allows the relative movement of warp and weft yarns. As

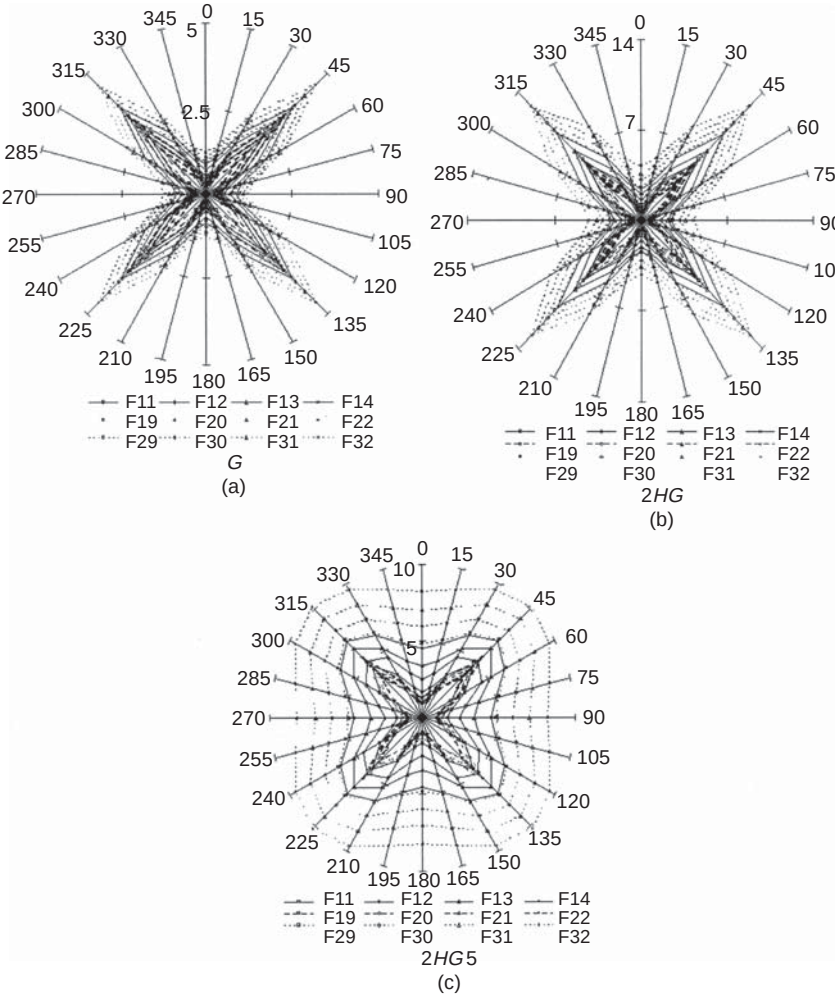

6.24 Effect of weft density on the polar diagrams of shear parameters: (a) *G;* (b) 2*HG;* (c) 2*HG*5.

a result, loose fabrics have the lowest shear rigidity and shear hysteresis. On the other hand, a tight structure avoids yarn movement, thus increasing the shear hysteresis of the fabrics. Therefore, a larger value of shear rigidity and shear hysteresis leads to an increase in the size of the polar diagram.

6.4.4 Relationship between shear rigidity and hysteresis in various directions

Existing literature shows a strong relationship between shear rigidity and shear hysteresis (Collier, 1991; Hu, 1994; Jeong and Phillips, 1998). The

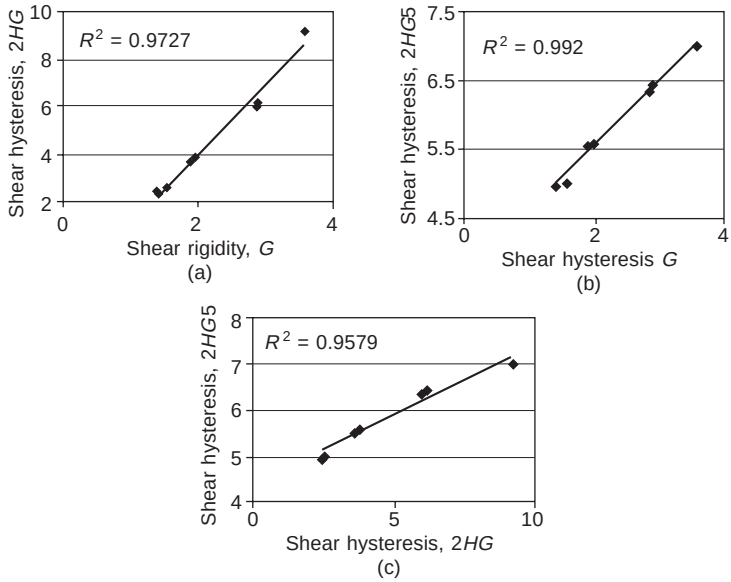

6.25 Relationship between shear rigidity and hysteresis in various directions: (a) 2*HG* and *G;* (b) 2*HG*5 and *G;* and (c) 2*HG*5 and 2*HG.*

relationships between shear rigidity (*G*) and shear hysteresis (2*HG* and 2*HG*5) of a fabric sample in various directions are illustrated in Fig. 6.25 parts (a)–(c) respectively. It can be seen that a strong linear relationship exists between shear properties in different directions. The coefficient of determination R^2 for 2*HG* and *G* in various directions is 0.9727, for 2*HG*5 and *G* in various directions is 0.9920 and for 2*HG*5 and 2*HG* in various directions is 0.9579. These strong linear relationships between shear rigidity and shear hysteresis at two angles, $R^2 > 0.90$, are also held in many other types of woven fabrics.

From these facts, it can be assumed that a similar mechanism operates for shear rigidity and hysteresis between both principal directions and bias directions. As shear rigidity of a fabric is mainly caused by the frictional forces existing in the yarns, shear hysteresis is also governed by its corresponding frictional force and the occurrence of the frictional force is continuous in the whole shear cycle. Higher values of shear rigidity appear in the bias directions and larger magnitudes of shear hysteresis can be found in these directions too.

6.5 Summary

Whenever bending occurs in more than one direction, so that the fabric is subject to double curvature, shear deformations of the fabric are involved. It

is thus not strange to find a strong relationship between the shear property and the bending property. Shear deformation is very common during the wearing process since the fabric needs to be stretched or sheared to a greater or lesser degree as the body moves. This chapter provides a comprehensive knowledge of the shear properties of woven fabrics and the conclusions reached include:

(1) The statement that bending and shear have identical nature is doubtful. The hardening of warp yarns has little effect on shear properties, but cover factor has a definite influence. Generally, large cover factor will produce large shear stiffness and shear hysteresis before the jammed condition is reached. After that, this effect is not apparent. The relation between bending and shear is not as strong as some literature has stated and, for some fabric types, like shengosen fabrics, they are totally different. This is because the two deformation modes operate in different ways although they both involve friction and yarn bending.

(2) The shear modulus and curves obtained on the KES shear tester are significantly different from those under the pure shear state, but they are still a good reflection of the shear properties of woven fabrics. Finite-element analysis can be successfully used to analyse the distribution of shear stresses and strains determined on the KES tester. The exact shear stress–strain relationship and actual shear modulus need modification for complex fabric deformation.

(3) A model derived from Kilby's work can be successfully used to predict the shear rigidity in all directions and extended to predict the shear hysteresis due to a strong linear relationship between them, which exists not only in the warp and weft directions but also in the bias directions. The shape of polar diagram of fabric shear properties is symmetrical to the warp and weft directions and has a crest given the maximum values in ± 45° directions. Moreover, the polar diagrams of shear rigidity and shear hysteresis will move outwards with the increase in weave density.

6.6 References

Behre B (1961), Mechanical properties of textile fabrics part I: shearing, *Text Res J*, **31**(2), 87–99.

Chapman B M (1980), Viscoelastic, frictional and structural effects in Fabric Wrinkling, in *Mechanics of Flexible Fibre Assemblies* (NATO Advanced Study Institute Series No. 38), Hearle J W S, Thwaites J J and Amirbayat J (eds), The Netherlands, Alpen ann den Rijn, Sijhoff and Noordhoff.

Collier B J (1991), Measurement of fabric drape and its relation to fabric mechanical properties and subjective evaluation, *Clothing & Text. Res J*, **10**(1), 46–52.

Collier J R, Collier B J, Toole G O and Sargrand S M (1991), Drape prediction by means of finite element analysis, *J Text Inst*, **82**(1), 96–107.

Cusick G E (1961), The resistance of fabrics to shearing forces, *J Text Inst*, **52**(9), T395–406.

Dawes V and Owen J D (1971), The assessment of fabric handle, *J Text Inst*, **62**, 233.

Dreby E C (1941), The planoflex: a simple device for evaluating the pliability of fabrics, *American Dyestuff Reporter*, **30**, 651–666.

Gan L, Steven G P and Ly N (1991), A finite element analysis of the draping of fabric *Proc 6th, Int Con in Australia on Finite Element Methods*, University of Sydney, Australia, July 8–10, 7.

Go Y, Shinohara A and Matsuhashi F (1957), Viscoelastic studies of textile fabrics part III: on the shearing buckling of textile fabrics, *Sen-i Gakkaishi*, **13**, 460–65.

Grosberg P and Park B J (1966), The mechanical properties of woven fabrics part V: the initial modulus and the frictional restraint in shearing of plain woven fabrics, *Text Res J*, **36**, 420–431.

Hu J L (1994), *Structure and Low Stress Mechanics of Woven Fabrics* (PhD thesis, University of Manchester Institute of Science and Technology).

Hu J L and Newton A (1993), Modelling of tensile stress–strain curves of woven fabrics, *J China Text Univ*, **4**, 49–61.

Jeong Y J and Phillips D G (1998), A study of fabric-drape behaviour with image analysis part II: effect of fabric structure and mechanical properties on fabric drape, *J Text Inst*, **89**(1), 70–79.

Kang T J, Lee J, Yu W R and Oh K H (1994), Prediction of woven fabric deformation using finite element method, *Proceedings of the International Symposium on Fibre Science and Technology*, **8**, 480.

Kawabata (1972), *Kawabata's Evaluation System for Fabric (KES-FB) Manual*, Kyoto, Kato Tech Co Ltd.

Kawabata S (1980, July), *Standardisation and Analysis of Hand Evaluation, 2nd ed*, Osaka, Textile Machinery Society of Japan.

Kawabata S, Niwa M, Ito K and Nitta M (1972), Application of objective measurements to clothing manufacture, *Int J Clothing Sci & Tech*, **2**(3/4), 8–31.

Kilby W F (1961), Shear properties in relation to fabric hand, *Text Res J*, **31**, 72–73.

Kilby W F (1963), Planar stress–strain relationships in woven fabrics, *J Text Inst*, **54**, T9–27.

Lindberg J, Behre B and Dahlberg B (1961), Mechanical properties of textile fabrics part III: shearing and buckling of various commercial fabrics, *Text Res J*, **31**(2), 99–122.

Lloyd D W, Shanahan W J and Konopasek M (1978), The folding of heavy fabric sheets, *Int J Mech Sci*, **20**, 521–527.

Lo W M (2001), *A Study of Fabric Anisotropy* (PhD Thesis, The Hong Kong Polytechnic University).

Lo W M and Hu J L (2002), Shear properties of woven fabrics in various directions, *Text Res J*, **72**(5), 383–390.

Lucas (1994), *FEA User's Manual and Theory Manual*, UK, Finite Element Analysis Ltd, Surrey.

Mahar T J, Dhingra R C and Postle R (1989), Fabric mechanical and physical properties relevant to clothing manufacture part I: fabric overfeed, formability, shear and hygral expansion during tailoring, *Int J Clothing Sci & Tech*, **1**(1), 12–20.

Mahar T J, Dhingra R C and Postle, R (1990), Measuring and interpreting low stress fabric mechanical and surface properties, *Textile Research Journal*, **60**, 7–17.

Mark C and Taylor H M (1956), Fitting of woven cloth to surfaces, *J Text Inst*, **47**, T477.

Morner B and Eeg-Olofsson T (1957), Measurement of the shearing properties of fabrics, *Text Res J*, **27**, 611–614.

Okabe H and Akami H (1984), The estimation of the three dimensional shapes of garments, *Report to the Polymer Materials Research Institute*, Japan, No, 142.

Oloffson B (1967), Study of inelastic deformations of textile fabrics, *J Text Inst*, **58**, 211.

Postle R, Carnaby G A and de Jong S (1976), Woven fabric shear and bending, *The Mechanics of Wool Structures*, Chichester, Ellis Horwood, 340–366.

Skelton J S (1976), Fundamentals of fabric shear, *Text Res J*, **46**, 862–869.

Skelton J S (1980), Shear of woven fabrics, in *Mechanics of Flexible Fibre Assemblies* (*NATO Advanced Study Institute Series; E Applied Sciences No. 38*), Hearle J W S, Thwaites J Je and Amirbayat J (eds), The Netherlands, Alpen ann den Rijn, Sijthoff and Noordhoff, 211–227.

Skelton J S and Schoppee M M (1976), Frictional damping in multicomponent assemblies, *Text Res J*, **46**, 661.

7

Fabric complex deformation analysis and simulation

7.1 Introduction

Drape can be generally classified into two categories, namely two-dimensional drape and three-dimensional drape. A two-dimensional drape means that a fabric bends under its own weight in one plane while three-dimensional drape allows a fabric to be deformed into folds in more than one plane under its own weight. The study of three-dimensional drape was begun by Chu *et al.* (1950) when they established a measuring method for fabric drape using the F.R.L. Drapemeter. Chu quantified the drapeability of a fabric into a dimensionless value termed the drape coefficient which is defined as the percentage of the area from an angular ring of fabric covered by a vertical projection of the draped fabric. The apparatus was further studied by Kaswell (1953) and later revised by Chu *et al.* (1960, 1962). Finally, Cusick (1968) re-investigated the experimental method by using a parallel light source which reflects the drape shadow of a circular specimen from a hanging disc onto a paper ring (Fig. 7.1). He also modified the calibration of Chu's drape coefficient in terms of paper-weighing method. In recent years, the emphasis has been on improving the efficiency and accuracy of Cusick's drapemeter by using digital readout of the drape shadow from photovoltaic cells (Collier,

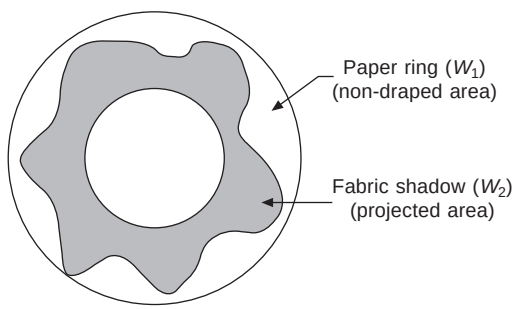

7.1 Measurement of the drape coefficient using image analysis.

1991), as well as computerised image analysis (Vangheluwe and Kiekens, 1993).

Both subjective and objective evaluations can be found in the literature on fabric drape study. Objective evaluation of fabric drape involves the measurement of the drapeability in terms of drape coefficient, drape profile and node analysis from Cusick's drapemeter (1962, 1965, 1968), and simulating fabric drape by various mechanical methods such as finite-element analysis (1962, 1965, 1968). On the other hand, fabric drape is also affected by psychological factors which relate to human perceptions and fashion. Subjective evaluation of the drape of a fabric involves the rating of drapeability on a garment such as a skirt, and image analysis on circular fabrics (Dowlen, 1976). Generally, subjective evaluation of fabric drape can provide understanding which relates to person, place, custom and fashion trends. Thus, subjective evaluation of fabric drape is an investigation aimed at understanding the human perception of drape of fabrics.

Basically, fabric drape is not an independent fabric property. It relates to fabric bending, shear, tensile, fabric thickness and fabric weight (Niwa and Seto, 1986; Collier, 1991; Hu and Chan, 1998). A fabric bends under its own weight during draping. Fabrics bend differently according to different fabric directions. Peirce (1930) also termed fabric bending under its own weight as drape stiffness. Since drape behaviour in two dimensions can be evaluated by a cantilever test in which bending length and bending rigidity are the measurable objective values for describing the two-dimensional drapeability of fabrics, the use of bending length and bending rigidity as the indices to trace the drape properties is important.

7.2 Drape categories and fabric cantilever

7.2.1 Three-dimensional drape

7.2.1.1 Objective measurement

Chu *et al*. (1950) had quantified the drapeability of a fabric into a dimensionless value termed the drape coefficient (*DC*%). The apparatus was further studied by Kaswell (1953) and later revised by Chu *et al.* (1960, 1962). At last, Cusick (1965, 1968) investigated again the experimental method by using a parallel light source which reflects the drape shadow of a circular specimen from a hanging disc onto a paper ring. In Cusick's modified formula, the drape coefficient is defined as the ratio of the paper weight from the drape shadow W_2 to the paper weight of the full specimen W_1. The formula is shown in dimensionless quantities in equation 7.1. The quantitative value of *DC*% can represent the drapeability of fabrics in three dimensions. *DC*% is high on stiff fabrics but *DC*% is low on limp fabrics.

$$DC\% = \frac{W_2}{W_1} \times 100\ (\%) \qquad [7.1]$$

Cusick's experimental method consists of hanging a 15 cm radius fabric specimen over a 9 cm radius supporting disc, a parallel light source inside the drapemeter will then form a shadow from the draping specimen on a piece of paper. The shadow pattern on the paper can be traced out and (*DC*%) can then be calculated. Alternative specimen sizes can be adopted according to different fabric properties. An 18 cm radius specimen may be used for a stiff fabric if its *DC*% on a 15 cm radius specimen is greater than 85 %. In another case, a 12 cm specimen may be used for a very limp fabric if its *DC*% on a 15 cm radius specimen is smaller than 30 %.

More recently Collier *et al*. (1991) designed a digital drapemeter to evaluate drape coefficient by using photovoltaic cells. Cusick's experimental drapemeter was used but photovoltaic cells were applied to the bottom surface of the Cusick paper to determine the amount of light blocked by a fabric specimen draped on a pedestal. A digital display gives the amount of light being absorbed by the photovoltaic cells, which is related to the amount of drape of the fabric specimen. The method is more convenient and accurate than the paper tracing method.

Vangheluwe and Kiekens (1993) measured the drape coefficient using image analysis. A charge coupled device (CCD) camera was mounted centrally above the drapemeter. This camera sent the image to a monitor and a frame grabber in a personal computer, and the frame grabber digitised the image. Calibration of the drape coefficient was preceded by recording the image from the drape tester in terms of area. The image analysis system saves both time and paper. The drape coefficient can be evaluated accurately within a few seconds. Because the measuring system is more time-efficient, change of drape can be measured and comparisons made within a short time.

Stylios *et al*. (1996) developed a new generation of drapemeter which measured the drape of any fabric both statically and dynamically in three dimensions by using a CCD camera as a vision sensor. This system, called the Marlin Monroe Meter (M^3), was used to measure the drape behaviour of fabric without being restricted to small circular fabric specimens, and to verify the theoretical prediction model. The draped profile of the specimen was taken and presented on a computer. In addition to this, evaluation of three-dimensional drape on a real garment can also be carried out using the Moiré Camera System (Iwasaki and Niwa, 1983; Niwa and Suda, 1984). The system can convert images into digital data; for example the three-dimensional drape image of a flared skirt can be successfully predicted and presented on paper.

7.2.1.2 Subjective measurement

The numerical value from the drape coefficient is not sufficient to represent drape behaviour. Drape is differentiated even when fabrics have the same value of *DC*%. In practice, using only the numerical value of *DC*% drape appearance cannot be fully described. Thus, Cusick's drape study involves not only objective measurement through a numerical value of drape coefficient, but also subjective evaluation. Rating of drape profile is a very typical example of subjective measurement of fabric drape; the rating result depends on person, place, custom, fashion trends, etc. The node analysis will usually involve the counting of node number, the measurement of the node length, as well as the observation of drape behaviour (Hearle, 1969).

Cusick (1962) mounted semi-circular fabrics with various cottons and rayons in the shape of a skirt on a model. The model was rated to see which skirt could drape most. The results indicated that a good drape as assessed by objective measurement almost matches one assessed by subjective selection. The subjective rating of fabric drape is rather inconsistent. However, the fabric with the most drape may not be the preferred one. The subjective study pointed out that the drape of fabric is also a psychological phenomenon which is related to human perceptions and fashion trends.

Collier (1991) reported that subjective drape is affected by the length of draping fabric on the pedestal. He carried out experiments comparing the subjective rating of drape as 'not preferred' with the objective experimental results. He found that results can be accurately predicted by garment professionals; however, he also pointed out that subjective measurement is closely related to the fashion trends in certain time periods.

Ayada and Niwa (1991) found that fabric mechanical properties are highly related to fabric drape. They made 24 skirts for subjective evaluation of total quality and visual beauty of skirts. It was found that bending, shear and fabric weight are the important factors influencing the garment appearance. In addition, dynamic drape of fabrics is also related to the mechanical properties. Subjective evaluation of dynamic drape (Izumi and Niwa, 1985; Mamiya and Kanayama, 1985; Niwa and Seto, 1986) is found to be highly correlated with dynamic bending and shear properties, as well as the hand feel. The results of the investigation are important in targeting and responding to customer demand.

7.2.2 Two-dimensional drape

7.2.2.1 Evaluation methods of fabric cantilever

Peirce (1937) initiated the study of fabric drape using the fabric cantilever in 1930. In this section, fabric drape can be evaluated using the cantilever test in which bending length, a numerical term in equation 7.2 for evaluating

fabric stiffness and drape of the cantilever, can be obtained. Bending property can also be quantified into a series of mathematical functions such as flexural rigidity and bending modulus in equations 7.3 and 7.4. In theory, the easier the fabric is to drape, the shorter is the bending length. Thus, Peirce termed the bending length drape stiffness. Peirce's mathematical expressions of bending length could not be solved analytically; thus Peirce used Hummel and Morton's (1927) approximation method to evaluate bending length. In Peirce's study, evaluation methods can be adopted for fabrics in the two extreme categories – very stiff and very limp. For very stiff fabrics, a weight can be added to the free-end of the specimen; the evaluation of bending length for stiff fabric can be modified into equation 7.5. For very limp fabrics, bending length can be obtained from equation 7.6 from a heart loop test. Pierce assumed a general fabric cantilever, which deformed under its own distributed weight, and a stiff fabric cantilever deformed by the concentrated weight at the tip end.

Postle and Postle (1992) also provided a very detailed explanation for the weight effect on drape of a fabric cantilever. They used bending length in the drape study, and taking advantage of the wide availability of computers, solved the differential equation by the finite-difference method.

Grosberg and Swani found that drape of a fabric cantilever is the combined effect of both the distributed and concentrated weight (Grosberg, 1966; Grosberg and Swani, 1966). A draped cantilever is divided into two sections. The first section near the hanging edge bends under its own distributed weight and a concentrated weight from the second section. They assumed that the second section of the fabric cantilever is straight and will not bend during draping. Also, fabric weight of the second section exists as a concentrated point load at the centre of this section. The total deflection of the fabric cantilever is the combined deflections of these two sections. The point O is the junction of these two sections at which bending moment is equal to M_o. If an applied moment M is greater than M_o, the fabric will bend. If an applied moment M is smaller than M_o, the fabric will remain straight. The analytical solution is obtained by Bickey's approximated methods (1936). His frictional couple theory is one of the non-linear models which can explain the bending property in terms of bending rigidity, frictional couple and curvature of cloth. The model can specify the real situation existing on the cantilever.

However, Peirce's beam theory assumed a linear bending behaviour for fabrics and is known as the classical linear model. In fact, most fabrics bend in a non-linear way. Besides, Peirce's evaluation method only provides an average value for the fabric drape and bending behaviour. Therefore, other non-linear models, including bilinear bending theory, indirect measurement of moment–curvature and large deformation (Clapp *et al*., 1990; Grosberg and Swani, 1966; Huang, 1979; Leaf and Anandjiwala, 1985; Potluri *et al*., 1996), have been developed. They are all non-linear studies of bending

behaviour. Equations for bending length C, bending rigidity B and bending modulus q are given by:

$$c = l\left(\frac{\cos 0.5\theta}{8\tan\theta}\right)^{1/3} \quad [7.2]$$

and $$B = wc^3 \quad [7.3]$$

$$q = \frac{12B}{t^2} \quad [7.4]$$

where l is fabric length, θ is bending angle, t is fabric thickness and W is distributed weight. Hence

$$c = l\left(\frac{W}{2wbl} + 0.13\right)^{\frac{1}{3}}\left(\frac{\cos 0.93\theta}{\tan\theta}\right)^{\frac{1}{3}} \quad [7.5]$$

and

$$c = 0.1337L \cdot f_2(\theta) \quad [7.6]$$

where

$$f_2(\theta) = \left(\frac{\cos\theta}{\tan\theta}\right)^{\frac{1}{3}},\ \theta = 32.85^\circ\ \frac{l - 0.1337L}{0.1337L}$$

and b is the width of the fabric strip, L is the length of the beam and f_2 denotes a function of θ.

7.2.2.2 Theories of fabric cantilever with different weight distributions

Classical beam theory

Potluri *et al*. (1996) conducted differential equations to describe the drape profile of the fabric cantilevers having distributed weight and concentrated weight at the tip. They reported that Peirce's cantilever study is based on the concept of the classical beam theory from which fabric beam is assumed to satisfy the Bernolli–Euler law. The Euler law states that the bending moment of a beam is proportional to the radius of curvature of the beam R caused by that moment, as shown in equation 7.7. Two assumptions are made when the theory is applied to a cantilever. It is assumed that the curvature is evaluated by the approximate equation and change in length of moment arm during beam deflection is ignored. Since $1/R \cong \mathrm{d}^2y/\mathrm{d}x^2$

$$M = B\frac{\mathrm{d}^2y}{\mathrm{d}x^2} \quad [7.7]$$

By simple mechanical theory, the applied bending moment of the beam is also equal to the product of the applied load on the cantilever to the perpendicular distance of the line of action x. Two cases of applied loading are studied: one with weight and one with distributed weight.

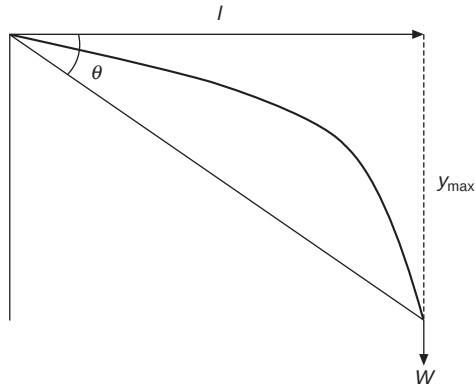

7.2 Cantilever beam with concentrated load *W*.

Fabric cantilever with concentrated weight
In this case the applied load *W* is acting on the free tip end of the cantilever as shown in Fig. 7.2, and equation 7.8 is developed:

$$M = B\frac{d^2y}{dx^2} = -Wx \qquad [7.8]$$

By double integrating equation 7.8 and applying the boundary condition, equation 7.9 is obtained where bending rigidity of the beam can be found from the deflection angle.

$$\tan\theta = \frac{Wl^2}{3B} \qquad [7.9]$$

Peirce developed an empirical relation from his experimental results by multiplying the right side of equation 7.9 by a factor of cos 0.93θ. As a result, the Peirce bending equation for a concentrated weight at the tip end of the cantilever is formed in equation 7.10.

$$\frac{B}{Wl^2} = \frac{\cos 0.93\theta}{3\tan\theta} \qquad [7.10]$$

Fabric cantilever with distributed weight
The deflection of a cantilever due to the distributed load from its own weight can be seen in Fig. 7.3. A uniformly distributed weight *w* is applied along the length of the cantilever and thus equation 7.9 can be rewritten to form equation 7.11.

$$M = B\frac{d^2y}{dx^2} = -\frac{wx^2}{2} \qquad [7.11]$$

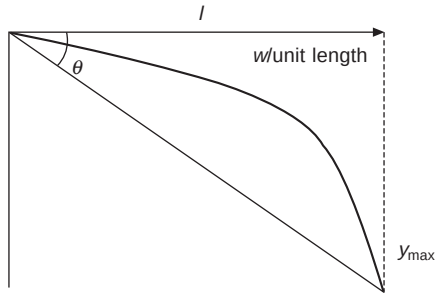

7.3 Cantilever beam with uniformly distributed load *w*.

Again, by double integrating equation 7.11 and applying the boundary conditions, equation 7.12 is obtained where bending rigidity of the beam can be found from the deflection angle.

$$\tan\theta = \frac{wl^3}{8B} \qquad [7.12]$$

Peirce developed an empirical relation from his experimental studies by multiplying the right-hand side of equation 7.12 by a factor of cos 0.5θ. As a result, Peirce's bending equation for the distributed weight is formed in equation 7.13.

$$\frac{B}{wl^3} = \frac{\cos 0.5\theta}{8\tan\theta} \qquad [7.13]$$

In Peirce's paper (1930), he defined the term B/w as equal to the cube of the bending length c where bending length is a quantitative value to measure a strip's drapeability in two dimensions. Equation 7.13 can be rewritten as equation 7.14 from which bending length can be evaluated from the extended fabric length l that bends to an angle θ under its own weight. Peirce's cantilever formula as shown in equation 7.14 is extensively adopted to describe the characteristics of fabric stiffness and fabric drape in two dimensions.

Since $c^3 = B/w$

$$c^3 = l^3\frac{\cos 0.5\theta}{8\tan\theta} \qquad [7.14]$$

7.2.2.3 Testing methods of fabric cantilever

In Peirce's theory, bending length c of the fabric cantilever can be evaluated either by measuring the extended fabric length (l) under a fixed angle or by measuring an angle from the extension of a fixed length l. The Flexometer shown in Fig. 7.4 can be used as a testing instrument for measuring the

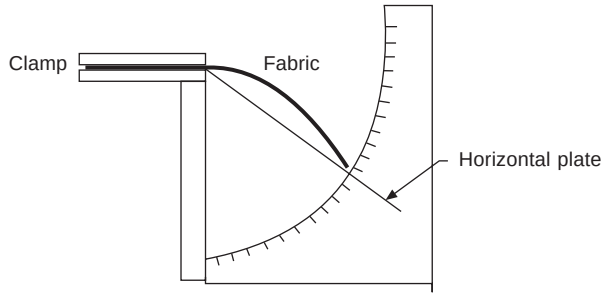

7.4 Flexometer.

bending angle θ of a draped cantilever with a constant length l. Bending length c can be evaluated from this bending angle by the mathematical formula shown in equation 7.14.

A bending tester from the Shirley Institute (Booth, 1968; Feather, 1970) is specially designed for measuring an extended length l with a fixed angle. The extended fabric bends under its own weight until the free end intercepts a plane at an angle of 41.5° from the horizon. Figure 7.5 shows the concept of Shirley's bending tester. With this fixed angle, the expression $(\cos 0.5\theta/8 \tan \theta)^{1/3}$ in equation 7.14 will be equal to 0.5. Thus, the bending length is calculated by a simple formula from equation 7.15. If $\theta = 41.5°$,

$$c = 0.5l \qquad [7.15]$$

In recent years, the experimental process has been simplified more. The Fabric Assurance by Simple Testing (FAST) system consists of cantilever bending meter. The FAST-2 Bending meter can be used to measure the bending length using the same concept as the Shirley Stiffness Tester. A photocell detector for detecting the free end is used. The extended fabric l bends under its own weight until the free end intercepts at an angle of 41.5°

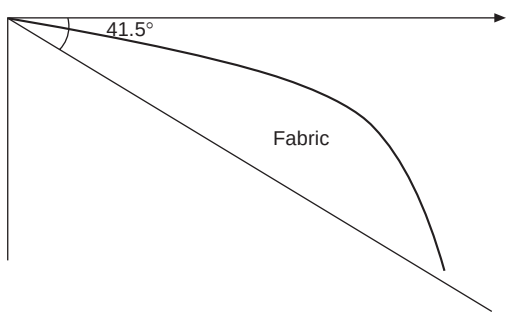

7.5 Concept of Shirley's and FAST bending meters.

from the horizon. Then, a photocell detector inside the measuring cavity detects the length of *l*. Experimental results are recorded directly in the computer. Bending length evaluated from equation 7.15 can be displayed digitally.

Clapp *et al*. (1990) developed an indirect method of measuring the moment–curvature relationship for fabrics. At the same time, they developed a method to measure the draped profile of the fabric cantilever. Deformed co-ordinates were recorded as a fabric sample was cantilevered under its own weight from a fixed support. The advantage of this method is that fabric non-linear bending behaviour, inherent in most fabrics, is readily obtained, unlike in the traditional cantilever beam test. The draped image obtained by using a laser sensor can be used to verify the numerical simulation results.

Potluri *et al*. (1996) also developed an experimental technique to verify their numerical method for the capability to simulate in general situations. A laser triangulation sensor, attached to a robot arm, was used to measure the cantilever profile of the fabric samples. A manipulating device positions the fabric sample as a fabric cantilever of specified length. The laser scans along the centre line of the fabric cantilever. The *x* co-ordinates are obtained from the robot position and the *y* co-ordinates from the output signal of the triangulation sensor.

7.2.3 Relationship between fabric drape and mechanical properties

The drape coefficient provides an objective description of drape deformation in three dimensions, but the study of three-dimensional fabric drape is not independent. In general, fabric drape is closely related to fabric stiffness (Hearle and Amirbayat, 1986a,b,c). Very stiff fabrics have drape coefficients approaching 100 %; very limp, loose, or open-weave rayon fabrics have *DC*% about 30 %. *DC*% is about 90 % for a starched cotton gingham. The drape coefficient provides an objective description of drape deformation in three dimensions, but the study of three-dimensional fabric drape is not independent. In other words, the study of three-dimensional drape in terms of *DC*% is empirically related to two-dimensional drape in terms of bending properties.

Chu *et al*. (1960) found that drapeability is dependent on three basic fabric parameters: Young's modulus *Y*, the cross-sectional moment of inertia *I*, and weight *W*. From their study, an equation was generated in which drape coefficient is equal to $f(YI/W)$. Later, Yamada *et al*. (1995) also reported that the drape area changes positively to $(EI/W)^{1/3}$ with a scale factor. When bending rigidity per weight (EI/W) of fabric is similar to each other, *DC*% and deflection angle obtain similar values.

Cusick (1965) proved by statistical evidence the hypothesis that fabric drape involves curvature in more than one direction, and that the deformation is dependent on the shear angle A in addition to bending length c. He used 130 fabrics for his multiple regressions. Regression equations were formulated for the relationship between drape coefficient, bending length and shear angle:

$$DC = 35.6c - 3.61c^2 - 2.59A + 0.0461A^2 + 17 \quad [7.16]$$

For this equation, residual sum of squares of the regression is the smallest when c and A are both considered to be the main factors influencing the DC%.

Mooraka and Niwa (1976) generated an equation to predict fabric drape using data from the KES system and concluded that fabric weight and bending rigidity were the most important factors. In their study, DC% is found to be determined by $(B/W)^{1/3}$. The correlation coefficient r between DC% and $(B/W)^{1/3}$ is 0.767 which is greater than the value of 0.686 for DC% and B only. The use of bending rigidity from the warp, weft and bias on a regression equation allows for better prediction of DC% than by using a mean bending rigidity. Physical properties which contribute greatly to the DC% are bending properties followed by weight and thickness, and then the shear properties. When bending and shearing hysteresis is large, DC% would be large and unstable.

Collier (1991) authored a paper in which six parameters were measured: shear stiffness, bending hysteresis, bending stiffness, shear hysteresis at 0.5°, shear hysteresis at 5°, from the KES testers, and bending rigidity from cantilever. He found that both bending stiffness from the KES and bending rigidity from the cantilever, as well as shear hysteresis and thickness, were significant in the model predicting the drape coefficient. However, shear hysteresis and bending stiffness from the KES explained most of the variation, with the other two variables being less important. They concluded that shear hysteresis is more important.

Niwa and Seto (1986) published a paper concerned with the relationship between drapeability and mechanical properties of fabrics. They used mechanical parameters $(B/W)^{1/3}$, $(2HB/W)^{1/3}$, $(G/W)^{1/3}$ and $(2HG/W)^{1/3}$ as independent variables, where B, $2HB$, W, G and $2HG$ are bending rigidity, bending hysteresis, weight per unit area, shear stiffness and shear respectively. These parameters were derived from the analysis of the bending of a cantilever of fabric having hysteresis in bending and shear by applying the heavy elastica theory. An equation to describe drape coefficient was then introduced.

From the above studies, three-dimensional drape in terms of DC% is closely associated with two-dimensional drape study in terms of bending length and bending rigidity. Nevertheless, DC% from three-dimensional drape study is also influenced by other fabric physical properties which include

shear and tensile properties as well as fabric weight and fabric thickness (Hu and Chan, 1998; Hu *et al*., 2000; Suda *et al*., 1984a,b; Tanabe *et al*., 1975). In addition, mechanical fabric properties also proved to be correlated to subjective drape evaluation (Okabe and Akami, 1984; Yamakawa and Akiyama, 1996). Although two-dimensional drape study is only a partial measure of drape behaviour, it is the most important index for predicting three-dimensional drape behaviour. Many numerical and theoretical investigations of fabric drape used the two-dimensional drape of a fabric cantilever to verify their mechanics models or the accuracy of their software programs (Gan and Steven, 1995).

7.3 Modelling of fabric drape profile

7.3.1 Background

Drape profile (*DP*) of a fabric is a projected two-dimensional image taken from the Cusick Drapemeter. It is characterised in terms of drape coefficient, node locations and node numbers of the projected image of a fabric. This section will introduce an attempt made to develop a model for the prediction of *DP* of fabrics using polar co-ordinates directly measured from the drapemeter. Drape coefficient, node locations and number of the drape profile of a fabric can all be determined by this model. Polar diagrams of the *DP* model will also be provided. The constants in the *DP* model can be either estimated using the polar co-ordinate fitting technique, or directly calculated from fabric bending and shear properties using regression analysis.

7.3.2 Modelling

A fabric drape profile can be captured in a two-dimensional image projected from a three-dimensionally draped fabric sample on the so-called Cusick Drapemeter by digital camera. From this image, node locations and numbers and the detailed shape of the drape profile can be observed from the computer screen, and the fabric drape coefficient can be accurately and automatically calculated by Leica QWin image analysis software. Although the nodes are not uniform, the drape profile exhibits a cyclic change in polar co-ordinates. Some assumptions, which have to be made to establish a mathematical model for the description/prediction of fabric drape profile measured by the above method using polar co-ordinates, are listed as follows:

(1) the fabric freely hangs under its own weight;
(2) nodes are evenly distributed around the plate and all node shapes are identical;
(3) the average value of node numbers of one fabric sample is a positive integer.

A trigonometric function is selected for the modelling,

$$r = p + q \sin (k\theta + \alpha) \qquad [7.17]$$

where p is the average radial length taken between the peaks and troughs of the draped profile, q is the half depth of the draped node, r is the radius of the projected drape profile, k is the number of nodes (peaks) in the drape profile while α is a constant which represents an angle between the fabric warp direction and its neighbour peak. The details are demonstrated in Fig. 7.6b. Figure 7.6a illustrates the image analysis system used for the measurement of fabric drape profile, in which a digital camera connected to a personal computer is used to capture the projected two-dimensional draped image directly from the drapemeter while the printer and digitiser are used to print out the drape profile results. Computer software, Leica QWin image analyser, serves the function of automatically calculating the drape coefficient from the captured image.

The constants p, q and k in the model can be either estimated by polar co-ordinate fitting technique or determined using multiple and stepwise regression analysis from SPSS based on the relationship between fabric mechanical properties and fabric drape. With the values of the constants known, the drape coefficient, node locations, node numbers and node shape of the drape profile of a fabric can be automatically predicted by this model. In particular, the projected area A_2 under the fabric drape profile is calculated in the following:

$$\begin{aligned} A_2 &= \int_0^{2\pi} \frac{1}{2} r^2 \mathrm{d}\theta \\ &= \frac{1}{2}\int_0^{2\pi} [p + q \sin (k\theta)]^2 \, \mathrm{d}\theta \\ &= \pi\left(p^2 + \frac{q^2}{2} \right) \end{aligned} \qquad [7.18]$$

Drape coefficient (DC%) is defined as the ratio of the projected area of draped fabric to the original non-draped area A_1 multiplied by 100:

$$DC\% = \frac{A_2}{A_1} \times 100\ \% \qquad [7.19]$$

Node location is defined as the position of a peak found in the drape profile (polar diagram) expressed in degrees. Node number is the number of nodes (peaks) in the drape profile while node profile is defined as the shape of each draped node.

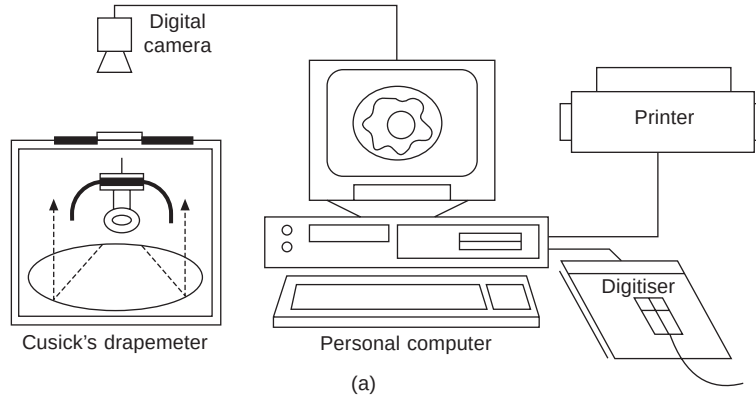

(a)

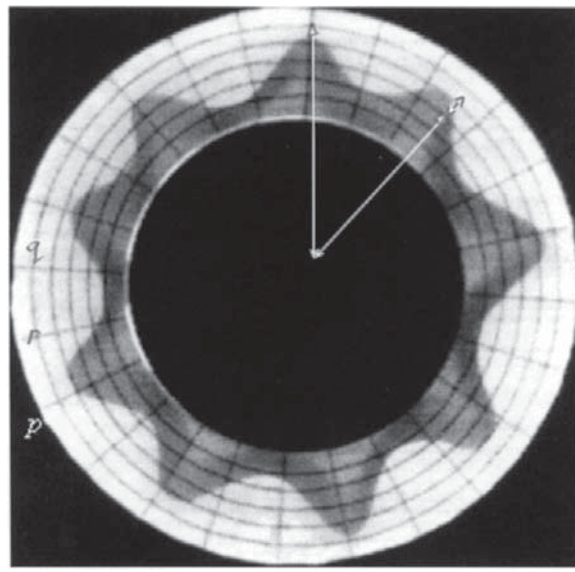

(b)

7.6 The set up for the measurement of fabric drape profile: (a) image analysis system; (b) captured image on the drapemeter.

7.3.3 Prediction of *DP* using constants from polar co-ordinate fitting

The three constants p, q and k in equation 7.17 can be determined by the polar co-ordinate fitting technique using a computer program written in the MATLAB software package. The input parameters of the computer program

are the co-ordinates (r, θ) of the draped profile with θ from 0–352.5° at every 7.5°. The predicted graphical drape profile is presented in the form of a polar diagram.

7.3.3.1 Drape profile

The drape profiles (*DP*) of plain, twill and satin woven fabrics are illustrated in Figs 7.7a–c. It can be seen that the theoretical model gives good agreement with the experimental data with some deviations in the node numbers and locations in the drape profile. The deviation between the theoretical and experimental *DP* of different woven fabrics is not more than 10 %.

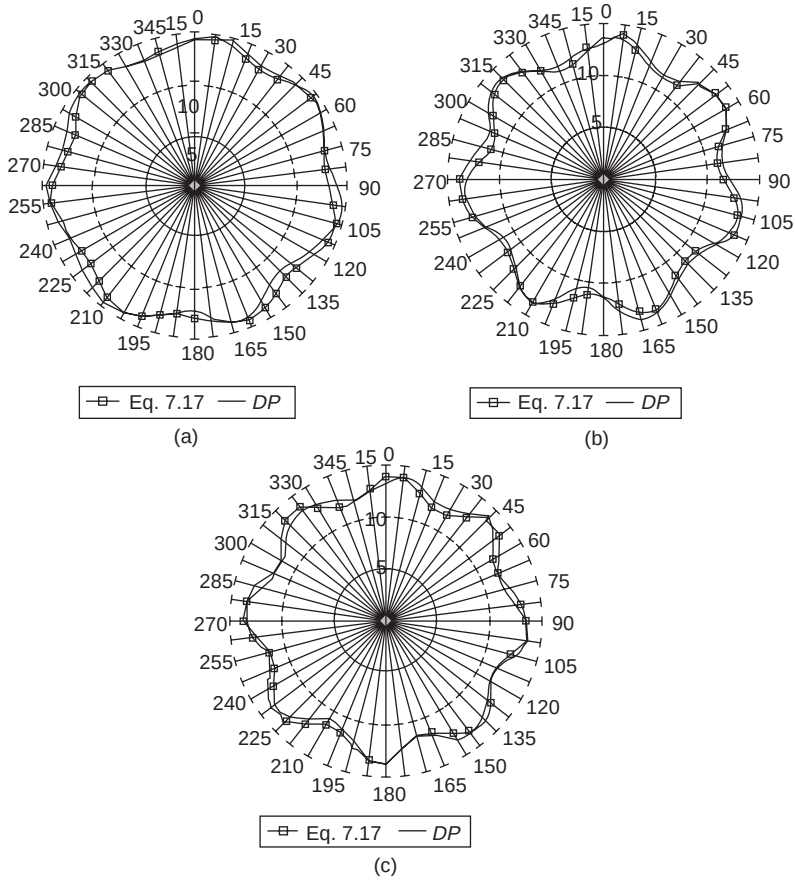

7.7 Theoretical and experimental results of drape profile of woven fabrics: (a) plain weave; (b) twill weave; (c) satin weave.

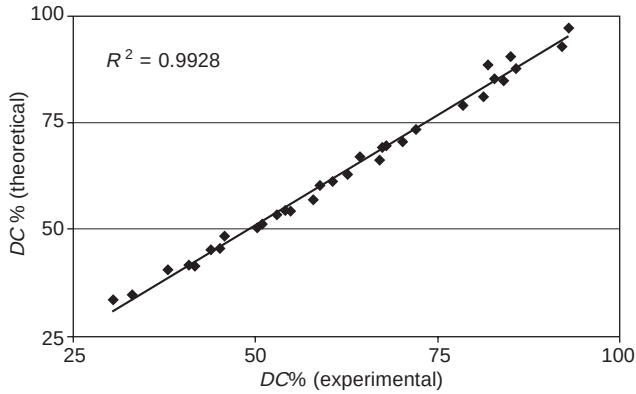

7.8 Relationship between theoretical and experimental *DC*%.

7.3.3.2 Drape coefficient

The validity of the model described above for the prediction of fabric drape profile can be further verified using excellent agreement between the theoretical and experimental results for drape coefficient (*DC*%) of 35 different types of fabrics exemplified in Fig. 7.8. That is, the experimental and the theoretical *DC*% have high coefficient of determination (R^2 = 0.9928). This means that over 99 % of experimental *DC*% can be explained by the theoretical *DC*%. The deviation between the theoretical *DC*% predicted from the *DP* model and the experimental *DC*% is smaller than 8.3 %.

7.3.3.3 Node number and location

As can be seen from Fig. 7.8, the theoretical model gives good agreement with some of the experimental data with some deviations in the node numbers and locations in the drape profile. This section shows that the model is applicable in average terms. This is because, although node numbers and their locations may vary from time to time, perhaps, on average a certain fabric should have a certain number of nodes and node locations. Some evidence is presented below.

The repetitions of the node numbers of one draped fabric sample under different drape tests are shown in Figs 7.9a and b. The results obtained from Fig. 7.9a imply that the drape node numbers of one fabric sample are 6, 7 and 8. The repetitions of 6, 7 and 8 nodes within 12 trials are 1, 9 and 2 respectively while 7 nodes give the majority in this sample. Therefore, in this case, the mean value of node number calculated from 12 trials is equal to 7.08. As the number of nodes in the fabric drape test must be a positive integer, we round off the mean value of the node number to get 7 nodes for this fabric sample. This result is very close to the mean value of node number, 7.08, with deviation 1.14 % and proves that the mean value obtained from

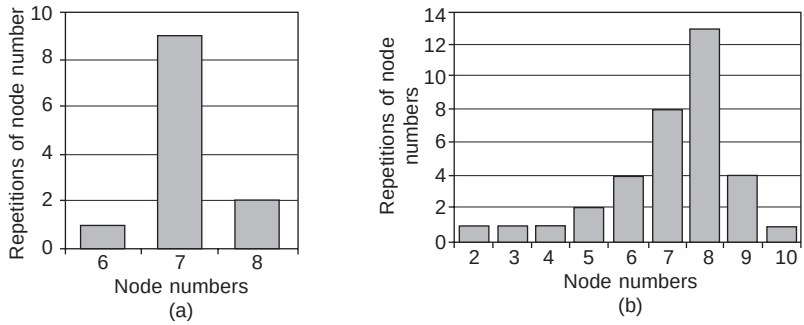

7.9 The repetitions of the node numbers within (a) one fabric sample and (b) 35 woven fabrics.

constant k in the *DP* model is acceptable in the prediction of draped node numbers.

If the same test is extended to a total of 35 woven fabrics, it is found that 8 nodes is the most frequent number to appear in the 35 woven fabrics, as shown in Fig. 7.9b. Selecting those fabrics having 5–10 nodes for analysis, a comparison is presented in Table 7.1 of their theoretical and experimental node locations, where the peaks are found in the polar diagram, which indicates

Table 7.1 Correlation coefficient between each constant in *DP* model and all selected fabric mechanical properties

Mechanical properties	**Average of mechanical property in the warp and weft directions**			**Average of mechanical property in the warp, weft and ±45° directions**		
	p	***q***	***k***	***p***	***q***	***k***
B	0.497*	0.474*	0.556*	0.617*	0.604*	0.652*
2*HB*	0.542*	0.529*	0.551*	0.682*	0.632*	0.672*
G	0.672*	0.679*	0.678*	0.723*	0.723*	0.612*
2*HG*	0.715*	0.724*	0.625*	0.740*	0.724*	0.676*
2*HG5*	0.730*	0.721*	0.690*	0.780*	0.750*	0.682*
LT	0.451*	0.407	0.456*	0.408*	0.343	0.450*
WT	0.429*	0.482*	0.291*	0.388	0.444*	0.225
RT	0.206	0.239	0.159	0.258	0.298	0.172
EMT	0.040	0.107	0.085	0.085	0.159	0.067
W	0.415*	0.344	0.435*	0.415*	0.344	0.435*
T	0.265	0.321	0.236	0.265	0.321	0.236
$\sqrt[3]{B/W}$	0.370	0.290	0.481	0.444*	0.376	0.539*
$\sqrt{2HB/W}$	0.600*	0.540*	0.615*	0.634*	0.582*	0.638*
$\sqrt[3]{G/W}$	0.487*	0.435*	0.470*	0.627*	0.583*	0.600*
$\sqrt{2H/W}$	0.523*	0.474*	0.471*	0.663*	0.664*	0.511*
$\sqrt{2HG5/W}$	0.636*	0.555*	0.616*	0.684*	0.636*	0.651*
Stepwise regression	0.684	0.664	0.700	0.847	0.750	0.782

*Significant value at $p < 0.005$

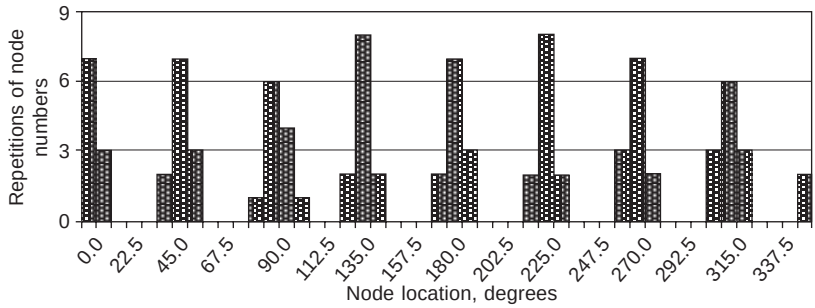

7.10 Node locations of 8 nodes in various directions.

a close relationship with deviation as low as 0.9°. Figure 7.10 illustrates the node location of each respective node for a fabric with 8 nodes, which indicates clearly that the probability of node repetition is comparatively high at 0°, 45°, 90°, 135°, 180°, 225°, 270° and 315° for 8 node numbers. Undoubtedly, the above facts also indicate that constant *k* in the *DP* model is not applicable only in predicting the node numbers, but also in determining the node locations.

Another conclusion which can be reached is that the higher the value of *DC*%, the lower the number of nodes: for stiffer or heavy fabrics with a *DC*% value larger than 85 %, 2–5 node numbers are recorded; for those medium fabrics whose *DC*% values fall in the range 50–85 %, they exhibit 6–8 node numbers; while for loose or light woven fabrics with a *DC*% value between 30 % and 50%, 9 or 10 node numbers can be observed. These facts confirm the findings of Cusick (1962) that the number of nodes is governed by the fabric stiffness.

7.3.3.4 Node profile

Since a woven fabric is anisotropic and exhibits different values of mechanical properties in different directions, each draped node may exhibit different shape. However, it is found that the agreement between the theoretical and experimental node profile has only minor deviations as demonstrated in Fig. 7.8. This may reveal that all node shapes in the drape profile can be assumed to be similar to each other and the mean value of node profile assumed in the *DP* model is acceptable in predicting the fabric drape profile.

7.3.4 Prediction of *DP* using fabric mechanical properties from regression analysis

In addition to polar co-ordinate fitting, the fabric drape profile can also be predicted from fabric mechanical properties using regression analysis. In

addition, stepwise regression can be adopted to determine which combination of mechanical properties gives the best description in predicting the fabric drape profile.

7.3.4.1 Drape profile

Sixteen mechanical properties are used in regression analysis, including bending (*B* and 2*HB*), shear (*G*, 2*HG* and 2*HG*5) and tensile (*WT*, *EMT*, *LT* and *RT*) properties, fabric weight (*W*) and fabric thickness (*T*). Among the selected mechanical properties, bending and shear properties give significant correlations with the constants *p*, *q* and *k* in the drape profile (*DP*) model while bending hysteresis and shear hysteresis have higher correlation coefficient, *r*, than their rigidities. In addition, the results indicate that the values of mechanical properties taken in the warp, weft and ± 45° directions have higher *r* than those taken only in the warp and weft directions. With all correlation coefficients between the constants in the *DP* model and the mechanical properties, the best combination in predicting the fabric profile can be found by using stepwise regression. The criterion of stepwise regression for entering a parameter was $p = 0.05$ and that for removal was 0.1.

After the removal of all variables that correlated with each other and were within the same mechanical property group, the most important properties are entered into the final equations given below:

$$p = 10.795 + 7.458(2HB_T) + 0.1087(2HG5_T) \quad [7.20]$$

$$q = 0.5116 + 1.861(2HB_T) - 0.122(2HG_T) \quad [7.21]$$

and

$$k = 2.753 + 0.8153(2HB_T) - 0.469(2HG5_T) \quad [7.22]$$

where 2*HB*, 2*HG* and 2*HG*5 are the bending hysteresis, shear hysteresis at 0.5° and shear hysteresis at 5° respectively. Suffix *T* is the mean value of its property obtained in the warp, weft and ± 45° directions. Equations 7.20–7.22 show that these constants can be directly calculated from the bending hysteresis and shear hysteresis along different directions.

As indicated by Fig. 7.11a–c, the constants *p*, *q* and *k* in the *DP* model can be determined from bending hysteresis and shear hysteresis in various directions. This indicates that draped nodes and locations of a fabric are affected by these properties not only in the warp and weft directions but also in other directions.

7.3.4.2 Drape coefficient

Substituting the experimental data of bending and shear hysteresis into equations 7.20–22, constants *p*, *q* and *k* can be identified and thus the drape

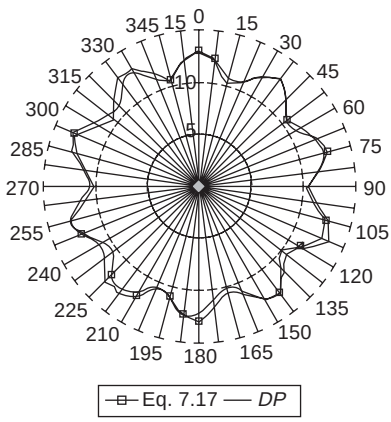

(a)

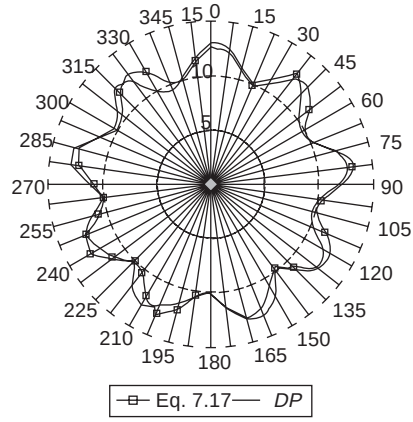

(b)

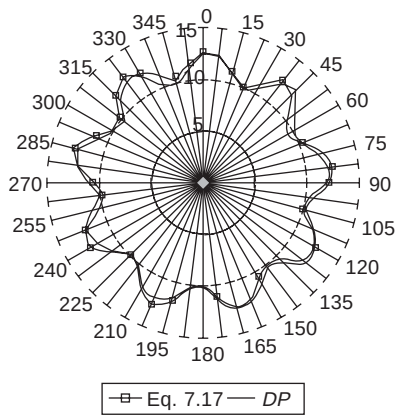

(c)

7.11 Theoretical and experimental results of drape profile of woven fabrics: (a) plain weave; (b) twill weave; (c) satin weave.

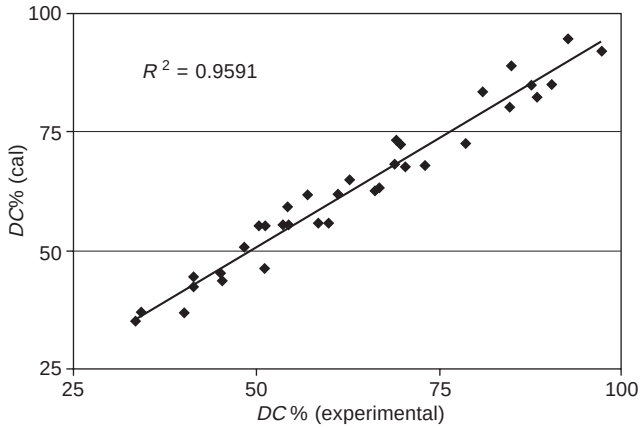

7.12 Comparison between theoretical *DC*% value and experimental *DC*%.

profile and drape coefficient can be predicted from the *DP* model. Figure 7.12 illustrates a comparison between the theoretical output of the *DP* model and the experimental drape coefficient (*DC*%), which indicates a high correlation between them ($R^2 = 0.9591$). It further implies that the *DP* models are applicable for the prediction of fabric drape profile from the values of fabric bending and shear hysteresis in various directions using the regression method.

7.4 References

Ayada M and Niwa M (1991), Relation between the comfort of gathered skirts and the fabric mechanical properties, *Sen-I Gakkaishi*, **47**(6), 291–298.

Bickley W G (1936), The numerical summation of slowly convergent series of positive terms, *Phil Mag*, **17**, 603.

Booth J E (1968), Fabric dimensions and properties, *Principles of Textile Testing*, 282–288.

Chu C C, Cummings C L and Teixeira N A (1950), Mechanics of elastic performance of textile material part V: a study of the factors affecting the drape of fabrics – development of a drape meter, *Text Res J*, **20**, 539–548.

Chu C C, Platt M M and Hamburger W J (1960), Investigation of the factors affecting the drapeability of fabrics, *Text Res J*, **30**, 66–67.

Chu C C, Hamburger W J and Platt M M (1962), *Report A R S*, Agricultural Research Service, United States Department of Agriculture, Washington D C.

Clapp T G, Peng H, Ghosh T K and Eischen J W (1990), Indirect measurement of the moment-curvature relationship for fabrics, *Text Res J*, **60**(4), 525.

Collier B J (1991), Measurement of fabric drape and its relation to fabric mechanical properties and subjective evaluation, *Clothing & Text Res J*, **10**(1), 46–52.

Collier J R, Collier B J, O'Toole G and Sargand S M (1991), Drape prediction by means of finite-element analysis, *J Text Inst*, **82**(1), 96–107.

Cusick G E (1962), *A Study of Fabric Drape*, PhD thesis, University of Manchester.
Cusick G E (1965), The dependence of fabric drape on bending and shear stiffness, *J Text Inst*, **56**, T596–606.
Cusick G E (1968), The measurement of fabric drape, *J Text Inst*, **59**, 253–260.
Dowlen R (1976), *Drape of Apparel Fabrics*, Agricultural Research Service, United States Department of Agriculture, Southern region, New Orleans (i) (ARS-S-149, (9), 1–9.
Feather D G (1970), Measuring fabric stiffness as a guide to drape and handle, *WIRA report 108*, 7.
Gan L, Ly N G and Steven G P (1995), A study of fabric deformation using nonlinear finite elements, *Text Res J*, **65**(11), 660–668.
Grosberg P (1966), The mechanical properties of woven fabrics part II: the bending of woven fabrics, *Text Res J*, **36**, 205–211.
Grosberg P and Swani N M (1966), The mechanical properties of woven fabrics part IV: the determination of the bending rigidity and frictional restraint in woven fabrics, *Text Res J*, **36**, 338.
Hearle J W S (1969), Shear and drape of fabrics, in *Structural Mechanics of Fibers, Yarns, and Fabrics*, Hearle J W S, Grosberg P and Backer S (eds), New York, Wiley-Interscience, 371–410.
Hearle J W S and Amirbayat J (1986a), Analysis of drape by means of dimensional groups, *Text Res J*, **56**, 727–733.
Hearle J W S and Amirbayat J (1986b), The complex buckling of flexible sheet materials part I: theoretical approach, *Int J Mech Sci*, **28**(6), 339–358.
Hearle J W S and Amirbayat J (1986c), The complex buckling of flexible sheet materials part II: experimental study of three-fold buckling, *Int J Mech Sci*, **28**(6), 359–370.
Hu J L, and Chan Y F (1998), Effect of fabric mechanical properties on drape, *Text Res J*, **68**(1), 57–64.
Hu J L Chen S F and Teng J G (2000), Numerical drape behaviour of circular fabric sheets over circular pedestals, *Text Res J*, **70**(7), 593–603.
Huang N C (1979), Finite biaxial extension of completely set plain woven fabrics, *J Appl Mech*, **46**, 651.
Hummel F H and Morton W B (1927), On the large bending of thin flexible strips and the measurement of their elasticity, *Philosophical Magazine*, **4**(7), 348.
Iwasaki K and Niwa M (1983), The drape of knitted fabrics, in *Objective Evaluation of Apparel Fabrics*, Postle R and Kawabata S (eds), Osaka 550, Textile Machinery Society of Japan, 373–378.
Izumi K and Niwa M (1985), Evaluation of dynamic drape of ladies dress fabrics', *Proc 3rd Japn/Aust joint symposium on objective measurement: application to product design and process control* (*preprint abstracts*), 725–734.
Kaswell E R (1953), *Textile Fibres, Yarns and Fabrics*, New York, Reinhold.
Leaf G A V and Anandjiwala (1985), A generalized model of plain woven fabric, *Text Res J*, **55**, 93.
Mamiya T F and Kanayama M M (1985), Evaluation of dress silhouette and fabric mechanical properties, *The 3rd Japn/Aust joint symposium on objective measurement: application to product design and process control* (*preprint abstracts*), 735–742.
Morooka H and Niwa M (1976), Relation between drape coefficients and mechanical properties of fabrics, *J Text Mach Soc of Japan*, **22**(3), 67–73.
Niwa M and Seto F (1986), Relationship between drapeability and mechanical properties of fabrics, *J Text Mach Soc of Japan*, **39**(11), 161–168.

Niwa M and Suda N (1984), Technique of measurements for three-dimensional shapes of flared-skirts and examination on the shape of node formed by draping, *Bulletin of Research Institute for Polymers and Textiles*, **9**(142), P5–24.

Okabe H and Akami H (1984), The estimation of the three dimensional shapes of garments, *Report Polymer Materials Res Inst Japan*, No 142.

Peirce F T (1930), The handle of cloth as a measurable quantity, *J Text Inst*, **21**, 337–416.

Peirce F T (1937), The geometry of cloth structure, *J Text Inst*, **28**, T45–96.

Postle J R and Postle R (1992), Fabric bending and drape based on objective measurement, *Int J Clothing Sci & Tech*, **4**(5), 7–15.

Potluri P, Atkinson J and Porat I (1996), Large deformation modelling of flexible materials, *J Text Inst*, **87**, Part 1 (1), 129–151.

Stylios G, Wan T R and Powell N J (1996), Modelling the dynamic drape of garments on synthetic humans in a virtual fashion show, *Int J Clothing Sci & Tech*, **8**(3), 95–112.

Suda N and Nagasaka T (1984a), Dependency of various sewing conditions on the bending property of seams, *Report of Polymeric Materials Res Ins Japan*, No 142, 39–45.

Suda Noriko and Nagasaka Tsune (1984b), Influence of the partial change of bending property on the formation of nodes, *Report of Polymeric Materials Res Ins Japan*, No 142, 47–55.

Tanabe H, Akamatsu A, Niwa M and Furusato K (1975), Determination of a drape coefficient from the basic mechanical properties of fabrics, *J Japan Res Assoc Text End-uses*, **16**(4), 116–120.

Vangheluwe L and Kiekens P (1993), Time dependence of the drape coefficient of fabrics, *Int J Clothing Sci & Tech*, **5**(5), 5–8.

Yamada T, Nakazato Y, Akiyama H and Suh J (1995), Flexural rigidity and drapability of fabrics, *J Japan Res Assoc Text End-uses*, **36**(7), 495–501.

Yamakawa M and Akiyama T (1996), Method for predicting the shape of flared skirts from paper patterns and mechanical characteristics of fabrics using multiple regression, *J Text Mach Soc Japan*, **49**(9), T245–251.

8

Mechanical properties of fabrics with seams

8.1 Introduction

A seam is the assembly method that joins fabric pieces together to form the parts or whole of a garment. Seam assembly is the method most typically used on garments. In order to create a seam, a fabric is cut into pieces and sewn together with stitches. Various seams can be obtained by combining different fabric cutting, joining and stitching parameters, and this will lead to substantial variation in fabric drape performance. Thus, investigation of the impact of a seam on fabric drape performance can help with understanding, evaluation and assurance of the appearance of the final garment.

8.2 Effect of seams on fabric bending/drape properties

8.2.1 Classification of fabric seams

The plain seam is the one most extensively found in apparel. It is the simplest seam type – a single row of lockstitches joins two pieces of fabric together. Thus, investigation of the effect of a plain seam on fabric drape has significant value for both the textile and the clothing industries. Plain seams can be classified into four types, i.e. vertical seam, horizontal seam, radial seam and circular seam. A vertical seam is a plain seam lengthwise sewn in the middle on a rectangular fabric strip, and is perpendicular to the bending axis as shown in Fig. 8.1. A horizontal seam is a plain seam located in the direction parallel to the bending axis of a fabric cantilever (see Fig. 8.2). Fabrics with both vertical and horizontal seams will drape in two dimensions. Radial seam refers to the kind of plain seam which is sewn across a circular specimen through its centre, as illustrated in Fig. 8.3. Usually, a radial seam drapes under its own weight perpendicular to the tangent of the pedestal, while a circular seam is the kind of plain seam sewn around a circular specimen with a radius from the specimen's centre, as illustrated in Fig. 8.4. A circular seam

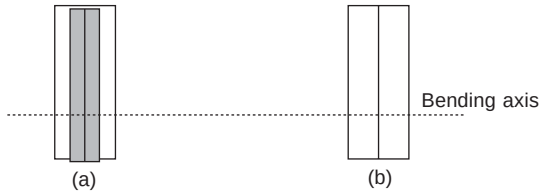

8.1 Fabric strip with vertical seams: (a) back side of fabric with seam allowances; (b) front side of fabric with a plain seam at centre.

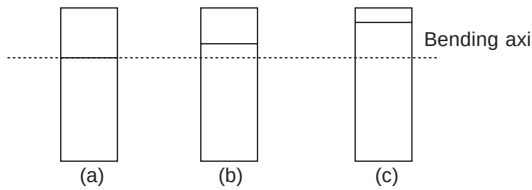

8.2 The horizontal seam at three positions from the free tip end respectively: (a) 0 mm; (b) 25 mm; and (c) 5 mm.

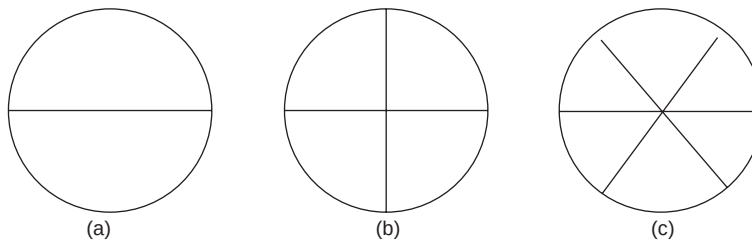

8.3 Radial seams along different directions: (a) one radial seam on the weft of a fabric; (b) two radial seams on the warp and weft of a fabric; (c) four radial seams on the warp, weft, 45° and 135° bias directions.

can be located either in-plane or out-of-plane of the pedestal, depending on the seam position. It drapes in a direction parallel to the circumference of the pedestal. Fabrics with radial and circular seams thus usually drape in three dimensions.

Another seam classification method is based on the direction of drape: vertical seam drape is associated with vertical and radial seams while horizontal seam drape is associated with horizontal and circular seams. Hence the difference between vertical and radial seams lies in the fact that fabrics with a vertical seam drape in two dimensions while fabrics with a radial seam drape in three dimensions. In addition to this, measuring methods for drape of fabrics with vertical and radial seams are also different. Usually, bending length is used to evaluate drape of fabrics with a vertical seam while drape of fabrics with radial seams can be evaluated using the drape coefficient.

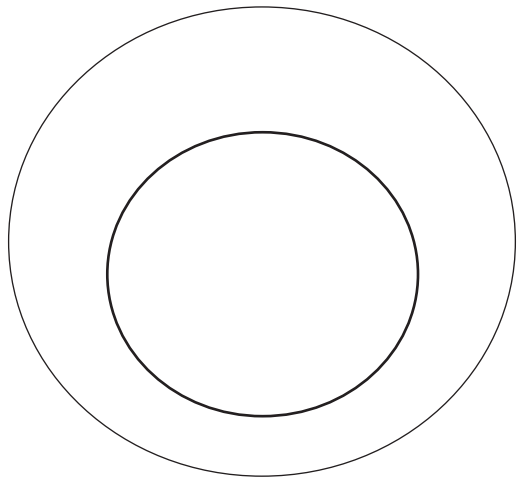

8.4 A circular seam on a circular fabric.

Both horizontal and circular seams drape horizontally to the gravity. Similarly, bending length is used to evaluate two-dimensional drape of fabrics with a horizontal seam while the drape coefficient is used to evaluate three-dimensional drape of fabrics with a circular seam. Therefore, horizontal and vertical seams will greatly influence fabric bending properties while circular and radial seams are more associated with drape properties.

8.2.2 Effect of seams on fabric bending properties

Dhingra and Postle (1980–81) measured bending rigidity by the KES system. Two plain seams, one vertical (perpendicular) and one parallel (horizontal) to the bending axis, were tested. With the introduction of the vertical seam, bending properties were greatly increased and they were further increased when the seam allowance was increased to 10 mm. Since the seam allowances of the vertical seam are clamped by the fabric holders during testing, their relative movement is restricted. Their results for bending rigidity from the KES fabric tester may not reflect the real drapeability as measured by the fabric cantilever test. Moreover, the range of seam allowances used in the experiment was kept to 1–10 mm; a limitation which made it difficult to fully trace out the drapeability of a seamed fabric. In contrast, they reported that the parallel (horizontal) seam had little influence on the bending rigidity of fabric. However, the experimental result cannot reflect the real drape situation of the seamed cantilever because the parallel seam can be parallel to any points from the free end to the hanging edge of the fabric cantilever. Differences may exist on a fabric cantilever with a parallel seam on different positions and with different seam allowances. Cantilever tests on fabrics

with vertical and parallel seams with a wide range of seam allowances and different seam positions are needed to investigate the validity of the argument.

8.2.3 Effect of seams on fabric drape properties

The study of fabric drape is undoubtedly very important for the appearance of the final garment but fabrics must be sewn to form a garment. Thus in practical situations, any assessment of the drape performance of a garment must take into account the influence of seams.

From the work of Suda and Nagasaka (1984a,b), the effect of the seam and hem of a flared skirt on the drape profile was studied by bonding narrow strips of non-woven fabrics at the edge or along the radial directions of circular fabrics. They observed that the bending rigidity of the bonded part increased with the width and the number of bonded layers of the non-woven fabric. In the samples with bonding only at their edge, the drape coefficient increased, and there was a negative correlation between the number of nodes formed and the rigidity of the bonded layers. In the case of samples with bonded strips in radial directions, the fourth layer of non-woven fabric seemed to have a distinctive influence on node formation. They concluded that the bending coefficient of the bonded part increased with the width and number of bonded layers of the non-woven fabrics.

Although thread balance during sewing, thread crimps, width, layers and thickness of the seamed piles (Ajiki, 1985; Gupta, 1992; Mahar *et al*., 1982a,b) are important factors affecting the drape of fabrics, the existence of seam allowance is also a key factor. In fact, a seam with seam allowance is commonly found on a garment. The effect of seam on fabric drape is not related only to the thread characteristics of the seam, but is also influenced by variations in seam allowance and seam directions (Suda and Nagasaka, 1984a,b). Suda and Nagasaka developed a good three-dimensional fabric drape simulation of the effect of seam directions and seam layers. However, the results were limited due to the method used of sticking a fabric stripe on fabrics. Using a real seam would make the tests more effective. Dhingra and Postle (1980–81) on the other hand, demonstrated bending properties of seamed fabrics with seam allowances in directions vertical and horizontal to the bending axis. However, their experiments were restricted to the KES bending tester; the results were also limited by the narrow range of tested specimens and seam allowances. Real two-dimensional drape from the fabric cantilever is not fully reflected in their results.

8.3 Effect of two-dimensional seams on fabric bending/drape properties – horizontal seams

Peirce (1930) considered the evaluation of bending length in the case of general and stiff fabrics. For general fabric, fabric weight is evenly distributed

in the fabric cantilever. Another specific method is set up for very stiff fabric in which the fabric weight is added and concentrated at the free end of the fabric cantilever. Postle and Postle (1992) provided a very detailed explanation of the distributed and concentrated weight effects of fabric bending. Grosberg's model (Grosberg and Swani, 1966) is able to specify the real situation existing on the fabric cantilever with both distributed and concentrated weight. However, their research was limited to the situation without seams. A parallel (horizontal) seam will bring in an additional weight from seam allowance at any positions of the fabric cantilever. The weight distribution on a seamed fabric is no longer restricted to only the distributed weight and the weight concentrated at the tip end. A method thus needs to be established to evaluate the fabric deflections from a fabric cantilever with a parallel (horizontal) seam. Seam allowances and seam positions can be varied on the seamed fabric cantilever. Thus, the draped effect can be measured by using Peirce's flexometer principle.

Horizontal seams play an important role in altering the drape of fabric, and this is an essential factor to be considered in both the clothing and upholstery industries. It affects the structural design of a garment with respect to features such as the appearance in the shoulder joins and the waist line as well as the hem. At the time of writing, only a few papers have been presented in this area and they contribute valuable but limited findings. From the scattered information, it has been found that the drape of fabric decreases and stiffness increases when a vertical seam is introduced (Dhingra and Postle, 1980–81; Suda and Nagasaka, 1984a,b). Nevertheless, literature on the effect on drape of a horizontal seam is limited.

8.3.1 Theory

In Peirce's mathematical expression (as shown in equation 8.1), bending length c from the fabric cantilever can be evaluated either by measuring the extended fabric length l with a fixed angle or by measuring an angle from the extension of a fixed length:

$$c = l\,(\cos 0.5\theta / 8 \tan \theta)^{1/3} \qquad [8.1]$$

A bending tester from the Shirley Institute (1957) is specially designed to measure an extended length l with a fixed angle. The extended fabric bends under its own weight until the free end intercepts a plane at an angle of 41.5° from the horizon. With this fixed angle, the expression $(\cos 0.5\theta/8 \tan \theta)^{1/3}$ in equation 8.1 will be equal to 0.5. Thus, the bending length is calculated by a simple formula from equation 8.2. Since $\theta = 41.5°$, $(\cos 0.5\,\theta/8 \tan \theta)^{1/3} = 0.5$, then

$$c = 0.5l \qquad [8.2]$$

More recently, the experimental process has been further simplified. The FAST-2 bending meter (De Boos and Tester, 1990) can be used to measure

the bending length using the same concept as Shirley, but with a photocell detector attached to detect the length of l and experimental results recorded directly from the computer. The effect of the position of a horizontal seam on a cantilever cannot be measured with either the Shirley or the FAST bending meter when the seam position varies with the extended fabric length l in the experiments. Peirce's flexometer (Peirce, 1930) is an instrument for measuring the drape of a fabric cantilever using bending angle θ from the fixed extended fabric length.

8.3.2 The flexometer

The flexometer can be used as a testing instrument for measuring the bending angle of a fabric cantilever with a constant length l. In a fabric cantilever with a horizontal seam, the seam can be placed in different positions on the fabric cantilever. Thus, the numerical value of bending length obtained from equation 8.2 is not applicable. On the other hand, a flexometer is a suitable instrument for measuring the bending angle from a constant extended fabric length l. To measure the bending angle and the chord l_0 from the hanging edge to the free end of a fabric cantilever, a modified flexometer is adopted as shown in Fig. 8.5, in which a guide is used to fix the required fabric length l from all specimens as shown in Fig. 8.6a. A hollow plate planted with a thin ruler at the centre is used to measure the chord l_0. The compass for measuring the bending angle is attached to the plate and can be rotated as shown in Fig. 8.6b. The values of bending angle θ and chord l_0 from the extended fabric length can thus be recorded. The horizontal x and vertical y displacements of

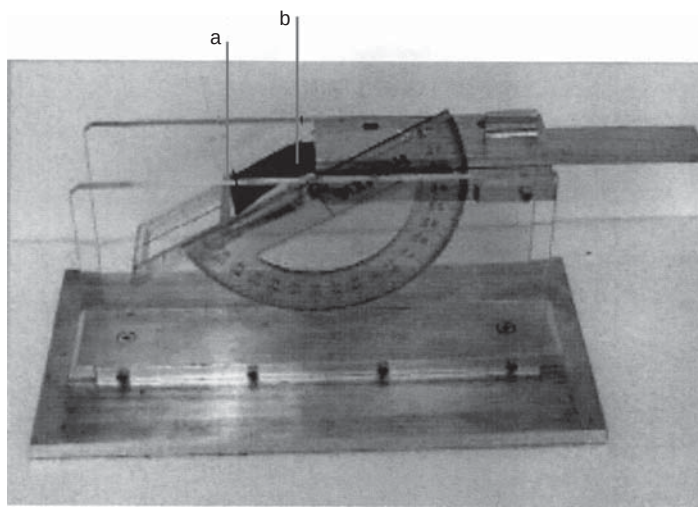

8.5 Modified flexometer: (a) a thin ruler for measuring the chord l_0; (b) a guide for fixing extended fabric length l.

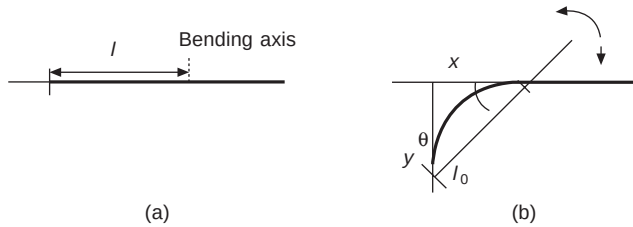

8.6 Measurement of bending angle θ and chord l_0; (a) before deflection; (b) during deflection.

a fabric cantilever can be evaluated from the value of l_0 as shown in equations 8.3 and 8.4 respectively:

$$x = l_0 \cos \theta \qquad [8.3]$$

and

$$y = l_0 \sin \theta \qquad [8.4]$$

8.3.3 Effect of seam allowance on drape of fabric cantilevers with a horizontal seam

The effect of seam allowance on the drape of a fabric cantilever with a horizontal seam can be represented by bending length – the smaller the value of the bending length, the larger the drapeability of the fabric cantilever. It has been found that the influence of seam allowances on drape of a fabric cantilever is highly dependent on the seam position, as well as the warp and weft directions of fabrics.

When a horizontal seam is added on a fabric cantilever, three situations will arise. Firstly, there is a horizontal seam on the supporting plane of the fabric cantilever when it is placed at the hanging edge as in the test of Fig. 8.7a. Then, in all other situations, the seam is out of the supporting plane. In the second situation, the seam allowance of a horizontal seam may be partially free hanging on the fabric cantilever as can be found from the test shown in

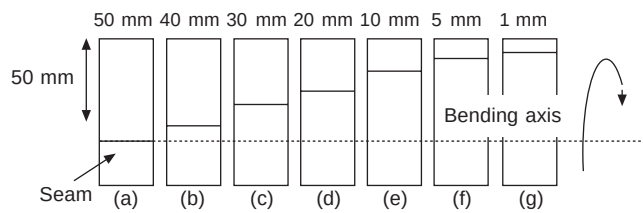

8.7 Extended fabric with a horizontal seam at different locations (50 mm, 40 mm, 30 mm, 20 mm, 10 mm, 5 mm and 1 mm respectively from the free tip end).

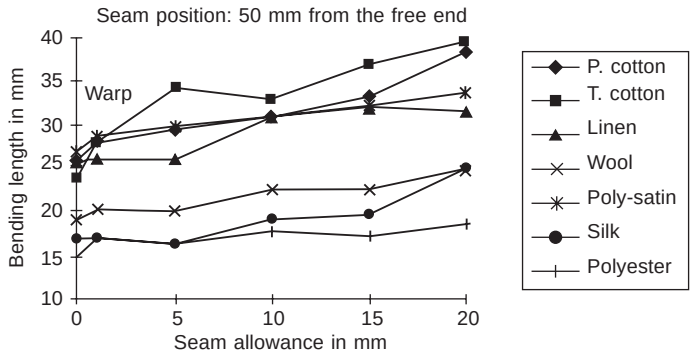

8.8 Bending length against seam allowance of fabric cantilever with a horizontal seam at the hanging edge (seam position: 50 mm from the free end).

Fig. 8.7b. In the third situation the seam allowance may be just appended to the hanging edge as can be found in Fig. 8.7c. Also, in the final situation, the seam allowance of a horizontal seam may be totally free hanging on the fabric cantilever as shown in Fig. 8.7d–g. Thus, different end results for the drape of fabric cantilevers can be observed in each supporting situation.

8.3.3.1 Seam at the hanging edge

When the seam is put on the hanging edge, that is the bending axis, it is located at 50 mm from the free end of the extended fabric as shown in Fig. 8.7a. The experimental result for fabric bending on the warp is shown in Fig. 8.8. It has been found that the increase in seam allowance in this position increases the bending length. Fabrics are stiffer and drape less with increased seam allowance. On the other hand, the result for fabric bending on the weft is different, as can be seen from Fig. 8.9. It is found that when a horizontal seam is introduced with a small seam allowance of 1 mm, the bending length increases sharply. When the seam allowance is further increased from 1 mm, the bending length does not change significantly. However, the bending length decreases when the seam allowance is increased from 15 mm to 20 mm. As a result, fabric bending in different fabric directions behaves differently when the seam allowance is changed.

8.3.3.2 Seam near the free tip end

When a horizontal seam is found near the free tip end of a fabric cantilever, the seam will be entirely free hanging on the fabric cantilever as shown in Figs 8.7d–g. No seam allowance is appended to the hanging edge in this situation. In the example of Fig. 8.7f, the addition of a horizontal seam and the increase in seam allowance cause a decrease in bending length and an increase in drapeability of a fabric cantilever. From Figs 8.10a and b, it can

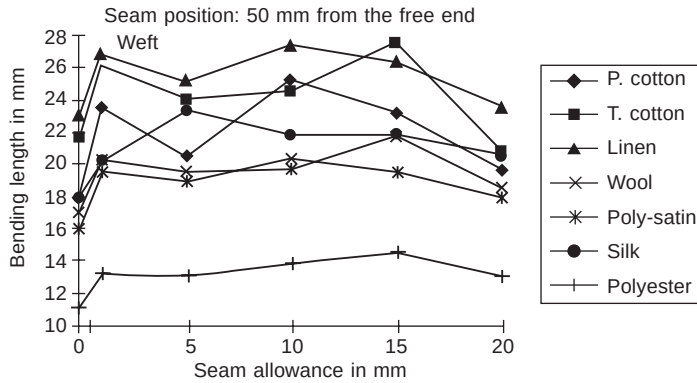

8.9 The bending length against seam allowance of fabric cantilever with a horizontal seam at the hanging edge (seam position: 50 mm from the free end).

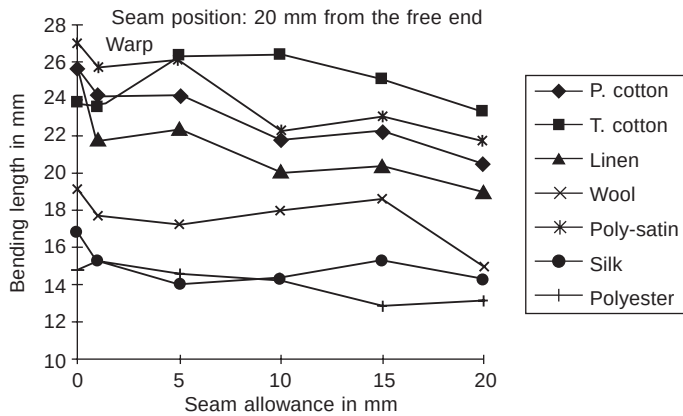

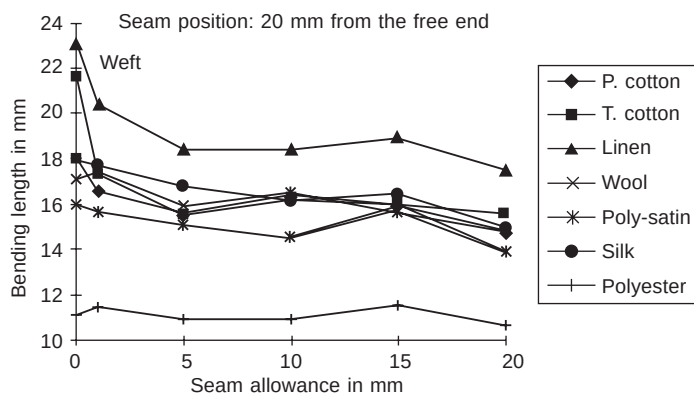

8.10 The bending length against seam allowance of fabric cantilever. Seam allowance of a horizontal seam is free hanging (seam position: 20 mm from the free end).

be seen that with increased seam allowance bending length reduces on fabric cantilevers in both the warp and weft directions.

8.3.3.3 Seam near the hanging edge

When a seam is located near the hanging edge with a large value of seam allowance, the seam allowance will partially append to the hanging edge. Seam allowance placed at 40 mm from the free end in Fig. 8.7b represents this situation. Figures 8.11a and b show the effects of seam allowance on bending length of fabric cantilevers in the warp and weft directions respectively. The seam is free hanging when *SA* is less than 10 mm. Thus, bending length and stiffness of the fabric cantilever will decrease when the fabric cantilever is seamed with 1 mm *SA*. Then, a gradual increase in seam allowance from

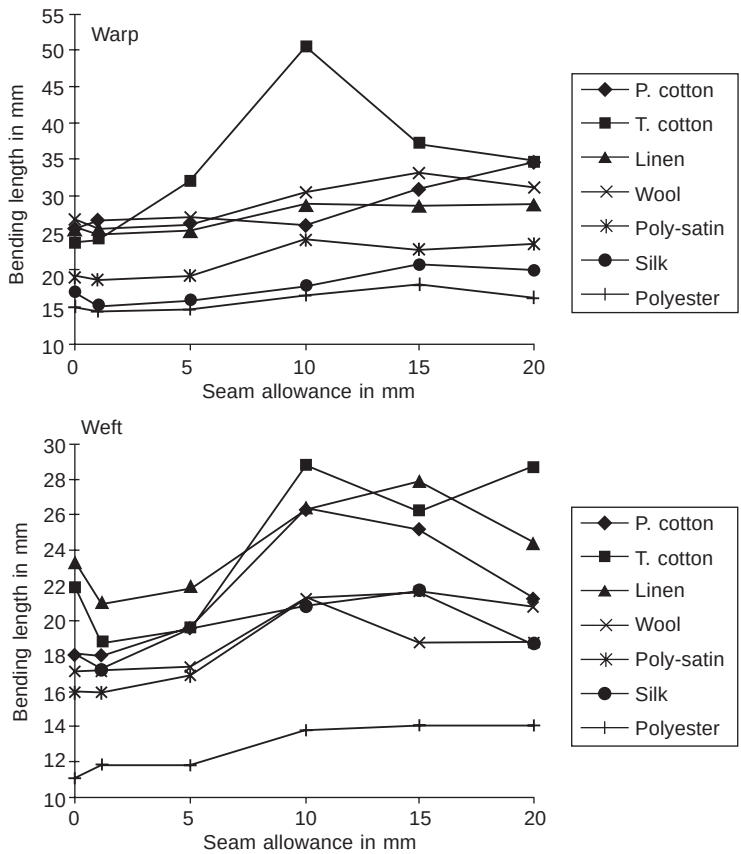

8.11 The bending length against seam allowance of fabric cantilever with a horizontal seam at 40 mm from the free end.

1 mm to 10 mm increases the bending length. Nevertheless, it is found that bending length increases sharply at 10 mm *SA* on the weft direction of the fabric cantilever where the edge of seam allowance is just appended to the hanging edge. When *SA* is increased to 20 mm, the further increase moderates the increased rate of bending length on the warp of the fabric cantilever, but greatly reduces the bending length and increases the drapability on the weft of the fabric cantilever.

8.3.4 Effect of seam position on drape of fabric cantilever with a horizontal seam

8.3.4.1 Completely free hanging of seam allowance

A horizontal seam with seam allowance 5 mm is generated at different positions on a fabric cantilever. The seam allowances are free hanging along the fabric cantilever when the seam is draping out of the platform. The positional effect of a horizontal seam on the drape of the fabric cantilever can be seen from Figs 8.12a and b. It has been found that the bending length of the fabric cantilever increases when the horizontal seam is moved away from the free tip end. A small value of bending length can be found when the seam is placed near the free tip end and a large value can be observed when the seam is positioned at the hanging edge of the fabric cantilever. The increased seam position gives rise to an increase in bending length which is steadier on the warp than on the weft of fabric cantilevers.

8.3.4.2 Partially free hanging of seam allowance

If either the seam allowance is too wide or the seam is too near the hanging edge, then the horizontal seam is not completely free hanging on the fabric cantilever. If the edge of seam allowance on a horizontal seam is too wide and appended to the hanging edge, the bending length will not increase markedly. A decrease in bending length can be seen on some fabrics as shown in Fig. 8.13. For fabrics such as twill cotton, wool, polyesters and silk, the bending length will be notably reduced from the seam positions of 40–50 mm from the tip end of the fabric cantilever since the seam with allowance 15 mm is still appended to the hanging edge of the fabric cantilever.

On the other hand, if a horizontal seam on a fabric cantilever is set in a position such that the edge of the seam allowance is just appended to the hanging edge (i.e. the edge of the seam allowance is dabbed to the edge of the hanging platform) the bending length of the fabric cantilever is increased for heavy weight fabrics. In Fig. 8.14, a prompt increase in bending length can be seen on the fabric cantilever with seam allowance of 10 mm at the seam position 40 mm from the tip end. An increase in bending length at this

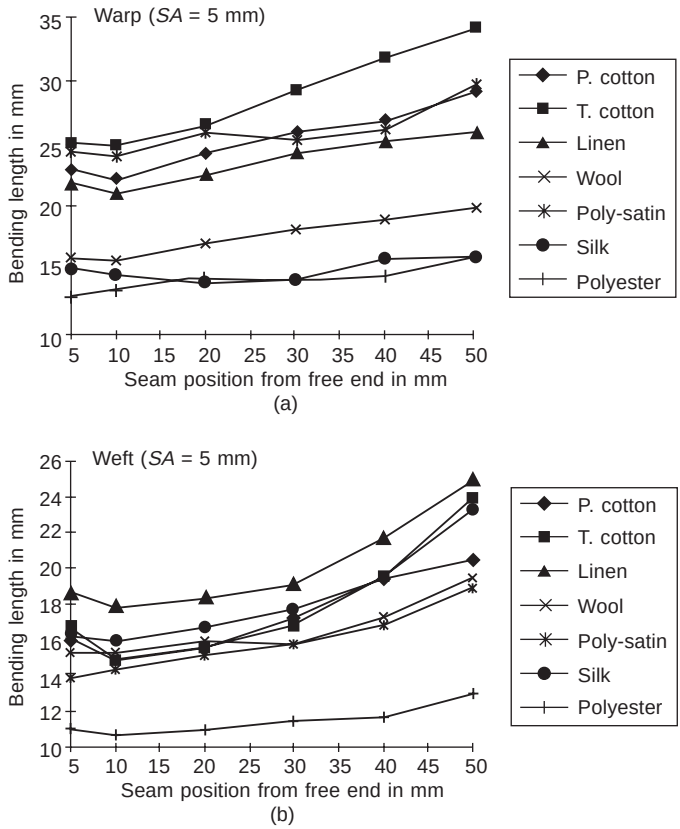

8.12 Bending length against seam position on the weft of fabric cantilever with a horizontal seam (seam allowance = 5 mm).

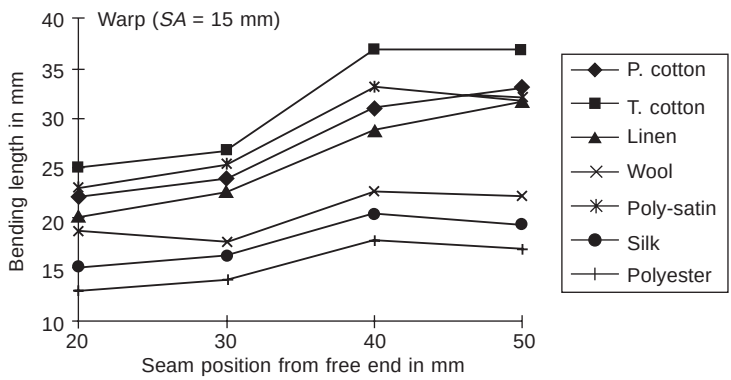

8.13 Bending length against seam position of fabric cantilever with a horizontal seam. Seam allowance is partially free hanging on the fabric cantilever at the seam positions of 40–50 mm from the free end (seam allowance = 15 mm).

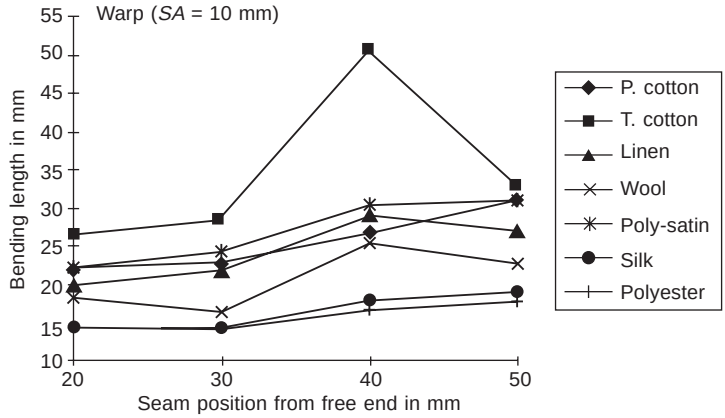

8.14 Bending length against seam position of fabric cantilever with a horizontal seam. Bending length promptly increases on heavy weight fabrics when seam allowance is dabbed to the hanging edge at the seam position of 40 mm from the free end (seam allowance = 10 mm).

seam position is obviously found for the heavy weight fabrics such as wool, linen and twill cotton.

8.3.4.3 Example using linen fabric

The linen fabric shown in Fig. 8.15 is an example which describes the effect of seam position and seam allowance on drape of a fabric cantilever. The bending length of linen with the seam position at 50 mm from the free end is greater than that at 40 mm. Bending length measured from the seam

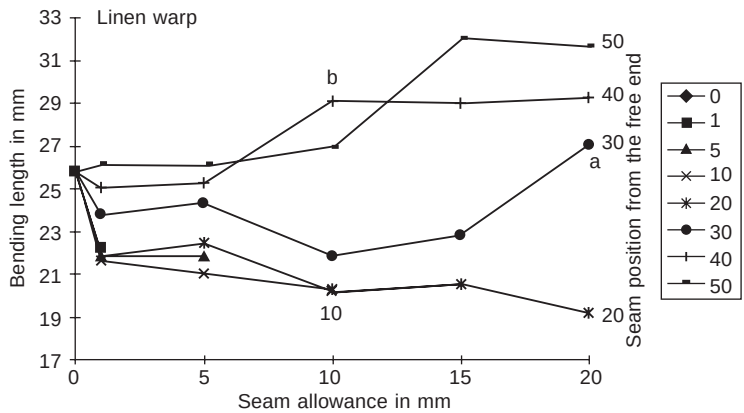

8.15 The bending length against seam allowance of linen fabric.

position at 30 mm is greater than that at 20 mm and 20 mm is greater than 10 mm. Nevertheless, it is difficult to compare the variance of bending length when the seam positions are less than 10 mm from the free end. Generally speaking, when a horizontal seam is positioned far from the hanging edge of a fabric cantilever, bending length will be smaller.

On the other hand, increase in seam allowance will either increase or decrease the drape of a fabric cantilever. Bending length of a fabric cantilever with a horizontal seam increases when the seam allowance is positioned at the hanging edge along the warp direction; otherwise, bending length decreases when the seam allowance is freely hanging along both fabric directions.

Moreover, the seam with seam allowance just dabbed to the hanging edge will markedly increase the stiffness of fabric. This situation can be seen at points a and b from the example of a linen fabric shown in Fig. 8.15. The seam allowance and seam position are 10 mm and 40 mm at point b, 20 mm and 30 mm at point a, respectively. The two seams with seam allowances are just dabbed to the hanging edge. Thus, bending length is instantly increased.

8.4 Effect of two-dimensional seams on fabric bending/drape properties – vertical seams

Dhingra and Postle (1980–81) studied the effect of a plain seam on bending rigidity using the KES-F bending tester. It was found that a plain seam has little effect on fabric shear rigidity and hysteresis, but has a great deal of influence on bending rigidity. The effect was found to be especially significant with the vertical seam. They also pointed out that the bending hysteresis and the bending rigidity were strongly affected by seam allowances. When SA = 1 mm, the ratio of bending hysteresis of seamed fabric was 9–11 times that of the no-seam fabric. This ratio was increased to 26–33 times the unseamed fabric when SA was increased to 10 mm. The investigation provides useful information for the study of fabric bending with a plain seam.

In another study by Shishoo *et al.* (1971), it was found that bending rigidity of a seamed multi-layer fabric was about 4–10 times that of the single one. The bending length of the multi-layer fabric was the approximated sum of that of the individual single layer fabrics.

Ajiki (1985) found that bending rigidity was affected by the level of sewing thread crimp in the seams. The sewing thread crimp is a linear function of thickness multiplied by the stitch density of the composite fabric layers. In addition, bending rigidity increased with the increase in the number of layers of fabrics.

Mahar *et al.* (1982a,b) reported that bending rigidity of fabrics was related to the balance of the thread tension. They joined two layers of fabrics with a row of lockstitches without obtaining any seam allowance. The bending properties were tested on both the top and bottom of the two-ply fabrics. An

asymmetric bending moment was obtained on each side of the fabric sheets if the thread tension was not balanced.

Among the studies, thread crimp, number of layers and thickness of the seamed sheets are the the important factors affecting fabric bending. However, the effect of seam on fabric bending is also related to the existence of seam allowance. In practice, a seam with seam allowance is commonly found on a garment. Dhingra and Postle's (1980–81) study provides fundamental understanding of the effect of a vertical seam on fabric bending of woven fabrics.

8.4.1 Theory

8.4.1.1 Elastic bending theory

By simple bending theory, the moment of resistance of a strip to bending is equal to the applied moment M at equilibrium. The total bending moment M for the whole cross-sectional area about the neutral axis is shown in equation 8.5 where Young's modulus E and radius of curvature R are assumed to be constant along the material strip.

$$M = \frac{E}{R} I = \frac{B}{R} \qquad [8.5]$$

The function $\int y^2 \delta A$ is called the second moment of area I of the cross-section where δA is defined as the area of an element of the cross-section at a distance y from the neutral axis. The neutral axis is a horizontal line which passes through the centroid of the cross-section. The distance of the neutral axis is a vertical distance from the fabric surface to the horizontal line of the neutral axis of the cross-section.

It has been noted that the bending moment changes with second moment of area of the cross-section. From equation 8.6, the bending rigidity of a strip is a linear function of the second moment of area I of the cross-section when Young's modulus E is assumed to be constant along the strip:

$$B = EI \qquad [8.6]$$

Enlightened by this principle, we may attempt to find the relationship between bending rigidity and the second moment of area for fabrics with a vertical seam. It is assumed that $B = \beta I^{\lambda}$, where β and λ are two constants and β may be related to Young's modulus E.

8.4.1.2 Second moment of area of seamed and unseamed fabrics

In order to find the difference between seamed and unseamed fabrics, their cross-sections are magnified under the microscope as shown in Figs 8.16a and b. Comparing the figures, a structural change can be seen for the seamed

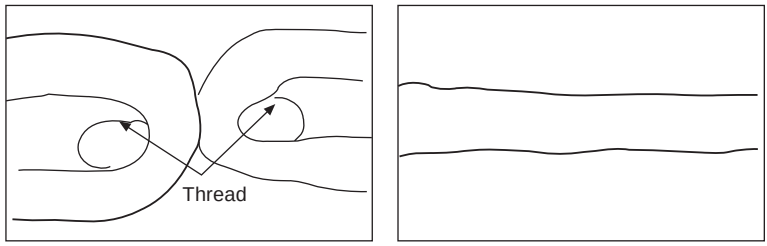

8.16 Cross-section of a fabric strip (× 200) with (a) a vertical plain seam and (b) no seam.

fabric in that seamed parts are forced to bend and seam allowances are formed on the reverse of the fabric. Besides, two gap areas are found between the top fabric and the bottom seam allowances. Both the cross-sectional area and the cross-sectional thickness are significantly increased on the seamed fabric. Sewing thread and seam structure are found to be the general elements affecting the bending properties of a fabric strip.

Geometrical models of the fabric cross-sections for seamed and unseamed fabrics are set up in Figs 8.17a and b. The assumptions followed in the modelling include:

(1) the cross-section of an unseamed fabric is rectangular in shape and the cross-section of the seamed fabric is I-shaped;
(2) free space areas between the top and the bottom plies of the seamed fabric are rectangular in shape;
(3) no external force from the sewing thread, stitch tension and balance of stitch tension is applied on the seamed model;
(4) the increased fabric weight due to the increased seam allowance is assumed to be uniformly distributed along the fabric strip.

For the unseamed fabric, the distance of the neutral axis from the fabric surface of the cross-section y is $t_0/2$ in equation 8.7.

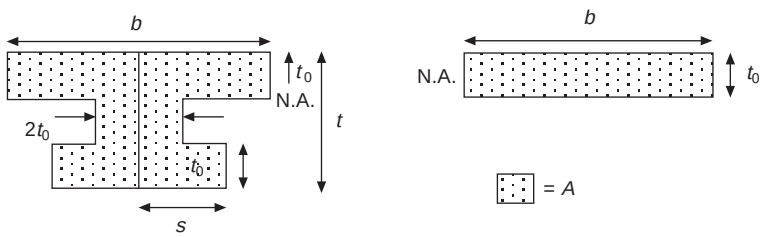

8.17 Geometrical models and cross-section areas of a fabric with (a) a vertical seam and (b) no seam.

$$y = \frac{t_0}{2} \qquad [8.7]$$

The second moment of area I of the cross-section with width b and thickness t_0 can be evaluated from equation 8.8.

$$I = \frac{bt_0^3}{12} \qquad [8.8]$$

However, the cross-section of an unseamed fabric strip shown in Fig. 8.16b is different from a fabric strip with a vertical seam shown in Fig. 8.16a.

From Fig. 8.16a, formation of a vertical seam creates a seam thickness at the cross-section and space areas are found between the top and bottom sheets of a seamed fabric strip. Moreover, a larger cross-sectional area is found for the seamed fabric than the unseamed fabric. Seam thickness t, fabric thickness t_0, width of fabric strip b, width of seam allowance s and the distance of the neutral axis y are the important factors which determine the cross-sectional area of the seamed fabric strip. According to equations 8.9 and 8.10, the distance of the neutral axis y and the second moment of area I_{seam} of the cross-section of the seamed fabric strip can be evaluated respectively using the measurable values of seam thickness t, fabric thickness t_0, width of fabric strip b and width of seam allowance s:

$$y = \frac{t_0(2s - 4t - b) + 2t(t + b)}{2(2s + 2t - 4t_0 + b)} \qquad [8.9]$$

and

$$I_{seam} = \frac{1}{3}[b(t-y)^3 - (b-2t_0)(t-t_0-y)^3 + 2sy^3 - 2(s-t_0)(y-t_0)^3] \qquad [8.10]$$

Rewriting equation 8.10, equation 8.11 is formed.

$$I_{seam} = \frac{t_0}{3}\left\{\begin{array}{l} 2t^2 + 3(b - 2t_0 - 2y)t^2 + 3[t_0(2t_0 + 4y - b) + 2y(y - b)]t \\ + 2(t_0^2 - 3t_0y + 3y^2)s + [bt_0^2 - 4t_0^3 + 3y(b - 4y)t_0 + 3by^2] \end{array}\right\} \qquad [8.11]$$

I_{seam} is a polynomial function of the seam thickness t in the third order. When a seam is added on a fabric strip with a small seam allowance, the change of I_{seam} is related to the change of t, y and s if t_0 and b are constant. When the seam allowance is small, the change in y will be mainly due to the change in t. Thus, the increased bending moment of a fabric strip from an added seam is mainly due to the increase in seam thickness t. When the seam allowance of a seamed strip is increased and t_0 and b are constant, the seam thickness becomes a constant. I_{seam} changes with y and s only:

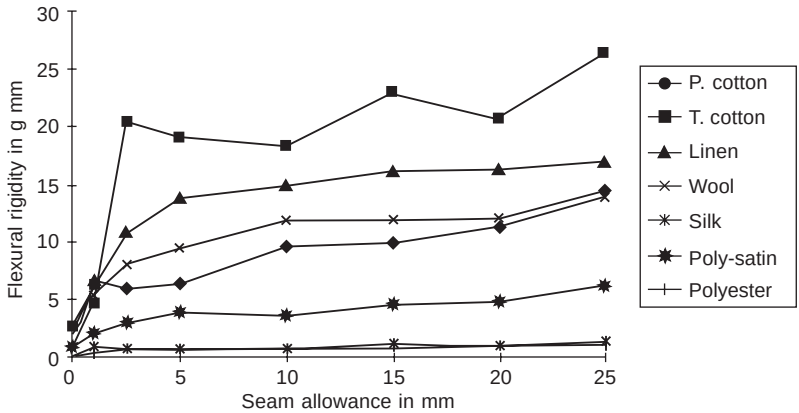

8.18 Experimental bending rigidity with the increased fabric weight due to the increase in seam allowance.

8.4.2 Relationship of bending rigidity *B* and second moment of area (I_{seam})

The bending rigidity B of a seamed fabric strip with various seam allowances can be evaluated from experimental bending length c from $B = Wc^3$ as shown in Fig. 8.18 where W is the fabric weight. The calculated results of I_{seam} with different seam allowances are shown in Table 8.1. The relations between the bending rigidity and the second moment of area of different fabrics can be expressed in equation 8.12

$$B = \beta I_{seam}^{\lambda} \qquad [8.12]$$

where β and λ are constants. The power relation of different fabrics is shown in Table 8.2. The correlation coefficient r averages 0.95 with a high confidence level for all fabrics.

From Table 8.2, it is found that the power λ in equation 8.12 of all seven

Table 8.1 Second moment of area in mm^4 of a seamed fabric strip with increased seam allowance

***SA*, mm**	**0**	**1**	**2.5**	**5**	**10**	**15**	**20**	**25**
Plain cotton	0.17	0.45	1.13	1.55	3.70	4.04	4.81	5.57
Cotton twill	0.41	2.04	4.02	3.80	6.24	8.92	10.21	13.60
Linen	0.37	1.06	1.60	2.92	3.50	4.91	6.32	7.52
Wool	0.65	2.24	3.50	4.56	9.21	11.94	18.95	20.49
Silk	0.00	0.04	0.08	0.11	0.17	0.28	0.23	0.42
Poly-satin	0.02	0.20	0.35	0.51	1.06	1.21	1.39	1.77
Polyester	0.01	0.08	0.18	0.15	0.39	0.50	0.72	0.74

Table 8.2 Relation of bending rigidity and second moment of area of fabric strip with various seam allowances

Fabric	Relation of B and I_{seam}	r
Plain cotton	$B = 5.33\ I_{seam}^{0.52}$	0.91
Twill cotton	$B = 4.95\ I_{seam}^{0.70}$	0.93
Linen	$B = 6.53\ I_{seam}^{0.56}$	0.96
Wool	$B = 2.60\ I_{seam}^{0.62}$	0.92
Silk	$B = 1.80\ I_{seam}^{0.41}$	0.95
Polyester satin	$B = 4.24\ I_{seam}^{0.38}$	0.98
Polyester	$B = 1.10\ I_{seam}^{0.38}$	0.98
Average		0.95

B = Bending rigidity
I_{seam} = Second moment of area from SA = 0 to SA = 25 mm

fabrics is close to 0.5. Thus, substituting 0.5 to the power λ in equation 8.12, equation 8.13 is formed.

$$B = \beta\sqrt{I_{seam}} \qquad [8.13]$$

Linear regressions of plot of bending rigidity against $\sqrt{I_{seam}}$, where β is a constant on a particular fabric, yield correlation coefficients of B in Table 8.3. The average correlation coefficient of all sample fabrics is 0.9 and the relationship is significant at the 0.05 level. Thus, the bending rigidity from various values of I_{seam} due to the change in seam allowance can be expressed by a simple formula:

Table 8.3 Linear relation of bending rigidity (B) and $I_{seam}^{0.5}$ of a fabric strip with various seam allowances

Fabric	Relation of B and $I_{seam}^{0.5}$ in equation 8.10	r
Plain cotton	$B = 5.43\ I_{seam}^{0.5}$	0.93
Twill cotton	$B = 7.34\ I_{seam}^{0.5}$	0.89
Linen	$B = 6.98\ I_{seam}^{0.5}$	0.94
Wool	$B = 3.30\ I_{seam}^{0.5}$	0.90
Silk	$B = 1.98\ I_{seam}^{0.5}$	0.82
Polyester satin	$B = 4.24\ I_{seam}^{0.5}$	0.95
Polyester	$B = 1.18\ I_{seam}^{0.5}$	0.90
Average		0.91

B = Bending rigidity
$I_{seam}^{0.5}$ from SA = 0 to SA = 25 mm

8.4.3 Relationship of bending length *c* and second moment of area (I_{seam})

The relationship between bending length c and bending rigidity B can be expressed by equation 8.14.

$$B = Wc^3 \qquad [8.14]$$

When equations 8.13 and 8.14 are combined, equation 8.15 is formed which shows the relation between the second moment of area (I_{seam}) and the bending length.

$$c = (\beta/W)^{\frac{1}{3}}\ I_{seam}^{1/6} \qquad [8.15]$$

The calculated results of bending length c_2 from equation 8.15 are shown in Table 8.4. As compared with a group of experimental data of bending length c_1 with various seam allowances (as shown in Table 8.5), we found that the correlation coefficients r are high and the predicted slope is 1, that is $c_1 = c_2$, for different fabrics as shown in Fig. 8.19. The overall correlation coefficient is 0.89. Since the correlation coefficient exceeds the critical value of 0.622 at the 0.05 level, the relation of bending length and second moment of area of a vertical seam with various seam allowances shown in equation 8.15 can be accepted at the 0.05 significance level:

Table 8.4 Calculated bending length (c_2) in mm

SA, (mm)	**0**	**1**	**2.5**	**5**	**10**	**15**	**20**	**25**
Plain cotton	24.85	28.14	32.84	33.67	37.03	36.17	35.65	35.14
Twill cotton	26.70	35.09	37.24	35.96	37.08	38.05	38.17	38.97
Linen	26.66	31.60	32.17	34.25	33.47	35.01	35.34	35.52
Wool	22.11	26.69	28.20	28.60	30.27	31.06	32.39	31.85
Silk	13.58	19.54	21.30	22.10	22.16	23.78	22.11	23.39
Polyester satin	16.86	24.68	26.89	27.85	29.82	30.06	29.17	29.86
Polyester	11.56	15.24	17.84	16.97	18.61	19.00	19.54	19.00

Table 8.5 Experimental bending length (c_1) in mm

***SA*, (mm)**	**0**	**1**	**2.5**	**5**	**10**	**15**	**20**	**25**
Plain cotton	21	34.5	33.25	33	36	35	35	36.5
Twill cotton	22	27	41.5	39.5	37	38.5	36.5	38.5
Linen	24	30.75	34.5	36	35	35.5	34.5	34
Wool	17	27.5	31	31.5	32	31.5	30.5	31
Silk	14.5	24.5	22.5	23	22	23.5	21.8	22.5
Polyester satin	20	25.5	28.5	30	28	29.5	28.5	30.5
Polyester	13	17.5	19.5	18	19	18.2	19.2	18.5

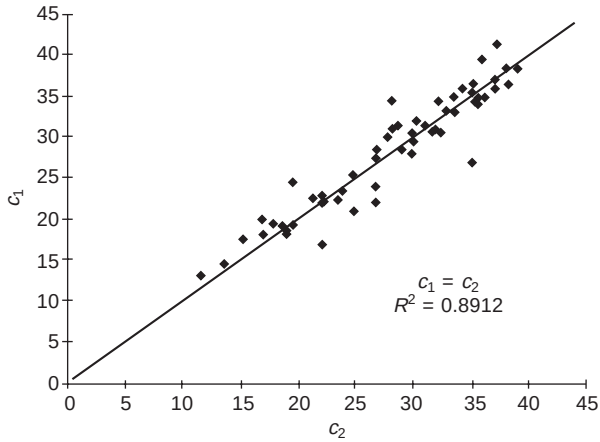

8.19 Bending length of seven fabrics from experimental results c_1 and calculated results c_2.

8.4.4 Difference of vertical and horizontal seams on drape of fabrics

The bending length of a fabric with a vertical seam is higher than that with a horizontal seam. Fabrics with a horizontal seam drape more easily than fabrics with a vertical seam. The effect of seam allowance on a horizontal seam is different from that on a vertical seam.

When a horizontal seam is added on a fabric cantilever, three situations are found. First, the seam allowance of a horizontal seam is supported on the plane when it is placed at the hanging edge, which is 50 mm from the free end in Fig. 8.2. In the second situation, the seam allowance of a horizontal seam is just appended to the hanging edge, that is 25 mm seam allowance at a seam position 25 mm from the free end. In the final situation, the seam allowance of a horizontal seam is fully free hanging on the fabric cantilever, which is 5 mm from the free end in Fig. 8.2. Different results for the drape of fabric cantilevers can be observed.

When a seam is located 50 mm from the free end, it is attached to the hanging edge. Bending length increases sharply when *SA* increases from 1 mm to 15 mm. Further increase in seam allowance brings a drop in bending length. When a horizontal seam is free hanging in a fabric cantilever, the addition of a horizontal seam and the increase in seam allowance cause a decrease in bending length. However, if the seam allowance of a horizontal seam is just appended to the hanging edge, bending length increases instantly.

8.5 Effect of three-dimensional seams on fabric bending/drape properties

8.5.1 Drape performance of fabrics with radial seams

8.5.1.1 Relation between vertical seams and radial seams in terms of bending length and drape coefficient

From Fig. 8.20, it can be seen that a linear correlation exists between two-dimensional and three-dimensional drape in terms of bending length *c* and *DC*% respectively. For the no-seam fabrics shown in Fig. 8.20a, a linear relation between *c* and *DC*% of different fabrics is shown in equation 8.16 with a correlation coefficient of 0.92.

$$DC\% = 4.37c - 33.11 \quad [8.16]$$

When a seam is added, a linear relation can also be seen between *c* and *DC*% as shown in Fig. 8.20b. However, the linear regression becomes equation 8.17 with correlation coefficient of 0.88,

$$DC\% = 3.45c - 42.6 \quad [8.17]$$

which shows that both the slope and the constant from equation 8.16 are changed with the addition of seams.

When seam allowance increases from 2.5 mm to 25 mm as shown in Fig. 8.20c, it is interesting to see that all the linear regressions in this *SA* range are similar to each other. The regressions can be combined and presented in equation 8.18 with correlation coefficient of 0.98.

$$DC\% = 2.79c - 30.97 \quad [8.18]$$

The linear regression shows that there is no significant change in relationship between *DC*% and *c* with *SA* in the range 2.5–25 mm, which means the change of seam allowance has little effect on the relation between *DC*% and *c*. However, the linear relationship of this *SA* range is different from *SA* = 1 mm in equation 8.17.

8.5.1.2 Drape coefficient of fabrics with one and two radial seams

The changes in drape coefficients (*DC*%) for fabrics with one or two radial seams are rather unstable when compared with those with four seams. However, the trends of *DC*% corresponding to various seam allowances are similar to each other. Generally speaking, drape coefficients increase rapidly with the addition of a seam from *SA* 0 mm (no seam) to 1 mm. Further increase in *DC*% is observed on some fabrics when *SA* is increased from 1 mm to 2.5 mm. However, *DC*% slightly increases after seam allowance is greater than 2.5 mm. In addition, light weight fabrics such as 100 % silk and 100 %

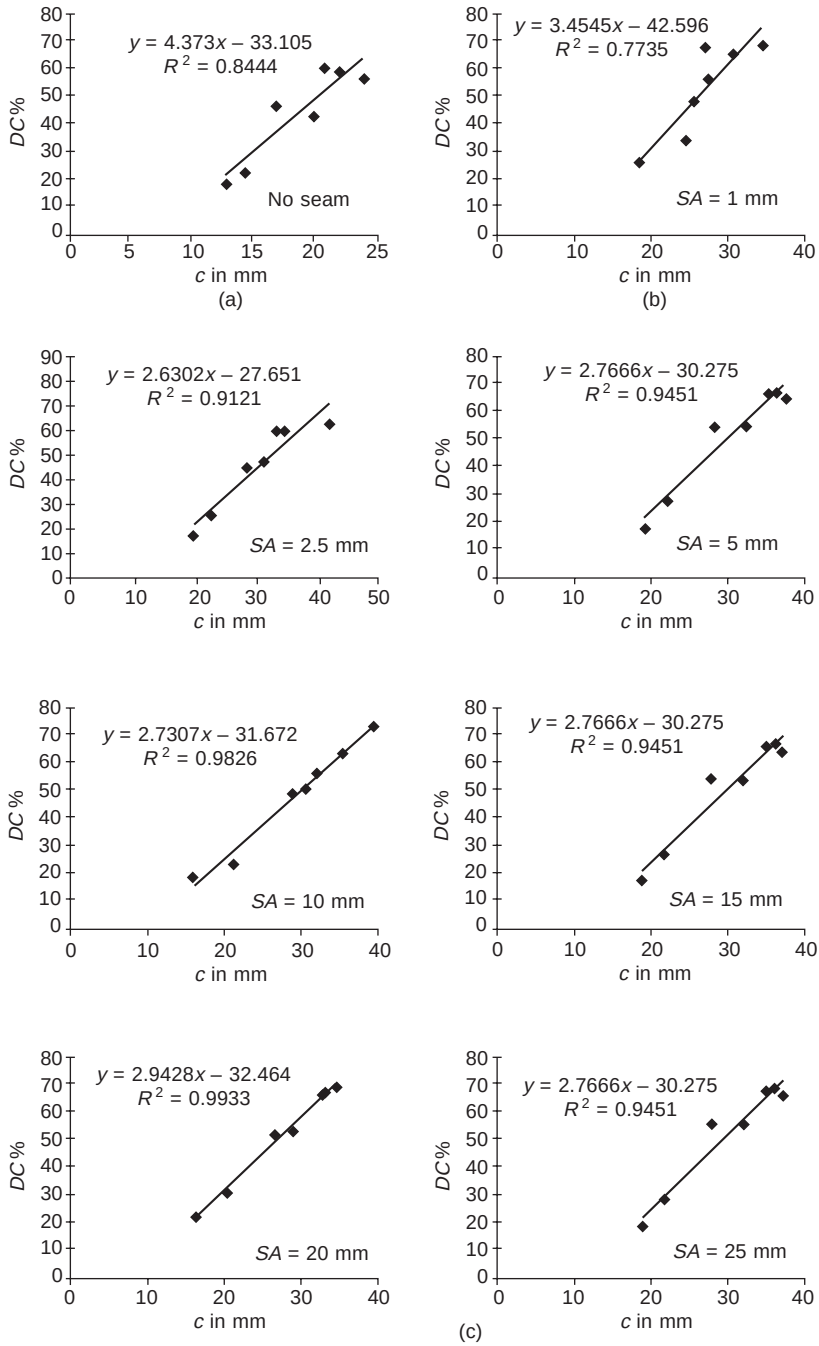

8.20 Relations between *DC* % and bending length *c* of different fabrics: (a) no seam; (b) seam allowance = 1 mm; (c) seam allowance = 2.5 ~ 25 mm.

polyester exhibit a much smaller change in *DC*% with the addition of one or two radial seams, which is different from heavy weight fabrics. Thus the effects of both one and two radial seams on light weight fabrics are very limited.

8.5.1.3 Drape coefficient of fabrics with four radial seams

Figure 8.21 shows that drape coefficient (*DC*%) increases when four seams are sewn on the fabric. An increased seam allowance initially increases *DC*% rapidly in the small region located between 1 and 5 mm *SA*; then, a negligible increase in *DC*% occurs on any further increase in seam allowance. The *DC*% of a fabric with four seams is relatively consistent and stable when compared with the results for one or two seams. In an example of 10 mm seam allowance, the change in *DC*% with respect to the seam number is shown in Fig. 8.22. The increased *DC*% with the addition of seams is highest when a fabric has four seams, and is minimal with one seam. In this case, the effect of radial seams on three-dimensional drape is influenced by the increase in seam numbers. Fabric weight also impacts on this effect. In Fig. 8.22 again, it can be shown that heavy weight fabrics have an increase in *DC*% value when seam numbers increase, but the increased seam numbers are less inclined to increase the *DC*% of light weight fabrics.

8.5.1.4 Drape profile of fabrics with radial seams

The instability of a draped fabric can be seen on fabrics with no seams, where node numbers may vary on every drape. However, the drape profile is

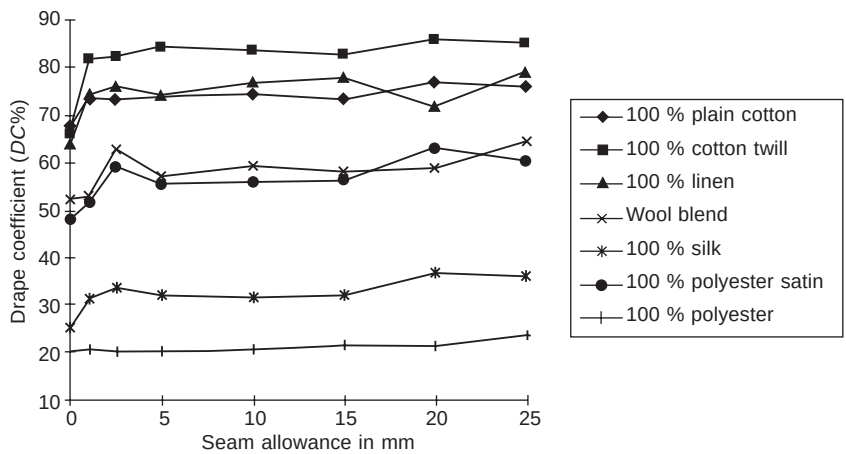

8.21 Drape coefficient (*DC*%) of four radial seams on the warp, weft and two biases.

Table 8.6 Node length of two radial seams with four nodes on various fabrics. Node length in cm from the edge of the pedestal

***SA* mm**	**Highest node**	**Seamed node 1**	**Seamed node 2**	**Seamed node 3**	**Seamed node 4**	**Lowest node**
(a) Wool						
0	5.4	–	–	–	–	4
1	5.4	5.4	5.2	5.1	4.9	4.1
2.5	5.5	5.5	5.3	5.2	5.2	4.1
5	5.6	5.6	5.4	5.1	5	4
10	5.7	5.7	5.5	5.3	5.3	3.9
15	5.4	5.4	5.2	5.2	4.9	4.3
20	5.4	5.4	5.4	5.3	5	4.2
(b) Silk						
0	4.2	–	–	–	–	3
1	4.5	4.5	4.5	4.3	4.2	3
2.5	4.7	4.7	4.1	4	3.8	3.5
5	4.5	4.5	4.1	3.8	3.4	3.2
10	4.9	4.9	4.6	4.2	4.1	3.5
15	4.7	4.7	4.6	3.9	3.7	3.2
20	4.9	4.9	4.3	4	4	3.3
(c) Polyester						
0	3.9	–	–	–	–	2.1
1	4.1	4.1	3.9	3.8	3.6	2.6
2.5	4.4	4.4	4	3.6	3.6	2.9
5	4.2	4.2	4.1	3.8	3.5	2.7
10	3.8	3.8	3.6	3.6	3.3	2.5
15	4	4	3.6	3.5	3.5	2
20	4	4	3.6	3.3	3.3	2.6

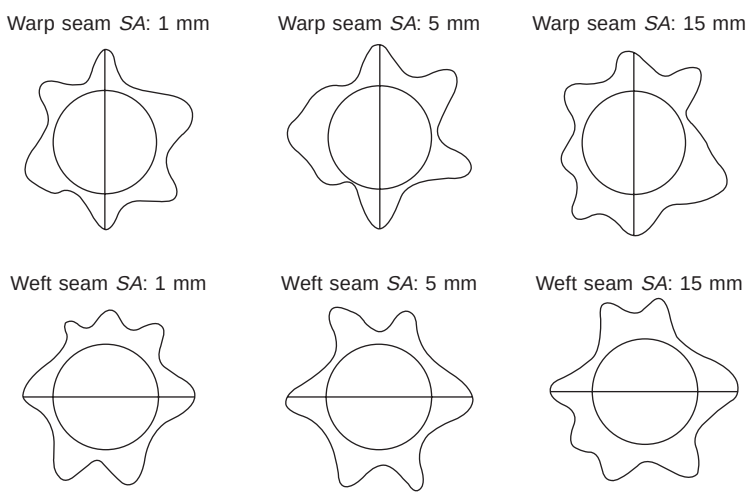

8.23 The drape profiles of one seam on plain cotton fabric with various seams.

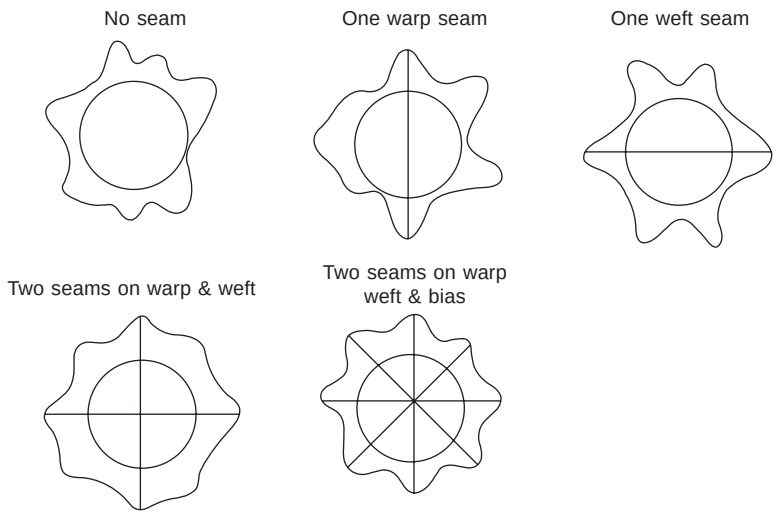

8.24 The drape profile of plain cotton with various seam numbers.

be evenly distributed in an octagonal arrangement along the seam directions. Increasing the seam allowances for four radial seams has little influence on changing the orientation of the drape profile. Drape profiles of fabrics with four radial seams are similar to those for fabrics with two seams, but the former are more stable than the latter and are not affected by variations in seam allowance. The drape profile of the specimen with four radial seams shows no significant change between each drape no matter how many times it drapes on the pedestal, because the free distribution of nodes is highly restricted by the additions of four seams.

From Fig. 8.24, it can be seen that the drape profile of a fabric is greatly affected by the number of radial seams. The more seams are added to a fabric, the more stable is the drape profile. Thus, drape profiles of fabrics with both two seams and four seams have a more regular node arrangement than those with one seam. It is also noted that added seams have less influence on the drape profiles of light weight fabrics: that is, the node number and drape appearance of light weight fabrics cannot be altered significantly by introducing seams and changes in seam allowance.

8.5.2 Drape performance of fabrics with circular seams

Two-dimensional and three-dimensional drape behave similarly when seam positions are changed. Both bending length and *DC*% increase when the seam is located just out of the hanging edge. Bending length and *DC*% decrease when the seam is fully free hanging and far from the hanging edge. In addition, bending length and *DC*% are lowest when the seam moves near the free end.

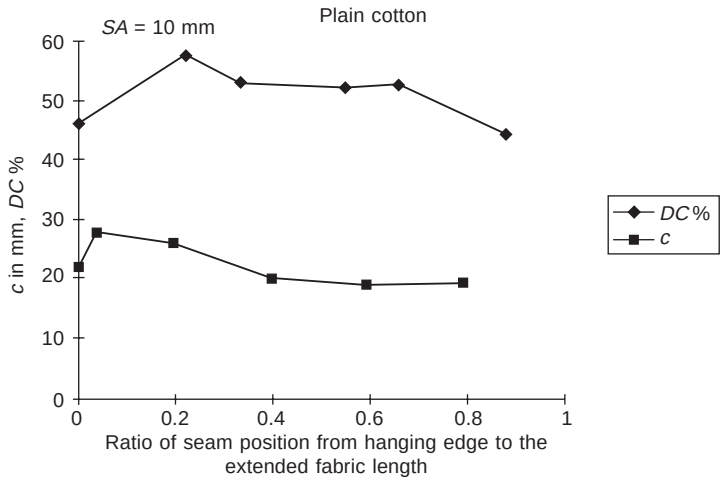

8.25 DC % and bending length *c* against ratio of seam position from hanging edge of the extended fabric length to the free end (seam allowance = 10 mm).

According to Fig. 8.25, the drape coefficient is highest when a circular seam is located just off the edge of the pedestal. This is because the seam allowance is still hanging at the edge of the pedestal where a supporting path is developed. If the seam is moved further outward from the pedestal, the *DC*% will drop quickly from a 14 cm to a 15 cm seam radius. The *DC*% will decrease continuously as the seam moves to the edge of a fabric. When the seam is located near the edge of the specimen, the drape coefficient is lowest. From these results, it can be seen that the effect of seam position on fabric drape is significant with respect to the *DC*% for fabrics with a circular seam.

The drape profile of a fabric with a circular seam is entirely different from the drape profile of a fabric with radial seams. Nodes do not stay at any specific positions. Moreover, there is no consistent change of node number in the fabric, as shown in Table 8.7.

Table 8.7 The node number of drape shadow, highest and lowest node with respect to different seam radii (*r*)

	Seam radius, *r*							
	0	**7**	**9**	**11**	**12**	**14**	**15**	**17**
Node number	6	6	6	6	4	4	4	4
Highest node length, cm	7.8	8	7.5	8	8.4	8.2	8.5	8
Lowest node length, cm	6.1	5.3	6.5	6.2	7	6.5	6.8	7.2

r is the radius of a circular seam.

8.6 Summary

This chapter has examined the effect of seams on the bending and drape properties of woven fabrics. It is hoped that the results can provide a deeper understanding of drape and bending of a seamed fabric. The following conclusions have thus been reached:

(1) The bending of a fabric strip with a vertical seam is related to the second moment of area of a seamed fabric. Fabric thickness, seam thickness, distance of the neutral axis from the surface of the seam cross-section, width of fabric strip and width of seam allowance are the key elements involved in the analysis of seam structure. The effect of the second moment of area on the bending rigidity of a fabric strip with a vertical seam of various seam allowances can be presented as $B = \beta\sqrt{I_{\text{seam}}}$ from which β is a constant for a particular fabric. The relationship of bending length to the second moment of area of a fabric strip with a vertical seam can be expressed as $c = (\beta/W)^{1/3} I_{\text{seam}}^{1/6}$.

(2) Bending of a fabric with a vertical plain seam is mainly affected by the seam structure, which involves the study of fabric thickness, seam thickness, seam allowance, distance of neutral axis from the surface of fabric cross-section and width of the fabric strip. It is found that the 'second moment of area' of the seamed cross-section determines the bending behaviour of a fabric strip with a vertical seam. Bending length and bending rigidity of seamed fabrics are highly related to the second moment of area of the fabric cross-section.

(3) In the cantilever test with a horizontal seam, it can be seen that the bending length of a fabric with a horizontal seam is lower than that of a vertical seam. The location of a horizontal seam is a significant factor in determining the bending length. The nearer the seam is to the free end, the smaller is the bending length. Seam allowance has different effects on bending length according to seam locations.

(4) It has been found that drape coefficient is increased by the addition of a radial seam. The effect of radial seams on fabric drape is clearly shown by the dramatic increase in seam numbers. The *DC*% is highest when a fabric has four seams. The drape profile of an unseamed fabric is not stable and node numbers vary on every drape. The drape profiles of fabrics with one radial seam have irregular node orientations at the unseamed parts. However, the drape profiles of fabrics with four radial seams are more stable and regular. The node numbers are normally fixed at seven or eight in an octagonal arrangement. Increase in seam allowance has little influence on changing the node orientation along the seamed parts of four radial seams.

(5) With respect to fabric drape with a circular seam, the highest drape coefficient has been found when a circular seam is located just out of

the pedestal. Any outward movement of the seam causes *DC*% to fall. The drape coefficient is lowest when the circular seam is located at the edge of the fabric. Hence, varying the seam position of a circular seam has a significant effect on fabric drape.

8.7 References

Ajiki I (1985), Bending properties of seamed fabrics. *The 3rd Japan/ Aust joint symposium on objective measurement: applications to product design and process control (preprint abstracts)*, 319–327.

De Boos A G and Tester D H (1990), The FAST approach to improved fabric performance in textile objective measurement and automation in garment manufacture, *Proc First International Clothing Conference*, July 9–11, University of Bradford, Chichester, Ellis Horwood.

Dhingra R C and Postle R (1980–1981), Some aspects of the tailorability of woven and knitted outerwear fabrics, *Clothing Res J*, **8–9**, 59–76.

Grosberg P and Swani N M (1966), The mechanical properties of woven fabrics part IV: the determination of the bending rigidity and frictional restraint in woven fabrics, *Text Res J*, **36**, 338.

Gupta B S, Leek R L, Buchanan D R and Little T J (1992), Directional variations in fabric properties and seam quality, *Int J Clothing Sci & Tech*, **4**(2/3), 71–78.

Mahar T J, Ajiki I and Postle R (1982a), Fabric mechanical and physical properties relevant to clothing manufacture part 2: structural balance, breaking elongation and curvature of seams, *Int J Clothing Sci & Tech*, **1**(2), 5–10.

Mahar T J, Dhingra R C and Postle R (1982b), Fabric mechanical and physical properties relevant to clothing manufacture part 1: fabric overfeed, formability, shear and hygral expansion during tailoring, *Int J Clothing Sci & Tech*, **1**(1), 12–20.

Peirce F T (1930), The handle of cloth as a measurable quantity, *J Text Inst*, **21**, 377–416.

Postle J R and Postle R (1992), Fabric bending and drape based on objective measurement, *Int J Clothing Sci & Tech*, **4**(5), 7–15.

Shirley Inst Bull (1957), **30**, 215.

Shishoo R L, Klevmar P H, Cednas M and Olofsson B (1971), *Text Res J*, **41**, 669.

Suda N and Nagasaka T (1984a), Influence of the partial change of bending property on the formation of nodes, *Report of Polymeric Materials Research Institute*, No **142**, 47–55.

Suda N and Nagasaka T (1984b), Dependency of various sewing conditions on the bending property of seams, *Report of Polymeric Materials Research Institute*, No **142**, 39–45.

9

Modelling drape deformation of woven fabrics and garments – theory

9.1 Introduction

The key to developing CAD (computer-aided design) systems for clothing products is the establishment of physically-based numerical models which can efficiently and accurately simulate the drape and other complex deformations of fabrics (Hu and Teng, 1996), in particular woven fabrics which are the commonly used fabric material. Woven fabrics are complex mechanisms made up of intersecting threads or yarns. Although they may be treated as continuous sheet materials, when undergoing overall deformations like draping, the complex and discrete microstructure and their very small thickness lend these fabrics many special properties that differ from those of other conventional sheet materials such as steel and glass. Fabrics have a very small bending stiffness compared to their membrane stiffness and have different mechanical properties in the warp and weft directions. They are easily deformable, suffering large deflections and rotations even under their own weight and in daily use. The maximum deflection involved in fabric deformations may be of the order of hundreds of times the thickness, and the final deformed shape may be extremely complicated, with many doubly-curved folds. The deformations are large although the strains are generally small. Analysis of complex fabric deformations is therefore a difficult task and one that was impossible, except for a few very simple cases, before the computer era.

Over the last two decades computer technology has made great advances. These advances have made it possible to model complex fabric deformations such as fabric draping using computer simulation techniques. There have been many successes and considerable progress in this area during the period (Hu and Teng, 1996; Ng and Grimsdale, 1996). Most early works (Weil, 1986; Dhande *et al.*, 1993) in the area are geometrically based, with an emphasis on reproducing the cloth-like appearance of a fabric sheet on a computer. These models cannot simulate fabric behaviour physically since no mechanical properties are included in them. Many other workers,

however, have adopted various physically-based models (Hu and Teng, 1996).

Feynman (1986) proposed an energy-based physical model for simulating the appearance of cloth. The simulations included hanging cloth and cloth draped over a sphere. The total energy function of the model contains tensile strain, bending strain and gravity terms, but shear deformations are not considered. Terzopoulos *et al.* (1987) introduced an elastically deformable model for generalised flexible objects including fabrics. Since the model was developed for general use in computer graphics, it is not capable of directly incorporating standard engineering parameters such as Young's modulus. The solution procedure for the equations arising from the model is also computationally intensive. Many other works (Thalmann and Yang, 1991; Thalmann and Thalmann, 1991; Carignan *et al.*, 1992) were reported using and extending Terzopoulos *et al.*'s deformable model. These works were focused on the computer visualisation and animation of garments.

Breen *et al.* developed a particle-based model to simulate the draping behaviour of woven cloth (Breen 1993; Breen *et al*. 1991, 1992, 1994). In their model, the cloth is treated as a collection of particles that conceptually represent the crossing points of warp and weft threads in a plain-woven fabric. Separate empirical energy functions were proposed for yarn repelling, stretching, bending and trellising deformations. These functions were tuned using the KES, Kawabata Evaluation System (Kawabata, 1975), test data empirically in their later works (Breen *et al.*, 1992; Breen, 1993). The final position of the draped fabric was determined based on the minimisation of the total potential energy which is the sum of the deformation energy terms mentioned above and the potential energy of the self weight. While the model was conceptually based on the microstructure of cloth, continuum-based macrostructure properties were used in the simulation. The particle grid of 51×51 used for a 1 m $\times$ 1 m cloth in the numerical examples is also far from that necessary for a microstructural or thread level model. In addition, the solution procedure employing a stochastic searching process was reported to be very time-consuming. Recently Eberhardt *et al.* (1996) extended Breen's particle-based model by using a different, faster technique to compute the exact particle trajectories. Some promising simulations including cloth draped over a square table, a circular table and a sphere were presented.

Stylios *et al.* (1995, 1996) presented a physically-based approach using the deformable node-bar model (Schnobrich and Pecknold, 1973) to predict complex deformations of fabrics. In their approach, the fabric sheet is assumed to be a continuum shell with homogeneous, orthotropic and linearly elastic properties. Their drape simulation was compared with results from a fabric drape testing system. The modelling of a skirt attached to a synthetic lady was also described.

Several other researchers employed the finite-element method for the simulation of fabric draping behaviour. Lloyd (1980) was probably the first to apply the finite-element method to model fabrics and dealt only with in-plane deformations. Collier (1991) developed a large deflection/small strain analysis employing a 4-noded orthotropic flat shell element to predict the drape coefficient of cotton fabrics. Their results were reported to be in reasonably good agreement with experimental results. Gan *et al.* (1995) produced a similar analysis employing a curved shell element and presented simulation results for fabric sheets draped over square and circular pedestals. Kim (1991) described drape simulations using a geometrically exact shell theory proposed by Simo *et al.* (1989, 1990). Simo and Fox (1989), Deng (1994) and Eischen *et al.* (1996) extended the work of Kim to buckling, contact and materially non-linear problems.

Chen and Govindaraj (1995) predicted the draping of fabrics using a shear flexible shell theory. The predicted results of a square fabric sheet draped over a flat square surface and an animation sequence were presented. Yu *et al.*(1993) and Kang and Yu (1995) also developed a non-linear finite-element code to simulate the draping of woven fabrics. In their study, a flat shell element model based on a convected co-ordinate system (Simo and Fox, 1989; Simo *et al.*, 1989, 1990; Bathe, 1982) was used. The fabric was again assumed to be an elastic and orthotropic material. The predicted draped shapes were shown to agree reasonably well with those obtained experimentally.

Ascough *et al.* (1996) adopted a rather simple beam element model in their cloth drape simulations and the simulation results for a piece of fabric draped over a table corner do not appear to be close in shape to that seen in a corresponding photo. They also presented simulation results of the falling of a skirt from its initial position into contact with a human body. Their simulations were carried out as a dynamic analysis using Newmark's method.

As reviewed above, there exist basically two main approaches in the existing modelling approaches of fabric drape deformations: (a) the finite-element approach employing a shell element; (b) a more empirical approach developed specifically for fabric deformation analysis, among which the particle-based model of Breen *et al.* is representative and the most widely quoted (Breen 1993; Breen *et al.* 1991, 1992, 1994).

The studies of Stylios *et al.* (1995; 1996) and Ascough *et al.* (1996) do not fall neatly into either of the above two approaches, but both are closely related to the first approach.

The finite-element approach employing a shell element has been used by a number of researchers. It has a rigorous mechanical basis and can be easily understood and further developed by the computational mechanics community. As the method was not developed making use of the special characteristics of fabric drape deformations, it has a number of disadvantages. First, the method entails a high computational cost as high-order shape functions are

used and very large displacements have to be followed in a step-by-step manner. Second, when the popular degenerated shell elements are used, the bending stiffness and the membrane stiffness of the shell surface will be coupled, and this subsequently leads to difficulty in modelling fabric sheets due to their independent membrane and bending stiffness. Thirdly, the method is theoretically complex, making it more difficult to be readily accepted and understood by its users.

On the other hand, the widely cited particle-based model of Breen and its extension (Breen *et al*., 1991, 1992; Breen, 1993; Breen *et al.*, 1994; Eberhardt *et al.*, 1996) contains much empiricism in the establishment of the energy functions and uses definitions of deformations which do not follow a rigorous mechanics approach. The computational cost may also be very high.

9.2 Finite-volume formulation

9.2.1 Discretisation scheme

Fabric drape deformations involve very large deflections, but the associated strains are small. This is because fabric sheets are very thin and flexible, so most of the gross deformations come from bending; the amount of in-plane stretching is very small in comparison. This means that an initial patch of a fabric sheet would retain its original surface area and volume after drape deformations.

Based on this knowledge, the finite-volume method is adopted for simulating the complex deformations of fabrics. In this method, an initially flat fabric is first subdivided into a finite number of structured small patches finite volumes (or control volumes). One control volume contains one grid node. The deformations of a typical volume can be defined using the global co-ordinates of its grid node and several neighbouring grid nodes surrounding it. The strains and curvatures, and hence the in-plane membrane and out-of-plane bending strain energies, of the whole fabric sheet are then calculated very easily over all control volumes which retain their original surface areas and thicknesses. The equilibrium equations of the fabric sheet are derived employing the principle of stationary total potential energy. Geometric non-linearity and linear elastic orthotropic material properties of the fabric are considered in the formulation. This leads to a simple but rigorous way of formulating the equilibrium equations of a grossly deformed fabric sheet.

The concept of finite volume or control volume was originally used for the discretisation of differential equations, particularly in computational fluid dynamics (Patankar, 1980; Versteeg and Malalasekera, 1995). Using this discretisation approach, the calculation domain is first divided into many non-overlapping control volumes such that there is one volume surrounding each grid node. The differential equations are then integrated over each control volume, resulting in discretisation equations containing variables for

a group of grid nodes. The most attractive feature of the finite-volume formulation is that the integral conservation of physical quantities such as mass, momentum, and energy is exactly satisfied over any group of control volumes (including the limiting case of a single finite volume) and, of course, over the whole calculation domain (Patankar, 1980).

In recent years, the finite-volume method has also been applied to solid and structural mechanics problems (Fryer *et al*., 1991; Demirdzic and Martinovic, 1993; Demirdzic and Muzaferija, 1994; Onate *et al*., 1994; Bailey and Cross, 1995; Wheel, 1996, 1997), particularly for solid body stress analysis (Demirdzic and Martinovic, 1993; Demirdzic and Muzaferija, 1994; Onate *et al*., 1994; Bailey and Cross, 1995; Wheel, 1996).

Here we attempt to extend the finite-volume method to model fabric deformation, a highly non-linear problem of orthotropic sheet materials with unique features. The deformations and energies are calculated over all control volumes based on simple but reasonable assumptions. The discretised equations containing the global co-ordinates of grid nodes as unknowns are derived using the principle of stationary total potential energy. The proposed formulation gives the finite-volume method an explicit physical interpretation in fabric deformation modelling and extends the horizon for the application of the finite-volume method.

There is another major difference between the analysis of fabric drape deformation and a non-linear load-resisting structure. In fabric deformation analysis, attention is given to the final shape of the deformed fabric sheet under self weight with or without additional applied load, while in the analysis of a non-linear load-bearing structure, the maximum load that the structure can carry and the load-deflection response are of more interest. In addition, both the displacements and the internal forces need to be carefully determined in the analysis of load-bearing structures while, in fabric deformation analysis, the final displacements are the only focus. These aspects are exploited here in developing an efficient solution method.

9.2.2 Finite-volume discretisation

Before deformations, the fabric sheet is assumed to be flat. The whole fabric surface is taken to be the computational domain of the problem, over which an appropriate discretisation grid needs to be established.

9.2.2.1 General control-volume discretisation

Consider an initially flat fabric sheet, which consists of two orthogonal sets of threads, warp and weft yarns. Figure 9.1 illustrates the domain discretisation scheme of such a fabric sheet. The dashed lines in the two orthogonal directions (warp and weft or x- and y-) divide the whole fabric area into a finite number

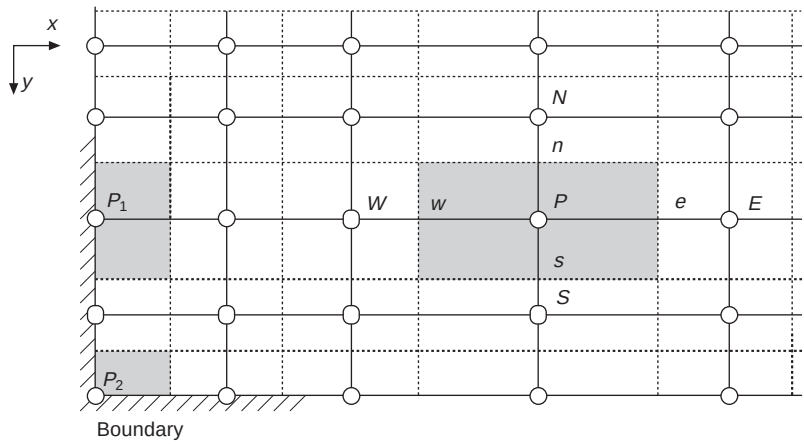

9.1 Two-dimensional non-uniform grid.

of structured sub-domains, called finite volumes (or control volumes). The solid lines are located midway between neighbouring dashed lines. Consequently, the crossings of solid lines, which are called grid nodes, lie exactly at the geometric centres of the control volumes, while the crossings of dashed lines and solid lines, which are called face nodes, lie at the mid-points of the respective finite-volume boundaries or faces.

A system of notation for each control volume is now established as shown in Fig. 9.1 for a typical internal volume. It contains one grid node which is identified by *P* and four face nodes which are identified by *w*, *e*, *n* and *s*, denoting the west, east, north and south side faces, respectively. The same letter *P* is also used to identify this typical volume. Four neighbouring grid nodes, identified by *W*, *E*, *N* and *S* respectively, are connected directly with the node *P*. Here nodes *W* and *E* are *x* direction neighbours of *P*, while *N* and *S* are the *y* direction neighbours. The two axes are assumed to be aligned with the two orthogonal directions of a woven fabric composed of warp and weft yarns. For simplicity of presentation here, the *x*-axis is assumed to be in the warp direction and the *y*-axis to be in the weft direction.

If the grid intervals (or finite-volume sizes) are non-uniform, the four face nodes will not lie midway between the grid node *P* and its four neighbouring grid nodes *W*, *E*, *N* and *S*, respectively. The positions of the four face nodes are, however, simply determined by a linear interpolation between the adjacent grid nodes. In particular, if a two-dimensional fabric drape problem is considered, the initial grid will be one-dimensional. This discretisation scheme is given in Fig. 9.2.

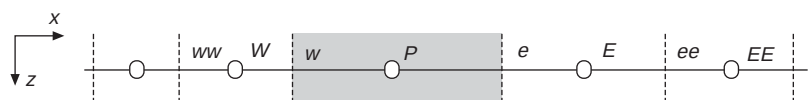

9.2 One-dimensional grid.

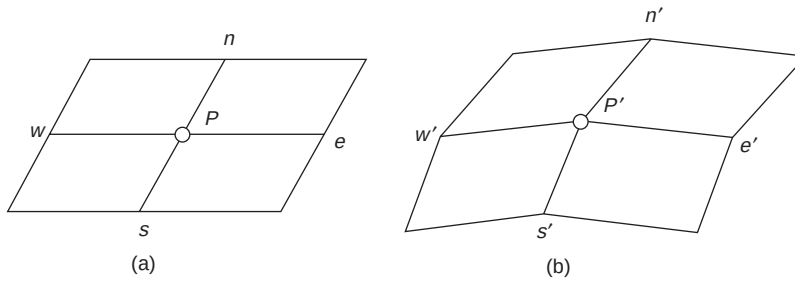

9.3 A typical control volume *P:* (a) before and (b) after deformation.

9.2.2.2 Assumptions about deformation

Deformation will lead to a subsequent change in the location and the overall shape of each control volume. For a typical control volume *P* (Fig. 9.3), this means that the grid node *P* and the face nodes *w*, *e*, *n* and *s* will move from their initial positions to their new positions. Since the fabric undergoes large displacements and rotations but small strains during the process of deformations, it may be reasonable to make the following assumptions in the analysis of fabric deformations:

(1) The fabric is an elastic and orthotropic material whose two principal directions of anisotropy coincide with the warp and weft directions of the yarns, respectively. Although the displacements may be very large, considering the small strains involved, the two directions of the warp and weft yarns are assumed to remain orthogonal throughout the deformation process.
(2) For a typical control volume, only uncoupled out-of-plane bending and in-plane tension or compression and shearing are produced during the deformation process. The contribution of twisting deformation to the strain energy is ignored.
(3) The surface area and thickness of the fabric sheet, and hence those of a control volume, do not change significantly during deformations.
(4) The strains and curvatures of a typical control volume can be determined using the positions of its grid node and four face nodes.
(5) The deformed position of each face node can be determined using a linear interpolation between its two adjacent grid nodes as in the undeformed state. For example, the deformed position of the face node *e* in Fig. 9.1 can be found by linear interpolation of the deformed positions of nodes *P* and *E*.
(6) Each grid node has three degrees of freedom: three global coordinates *x*, *y* and *z*.

Under the above assumptions, the deformations of an internal control volume will only depend on five grid nodes: the grid node of the volume itself and its four neighbours surrounding it.

In assumption 2, the twisting shear strain energy is assumed to be negligible. This assumption in fact has been involved in all fabric deformation models based on approach b, although it has never been discussed or even mentioned in these studies. Physically, the assumption may be justified by noting that the warp and weft yarns of a woven fabric structure can slide against each other under twisting shear stresses, a situation which also makes the in-plane shear stiffness much smaller than the tensile stiffness. The assumption of ignoring the resistance offered by twisting shear deformations is also supported by numerical comparisons later (Press *et al.*, 1992).

9.2.2.3 Boundary control volumes

So far, no discussion has been given on the control volumes that lie along the edges or at the corners of the computational domain. Since boundary conditions are usually imposed only on the grid nodes, the solid grid lines are placed along the domain edges, leading to half volumes along edges and quarter volumes at corners. That is, the typical edge volume P_1 (Fig. 9.1) may be viewed as a 'half' of an internal control volume and the corner volume P_2 (Fig. 9.1) a 'quarter' of an internal volume. Therefore, the deformations of the edge control volume P_1 will depend on four grid nodes instead of five, one of itself and three neighbours, and those of the corner control volume P_2 depend only on three grid nodes.

9.2.3 Strain energy

The out-of-plane bending and in-plane membrane strain energies of a typical control volume are considered in this section. The total strain energy of a control volume is the summation of these two types of strain energy. The total strain energy of the fabric sheet can be found by adding together the contributions from all control volumes.

9.2.3.1 Out-of-plane bending

The bending deformations of a typical control volume P are in general produced simultaneously in two directions: warp (or x) and weft (or y). Figure 9.4a illustrates the x-direction bending. Although the draped shape of a fabric sheet is in general a complicated curved surface, the radii of curvature in both the warp and weft directions of a small surface area are still much greater than its thickness. Therefore, if the control volume is sufficiently small, it is not difficult to derive the equivalent bending curvatures in the

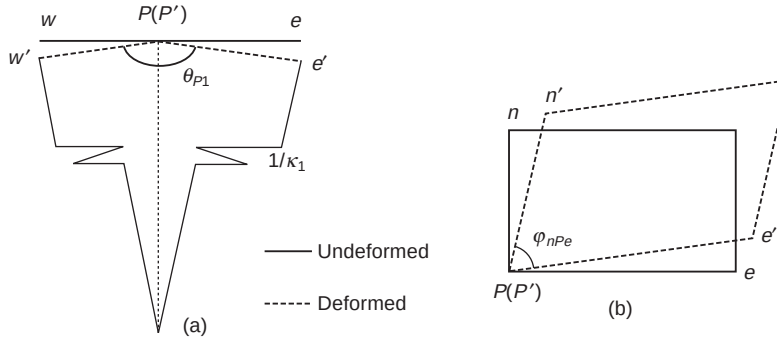

9.4 Deformations of a typical control volume *P:* (a) out-of plane bending in *x*-direction; (b) in-plane tension and shearing.

two directions from the two bending angles formed by its grid node and the four neighbours. For example, the radius of curvature of the deformed surface in the warp direction is found as the radius of a circular arc which has two end tangents coinciding with the deformed lines $P'w'$ and $P'e'$ for the control volume P (Fig. 9.4a). Therefore, the curvatures of the control volume P in the two directions are

$$\kappa_{P1} = 2\text{ctg}\,\frac{\theta_{P1}}{2}/l_{P1} \quad \text{and} \quad \kappa_{P2} = 2\text{ctg}\,\frac{\theta_{P2}}{2}/l_{P2} \qquad [9.1]$$

where κ_{P1} and κ_{P2} are the bending curvatures in the warp and weft directions, θ_{P1} and θ_{P2} are the corresponding bending angles (see Fig. 9.4a), l_{P1} and l_{P2} are the finite-volume sizes in the two directions, respectively. Based on assumptions 1–6 as given in the previous section, the bending strain energy is given as

$$U_{Pb} = \frac{1}{2}(D_1\kappa_{P1}^2 + 2D_{12}\kappa_{P1}\kappa_{P2} + D_2\kappa_{P2}^2) \cdot A_P \qquad [9.2]$$

where D_1 and D_2 are the bending rigidities in the warp and weft directions, respectively, D_{12} is the bending rigidity reflecting the Poisson's effect, and A_P is the in-plane surface area of volume P which is assumed to remain constant during deformations.

Based on the classical continuum bending theory which assumes that the tensile and compressive Young's moduli are the same and that they are also the same regardless of the nature of deformations, these bending rigidities can be related to the elastic moduli obtained from uniaxial tensile tests. For a woven fabric, however, the situation is quite different in that the measured bending rigidities are much smaller than those calculated using the conventional continuum mechanics approach. That is, a fabric has independent bending stiffness and stretching stiffness. Therefore, equation 9.2 is used directly with measured bending rigidities.

9.2.3.2 In-plane tension and shearing

The in-plane (or membrane) deformations of a control volume include tension/compression in the two principal directions and membrane shearing. In general, the surface of a control volume is not plane after deformations, so subdivision of the volume into smaller sections is desirable for a more accurate evaluation of the in-plane strain energy. Referring to the typical volume *P* as shown in Figs 9.1 and 9.3, the two lines *ew* and *ns* subdivide the whole volume into four sections, *nPe*, *nPw*, *sPe* and *sPw*. The in-plane deformations of the quarter section *nPe* are illustrated in Fig. 9.4b. The membrane strains of the section can then be evaluated as

$$\left.\begin{aligned}
\varepsilon_1 &= \varepsilon_{Pe} = \frac{\overline{P'e'} - \overline{Pe}}{\overline{Pe}} = \frac{\overline{P'E'} - \overline{PE}}{\overline{PE}} = \frac{d_{PE} - l_{PE}}{l_{PE}} \\
\varepsilon_2 &= \varepsilon_{Pn} = \frac{\overline{P'n'} - \overline{Pn}}{\overline{Pn}} = \frac{\overline{P'N'} - \overline{PN}}{\overline{PN}} = \frac{d_{PN} - l_{PN}}{l_{PN}} \\
\varepsilon_{12} &= \gamma_{nPe} = \frac{\pi}{2} - \varphi_{nPe}
\end{aligned}\right\} \qquad [9.3]$$

where l_{PE}, d_{PE} and l_{PN}, d_{PN} are the distances between grid nodes *P* and *E*, and *P* and *N*, before and after deformations, respectively; φ_{nPe} is the angle formed by lines *Pe* and *Pn* after deformations (Fig. 9.4b).

As the fabric is assumed to be an orthotropic elastic material, the corresponding stress resultants (force per unit length) in the section can be easily obtained as

$$\begin{Bmatrix} N_1 \\ N_2 \\ S_{12} \end{Bmatrix} = \begin{bmatrix} E_1 & E_{12} & 0 \\ E_{12} & E_2 & 0 \\ 0 & 0 & G \end{bmatrix} \begin{Bmatrix} \varepsilon_1 \\ \varepsilon_2 \\ \gamma_{12} \end{Bmatrix} = \begin{bmatrix} E_1 & E_{12} & 0 \\ E_{12} & E_2 & 0 \\ 0 & 0 & G \end{bmatrix} \begin{Bmatrix} \varepsilon_{Pe} \\ \varepsilon_{Pn} \\ \gamma_{nPe} \end{Bmatrix} \qquad [9.4]$$

where *G* is the shear rigidity and E_1, E_2, E_{12} are given by

$$\left.\begin{aligned}
E_1 &= \frac{E_{\text{warp}}}{1 - \nu_{\text{warp}}\nu_{\text{weft}}} \\
E_2 &= \frac{E_{\text{weft}}}{1 - \nu_{\text{warp}}\nu_{\text{weft}}} \\
E_{12} &= \frac{\nu_{\text{warp}} E_{\text{weft}}}{1 - \nu_{\text{warp}}\nu_{\text{weft}}} = \frac{\nu_{\text{weft}} E_{\text{warp}}}{1 - \nu_{\text{warp}}\nu_{\text{weft}}}
\end{aligned}\right\} \qquad [9.5]$$

Here, E_{warp} and E_{weft} are the membrane rigidities of the fabric sheet in the warp and weft directions respectively determined from tensile tests, and ν_{warp} and ν_{weft} are the corresponding Poisson's ratios. The in-plane strain energy of section *nPe* is therefore given by

$$U_{nPe} = \frac{1}{2}(E_1\varepsilon_{Pe}^2 + 2E_{12}\varepsilon_{Pe}\varepsilon_{Pn} + E_2\varepsilon_{Pn}^2 + G\gamma_{nPe}^2) \cdot A_{nPe} \qquad [9.6]$$

where A_{nPe} is the area of quarter section *nPe*.

The in-plane strain energy U_{nPw}, U_{sPw} and U_{sPe} of the other three quarter sections can be found in a similar manner. The in-plane (or membrane) strain energy of the whole control volume is the sum of the above four sections given by

$$U_{P\mathrm{m}} = U_{nPe} + U_{nPw} + U_{sPw} + U_{sPe} \qquad [9.7]$$

The total strain energy of the control volume P is the sum of bending and membrane strain energies, i.e.

$$U_P = U_{P\mathrm{b}} + U_{P\mathrm{m}} \qquad [9.8]$$

Consequently, the total strain energy of the whole fabric sheet consisting of r control volumes U_{df} is

$$U_{df} = \sum_{P=1}^{r} U_P \qquad [9.9]$$

9.2.4 Governing equations

Under its own weight and given boundary conditions, a fabric sheet always deforms into a final stable equilibrium state and forms a complicated surface, the process of which is called fabric draping. Complex deformations may also occur under additional applied loads. The final equilibrium state of the fabric can be determined by using the principle of stationary total potential energy. The total potential energy Π is the summation of the total strain energy as given by equation 9.9 and the potential energy of gravitational forces and other applied loads

$$\left.\begin{aligned} \Pi &= U_{df} + U_{\mathrm{g}} + U_{\mathrm{ex}} = \sum_{P=1}^{n}(U_{P\mathrm{b}} + U_{P\mathrm{m}} + U_{P\mathrm{g}} + U_{P\mathrm{ex}}) \\ U_{P\mathrm{g}} &= -m_P g z_P \end{aligned}\right\} \qquad [9.10]$$

where U_{g} and U_{ex} are the potential energies of gravitational forces and other applied loads respectively, m_P is the mass of the finite volume P, g is the gravitational acceleration, and z_P is the vertical co-ordinate. The equilibrium equations can be obtained using the variational principle that the total potential energy Π must be stationary;

$$\delta\Pi = \delta(U_{df} + U_{\mathrm{g}} + U_{\mathrm{ex}}) = 0 \qquad [9.11]$$

or

$$\frac{\partial\Pi}{\partial x_{Pi}} = \frac{\partial U_{df}}{\partial x_{Pi}} + \frac{\partial(U_{\mathrm{g}} + U_{\mathrm{ex}})}{\partial x_{Pi}} = 0 \quad (P = 1, 2, \ldots, r, i = 1, 2, 3) \qquad [9.12]$$

where x_{Pi} ($i = 1, 2, 3$) stands for the three global co-ordinates x_P, y_P and z_P of the position of node P at any point of time during deformation. Equation 9.12 leads to a set of non-linear algebraic equations with the global coordinates of all grid nodes as unknowns, which can be cast in the following form

$$\left.\begin{aligned} \boldsymbol{F} - \boldsymbol{R} &= 0 \\ \boldsymbol{F} &= \frac{\partial U_{df}}{\partial \boldsymbol{X}} \\ \boldsymbol{R} &= -\frac{\partial (U_g + U_{ex})}{\partial \boldsymbol{X}} \end{aligned}\right\} \qquad [9.13]$$

where $\boldsymbol{X} = [\cdots x_{W1}\ x_{W2}\ x_{W3}\ \cdots x_{P1}\ x_{P2}\ x_{P3}\ \cdots]^{\mathrm{T}}$ is the global nodal co-ordinate vector, $\boldsymbol{F}$ is the global nodal internal force vector and $\boldsymbol{R}$ is the global nodal load vector due to gravity and applied loads.

Using the Newton–Raphson iteration scheme (Bathe, 1996; Crisfield, 1991), equation 9.13 can be rewritten in the following iterative form

$$\left.\begin{aligned} \boldsymbol{K}\Delta\boldsymbol{X} &= \boldsymbol{R} - \boldsymbol{F} \\ \boldsymbol{X}^{(i+1)} &= \boldsymbol{X}^{(i)} + \Delta\boldsymbol{X} \\ \boldsymbol{K} &= \frac{\partial \boldsymbol{E}}{\partial \boldsymbol{X}} = \frac{\partial^2 U_{df}}{\partial \boldsymbol{X}\partial \boldsymbol{X}} \end{aligned}\right\} \qquad [9.14]$$

where $\boldsymbol{K}$ is the global tangent stiffness matrix of the fabric sheet, and $\boldsymbol{X}^{\{i\}}$ denotes the i-th iterative solution of the vector $\boldsymbol{X}$. From equation 9.9, the global internal force vector and the global tangent stiffness matrix may be written in the form of summations as

$$\left.\begin{aligned} \boldsymbol{F} &= \sum_{P=1}^{r} \frac{\partial U_p}{\partial \boldsymbol{X}} \\ \boldsymbol{K} &= \sum_{P=1}^{r} \frac{\partial^2 U_p}{\partial \boldsymbol{X}\partial \boldsymbol{X}} \end{aligned}\right\} \qquad [9.15]$$

Since the strain energy function U_P depends only on the co-ordinates of node P and its four neighbours W, E, N and S, only 15 components in the vector $\partial U_P/\partial \boldsymbol{X}$ are non-zero. Similarly, the matrix $\partial^2 U_P/\partial \boldsymbol{X}\partial \boldsymbol{X}$ contains only 15×15 non-zero elements. These non-zero elements form a sub-vector $\boldsymbol{F}^{\mathrm{e}}$ and a sub-matrix $\boldsymbol{K}^{\mathrm{e}}$, which are referred to as the element internal force vector and the element tangent stiffness matrix, respectively. Once all the element vectors $\boldsymbol{F}^{\mathrm{e}}$ and matrices $\boldsymbol{K}^{\mathrm{e}}$ are obtained, they can be assembled to form the global vector $\boldsymbol{F}$ and matrix $\boldsymbol{K}$, the procedure of which is similar to that in the finite-element method.

9.2.4.1 The element internal force vector

In this section, the internal force vector for a typical internal control volume P (referred to as element internal force vector here) is formulated. The vector is given by

$$\boldsymbol{F}^{\mathrm{e}} = \left[\frac{\partial U_P}{\partial x_{Wi}} \; \frac{\partial U_P}{\partial x_{Ni}} \; \frac{\partial U_P}{\partial x_{Pi}} \; \frac{\partial U_P}{\partial x_{Si}} \; \frac{\partial U_P}{\partial x_{Ei}} \right]^{\mathrm{T}} \qquad [9.16\}$$

and the corresponding element nodal co-ordinate vector is

$$\boldsymbol{X}^{\mathrm{e}} = [x_{Wi} \quad x_{Ni} \quad x_{Pi} \quad x_{Si} \quad x_{Ei}]^{\mathrm{T}} \qquad [9.17]$$

In equations 9.16 and 9.17, each component denotes a 3×1 vector, for example

$$\left\{ \frac{\partial U_P}{\partial x_{P_i}} \right\} = \left[\frac{\partial U_P}{\partial x_{P1}} \quad \frac{\partial U_P}{\partial x_{P2}} \; \frac{\partial U_P}{\partial x_{P3}} \right]^{\mathrm{T}} \quad \text{and} \quad \{x_{Pi}\} = [x_{P1} \quad x_{P2} \quad x_{P3}]^{\mathrm{T}} \qquad [9.18]$$

From equations 9.7 and 9.8, it is easy to see that

$$\left.\begin{aligned} \frac{\partial U_P}{\partial x_j} &= \frac{\partial U_{P\mathrm{b}}}{\partial x_j} + \frac{\partial U_{P\mathrm{m}}}{\partial x_j} \\ \frac{\partial U_{P\mathrm{m}}}{\partial x_j} &= \frac{\partial U_{nPw}}{\partial x_j} + \frac{\partial U_{nPe}}{\partial x_j} + \frac{\partial U_{sPw}}{\partial x_j} + \frac{\partial U_{wPe}}{\partial x_j} \\ (x_j &= x_{Wi}, x_{Ni}, x_{Pi}, x_{Si}, x_{Ei}, i = 1, 2, 3) \end{aligned}\right\} \qquad [9.19]$$

Noting that

$$\left.\begin{aligned} \kappa_{P1} &= \frac{2}{l_{P1}} \operatorname{ctg} \frac{\theta_{P1}}{2} = \pm \frac{2}{l_{P1}} \sqrt{\frac{1 + \cos\theta_{P1}}{1 - \cos\theta_{P1}}} = \pm \frac{2}{l_{P1}} \sqrt{\frac{1 + f_{wpe}}{1 - f_{wpe}}} \\ \kappa_{P2} &= \frac{2}{l_{P2}} \operatorname{ctg} \frac{\theta_{P2}}{2} = \pm \frac{2}{l_{P2}} \sqrt{\frac{1 + f_{nps}}{1 - f_{nps}}} \end{aligned}\right\} \qquad [9.20]$$

where f_{wPe} and f_{nPs} denote the cosines of the bending angles θ_{P1} and θ_{P2} respectively, the strain energies $U_{P\mathrm{b}}$, U_{nPw}, U_{nPe}, U_{sPw} and U_{wPe} can be expressed as functions of the nodal co-ordinates, that is

$$
\begin{aligned}
U_{Pb} &= \frac{1}{2}(D_1\kappa_{P1}^2 + 2D_{12}\kappa_{P1}\kappa_{P2} + D_2\kappa_{P2}^2)A_P \\
&= \frac{2D_1 l_{P2}}{l_{P1}}\frac{1+f_{wPe}}{1-f_{wPe}} \\
&\quad \pm 4D_{12}\sqrt{\frac{1+f_{wPe}}{1-f_{wPe}}\cdot\frac{1+f_{nPs}}{1-f_{nPs}}} + \frac{2D_2 l_{P1}}{l_{P2}}\frac{1+f_{nPs}}{1-f_{nPs}}
\end{aligned}
\qquad [9.21]
$$

and

$$
\left.
\begin{aligned}
U_{bPa} &= \frac{1}{2}(E_1\varepsilon_{Pa}^2 + 2E_{12}\varepsilon_{Pa}\varepsilon_{Pb} + E_2\varepsilon_{Pb}^2 + G\gamma_{bPa}^2)A_{bPa} \\
\gamma_{bPa} &= \frac{\pi}{2} - \arccos f_{bPa} \\
\varepsilon_{Pa} &= \frac{d_{PA} - l_{PA}}{l_{PA}} \quad (Pa = Pw, Pe, Pn, Ps;\ PA = PW, PE, PN, PS) \\
(bPa &= nPw, nPe, sPw, sPe)
\end{aligned}
\right\}
\qquad [9.22]
$$

where

$$
\left.
\begin{aligned}
f_{bPa} &= \frac{h_{bPa}}{g_{bPa}} \\
h_{bPa} &= \sum_{j=1}^{3}[(x_{Bj} - x_{Pj})(x_{Aj} - x_{Pj})] \\
g_{bPa} &= d_{PA}d_{PB} \\
d_{PA} &= \sqrt{\sum_{j=1}^{3}(x_{Aj} - x_{Pj})^2}\,,\ d_{PB} \\
&= \sqrt{\sum_{j=1}^{3}(x_{Bj} - x_{Pj})^2}\ (A, B = W, E, N, S) \\
(bPa &= wPe, nPs, \mathbf{nPw}, nPe, sPw, sPe)
\end{aligned}
\right\}
\qquad [9.23]
$$

where f_{bPa} denotes the cosine of the angle formed by grid lines PA and PB after deformations ($A, B = W, E, N$ or S), while d_{PA} and d_{PB} are the distances between grid nodes P and A, and P and B, respectively, after deformations. In equation 9.21 above, if the control volume deforms into an anticlastic surface, the second term on the right-hand side assumes the negative sign and otherwise the positive sign. Using equations 9.21–9.23, the first partial derivatives of the bending and membrane strain energy functions, namely the components of the element internal force vector $\boldsymbol{F}^e$, can be found as follows:

$$\left.\begin{aligned}
\frac{\partial U_{Pb}}{\partial x_{Wi}} &= \frac{4D_1 l_{P2}}{l_{P1}} \frac{1}{(1-f_{wPe})^2} \frac{\partial f_{wPe}}{\partial x_{Wi}} \\
\frac{\partial U_{Pb}}{\partial x_{Ni}} &= \frac{4D_2 l_{P1}}{l_{P2}} \frac{1}{(1-f_{nPs})^2} \frac{\partial f_{nPs}}{\partial x_{Ni}} \\
\frac{\partial U_{Pb}}{\partial x_{Pi}} &= \frac{4D_1 l_{P2}}{l_{P1}} \frac{1}{(1-f_{wPe})^2} \frac{\partial f_{wPe}}{\partial x_{Pi}} \\
&\quad + \frac{4D_2 l_{P1}}{l_{P2}} \frac{1}{(1-f_{nPs})^2} \frac{\partial f_{nPs}}{\partial x_{Pi}} \\
\frac{\partial U_{Pb}}{\partial x_{Si}} &= \frac{4D_2 l_{P1}}{l_{P2}} \frac{1}{(1-f_{nPs})^2} \frac{\partial f_{nPs}}{\partial x_{Si}} \\
\frac{\partial U_{Pb}}{\partial x_{Ei}} &= \frac{4D_1 l_{P2}}{l_{P1}} \frac{1}{(1-f_{wPe})^2} \frac{\partial f_{wPe}}{\partial x_{Ei}}
\end{aligned}\right\} \qquad [9.24]$$

and

$$\left.\begin{aligned}
\frac{\partial U_{bPa}}{\partial x_{Ai}} &= \left(E_1 \varepsilon_{Pa} \frac{\partial \varepsilon_{Pa}}{\partial x_{Ai}} + E_{12} \varepsilon_{Pb} \frac{\partial \varepsilon_{Pa}}{\partial x_{Ai}} + G\gamma_{bPa} \frac{\partial \gamma_{bPa}}{\partial x_{Ai}} \right) \cdot A_{bPa} \\
\frac{\partial U_{bPa}}{\partial x_{Pi}} &= \left(E_1 \varepsilon_{Pa} \frac{\partial \varepsilon_{Pa}}{\partial x_{Pi}} + E_2 \varepsilon_{Pb} \frac{\partial \varepsilon_{Pb}}{\partial x_{Pi}} + E_{12} \varepsilon_{Pa} \frac{\partial \varepsilon_{Pb}}{\partial x_{Pi}} \right. \\
&\quad \left. + E_{12} \varepsilon_{Pb} \frac{\partial \varepsilon_{Pa}}{\partial x_{Pi}} + G\gamma_{bPa} \frac{\partial \gamma_{bPa}}{\partial x_{Pi}} \right) \cdot A_{bPa} \\
\frac{\partial U_{bPa}}{\partial x_{Bi}} &= \left(E_2 \varepsilon_{Pb} \frac{\partial \varepsilon_{Pb}}{\partial x_{Bi}} + E_{12} \varepsilon_{Pa} \frac{\partial \varepsilon_{Pb}}{\partial x_{Bi}} + G\gamma_{bPa} \frac{\partial \gamma_{bPa}}{\partial x_{Bi}} \right) \cdot A_{bPa} \\
&(bPa = nPw, nPe, sPw, sPe)
\end{aligned}\right\} \qquad [9.25]$$

where

$$\frac{\partial \gamma_{bPa}}{\partial x_j} = -\frac{\partial \varphi_{bPa}}{\partial x_j} = \frac{1}{\sqrt{1-f_{bPa}^2}} \frac{\partial f_{bPa}}{\partial x_j},$$

$$(x_j = x_{Ai}, x_{Pi}, x_{Bi}, i = 1, 2, 3) \qquad [9.26]$$

For simplicity, in deriving equation 9.26, the coupling of bending in the two directions due to the Poisson's effect has been neglected (i.e. $D_{12} = 0$) and $A_P = l_{P1} l_{P2}$ has been used. There is currently little information on the Poisson's ratio of fabrics and its accurate measurement is difficult (Chen and Govindaraj, 1996). The effect of the Poisson's ratio is therefore ignored in almost all models belonging to the second approach. In finite-element shell models, while a non-zero Poisson's ratio can be easily handled and is quite often

included in numerical simulations, it has also been set to zero (Kim, 1991; Eischen *et al.*, 1996), a very small value (Kang and Yu, 1995) or not at all mentioned in the material properties (Gan *et al.*, 1995).

Collier (1991) compared the drape deformations of a circular piece of cloth draped over a circular pedestal using two very different values for the Poisson's ratios, 0.12 and 0.54 respectively, and showed that they led to some significant differences in the draped shape. A recent study by Chen and Govindaraj (1996) has, however, shown that the Poisson's ratio has no visible effect on fabric drape deformations for values between 0 and 0.5. Chen and Govindaraj (1996) also argued that Collier *et al.*'s results are not reliable due to the particular modelling approach used for their circular cloth pieces. It is also a pity that they did not include results for a Poisson's ratio of 0.3 which was used for other examples in their papers.

Even in the above two studies which give special attention to the effect of the Poisson's ratio, the definition of the Poisson's ratios is a little loose. Collier *et al.* does not even mention which of the two Poisson's ratios he was referring to when quoting the values, while Chen and Govindaraj define only one Poisson's ratio although the symmetry of the constitutive matrix is enforced. It thus appears to be wise to set the Poisson's ratios to zero. The theory presented here is, however, not limited to the case of zero Poisson's ratios, although a more involved derivation is required if a non-zero value is used. Numerical results given later in the section further justify the omission of the Poisson's effect.

In equations 9.24–9.26, the first derivatives of ε_{Pa} ($Pa = Pw, Pe, Pn, Ps$) and f_{bPa} ($bPa = wPe, nPs, nPw, nPe, sPw, sPe$) with respect to the nodal co-ordinates are given in the following four expressions

$$\left.\begin{aligned}\frac{\partial \varepsilon_{Pa}}{\partial x_{Pi}} &= \frac{x_{Pi} - x_{Ai}}{l_{PA} d_{PA}} \\ \frac{\partial \varepsilon_{Pa}}{\partial x_{Ai}} &= \frac{x_{Ai} - x_{Pi}}{l_{PA} d_{PA}}\end{aligned}\right\} (Pa = Pw, Pe, Pn, Ps; PA = PW, PE, PN, PS) \quad [9.27]$$

$$\left.\begin{aligned}\frac{\partial f_{bPa}}{\partial x_{Pi}} &= \frac{(2x_{Pi} - x_{Ai} - x_{Bi}) g_{bPa} - h_{bPa} \dfrac{\partial g_{bPa}}{\partial x_{Pi}}}{g_{bPa}^2} \\ \frac{\partial g_{bPa}}{\partial x_{Pi}} &= \frac{(x_{Pi} - x_{Ai}) d_{PB}}{d_{PA}} + \frac{(x_{Pi} - x_{Bi}) d_{PA}}{d_{PB}}\end{aligned}\right\} \quad [9.28]$$

$$\left.\begin{aligned}\frac{\partial f_{bPa}}{\partial x_{Ai}} &= \frac{x_{Bi} - x_{Pi}}{g_{bPa}} - \frac{h_{bPa}}{g_{bPa}^2} \frac{\partial g_{bPa}}{\partial x_{Ai}} \\ \frac{\partial g_{bPa}}{\partial x_{Ai}} &= \frac{(x_{Ai} - x_{Pi}) d_{PB}}{d_{PA}}\end{aligned}\right\} \quad [9.29]$$

and

$$\left.\begin{aligned}\frac{\partial f_{bPa}}{\partial x_{Bi}} &= \frac{x_{Ai} - x_{Pi}}{g_{bPa}} - \frac{h_{bPa}}{g_{bPa}^2}\frac{\partial g_{bPa}}{\partial x_{Bi}} \\ \frac{\partial g_{bPa}}{\partial x_{Bi}} &= \frac{(x_{Bi} - x_{Pi})d_{PA}}{d_{PB}}\end{aligned}\right\} \qquad [9.30]$$

By now, all components of the element internal force vector $\boldsymbol{F}^{\mathrm{e}}$ have been expressed as functions of the element nodal coordinate vector $\boldsymbol{X}^{\mathrm{e}}$. The global internal force vector $\boldsymbol{F}$ can then be formed by placing these components at appropriate positions according to the global grid-node numbering sequence.

9.2.4.2 The element tangent stiffness matrix

The element tangent stiffness matrix $\boldsymbol{K}^{\mathrm{e}}$ is a 15×15 symmetric matrix. For the typical internal control volume P, the matrix is

$$\boldsymbol{K}^{\mathrm{e}} = \begin{bmatrix} \dfrac{\partial^2 U_P}{\partial x_{Wi}\partial x_{Wk}} & & & & \\ \dfrac{\partial^2 U_P}{\partial x_{Ni}\partial x_{Wk}} & \dfrac{\partial^2 U_P}{\partial x_{Ni}\partial x_{Nk}} & & \textit{Sym.} & \\ \dfrac{\partial^2 U_P}{\partial x_{Pi}\partial x_{Wk}} & \dfrac{\partial^2 U_P}{\partial x_{Pi}\partial x_{Nk}} & \dfrac{\partial^2 U_P}{\partial x_{Pi}\partial x_{Pk}} & & \\ \dfrac{\partial^2 U_P}{\partial x_{Si}\partial x_{Wk}} & \dfrac{\partial^2 U_P}{\partial x_{Si}\partial x_{Nk}} & \dfrac{\partial^2 U_P}{\partial x_{Si}\partial x_{Pk}} & \dfrac{\partial^2 U_P}{\partial x_{Si}\partial x_{Sk}} & \\ \dfrac{\partial^2 U_P}{\partial x_{Ei}\partial x_{Wk}} & \dfrac{\partial^2 U_P}{\partial x_{Ei}\partial x_{Nk}} & \dfrac{\partial^2 U_P}{\partial x_{Ei}\partial x_{Pk}} & \dfrac{\partial^2 U_P}{\partial x_{Ei}\partial x_{Sk}} & \dfrac{\partial^2 U_P}{\partial x_{Ei}\partial x_{Ek}} \end{bmatrix} \qquad [9.31]$$

in which each component stands for a 3×3 sub-matrix. For example

$$\left[\frac{\partial^2 U_P}{\partial x_{Ni}\partial x_{Wk}}\right] = \begin{bmatrix} \dfrac{\partial^2 U_P}{\partial x_{N1}\partial x_{W1}} & \dfrac{\partial^2 U_P}{\partial x_{N1}\partial x_{W2}} & \dfrac{\partial^2 U_P}{\partial x_{N1}\partial x_{W3}} \\ \dfrac{\partial^2 U_P}{\partial x_{N2}\partial x_{W1}} & \dfrac{\partial^2 U_P}{\partial x_{N2}\partial x_{W2}} & \dfrac{\partial^2 U_P}{\partial x_{N2}\partial x_{W3}} \\ \dfrac{\partial^2 U_P}{\partial x_{N3}\partial x_{W1}} & \dfrac{\partial^2 U_P}{\partial x_{N3}\partial x_{W2}} & \dfrac{\partial^2 U_P}{\partial x_{N3}\partial x_{W3}} \end{bmatrix} \qquad [9.32]$$

Using equations 9.17 and 9.18, the second partial derivatives may be expressed as

$$\left.\begin{aligned}
&\frac{\partial^2 U_P}{\partial x_j \partial x_l} = \frac{\partial^2 U_{Pb}}{\partial x_j \partial x_l} + \frac{\partial^2 U_{Pm}}{\partial x_j \partial x_l} \\
&\frac{\partial^2 U_{Pm}}{\partial x_j \partial x_l} = \frac{\partial^2 U_{nPw}}{\partial x_j \partial x_l} + \frac{\partial^2 U_{nPe}}{\partial x_j \partial x_l} + \frac{\partial^2 U_{sPw}}{\partial x_j \partial x_l} + \frac{\partial^2 U_{sPe}}{\partial x_j \partial x_l} \\
&(x_j, x_l = x_{Wi}, x_{Ni}, x_{Pi}, x_{Si}, x_{Ei}, i = 1, 2, 3)
\end{aligned}\right\} \quad [9.33]$$

The second partial derivatives of the bending strain energy U_{Pb} can be obtained by differentiating equation 9.24 with respect to nodal co-ordinates once more, which leads to

$$\begin{aligned}
&\frac{\partial^2 U_{Pb}}{\partial x_{Pi} \partial x_{Pk}} \\
&= \frac{4 D_1 l_{P2}}{l_{P1}} \left[\frac{1}{(1 - f_{wPe})^2} \frac{\partial^2 f_{wPe}}{\partial x_{Pi} \partial x_{Pk}} + \frac{2}{(1 - f_{wPe})^3} \frac{\partial f_{wPe}}{\partial x_{Pi}} \frac{\partial f_{wPe}}{\partial x_{Pk}} \right] \\
&+ \frac{4 D_2 l_{P1}}{l_{P2}} \left[\frac{1}{(1 - f_{nPs})^2} \frac{\partial^2 f_{nPs}}{\partial x_{Pi} \partial x_{Pk}} + \frac{2}{(1 - f_{nPs})^3} \frac{\partial f_{nPs}}{\partial x_{Pi}} \frac{\partial f_{nPs}}{\partial x_{Pk}} \right]
\end{aligned} \quad [9.34]$$

and

$$\begin{aligned}
&\frac{\partial^2 U_{Pb}}{\partial x_{Wi} \partial x_{Wk}} \\
&= \frac{4 D_1 l_{P2}}{l_{P1}} \left[\frac{1}{(1 - f_{wPe})^2} \frac{\partial^2 f_{wPe}}{\partial x_{wi} \partial x_{Wk}} + \frac{2}{(1 - f_{wPe})^3} \frac{\partial f_{wPe}}{\partial x_{Wi}} \frac{\partial f_{wPe}}{\partial x_{Wk}} \right]
\end{aligned} \quad [9.35]$$

The other four terms $\partial^2 U_{Pb}/\partial x_{Pi} \partial x_{Wk}$, $\partial^2 U_{Pb}/\partial x_{Ei} \partial x_{Wk}$, $\partial^2 U_{Pb}/\partial x_{Ei} \partial x_{Pk}$ and $\partial^2 U_{Pb}/\partial x_{Ei} \partial x_{Ek}$ can be found by appropriate permutations in the subscripts of the nodal co-ordinates on both sides of equation 9.35. Similarly,

$$\begin{aligned}
&\frac{\partial^2 U_{Pb}}{\partial x_{Ni} \partial x_{Ni}} \\
&= \frac{4 D_2 l_{P1}}{l_{P2}} \left[\frac{1}{(1 - f_{nPs})^2} \frac{\partial^2 f_{nPs}}{\partial x_{Ni} \partial x_{Nk}} + \frac{2}{(1 - f_{nPs})^3} \frac{\partial f_{nPs}}{\partial x_{Ni}} \frac{\partial f_{nPs}}{\partial x_{Nk}} \right]
\end{aligned} \quad [9.36]$$

Again, the terms $\partial^2 U_{Pb}/\partial x_{Pi} \partial x_{Nk}$, $\partial^2 U_{Pb}/\partial x_{Si} \partial x_{Nk}$, $\partial^2 U_{Pb}/\partial x_{Si} \partial x_{Pk}$ and $\partial^2 U_{Pb}/\partial x_{Si} \partial x_{Sk}$ can be obtained by permutations in the subscripts on both sides of equation 9.36. The second derivatives of f_{bPa} (*bPa* = *wPs*, *nPs*, *nPw*, *nPe*, *sPw*, *sPe*) can be derived without difficulty. The second derivatives of the in-plane strain energy function U_{bPa} (*bPa* = *nPw*, *nPe*, *sPw*, *sPe*) can also be

obtained by differentiating equation 9.25 once more with respect to the nodal co-ordinates.

9.2.5 Boundary control volumes

In the previous sections, the element internal force vector $\boldsymbol{F}^{\mathrm{e}}$ and the element tangent stiffness matrix $\boldsymbol{K}^{\mathrm{e}}$ for internal control volumes are established. The corresponding matrices for boundary control volumes, such as the edge volume P_1 and the corner volume P_2 as shown in Fig. 9.1, are now derived. For an edge control volume such as the typical volume P_1 in Fig. 9.1, the strain energy U_{P1} only depends on four grid nodes. Therefore, the element internal force vector $\boldsymbol{F}^{\mathrm{e}}$ is a 12×1 vector and the element tangent stiffness matrix $\boldsymbol{K}^{\mathrm{e}}$ is a 12×12 matrix. They are expressed as follows

$$\boldsymbol{F}^{\mathrm{e}} = \left[\frac{\partial U_P}{\partial x_{Ni}} \; \frac{\partial U_P}{\partial x_{Pi}} \; \frac{\partial U_P}{\partial x_{Si}} \; \frac{\partial U_P}{\partial x_{Ei}} \right]^{\mathrm{T}} \qquad [9.37]$$

and

$$\boldsymbol{K}^{\mathrm{e}} = \begin{bmatrix} \dfrac{\partial^2 U_P}{\partial x_{Ni}\partial x_{Nk}} & & & \textit{Sym.} \\ \dfrac{\partial^2 U_P}{\partial x_{Pi}\partial x_{Nk}} & \dfrac{\partial^2 U_P}{\partial x_{Pi}\partial x_{Pk}} & & \\ \dfrac{\partial^2 U_P}{\partial x_{Si}\partial x_{Nk}} & \dfrac{\partial^2 U_P}{\partial x_{Si}\partial x_{Pk}} & \dfrac{\partial^2 U_P}{\partial x_{Si}\partial x_{Sk}} & \\ \dfrac{\partial^2 U_P}{\partial x_{Ei}\partial x_{Nk}} & \dfrac{\partial^2 U_P}{\partial x_{Ei}\partial x_{Pk}} & \dfrac{\partial^2 U_P}{\partial x_{Ei}\partial x_{Sk}} & \dfrac{\partial^2 U_P}{\partial x_{Ei}\partial x_{Ek}} \end{bmatrix} \qquad [9.38]$$

Similarly, for a corner control volume, such as the typical volume P_2 shown in Fig. 9.1, the strain energy U_{P2} depends only on three grid nodes, so $\boldsymbol{F}^{\mathrm{e}}$ is a 9×1 vector and $\boldsymbol{K}^{\mathrm{e}}$ a 9×9 matrix. These are given by

$$\boldsymbol{F}^{\mathrm{e}} = \left[\frac{\partial U_P}{\partial x_{Ni}} \; \frac{\partial U_P}{\partial x_{Pi}} \; \frac{\partial U_P}{\partial x_{Ei}} \right]^{\mathrm{T}} \qquad [9.39]$$

and

$$\boldsymbol{K}^{\mathrm{e}} = \begin{bmatrix} \dfrac{\partial^2 U_P}{\partial x_{Ni}\partial x_{Nk}} & & \textit{Sym.} \\ \dfrac{\partial^2 U_P}{\partial x_{Pi}\partial x_{Nk}} & \dfrac{\partial^2 U_P}{\partial x_{Pi}\partial x_{Pk}} & \\ \dfrac{\partial^2 U_P}{\partial x_{Ei}\partial x_{Nk}} & \dfrac{\partial^2 U_P}{\partial x_{Ei}\partial x_{Pk}} & \dfrac{\partial^2 U_P}{\partial x_{Ei}\partial x_{Ek}} \end{bmatrix} \qquad [9.40]$$

The procedure of derivation for all components in equations 9.37–9.40 is the same as that for internal control volumes as presented in the previous sections.

9.2.6 Solution method for the non-linear equations

9.2.6.1 Existing solution procedures in fabric deformation analysis

A variety of algorithms have been employed for the solution of the non-linear algebraic equations arising from a discretised fabric model. In Breen *et al*.'s work (Breen, 1993; Breen *et al*., 1994) the deformed shapes of square pieces of woven cloth draped over rectangular tables were simulated using a particle-system model. They used a three-phase solution procedure. The first phase accounts for the effect of gravity and the collisions between the cloth and the interacting object. The second phase is an energy minimisation phase in which a stochastic technique is used to reach a local minimum. In the third phase, a stochastic perturbation technique is used to produce a more natural final shape.

Eberhardt *et al*. (1996) used a Runge-Kutta method with adaptive step-size control and the Bulirsch-Stoer method (Press *et al*., 1992) as a numerical solver for the differential equations resulting from the particle-system model. The simulation examples presented include cloth sheets draped over a square table, a circular table and a sphere. Other researchers (Kim, 1991; Chen and Govindaraj, 1995; Gan *et al*., 1995; Kang and Yu, 1995) employed the incremental Newton–Raphson iteration method to solve the non-linear equilibrium equations derived from a finite-element formulation. Their simulation examples include the two-dimensional draping of fabric cantilevers, square cloth sheets draped over cubic objects or circular tables. Deng (1994) and Eischen *et al*. (1996) employed an adaptive arc-length algorithm (Riks, 1979; Schweizerhof and Wriggers, 1986) with an acceleration factor to deal with non-linear effects including material non-linearity and contact. The predicted results of fabric pieces draped over a block, hanging over a round rod, draped over intersecting cylinders were presented.

In the existing literature, little discussion has been found on an appropriate solution procedure for fabric deformation analysis which takes into account the special characteristics of these problems. This issue is considered first below, leading to the choice of the Newton–Raphson method (Crisfield, 1991; Bathe, 1996) in conjunction with the use of the line search technique (Crisfield, 1991). The effectiveness and efficiency of the solution procedure is then investigated, through comparison with the conventional step-by-step incremental iterative Newton–Raphson procedure in a numerical example.

9.2.6.2 Special characteristics of fabric deformation analysis

Fabric deformations generally involve very large displacements, often of the order of hundreds of times the thickness of the fabric sheet. This kind of gross deformation is not encountered in the analysis of load-bearing structures. The only obvious example in non-linear structural mechanics which is closely related to this class of deformations is the elastica problem. There are also some other major differences between a fabric drape deformation analysis and a non-linear analysis of load-bearing structures. First, the aim of a fabric deformation analysis is to determine the final deformed shape under self weight with or without additional applied loading, while in the non-linear analysis of load-bearing structures, the maximum load-carrying capacity and the load-deflection response are of interest. Second, both the displacements and the internal forces need to be carefully determined in the analysis of load-bearing structures, while in a fabric deformation analysis, the final displacements are the only item of interest.

It is easy to see that a step-by-step incremental iterative approach is well suited for the analysis of load-bearing structures, as the load-deflection response can be traced and internal forces and displacements can be computed at different levels of loading. For a fabric deformation analysis, a more direct and efficient approach is clearly desirable as the only information of interest is the final displacements of the cloth sheet.

9.2.6.3 The Newton–Raphson method

Based on the above rationale, the full Newton–Raphson iterative method (Crisfield, 1991; Bathe, 1996) is adopted for the solution of the non-linear equations of the fabric sheet with all the loading applied in a single step, instead of an incremental iterative approach. The solution process using the Newton–Raphson iterative method (Crisfield, 1991; Bathe, 1996) in a single step is described by the following two equations

$$\left.\begin{aligned} \boldsymbol{K}\Delta\boldsymbol{X} &= \boldsymbol{R} - \boldsymbol{F} \\ \boldsymbol{X}^{\text{new}} &= \boldsymbol{X}^{\text{old}} + \Delta\boldsymbol{X} \end{aligned}\right\} \qquad [9.41]$$

where $\boldsymbol{X}$ is the global nodal co-ordinate vector, $\boldsymbol{K}$ is the global tangent stiffness matrix, $\boldsymbol{F}$ is the global nodal internal force vector and $\boldsymbol{R}$ is the global nodal load vector due to gravity and other applied loads if any. Details of the computational steps will be given later.

9.2.6.4 The line search technique

To accelerate the convergence of the Newton–Raphson iterative solution process, the line search technique (Crisfield, 1991) is included in the iterative

solution process. In this technique, the incremental co-ordinate vector $\Delta \boldsymbol{X}$ obtained from the first part of equation 9.41 is now defined as an iterative direction for the actual co-ordinate increment. The co-ordinate vector is then updated using

$$\boldsymbol{X}^{\text{update}} = \boldsymbol{X}^{\text{old}} + \eta \Delta \boldsymbol{X} \qquad [9.42]$$

in which the scalar η is the iterative step length and the only variable for the line-search process. The scalar η can be determined using the linear interpolation method until the defined inner product

$$s(\eta) = \Delta \boldsymbol{X}^{\text{T}}(\boldsymbol{F} - \boldsymbol{R}) \qquad [9.43]$$

is small, i.e. until the following expression is satisfied

$$|s(\eta)| < \beta_{\text{ls}} |s(\eta = 0)| \qquad [9.44]$$

where β_{ls} is the line-search tolerance. In the numerical simulations to be presented later, the line-search technique was employed in the solution process for all-three dimensional cases and was found to be effective. For the two-dimensional draping analysis of fabric cantilevers, this technique was not used as it was not found to be useful.

9.2.6.5 Convergence criterion

A rational and realistic convergence criterion is an essential ingredient of an effective iterative solution procedure. As stated by Bathe (1996), 'if the convergence tolerances are too loose, inaccurate results are obtained, and if the tolerances are too tight, much computational effort is spent to obtain needless accuracy'. A number of convergence criteria have been used in non-linear analysis of load-bearing structures (Bathe, 1996), which may be either displacement-based or load-based. Bearing in mind that the concern in fabric drape deformation analysis is the final deformed shape, the convergence criterion adopted is the iterative change of the position vector at a grid node which is given by

$$\left.\begin{aligned} \beta &= \frac{|\Delta^{\text{new}} - \Delta^{\text{old}}|}{\Delta^{\text{new}}} \leq \beta_{\text{d}} \\ \Delta^{\text{new}} &= (\sqrt{x^2 + y^2 + z^2})^{\text{new}}, \Delta^{\text{old}} = (\sqrt{x^2 + y^2 + z^2})^{\text{old}} \end{aligned}\right\} \qquad [9.45]$$

where β_{d} is the displacement convergence tolerance, x, y and z are the three co-ordinates of the grid node. This criterion has to be satisfied by each grid node before convergence is deemed to have been reached. A value of 10^{-5} has been used and found to be satisfactory in all the numerical simulations presented below.

9.3 References

Ascough J, Bez H E and Bricis A M (1996), A simple finite element model for cloth drape simulation, *Int J Clothing Sci and Tech*, **8**(3), 59–74.

Bailey C and Cross M (1995), A finite volume procedure to solve elastic solid mechanics problems in three dimensions on an unstructured mesh, *Int J Numer Methods Eng*, **38**, 1757–1776.

Bathe K J (1982), *Finite Element Procedures in Engineering Analysis*, New Jersey, Prentice Hall.

Bathe K J (1996), *Finite Element Procedures*, New Jersey, Prentice Hall.

Breen D E (1993), *A Particle-based Model for Simulating the Draping Behaviour of Woven Cloth* (Doctoral dissertation, Rensselaer Polytechnic Inst., New York).

Breen D E, House D H and Getto P H (1991), A particle-based computational model of cloth draping behaviour, in *Scientific Visualization of Physical Phenomena*, Patrikalakis N M (ed), New York, Springer Verlag, 113–134.

Breen D E, House D H and Getto P H (1992), A particle-based particle model of woven cloth, *The Visual Computer*, **8**(5–6), 264–277.

Breen D E, House D H and Wozny M J (1994), A particle-based model for simulating the draping behaviour of woven cloth, *Text. Res J*, **64**(11), 663–685.

Carignan M, Yang Y, Thalmann N M and Thalmann D (1992), Dressing animated synthetic actors with complex deformable clothes, *Computer Graphics* (*Proc. siggraph)*, **26**(2), 99–104.

Chen B and Govindaraj M (1995), A physical based model of fabric drape using flexible shell theory, *Text Res J*, **65**(6), 324–330.

Chen B and Govindaraj M (1996), A parametric study of fabric drape, *Text Res J*, **66**(1), 17–24.

Collier B J (1991), Measurement of fabric drape and its relation to fabric mechanical properties and subjective evaluation, *Clothing & Text Res J*, **10**(1), 46–52.

Crisfield M A (1991), *Non-linear Finite Element Analysis of Solids and Structures, vol.1: Essentials*, Chichester, John Wiley & Sons.

Demirdzic I and Martinovic D (1993), Finite volume method for thermo-elasto-plastic stress analysis, *Comput Methods Appl Mech Eng*, **109**, 331–349.

Demirdzic I and Muzaferija S (1994), Finite volume method for stress analysis in complex domain, *Int J Numer Methods Eng*, **37**, 3751–3766.

Deng S (1994), *Nonlinear Fabric Mechanics Including Material Nonlinearity, Contact, and an Adaptive Global Solution Algorithm* Doctoral Dissertation, (North Carolina State University, Raleigh NC).

Dhande S G, Rao P V M and Moore C L (1993), Geometric modelling of draped fabric surfaces, *Graphics, design and visualization (Proc Int Conf on Computer Graphics)*, Mudur S P and Pattanaik S N (eds), Bombay, Jaico Publishing House, 173–180.

Eberhardt B, Weber A and Strasser W (1996), A fast, flexible particle-system model for cloth draping, *IEEE Computer Graphics and Applications*, **16**(5), 51–59.

Eischen J W, Deng S and Clapp T G (1996), Finite-element modelling and control of flexible fabric parts, *IEEE Computer Graphics and Applications*, **16**(5), 71–80.

Feynman C (1986), *Modelling the Appearance of Cloth*, Master's dissertation, Massachusetts Institute of Technology, Cambridge).

Fryer Y D, Bailey C, Cross M and Lai C H (1991), A control volume procedure for solving the elastic stress-strain equations on an unstructured mesh, *Appl Math Modelling*, **15**(11–12), 639–645.

Gan L, Ly N G and Steven G P (1995), A study of fabric deformation using nonlinear finite elements, *Text Res J*, **65**(11), 660–668.

Hu J L and Teng J G (1996), 'Computational fabric mechanics-present status and future trends', *Finite Element in Analysis and Design*, **21**, 225–237.

Kang T J and Yu W R (1995), Drape simulation of woven fabric by using the finite-element method, *J Text Inst*, **86**(4), 635–648.

Kawabata S (1975), *The Standardization and Analysis of Hand Evaluation*, Osaka, Hand evaluation and standardization committee of the Textile Machinery Society of Japan.

Kim J (1991), *Fabric Mechanics Analysis Using Large Deformation Orthotropic Shell Theory*, Doctoral Dissertation, North Carolina State University, Raleigh, N C).

Lloyd D W (1980), The analysis of complex fabric deformations, in *Mechanics of Flexible Fibre Assemblies (NATO Advanced Study Institute Series; E Appplied Sciences No. 38*), Hearle J W S, Thwaites J J and Amirbayat J (eds), The Netherlands Alpen aan den Rijn, Sijthoff & Noordhoff, 311–342.

Ng H N and Grimsdale R L (1996), Computer graphics techniques for modelling cloth, *IEEE Computer Graphics and Applications*, **16**, 28–41.

Onate E, Cervera M and Zienkiewicz O C (1994), Finite volume format for structural mechanics, *Int J Numer Methods Eng*, **37**(2), 181–201.

Patankar S V (1980), *Numerical Heat Transfer and Fluid Flow*, New York, Hemisphere Publishing Corporation.

Press W H, Flannery B P, Teukolsky S A and Vetterling W T (1992), *Numerical Recipes in C: The Art of Scientific Computing, 2nd edition*, New York, Cambridge University Press.

Riks E (1979), An acceleration approach to the solution of snapping and buckling problem, *Int J Solids Struc*, **15**, 524–551.

Schnobrich W C and Pecknold D A (1973), The lumped-parameter or bar-node model approach to thin shell analysis, numerical and computer methods, in *Structural Mechanics*, Perrone F and Schnobrich R (eds), London, Academic Press, 337–402.

Schweizerhof K H and Wriggers P (1986), Consistent linearization of path following methods in nonlinear FE analysis, *Comput Methods Appl Mech Eng*, **72**, 267–304.

Simo J C and Fox D D (1989), On a stress resultant geometrically exact shell model part I: formulation and parameterization, *Comp Methods Appl Mech Eng*, **72**, 267–304.

Simo J C and Fox D D and Rifai M S (1989), On a stress resultant geometrically exact shell model part II: the linear theory; computational aspects, *Comp Methods Appl Mech Eng*, **73**, 53–92.

Simo J C, Fox D D and Rifai M S (1990), On a stress resultant geometrically exact shell model, Part III, Aspects of nonlinear theory, *Comp Methods Appl Mech Eng*, **79**, 21–70.

Stylios G K, Wan T R and Powell N J (1995), Modelling the dynamic drape of fabrics on synthetic humans, a physical, lumped-parameter model, *Int J Clothing Sci and Tech*, **7**(5), 10–25.

Stylios G K, Wan T R and Powell N J (1996), Modelling the dynamic drape of garments on synthetic humans in a virtual fashion show, *Int J Clothing Sci and Tech*, **8**(3), 95–112.

Terzopoulos D, Platt J, Barr A and Fleischer K (1987), Elastically deformable models, *Computer Graphics*, **21**(4), 205–214.

Thalmann N M and Thalmann D (1991), Cloth animation with self-collision detection, in *Modelling in Computer Graphics*, Kunii T L (ed), Berlin, Springer-Verlag, 179–187.

Thalmann N M and Yang Y (1991), Techniques for cloth animation, in *New Trends in Animation and Visualization*, Thalmann N M and Thalmann D (eds), Chichester, John Wiley & Sons, 243–256.

Versteeg H K and Malalasekera W (1995), *An Introduction to Computational Fluid Dynamics, the Finite Volume Method*, Harlow, Longman Scientific & Technical.

Weil J (1986), The synthesis of cloth object, *Computer Graphics (Proc Siggraph)*, **20**(4), 49–54.

Wheel M A (1996), Finite volume approach to the stress analysis of pressurized axisymmetric structures, *Int J Pressure Vessels Piping*, **68**(3), 311–317.

Wheel M A (1997), A finite volume method for analyzing the bending deformation of thick and thin plates, *Comp Methods Appl Mech Eng*, **147**, 199–208.

Yu W R, Kang T J and Lee J K (1993), Drape properties of woven fabrics, *Proc 2nd Asian Textile Conf*, **1**, South Korea, 20 Oct, 455–459.

10

Modelling drape deformation of woven fabrics and garments – computation and simulation

10.1 Introduction

Due to its inherent extreme thinness and high flexibility, the drape deformation of a fabric sheet usually involves only very small strains even under very large deflections; most of these come from bending and only a small amount is due to in-plane stretching. As a result, a fabric sheet can still retain its original surface area and volume after drape deformation. For this reason, the finite-volume method is reasonably appropriate for simulating fabric drape deformation. In Chapter 9, the theoretical analysis of this method was developed, and in this chapter a detailed computational evaluation of the model is reported whereby its predictability and accuracy can be confirmed. In addition, a B-spline method is used to map fabric texture and colours to a three-dimensional draped garment.

10.2 Computation

The analysis starts with an initially flat fabric sheet which has been discretised into r control volumes. For a three-dimensional problem, the unknown vector $\boldsymbol{X}$ in equation 9.14 contains $3r$ co-ordinate vector components, i.e. the degrees of freedom of the problem are $3r$. The computational procedure including the line-search technique for a three-dimensional problem is as follows:

(1) Set up the initial grid and calculate the initial three-dimensional co-ordinates of all grid nodes.
(2) Calculate the nodal forces due to gravity and external loading (if any) and form the total load vector $\boldsymbol{R}$.
(3) Begin iterative loops: steps (4)–(14).
(4) Check if the grid node to be dealt with is an internal node or a boundary node.
(5) Form the element internal force vector, with appropriate different treatments for internal and boundary grid nodes.

(6) Form the element tangent stiffness matrix, with appropriate different treatments for internal and boundary grid nodes.
(7) Form the global internal force vector $\boldsymbol{F}$, the global tangent stiffness matrix $\boldsymbol{K}$ and the out-of-balance force vector $\boldsymbol{G} = \boldsymbol{F} - \boldsymbol{R}$.
(8) Calculate the old position vector at each grid node Δ^{old}.
(9) Impose the boundary conditions.
(10) Apply Crout factorisation to the tangent stiffness matrix $\boldsymbol{K}$ and then solve the first part of equation (9.14) to obtain the incremental co-ordinate vector $\Delta\boldsymbol{X}$.
(11) Compute the new co-ordinate vector $\boldsymbol{X}^{\text{new}} = \boldsymbol{X}^{\text{old}} + \Delta\boldsymbol{X}$.
(12) If necessary, carry out line searches to obtain an iterative step length η and then the updated co-ordinate vector $\boldsymbol{X}^{\text{update}} = \boldsymbol{X}^{\text{old}} + \eta\Delta\boldsymbol{X}$, otherwise go to step (13). The line search procedure (Crisfield, 1997) is as follows:

(i) Compute $s_0 = s(\eta = 0) = \Delta\boldsymbol{X}^{\text{T}}(\boldsymbol{F}^{\text{old}} - \boldsymbol{R})$. If it is positive, set $\eta = 1$ and go to step (13).
(ii) Set $\eta^{(1)} = 0$, $\eta^{(2)} = 1$ and $\eta = \eta^{(2)}$.
(iii) Compute $s(\eta) = \Delta\boldsymbol{X}^{\text{T}}(\boldsymbol{F} - \boldsymbol{R}) = \Delta\boldsymbol{X}^{\text{T}}g(\eta)$.
(iv) Check if the equation $|r_{\text{ls}}| = |s(\eta)/s_0| < \beta_{\text{ls}}$ is satisfied or the maximum or minimum allowed step length has been reached twice. If either condition is met, go to step (13).
(v) Find the step length η_- which is the minimum of all previously obtained step lengths with a negative ratio $r_{\text{ls}-}$. If such a step length does not exist, go to step (viii).
(vi) Find the step length η_+ which is the maximum of all previous step lengths with a positive ratio $r_{\text{ls}+}$ and is at the same time smaller than η_-
(vii) Calculate the new step length using the following linear interpolation:

$$\eta = \frac{r_{\text{ls}-} \cdot \eta_+ - r_{\text{ls}+} \cdot \eta_-}{r_{\text{ls}-} - r_{\text{ls}+}}$$

(viii) If the calculated step length $\eta > \eta_+ + 0.2(\eta_- - \eta_+)$, set $\eta = \eta_+ + 0.2(\eta_- - \eta_+)$ and go to step (x).
(ix) Calculate the new step length using a linear extrapolation between the current and previous step lengths.
(x) If the step length from (viii) $\eta > \alpha_{\text{ls}}\eta_{\text{maxp}}$, set $\eta = \alpha_{\text{ls}}\eta_{\text{maxp}}$, where α_{ls} is a predefined maximum amplification factor and η_{maxp} is the maximum of all previous step lengths.
(xi) Calculate the updated co-ordinate vector $\boldsymbol{X}^{\text{update}} = \boldsymbol{X}^{\text{old}} + \eta\Delta\boldsymbol{X}$.
(xii) If the maximum number of line searches has not been reached, return to step (iii), otherwise go to step (13).

(13) Calculate the updated position vector at each grid node Δ^{update}.

(14) Convergence is checked by evaluating the iterative change of the position vector at each grid node using equation 9.22. If $\beta \leq \beta_d$ is satisfied at all grid nodes, convergence is deemed to have been achieved; otherwise more iterations need to be carried out.

(15) If convergence has not been achieved and the maximum number of iterations specified at the beginning of the problem has not been reached, return to step (4), otherwise stop.

10.3 Two-dimensional drape simulations

10.3.1 Cantilever cloth strips

Numerical simulations using two-dimensional drape deformations of cloth cantilever strips are presented first. The simulations are for two cloth strips made of the same wool fabric, with their long directions along either the warp or the weft directions. These cloth strips have been experimentally studied before (Kang and Yu, 1995) where their mechanical properties were determined using the KES tester (Kawabata, 1975). The Poisson's ratio is assumed to be zero in the present study here and in all subsequent calculations. Both cloth strips are 5 cm long and 1 cm wide. A mesh with 56 grid nodes (or control volumes) was used in the simulations (Fig. 10.1a). The numerical results for fabric cantilevers were obtained using the full Newton–Raphson method without line searches as they were found not to be very useful for these cases.

10.3.2 Deformed shapes

The predicted deflected shapes and the corresponding experimental data (Kang and Yu, 1995) for the two strips are shown in Fig. 10.1b A close match in the draped shapes is evident.

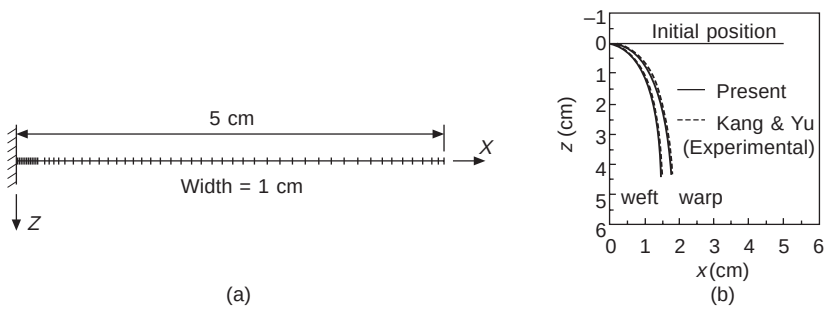

10.1 Fabric cantilevers: (a) geometry and mesh; (b) deflection curves.

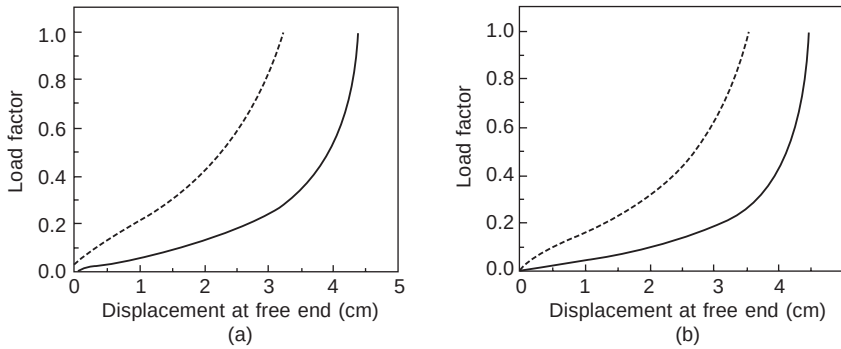

10.2 Load–displacement curves of fabric cantilevers: (a) warp direction; (b) weft direction. (Solid line = vertical displacement (w); dotted line = horizontal displacement ($-u$).)

10.3.3 Load–displacement curves

As discussed earlier, in conventional non-linear finite-element analysis of load-bearing structures, the step-by-step incremental approach is widely employed for solving the non-linear algebraic equations. As this method has also been popular in finite-element modelling of fabric deformations, it is of interest to examine the relative efficiency of the single-step full Newton–Raphson method adopted here and the incremental iterative method.

In the incremental iterative approach, the self weight of the fabric is seen as external loading and is applied to the fabric strip step-by-step. Figure 10.2 shows the load–displacement curves of the free end of the two fabric cantilevers obtained using a 50-step incremental iterative procedure, where the vertical axis represents the load factor with the self weight as the reference load. The calculated final deflection curves for the fabric strips are identical to those presented in Fig. 10.1b. The required computer time on a Pentium® II/266 personal computer for each simulation without line searches is listed as follows:

- 50-step: warp direction 8.35 seconds and weft direction 5.77 seconds;
- single-step: warp direction 0.39 seconds and weft direction 0.38 seconds.

Although variations in the control parameters of the incremental solution procedure may make it more efficient, the large difference in computer time makes it clear that the method adopted here is more efficient.

In all previous finite-element simulations of drape deformations, even though the step-by-step solution procedure was used, the load–displacement curves were seldom plotted. This is understandable since the result which is of practical interest is the final deformed shape. However, the shape of a load–displacement curve has much bearing on the success of a particular incremental solution procedure, so beneficial insight may be gained by plotting

some load–displacement curves. It was necessary to plot the load–displacement curves of the wool cantilevers here in order to explain the inefficiency of the 50-step approach. These load–displacement curves are of a geometrically stiffening type. Similar curves have been obtained for three-dimensional draping of fabrics by Kim (1991). This kind of curve is believed to be typical of fabric drape deformations as fabric sheets transform themselves from a bending deformation-dominant structure into a stretching deformation-dominant membrane during the draping process. The behaviour is highly non-linear in the initial stage of loading and then becomes more linear as deformations progress. A great deal of computer time may thus be consumed in tracing the early part of the load–displacement curve in a step-by-step solution process, although information on this part of the deformation is of no practical value in real fabric drape simulations. The single-step approach is thus more rational and efficient.

There may be concern that the single-step procedure could lead to a different final state from that determined by a step-by-step solution process if the solution is non-unique. A number of the problems studied below were checked by running the analysis using a step-by-step solution procedure and the same final shape was reached.

10.3.4 Convergence of the grid scheme

So far, the issue of convergence of the solution as the grid is refined has not been mentioned. This is considered here for the wool cantilever strip bent in the warp direction. The results are given in Table 10.1, where solutions in terms of the free end displacements are compared for different uniform discretisation schemes. It is seen that a coarse grid leads to a softer structure, and the solution converges towards the exact solution as more grid nodes are employed. Compared to the rate of convergence of a uniform grid, a non-

Table 10.1 Displacements at the free end of a fabric cantilever (warp-direction)

Uniform grid	**Horizontal displacement $-u$ (cm)**	**Vertical displacement w (cm)**
5×1	3.6132	4.6698
10×1	3.4798	4.5551
20×1	3.3763	4.4671
40×1	3.3100	4.4109
80×1	3.2825	4.3791
160×1	3.2527	4.3623
320×1	3.2270	4.3537
Non-uniform grid 56×1	3.2437	4.3552
Non-uniform grid 112×1	3.2395	4.3506

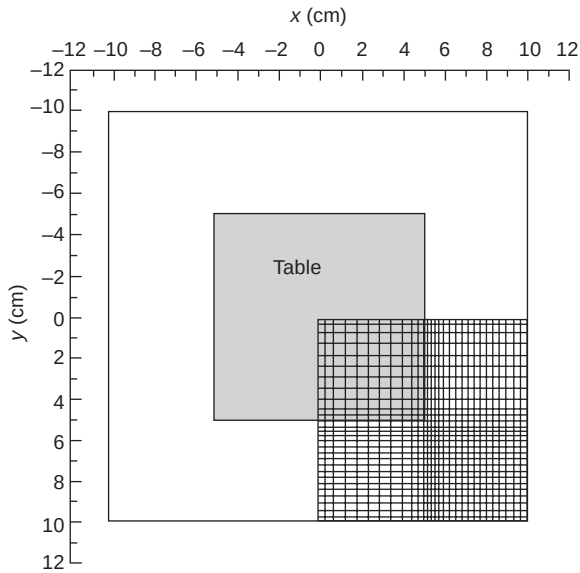

10.3 A non-uniform grid scheme for a square fabric sheet draped over a square table.

uniform grid as employed above (Fig. 10.3) proves to be much more effective for this problem. Doubling the grid density of the non-uniform grid employed above (56×1) leads to few differences (Table 10.1), indicating that the results from the 56×1 grid are accurate. The issue of grid convergence is not further discussed in this section, but all the grid schemes employed for the examples in this section are good enough to give accurate predictions.

10.4 Three-dimensional drape simulations

10.4.1 General

In this section, a number of three-dimensional drape simulations are presented. They are all initially flat and have a square undeformed shape. All numerical simulations were carried out on a Pentium® II/266 personal computer.

10.4.2 Square fabric sheet concentrically draped over a square table

The case of a square fabric sheet with a width of 20 cm concentrically draped over a 10 cm $\times$ 10 cm square table is considered here. Since both the geometry and the material properties are doubly symmetric about the axes of symmetry, only a quarter of the fabric sheet was modelled in the numerical analysis. Figure 10.4 shows the mesh used which features a non-uniform grid of

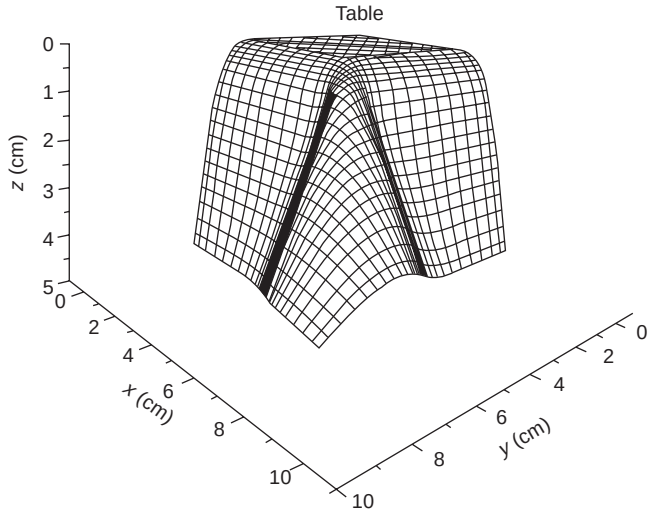

10.4 Shape of a fabric sheet draped over a square table.

31 × 31 nodes (or control volumes) adopted for the numerical simulation. The grid was finer near the edges of the table to cater for the more complex deformations here. The nodes which are in contact with the table were fixed in all directions.

Figure 10.4 shows the three-dimensional draped shape of the fabric sheet, while Fig. 10.5 shows its projection onto the horizontal (or *x*–*y*) plane. The

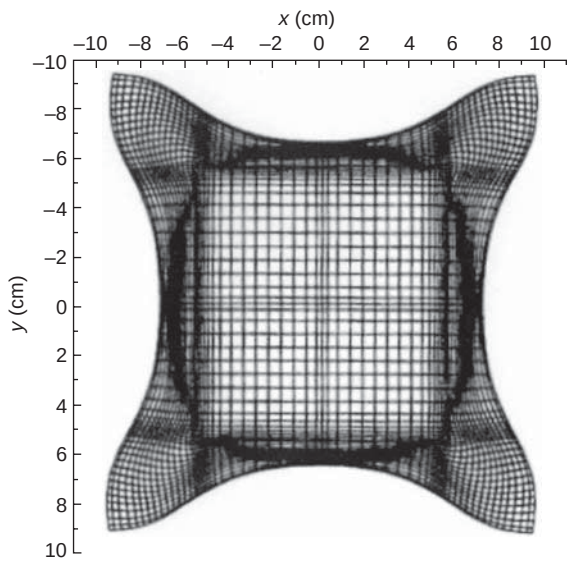

10.5 Horizontal projection of a fabric sheet draped over a square table.

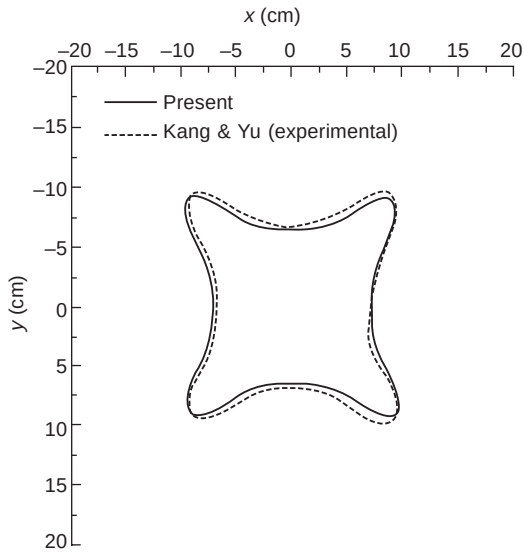

10.6 Draped shape of a fabric sheet: comparison between theoretical prediction and experiment.

projected image is compared in Fig. 10.6 with the experimental measurements given by Dhande *et al*. (1993). It is clear from Fig. 10.6 that the predicted draped shape matches the experimental result quite well. This further demonstrates the validity of the proposed method.

It has been found that previous authors often gave qualitative information (e.g. the appearance of the draped cloth sheet) rather than precise quantitative information when carrying out comparisons or presenting results. This makes precise numerical comparisons difficult, although such comparisons are important in verifying numerical results. Table 10.2 thus provides the final co-ordinates of the nodal points located on the two edges of the quarter model of the wool fabric sheet. These results should be useful as benchmark results for comparisons with predictions from other numerical methods.

10.4.3 Square fabric sheet eccentrically draped over a square table

To evaluate the model, a 15 cm × 15 cm fabric sheet eccentrically draped over the corner of a square table was also analysed. The area of the table corner in contact with the cloth is 7.5 cm × 7.5 cm and a non-uniform grid was adopted for the initially flat fabric sheet (Fig. 10.7). Again, the portion of the fabric sheet lying on the table was prescribed to have no displacements during the deformations. The predicted three-dimensional deformed shape using a 31 × 31 grid is given in Fig. 10.8.

Table 10.2 Co-ordinates of edge points on the wool fabric sheet before and after deformations

Point No.	Initial co-ordinates ($z = 0$)		Co-ordinates after deformations		
	x	***y***	***x***	***y***	***z***
1	0.0	10.0	0.0000	6.5289	4.5662
2	2.5	10.0	2.4892	6.7319	4.5169
3	5.0	10.0	4.8289	7.5258	4.2028
4	7.5	10.0	6.9641	8.7134	3.6763
5	10.0	10.0	9.3813	9.2186	3.6625
6	10.0	7.5	9.3281	6.8742	3.0236
7	10.0	5.0	8.2324	4.7471	3.7170
8	10.0	2.5	7.3465	2.4851	4.2436
9	10.0	0.0	7.1206	0.0000	4.3385

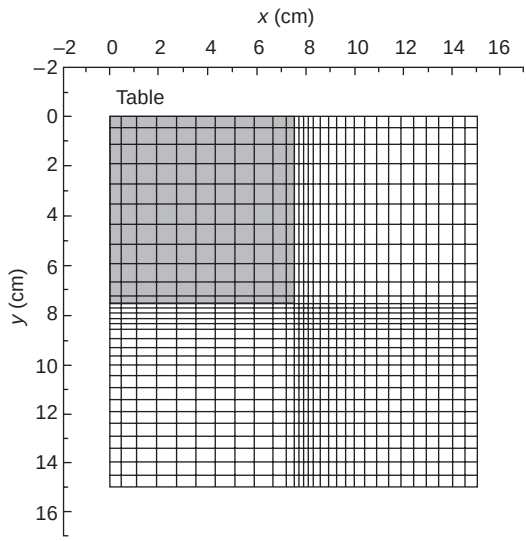

10.7 A non-uniform grid scheme for a fabric sheet eccentrically draped over a table.

10.4.4 Square fabric sheet supported at two diagonal corners

A numerical simulation was also carried out for the drape deformations of an initially flat square fabric sheet 15 cm × 15 cm in size fixed at two diagonal corners. A uniform grid scheme of 41 × 41 nodes was used in the simulation. The final draped shape predicted is shown in Fig. 10.9.

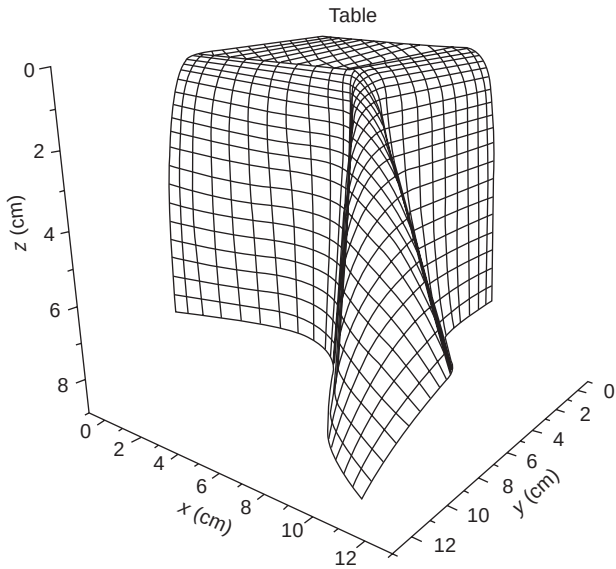

10.8 Shape of a fabric sheet eccentrically draped over a table.

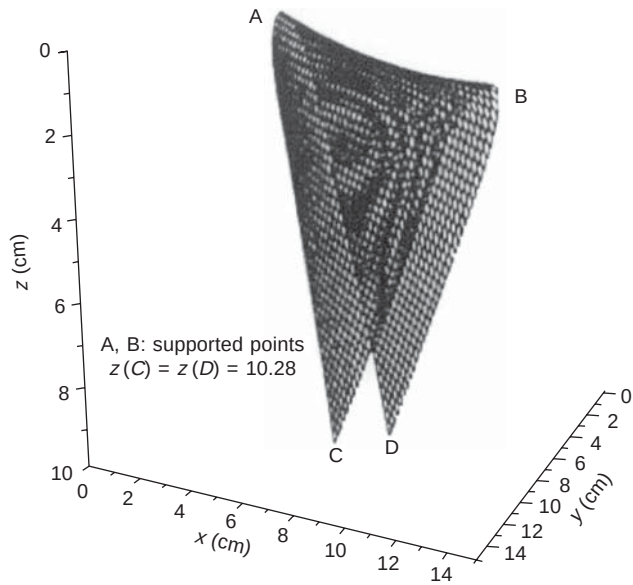

10.9 Draped shape of a fabric sheet supported at diagonal corners.

10.5 Fabric buckling simulation

Wrinkles often appear in cloth products in daily use. The phenomenon of wrinkle formation is one of buckling and post-buckling deformations in

terms of structural mechanics. Wrinkles appear easily because fabric sheets are very flexible in bending and can easily buckle when compressive stresses arise. It is therefore of interest to examine the ability of the model to simulate buckling and post-buckling deformations in fabric sheets.

Suppose that a square fabric piece is placed on a flat surface and a pair of pulling forces is exerted in the plane of the fabric surface on the two diagonal corners, one may be able to intuitively expect that out-of-plane deformations will arise. This kind of deformation can also be confirmed using simple experiments. The reason for the appearance of out-of-plane deformations is the non-uniformity of the applied stretching, which leads to compressive membrane stresses in the perpendicular direction. Consequently, wrinkles will appear unless the applied forces are very small. The following numerical simulations were conducted to capture this type of post-buckling deformation phenomenon.

The fabric considered here is a pure wool fabric with the properties of wool material. The fabric sheet is 15 cm $\times$ 15 cm, modelled by a 31 $\times$ 31 grid. As the fabric sheet is assumed to be lying on a table, the gravitational forces were assumed to be balanced by reactions from the table and were neglected in the analyses. The top left corner was prevented from any in-plane displacements and the top right corner was prevented from any horizontal displacement. These in-plane restraints were specified to avoid rigid body motions. In addition, the fabric sheet was supported vertically around its edge. The applied pulling force is 50 gf (1 gf = 0.0098 N).

Under these idealised conditions, the problem is a typical plane-stress problem and the model can predict only in-plane deformations (Fig. 10.10). However, it is recognised that the equilibrium state predicted by the model is not a stable one if the applied force is sufficiently large, and there exist other more stable equilibrium positions as discussed above.

In order to find the more stable post-buckling state, a small perturbation force was applied to the fabric sheet during the simulation. The perturbation force used was a small concentrated force at the centre of the fabric sheet in the negative direction of the z co-ordinate (upwards). Interestingly, different deformation modes were obtained depending on the amount of perturbation force (Fig. 10.11). When the perturbation force Q_p is below 7.795×10^{-5} gf, the deformed shape assumes a wavy pattern (Fig. 10.11a). With a slightly higher perturbation force ($Q_p = 7.800 \times 10^{-5}$ gf), the deformed shape assumes a roughly asymmetric shape about the stretched diagonal, featuring one major crest and one major trough. As the perturbation force is increased further, this asymmetric pattern gradually transforms into a roughly symmetric pattern (Figs 10.11c–h). The deformed shape is close to symmetric when the perturbation force is greater than 0.5 gf and features a single major crest.

These deformed shapes deserve further investigation and verification from other researchers in the future. In particular, the shape shown in Fig. 10.11a

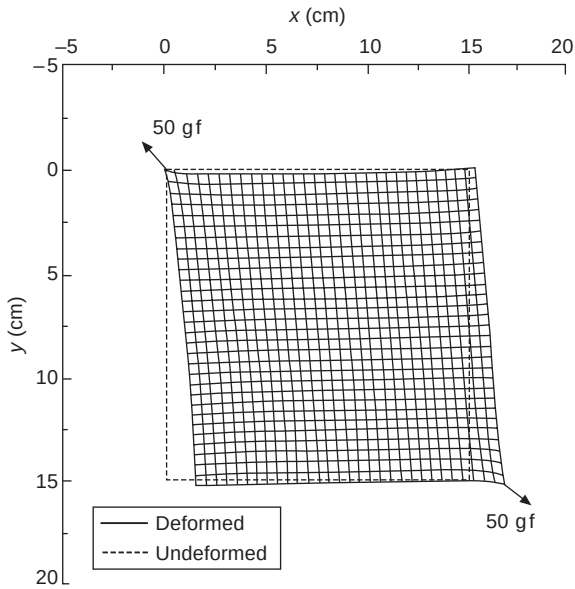

10.10 In-plane deformations of a fabric sheet under diagonal tension.

is difficult to produce by doing a simple experiment with a piece of cloth on a table. The shapes shown in Figs 10.11b–h appear to be obtainable in a simple experiment by appropriately perturbing the fabric cloth so that it is guided into the appropriate mode. These shapes (Figs 10.11b–h) have a clear load-path across the loaded diagonal and appear to be stable. The first mode shown in Fig. 10.11a may be one which needs such a small disturbance that it cannot be achieved in a simple experiment, although more elaborate experiments may prove otherwise. In addition, the conditions assumed in the numerical simulations are not exactly the same as those of a fabric sheet resting on a table under diagonal pulling. Explanations aside, these different modes do show that fabric deformations may be dependent on small perturbations.

10.6 Circular fabric sheets over circular pedestals

Numerical simulation of two circular sheets of different sizes made of two different fabrics (fabric A and fabric B) are presented in this section. The Poisson's ratio is taken as zero for both fabrics in the simulations.

10.6.1 Drape behaviour of a circular fabric sheet A

The circular fabric sheet made of fabric A is referred to as fabric sheet A and is considered first. The radius of the sheet is 12.7 cm, and that of the supporting

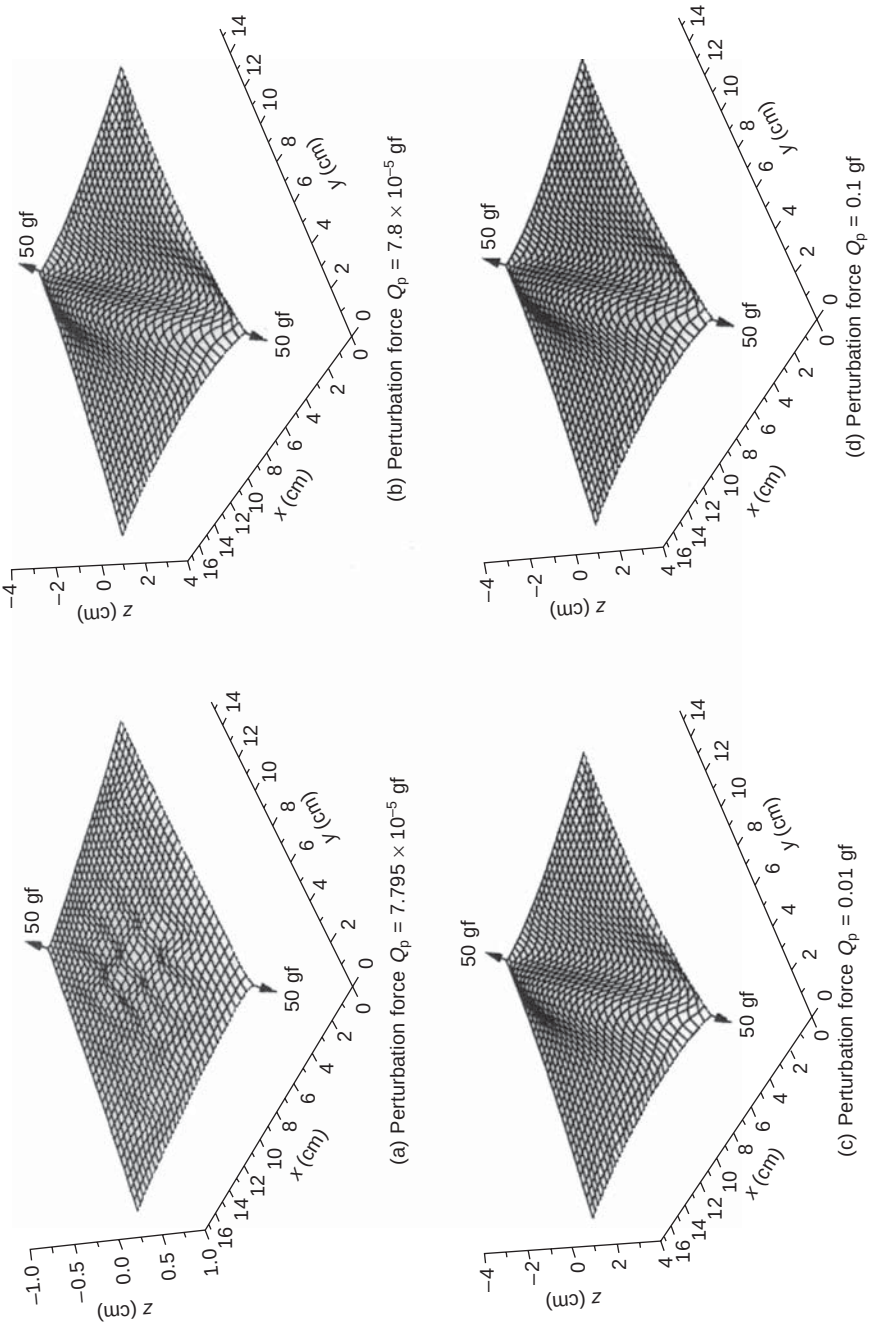

10.11 (a–h) Out-of-plane deformations of a fabric sheet under diagonal tension.

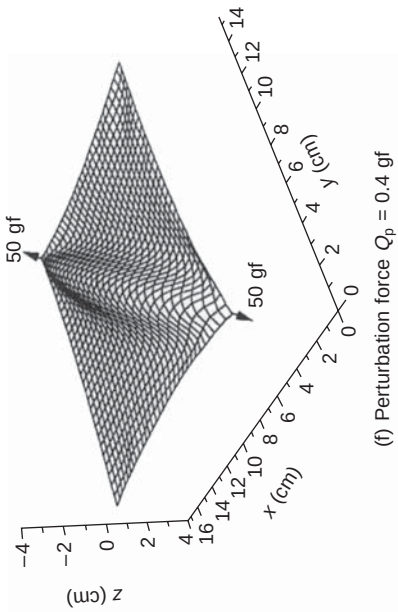

(e) Perturbation force $Q_p = 0.3$ gf

(f) Perturbation force $Q_p = 0.4$ gf

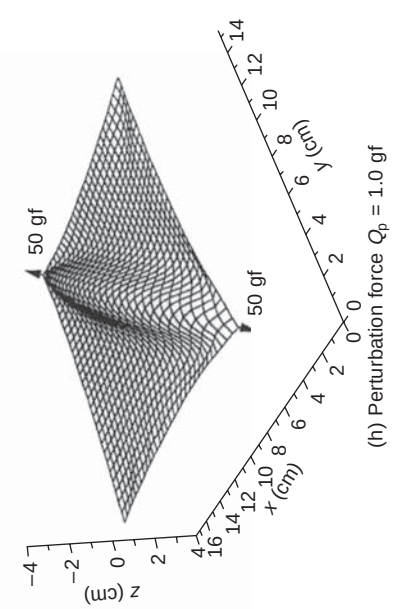

(g) Perturbation force $Q_p = 0.5$ gf

(h) Perturbation force $Q_p = 1.0$ gf

10.11 (cont.)

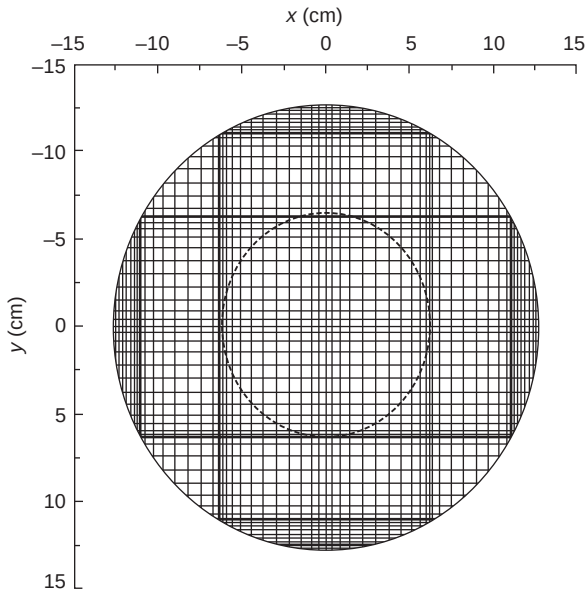

10.12 A grid scheme for fabric sheet A.

pedestal is 6.35 cm. A 65×65 non-uniform grid with 2365 nodes (or control volumes) was used in the simulation when the entire sheet was modelled. The grid is symmetric about the *x*- and *y*-axes, as shown in Fig. 10.12. The grid nodes which are in contact with the rigid pedestal were fixed in all directions.

Since both the geometry and the fabric material properties are doubly symmetric about the *x*- and *y*- (or warp and weft) axes, the deformed shape is expected to be doubly symmetric under fully idealised conditions (i.e. without any perturbation or initial imperfections). Consequently, a quarter section of the fabric sheet was first modelled with symmetric boundary conditions imposed along the two axes of symmetry. The same grid divisions as those used for a whole sheet model were adopted for the quarter section model, with a 33×33 grid. The drape shape predicted using this model features four curved folds (Fig. 10.13). It should be noted that Fig. 10.13, as well as all other figures, shows only the vertical projections of the drape shapes. It is believed that vertical projections can best illustrate the drape patterns, at least in terms of the number of waves and the degree of symmetry. Kang and Yu (1995) studied the same problem using the finite-element method, also employing a quarter section model. Their simulated deformed shapes together with their experimental shapes, both with four folds, are shown in Fig. 10.14 for comparison with the theoretical prediction.

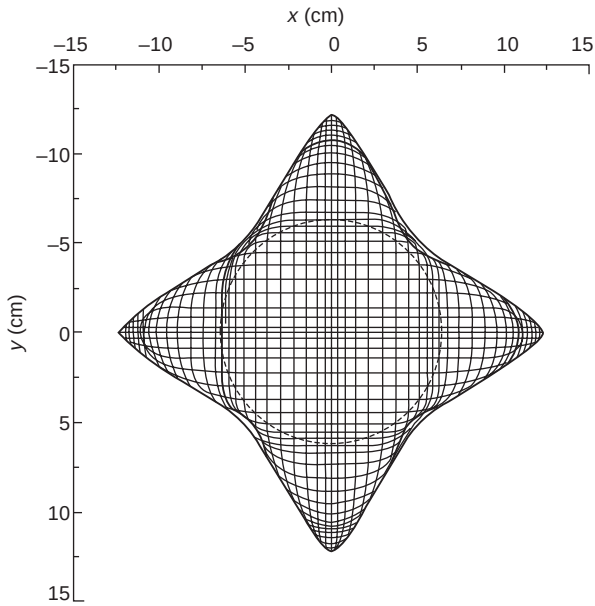

10.13 Doubly symmetric drape pattern of fabric sheet A.

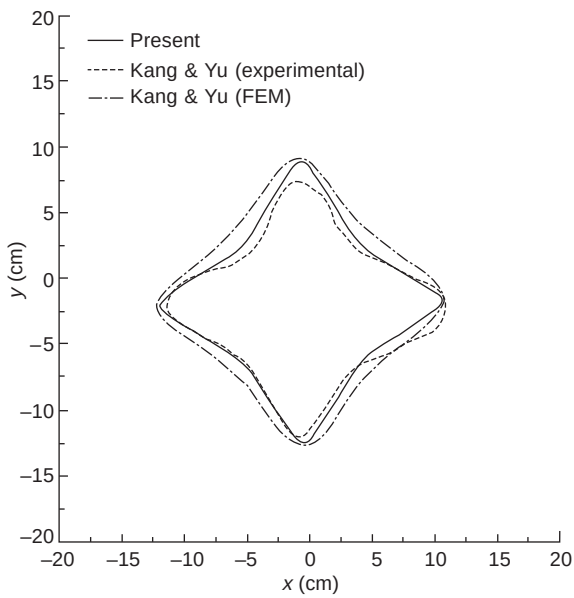

10.14 Comparison of doubly symmetric drape patterns of fabric sheet A.

It is clear from Fig. 10.14 that the present model presents a better fit with the experimental curve than that of Kang and Yu (1995). The simulated shape by Kang and Yu is too stiff as compared with the experimental shape. In addition, no other drape patterns were predicted or discussed in their study.

It is well known from simple experiments or daily experiences that the drape results of circular fabric sheets over circular pedestals are sensitive to any small perturbations or initial imperfections/deviations. Different drape patterns may appear in repeated experiments using the same fabric sheet on the same supporting pedestal. Studies on the buckling of thin shells show that the buckling and post-buckling deformations of shells are sensitive to initial imperfections and disturbances (Teng, 1996). As the drape deformations of circular fabric sheets are those of post-buckling deformations, it is expected that the final deformed pattern is sensitive to small perturbations or initial imperfections. This possibility has been briefly explored by Chen and Govindranaj (1995) for a tensioned square fabric sheet. The effect of small disturbances on the drape pattern of a circular fabric sheet is studied here in order to explain the multiplicity of drape patterns observed in experiments.

When the quarter section model was used, the doubly symmetric deformation pattern (Fig. 10.15) was ensured by imposing appropriate constraints along the axes of symmetry. When the whole fabric sheet was modelled using a 65×65 grid, the predicted drape pattern (Fig. 10.15a) featured six curved folds rather than four, and was asymmetrical about the original axes of symmetry. This asymmetric shape was obtained without applying any disturbance to destroy the double symmetry of the problem. This may appear surprising at first, but it should be realised that, although a bifurcation analysis was not carried out, the fabric sheet can deform into an asymmetrical shape through perturbations from numerical approximation and roundoff errors. The asymmetric drape is thus predicted to be the preferred shape if the sheet is not constrained during the deformation process.

So far two different drape patterns have been predicted for this fabric sheet without adding external perturbations. In order to find out whether other drape patterns exist for it, a small perturbation force was then applied to the fabric sheet during the simulation. The perturbation force used is a small concentrated force in the positive x-direction, applied at the point with the following initial co-ordinates: $x = 2.7$ cm and $y = 0$. Figures 10.15b–e show the drape patterns predicted with perturbation forces of different magnitudes. When the perturbation force is sufficiently small ($Q_p = 5 \times 10^{-5}$ gf), the drape shape retains the six-fold pattern (Fig. 10.15b). However, when Q_p reaches 1×10^{-4} gf or higher, the fabric sheet exhibits other drape patterns all with seven curved folds (Figs 10.15c–e). Drape patterns with seven curved folds appear to be more stable than other patterns since an increase in the perturbation force from 1×10^{-4} gf to 0.01 gf cannot change the number of folds.

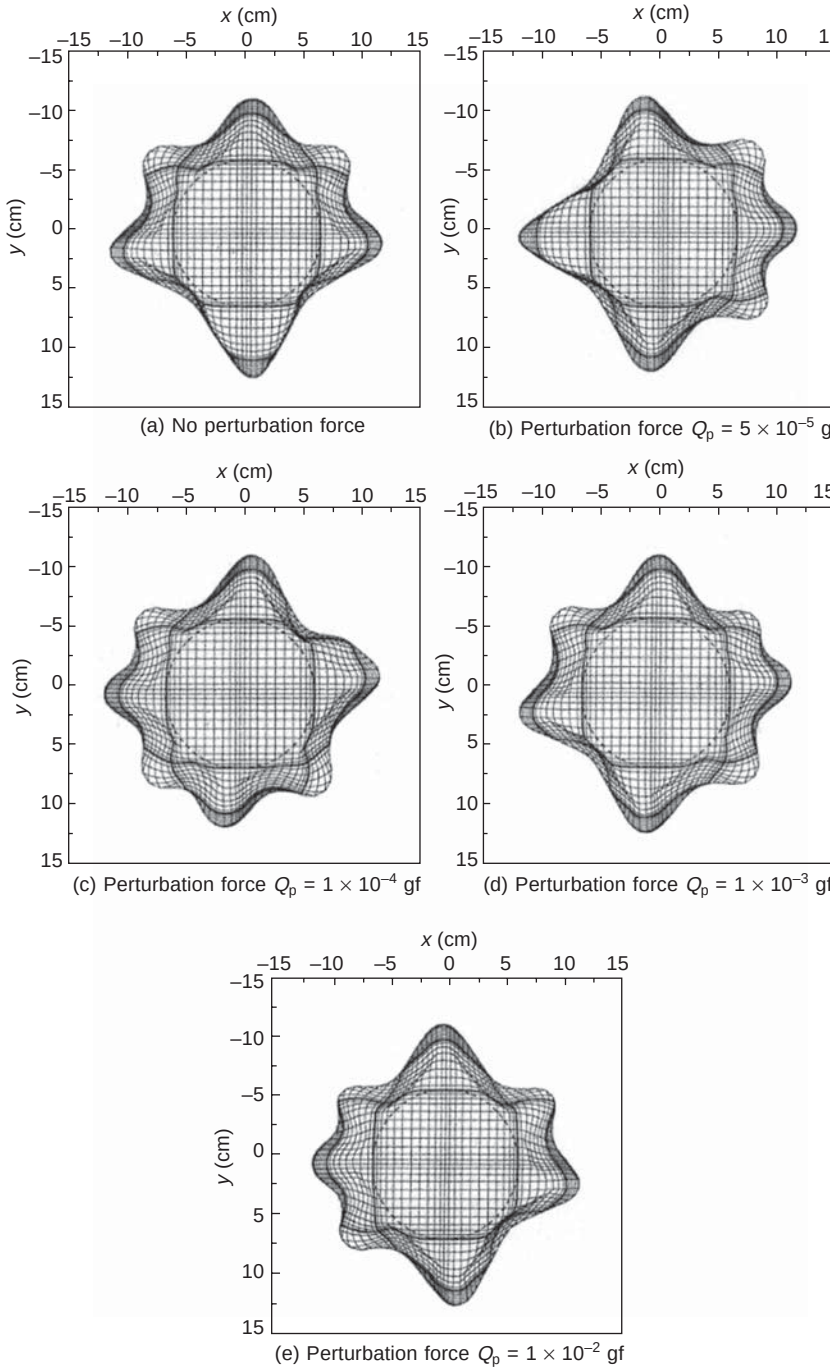

10.15 Drape pattern of fabric sheet A with a horizontal perturbation force.

10.6.2 Drape behaviour of a circular fabric sheet B

The sheet made of fabric B, referred to as fabric sheet B, has a radius of 15 cm and is supported by a pedestal of radius 9 cm. When the whole fabric sheet was modelled, a 69×69 division grid with 2649 nodes was adopted. The simulation procedure is similar to that for fabric sheet A discussed above. Figures 10.16a–e show the drape patterns predicted with a horizontal perturbation force of different magnitudes in the positive x-direction. The concentrated perturbation force was applied at the point with initial co-ordinates $x = 15$ cm and $y = 0$.

When the whole fabric surface was used in the simulation without a perturbation force, the deformed pattern was predicted to be unsymmetrical with nine folds instead (Fig. 10.16a). A similar deformed pattern with nine folds was found when a horizontal perturbation force $Q_p = 5 \times 10^{-5}$ gf was applied (Fig. 10.16b). Moreover, when Q_p reaches 1×10^{-4} gf, ten folds are present in the drape pattern (Fig. 10.16c). When $Q_p = 1 \times 10^{-3}$ gf, the deformed shape exhibits a different nine-fold pattern (Fig. 10.16d). When a relatively high Q_p of 1×10^{-2} gf was applied, the deformed shape returns to an eight-fold pattern (Fig. 10.16e) which is much closer to the doubly symmetric pattern.

The drape patterns of the fabric sheet B are seen to have eight to ten curved folds (Fig. 10.16), with nine-fold patterns appearing more often than others. With a relatively high perturbation force, the drape shape usually features eight folds, and the chance of seeing a ten-fold pattern is relatively small. Gan *et al*. (1995) studied the same fabric drape problem using the finite-element method and predicted an eight-fold drape pattern only for this fabric sheet. They also pointed out that in experiments the drape pattern of this fabric sheet had six to eight folds. This experimental observation does not match the numerical results presented above. This does not mean, however, that the numerical approach is flawed in any sense, as the discrepancy could have been caused by some or all of the many possible factors including deviations in shape, material properties and experimental conditions from those assumed in the analysis. The important fact that has been demonstrated is that small disturbances can change the drape patterns significantly.

10.7 Contact drape simulation of woven fabrics and garments

10.7.1 Contact determination algorithm

The two main methods adopted for the treatment of contact problems in non-linear finite-element analysis are the penalty method and the Lagrangian multiplier method (Crisfield, 1997). The penalty method is closely related to techniques which attempt to introduce a high stiffness for the contact region.

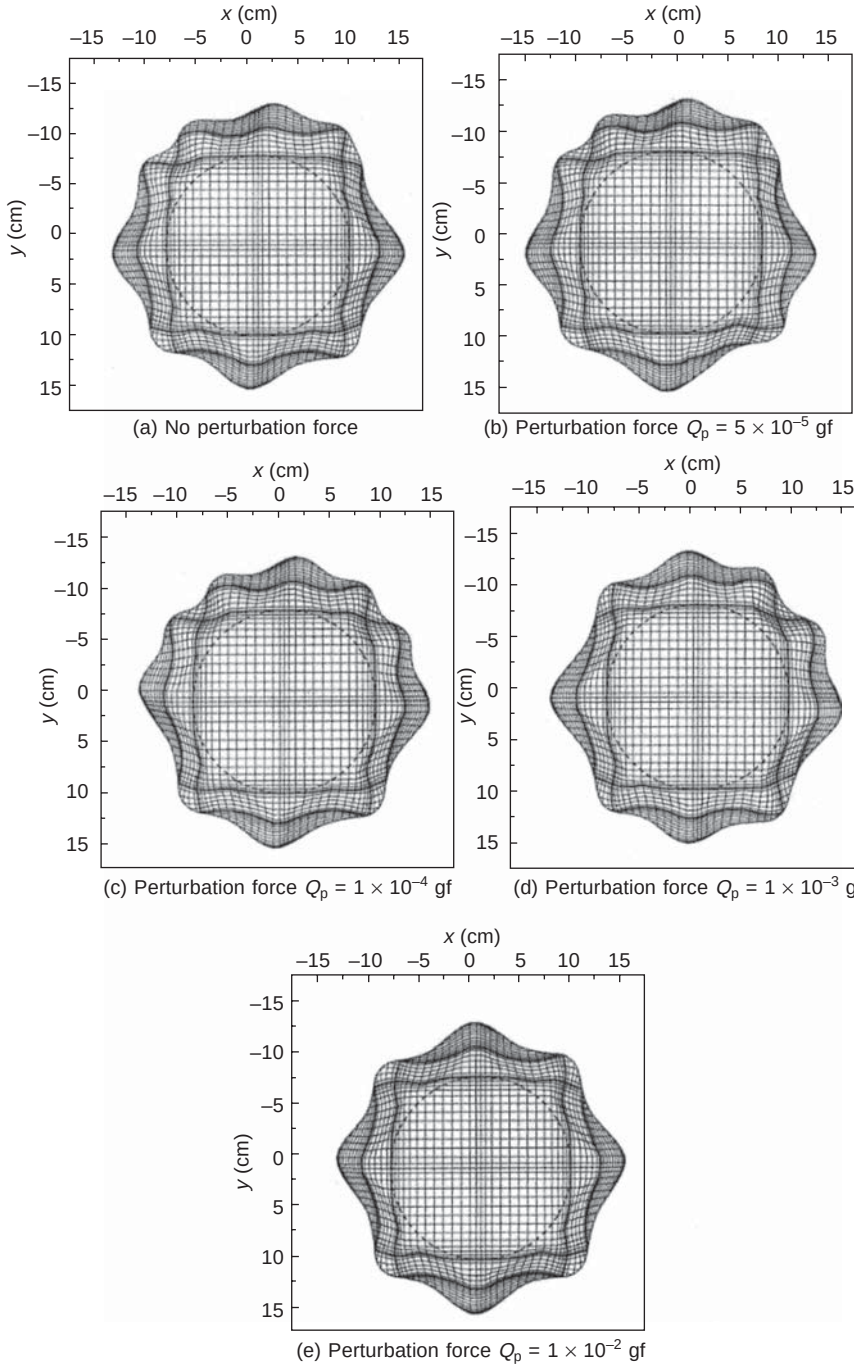

10.16 Drape patterns of fabric sheet B with a horizontal perturbation force.

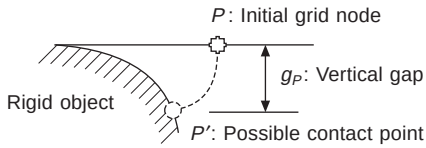

10.17 Two-dimensional case of fabric contact with rigid object.

However, in this approach, the magnitude of the penalty constant may affect the convergence of the iterative procedure. An excessively large constant can cause divergence. On the other hand, in the Lagrangian multiplier method, the number of equational unknowns must be increased, which leads to complexity and difficulty in computer implementation. In this study, a simpler but effective approach for dealing with the contact process between a cloth falling from an initial flat position and a rigid object is developed. This is described below.

Before deformation, the cloth is fully flat. The vertical distances between the initial positions of all grid nodes and their possible contact points (if any) are then calculated. The calculation is based on the plausible assumption that the in-plane stretching of the cloth is very small and an initial control volume retains its original surface area during the process of draping. Figure 10.17 shows a two-dimensional case of such a contact problem. During the numerical iteration, if the current increment makes the total vertical displacement of a grid node exceed its vertical gap, the condition that the vertical displacement increment is equal to the difference of the vertical gap and the displacement is imposed upon the grid node. As a result, the grid node is pulled back vertically. In this approach, there is no need to increase the number of equational unknowns or introduce large penalty constants which may cause numerical convergence problems. Therefore, the approach is rather simple and easy for computer implementation with the finite-volume method. Through the numerical simulations described in the next section this contact determination approach is proved to be both valid and efficient.

10.7.2 Simulation of contact drape

A number of numerical simulations of fabric pieces and simple garments are presented in this section. We start with the drape prediction of a square piece of full polyester fabric and a piece of pure wool fabric over a round rod; then a square piece of pure wool fabric and a piece of pure cotton fabric draped over a sphere are analysed. Finally the simulation results for a wool and a cotton skirt draped over and in contact with a synthetic body form from their initial flat positions are presented. The three types of fabric materials used here, namely polyester, wool and cotton materials, have been experimentally studied by Deng (1994) and Kang and Yu (1995), as listed in Table 10.3.

Table 10.3 Material properties of fabrics

Property	Notation	Polyester	Wool	Cotton
Tensile rigidity	E_{warp}	235724.7	1118.2	2531.6
(gf/cm)	E_{weft}	145680.8	759.5	1413.5
Bending rigidity	D_{warp}	0.322	0.083	0.068
(gf cm^2/cm)	D_{weft}	0.199	0.063	0.030
Shearing rigidity (gf/cm)	G	2800.0	41.8	250.7
Weight (gf/cm^2)	w	0.01715	0.019	0.0095
Thickness (cm)	h	0.0254	0.0593	0.0469

1 gf = 0.0098 N

10.7.2.1 Square fabric pieces draped over a round rod

Considering a fabric piece with the dimensions 20 cm × 20 cm, the problem involves the draping of the fabric piece on a round rod of radius 2.5 cm, which is placed diagonally under it. The simulation was first carried out for the polyester fabric material as the same problem was experimentally studied and numerically predicted using the finite-element method by Deng (1994). In his study, only bending rigidities in the warp and weft directions were experimentally obtained, while the tensile rigidities were derived from the bending rigidities using the approach in the classical plate/shell theory. In his finite-element analysis, however, Deng (1994) used an isotropic and geometrically non-linear shell element model, so only the warp-direction rigidities were actually included in the numerical simulation. The shear modulus was simply set equal to the tensile modulus, considering that the shear modulus showed relative insensitivity to the drape deformations, and the Poisson's ratio was set to 0.3. We presume that the fabric material is assumed to be linear elastic and orthotropic. The material properties in both the warp and weft directions, as listed in the third column of Table 10.3, were all included in the numerical simulation. The shear rigidity of the fabric was set to be 2800 gf/cm which is about 2 % of the weft-direction tensile rigidity, considering that the shear rigidity of the fabric is in general much smaller than the tensile rigidities. The effect of the Poisson's ratio was neglected in all simulations as mentioned earlier. A uniform grid of 33 × 33 nodes (or control volumes), as shown in Fig. 10.18, was adopted in the simulation.

Figure 10.19a shows the three-dimensional drape shape of this polyester fabric. Table 10.4 lists the three deformed co-ordinates of corner point A and compares them with the experimental data and those of the finite-element method of Deng (1994). It is seen from Table 10.4 that the predicted co-ordinates closely match the experimental results.

In order to compare the contact drape behaviour of different fabric materials, a simulation was also carried out for a wool fabric sheet of the same size

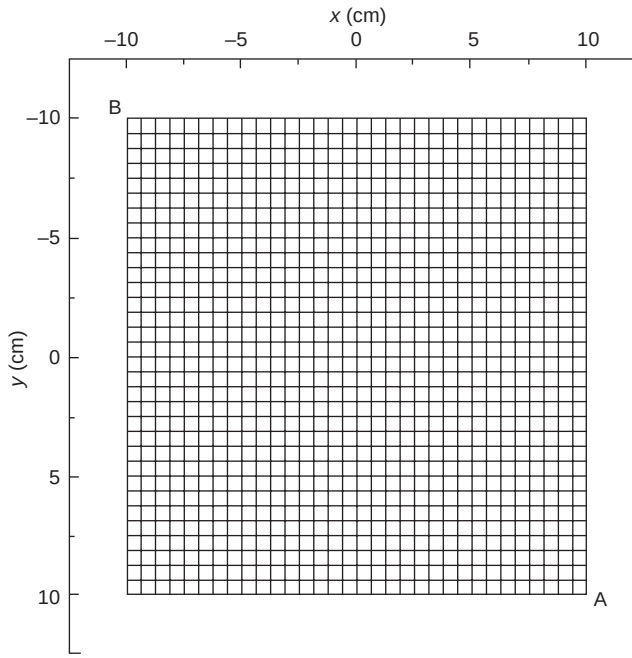

10.18 A uniform grid scheme for square fabric pieces draped over a rod.

draped over the same round rod. The simulated drape shape of the fabric is shown in Fig. 10.19b. The wool fabric piece is seen to exhibit a greater degree of draping than the polyester fabric counterpart. The calculated vertical co-ordinate of the corner point A (or B) of the former is larger than that of the latter and the corresponding horizontal co-ordinates of the former are smaller than those of the latter (Fig. 10.19). This demonstrates that the wool fabric has a better drapeability than the polyester fabric.

Both the above simulations were achieved on a Pentium® II/266 personal computer. The computational times required for the two simulations, are only 3 hours and 10 minutes for the polyester fabric and 28 minutes for the wool fabric. This shows that the drape simulation for the wool fabric with a greater drapeability is much faster than that for polyester fabric with stiffer mechanical properties. Much faster simulations can be achieved if a more powerful PC or workstation is used. Although precise comparison in computer time with other methods is not possible as different grid schemes, different computers and other variables are involved, the efficiency of the present method together with the proposed contact determination approach is easily demonstrated by noting that a draping simulation using a 51×51 grid requires one week on an IBM RS/6000 workstation.

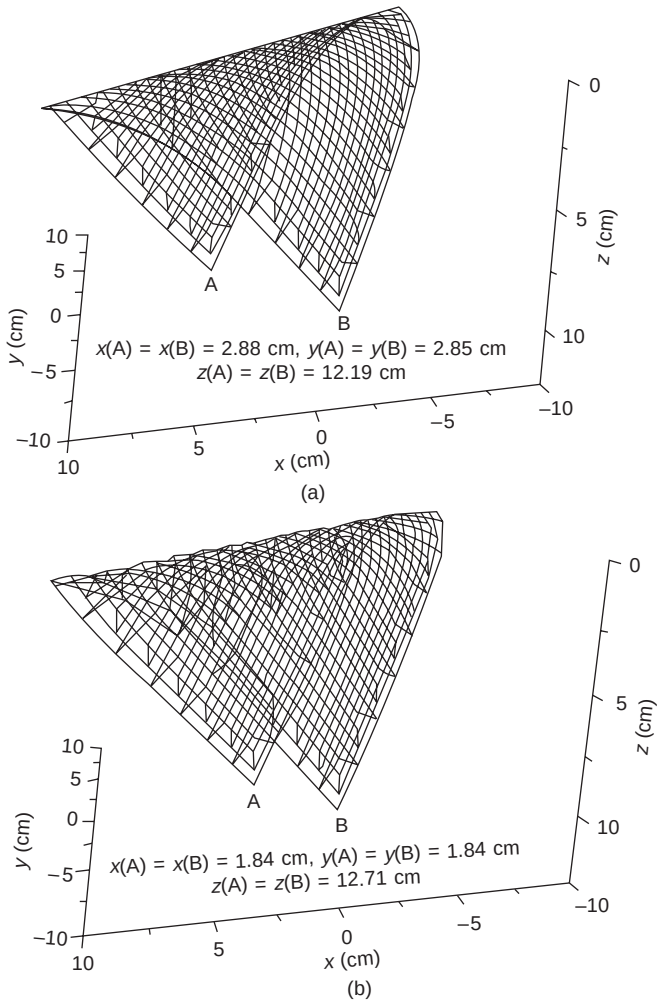

10.19 Drape shapes of square fabric pieces over a rod: (a) polyester fabric; (b) wool fabric.

Table 10.4 Deformed co-ordinates of point A of the polyester fabric piece

Co-ordinates of points A	***x* (cm)**	***y* (cm)**	***z* (cm)**
Initial co-ordinate	10	10	0
Theoretical prediction	2.88	2.85	12.19
Finite element prediction (Deng, 1994)	2.70	2.70	12.56
Experimental result (Deng, 1994)	3.27	3.27	12.25

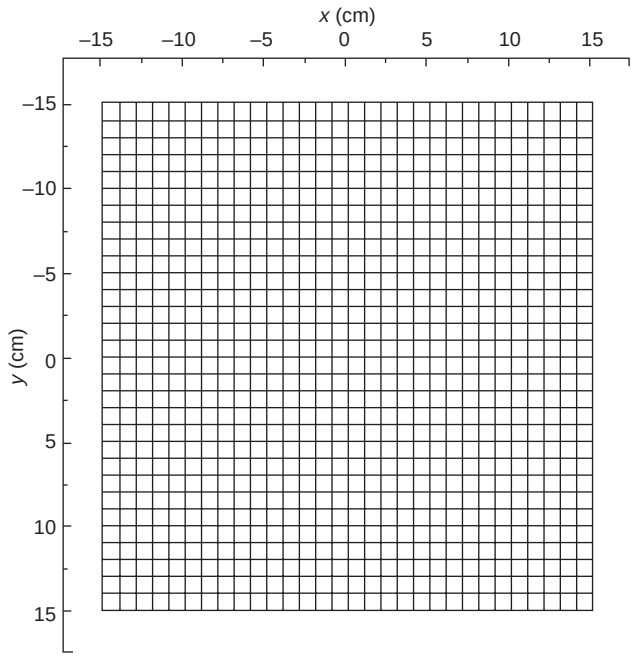

10.20 A uniform grid scheme for fabric pieces draped over a sphere.

10.7.2.2 Square fabric pieces draped over a sphere

In order to further investigate the validity and capacity of the present method and further compare the drapeability of different fabric materials, two square pieces of fabric 30 cm × 30 cm in size, one of wool material and one of cotton, concentrically draped over a sphere of 5 cm in radius were also analysed. Their mechanical properties are listed in Table 10.3. Both fabric pieces were modelled by a uniform grid of 31 × 31 nodes, as shown in Fig.10.20. The predicted drape shapes of the two fabric pieces are given in Figs 10.21a and b. Both shapes feature four main folds with smaller curved wrinkles between them. The wool fabric piece, however, is seen to exhibit a significantly greater degree of draping than the cotton fabric. The cotton fabric appears to be relatively stiff and does not drape so thoroughly over the sphere as the wool fabric does. This verifies the good drapeability of the wool fabric material in comparison with the cotton material.

The drape simulation of the two fabric pieces was again carried out using a finer grid scheme of 51 × 51 nodes, the results of which are shown in Fig. 10.22. The overall drape shapes of the two fabric pieces are similar to those presented in Fig. 10.21, demonstrating the reliability of the present method and the proposed contact determination approach. The northeast and southeast

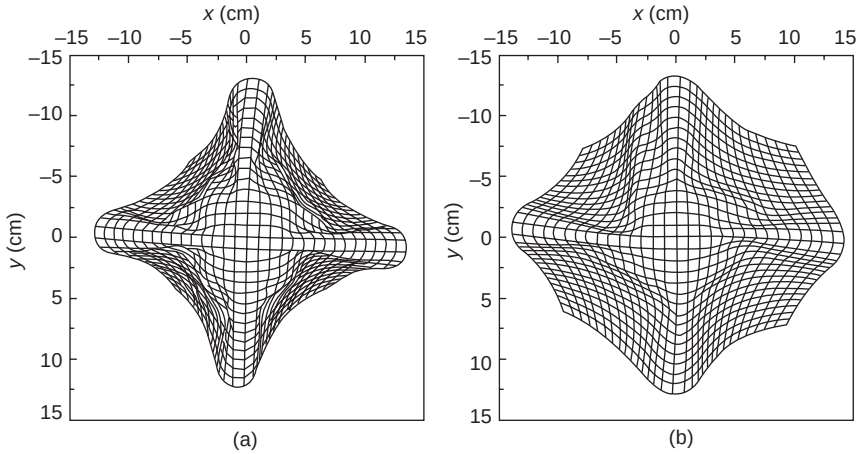

10.21 Drape shapes of square fabric pieces over a sphere: (a) wool fabric; (b) cotton fabric.

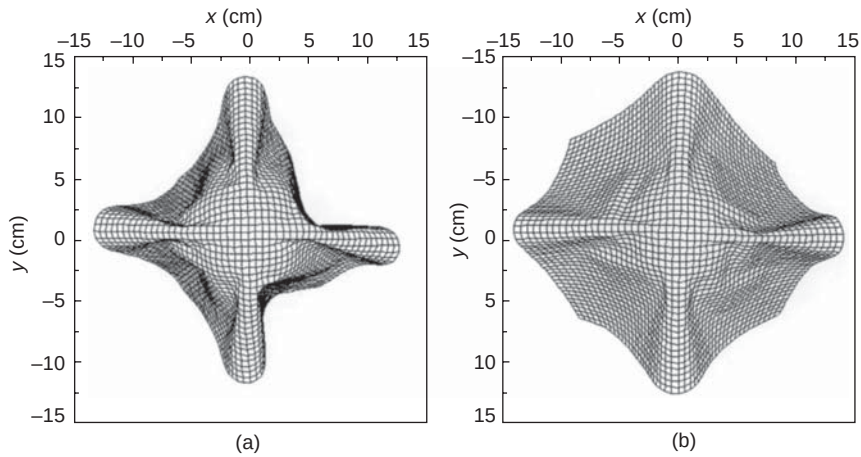

10.22 Drape shapes of square fabric pieces over a sphere using a finer grid: (a) wool fabric; (b) cotton fabric.

corners of the two fabric pieces in Fig. 10.22, however, undergo greater drape deformations than those presented in Fig. 10.21. This demonstrates that, using the present method, a fabric piece modelled by a coarse grid generally appears stiffer than one modelled by a finer grid. More importantly, the drape shapes predicted using a finer grid contain more detailed information of deformations including small curved wrinkles as shown in Fig. 10.22, particularly for the cotton fabric piece (Fig. 10.22b).

Naturally, the better results with a finer grid come with higher computational cost. The simulation of the drape shape of the wool fabric piece using a

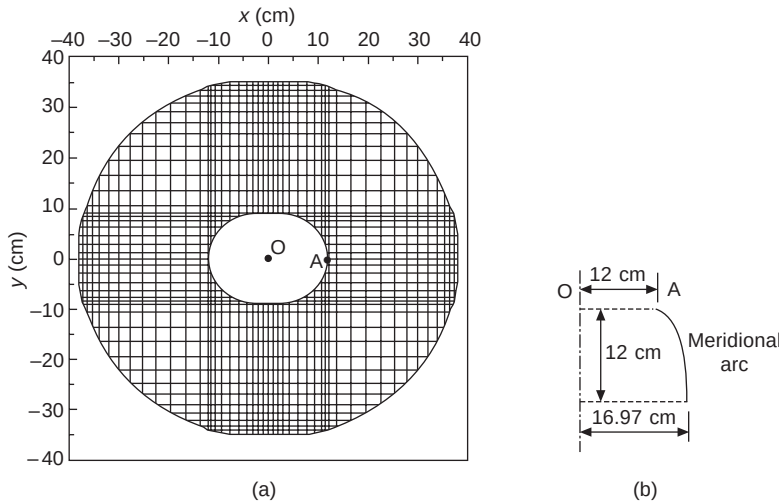

10.23 Modelling of a skirt attached to a human body: (a) non-uniform grid scheme; (b) meridional profile of body form.

31 × 31 grid as shown in Fig. 10.23a requires only 1 hour and 10 minutes, while the corresponding simulation using a 51 × 51 grid as shown in Fig. 10.22a requires 10 hours and 14 minutes, both on a Pentium® II/266 personal computer. Therefore, the choice of a grid needs to strike a balance between accuracy and computational time. For the cotton fabric, the simulations of the drape shapes as shown in Fig. 10.21b require 1 hour and 12 minutes and 17 hours and 10 minutes respectively. A comparison between the computer times required for the simulations of the wool and cotton fabric pieces again confirms that drape simulation is faster for fabric materials with a better drapability/softer mechanical properties, using the full Newton–Raphson iteration method with line searches as adopted here.

10.7.2.3 Skirts attached to a body form

The problem of a skirt draping over and interacting with a synthetic body form is considered here. The pre-drape configuration of the skirt is a flat cloth. The circumference of the body form at any vertical position was obtained by moving all points of the circumference at the top of the skirt (the inner boundary of the mesh shown in Fig. 10.23a) in the normal direction by the same amount. The distance between two corresponding points on any two circumferences was determined by the meridional profile adopted, which only had to be specified at one point around the circumference. Figure 10.23b shows the circular arc meridional profile used in the simulations described below.

Figure 10.23a shows the finite-volume grid scheme of the flat cloth used in the simulation. The non-uniform grid was used to suit the outer and inner boundaries of the skirt cloth. Two fabric materials, pure wool and pure cotton, with their mechanical properties as given in Table 10.3, were considered in the simulations. Figure 10.24 shows the three-dimensional drape shapes of the two skirts obtained using the present method, while Fig. 10.25 shows the corresponding vertical projections of the final shapes. The outlines of the two vertical projections are given in Fig. 10.26a and b, respectively. These figures were all produced by directly joining the calculated positions of all

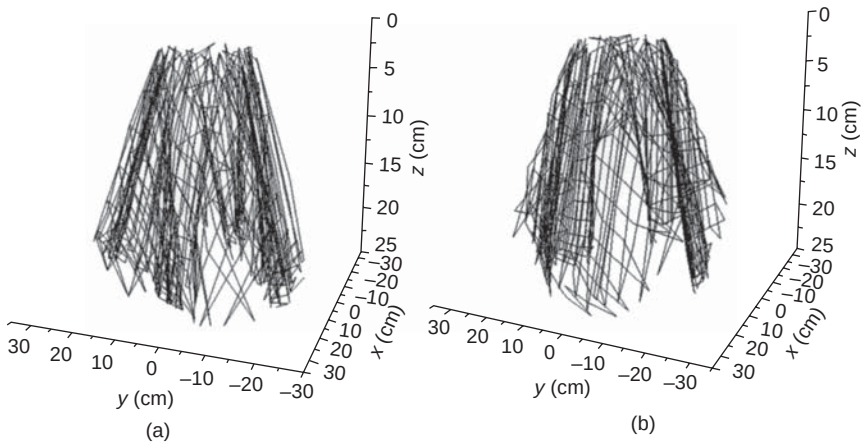

10.24 Three-dimensional drape shapes of skirts attached to a synthetic body form: (a) wool fabric; (b) cotton fabric.

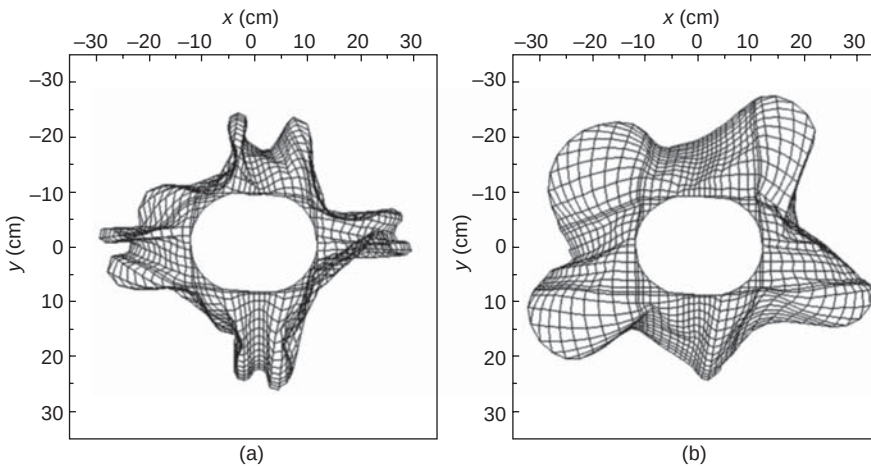

10.25 Vertical projections of skirts attached to a synthetic body form: (a) wool fabric; (b) cotton fabric.

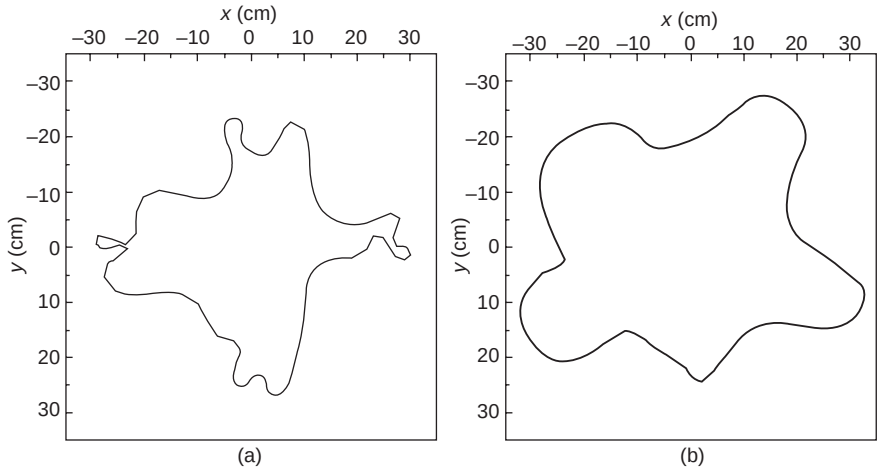

10.26 Outlines of vertical projections of skirts: (a) wool fabric; (b) cotton fabric.

grid nodes along the warp and weft directions by a straight line. Enhanced images with better visual effect can be obtained by using some curve- or surface-fitting plot software, which should be considered in future studies. The simulations for the wool and the cotton skirts took 2 hours and 31 minutes and 5 hours and 47 minutes on a Pentium® II/266 personal computer, respectively.

It is clear from Figs 10.24–26 that the two skirts exhibit complicated drape surfaces characterised by curved folds and wrinkles of various sizes. Although the initial geometry, material properties and boundary conditions of the two skirts are doubly symmetric about the *x*- and *y*-axis (Fig. 10.23), the deformed shapes do not retain the original symmetry again. Since bifurcation/buckling phenomena can occur during the process of draping, the skirts can deform into a preferred unsymmetrical shape through perturbations from numerical approximation and roundoff errors (Hu and Chung, 1998). It is seen from the comparison of parts (a) and (b) in Figs 10.24–26 that the wool skirt shows a greater degree of draping and a more complex drape shape than the cotton skirt. This again demonstrates the good drapeability of the wool fabric material studied here. Although there are no other available theoretical or experimental results for comparison with the present predictions, the results here do give realistic and reasonable shapes. This gives us confidence in the capability of the present method to model complicated contact drape problems of various clothing products including garments. It is thus suitable for use in the development of powerful clothing CAD systems.

10.8 Three-dimensional skirt simulation by using B-spline surface

It is well known that space spline surface has wide applications, including the modelling of objects such as robots, the design of cars, ships, aeroplanes, and computer simulation of virtual animals and humans. The B-spline paradigm for modelling smooth surfaces is limited by the requirement that the control point mesh must be organised as a regular rectangular structure. Ignoring this requirement by collapsing the control mesh edges leads to surfaces with ambiguous surface normal and degenerated parameterisation (Peirce, 1937). Many approximation approaches have been considered for modelling surfaces of arbitrary topological type by smoothly approximating an irregular control mesh. The limitation of this polishing method is that it does not satisfy the interpolation condition. A local interpolation method has also been discussed for constructing a piecewise smooth interpolation space surface (Hearle *et al.*, 1969, 1980; Skelton, 1974; Barker *et al*., 1985, 1986, 1987). A smooth piecewise quartic surface was constructed with triangular Bézier patches by Hearle *et al.* (1980). A cubic interpolation scheme for constructing GC^1 surface over space triangles and space quadrangles has also been presented. These methods are based on increasing the free-degrees of each surface patch by using increasing polynomial order or refinement of space mesh. In general, surface degree is not less quartic. In applying these methods, surface shapes depend on determination of parameter and estimation of gradient. It is concluded that local polynomial interplant generally produces unsatisfactory shapes (Kawabata, 1980a, b).

In this section, we consider an application of smooth interpolation space surface in clothing simulation. Combining both the fabric frame and the B-spline method generates a trimming B-spline interpolation surface over space mesh. The advantages of this technique are simplicity, efficiency and ease of display. The surface, as a whole parameter surface, is smooth and interpolates space mesh points.

The interpolation surface algorithm takes a space mesh as input. The mesh is extended to a regular rectangular mesh so that it fits into the product B-spline surface representation. Next, a B-spline surface is generated for interpolating the rectangular mesh vertices in which the boundary curves divide the interpolation surface into two parts, the initial and the extended surface. B-spline basis functions are chosen with equidistant knots and are bi-cubic. To compute the control points of the B-spline, it is necessary to solve the linear equation system which is recursively divided into small subsystems. The three-dimensional skirt surface is constructed by trimming the rectangular B-spline surface along with the boundary curves. Finally, a three-dimensional texture mapping technique is used to put the image texture on the skirt surface.

10.8.1 Background

This section gives a brief review of B-spline curve and surface. Some details can be found in Kawabata (1980), Oloffson (1967), Skelton and Schoppee (1976).

10.8.1.1 B-spline curve and surfaces

Given $m + p - 1$ space points $\{p_i \in R^3: i = 1, 2, \ldots, m + p - 1\}$ and a partition of the interval $[0, p]$, $s_1, s_2, \ldots, s_{2m+p-1}$, a degree m B-spline curve is defined as

$$p(s) = \sum_{i=1}^{m+p-1} p_i N_{i,m}(s) \quad s \in [0, p],$$

where

$$N_{i,1}(s) = \begin{cases} 1 & s_i \le s < s_{i+1} \\ 0 & \text{other} \end{cases}$$

and

$$N_{i,m}(s) = \frac{s - s_i}{s_{i+m-1} - s_i} N_{i,m-1}(s) + \frac{s_{i+m} - s}{s_{i+m} - s_{i+1}} N_{i+1,m-1}(s) \quad m > 1$$

are the basis function of B-spline.

The $m \times n$ B-spline surface is the tensor product of a two direction B-spline curve. Given space points $\{p_{ij} \in R^3 : i = 1, 2, \ldots, m + p - 1, j = 1, 2, \ldots, n + q - 1\}$ and two partitions, $s_1, s_2, \ldots, s_{2m+p-1}$, $t_1, t_2, \ldots, t_{2n+q-1}$ a degree $m \times n$ B-spline surface is defined as

$$p(s, t) = \sum_{i=1}^{m+p-1} \sum_{j=1}^{n+q-1} p_{ij} N_{i,m}(s) N_{j,n}(t) \quad (s, t) \in [0, p] \times [0, q].$$

B-spline surfaces, as a kind of parameter surface form, are widely applied in space surface representation, geometric design and object modelling. Low degree B-spline surface can be applied to surface rendering, shape control and collision detection.

10.8.1.2 B-spline interpolation

The B-spline interpolation means the construction of a B-spline surface so that it passes through the given space points. This can be described as follows. Given space points $\{Q_{ij} \in R^3 : i = 0, 1, \ldots, m + p - 1, j = 1, 2, \ldots, n + q - 1\}$ and two partitions, $s_1, s_2, \ldots, s_{2m+p-1}$, $t_1, t_2, \ldots, t_{2n+q-1}$, a B-spline surface $p(s)$ with given knots can be constructed so that the surface satisfies

the interpolation condition, that is

$$p(s_k, t_l) = \sum_{i=1}^{m+p-1} \sum_{j=1}^{n+q-1} p_{ij} N_{i,m}(s_k) N_{j,n}(t_l) = Q_{kl}$$

with

$$k = 0, 1, \ldots, m + p - 1, \; l = 1, 2, \ldots, n + q - 1$$

To compute the control points of the surface, it is necessary to solve a $m + p - 1 \times n + q - 1$ linear equation system. In fact, it can be translated to solve curve interpolation recursively. This can be represented as:

$$\begin{aligned} p(s, t) &= \sum_{i=1}^{m+p-1} \sum_{j=1}^{n+q-1} p_{ij} N_{i,m}(s) N_{j,n}(t) \\ &= \sum_{j=1}^{m+q-1} R_j(s) N_{j,n}(t) \\ &= \sum_{i=1}^{m+p-1} G_i(t) N_{i,m}(s). \end{aligned}$$

10.8.1.3 Texture mapping

Texture in graphics is an illumination function. It can be defined in both forms – mathematical model and image. This section adopts the latter. Let T be an $M \times N$ digital image. Divide the texture space into an $M \times N$ mesh and define a map from digital image to mesh vertices. The texture value in the mesh vertex takes the corresponding image value. The texture value inside the mesh can be computed by using interpolation methods. This defines a texture by digital image. Texture mapping is the process of building a mapping function from texture space to object surface. When computing light brightness in an illumination model, diffuse reflection shininess takes the texture function value.

10.8.2 Mesh extension

The three-dimensional skirt data come from a drape simulation computed by using a finite-volume method. It is deformed from a plane mesh. Because this mesh is not rectangular, it is necessary to extend the mesh to a rectangular one in order to construct an interpolation B-spline surface. This means adding some data to the original mesh along with its boundary. These three-dimensional space points are computed one by one from the boundary to the outside so that the whole mesh has a smooth shape (Fig. 10.27). It can be represented as follows.

If the extension point is connected with the boundary points in the vertical

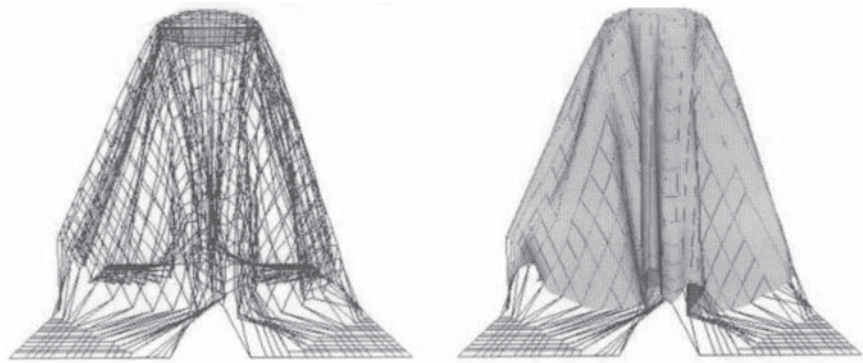

10.27 Extension mesh and trimming surface.

and horizontal directions, the point is set to be a linear combination of the four points that are connected in the two directions. If the extension point is connected with the boundary points in one direction, the point is set to be a linear combination of the two points that are connected in that direction.

10.8.3 B-spline surface interpolation

The extension rectangle mesh consists of 47 rows and 41 columns. The inside and outside boundaries are made up of 45 and 117 points respectively. For the extension rectangle mesh, we choose a bi-cubic B-spline surface with equidistant knots. The knots are the following:

- knots for parameter S:

  (0.0, 0.0, 0.0, 0.0, 1.0, 2.0, . . . , 42.0, 43.0, 44.0, 44.0, 44.0, 44.0)

- knots for parameter T:

  (0.0, 0.0, 0.0, 0.0, 1.0, 2.0, . . . , 36.0, 37.0, 38.0, 38.0, 38.0, 38.0)

  Let

  p_{ij}, $i = 1, 2, \ldots, 47$, $j = 1, 2, \ldots, 41$

  be the rectangle mesh points. The parameter interpolation points are chosen as:

- i-th column parameter points: $0, s_1^i, 1, 2, \ldots, 42, 43, s_2^i, 44$
- j-th row parameter points: $0, t_1^i, 1, 2, \ldots, 36, 37, t_2^i, 38$

  where

$$s_1^i = \frac{\| p_{i0} - p_{i1} \|}{\| p_{i0} - p_{i1} \| + \| p_{i1} - p_{i2} \|},$$

$$s_2^i = 44 - \frac{\| p_{i47} - p_{i46} \|}{\| p_{i47} - p_{i46} \| + \| p_{i45} - p_{i46} \|}$$

$$t_1^i = \frac{\| p_{0j} - p_{1j} \|}{\| p_{0j} - p_{1j} \| + \| p_{1j} - p_{2j} \|},$$

$$t_2^i = 38 - \frac{\| p_{41j} - p_{40j} \|}{\| p_{41j} - p_{40j} \| + \| p_{39j} - p_{40j} \|}$$

$i = 1, 2, \ldots, 41, j = 1, 2, \ldots, 47$

The B-spline parameter surface $P(s, t)$ defined on $[0,44] \times [0,38]$ is determined by the interpolation condition.

$$P(s_i, t_j) = p_{ij},\ i = 1, 2, \ldots, 47, j = 1, 2, \ldots, 41$$

10.8.4 Trimming surface

The previous section shows the construction of an interpolation B-spline surface for an extension mesh. To generalise the interpolation surface of original mesh, it is necessary to determine the boundary curves on the interpolation surface. A method of representing the boundary curves is to determine the parameter curves in the parameter field of the previous interpolation B-spline surface so that its mapping curves in the B-spline function are the boundary curves of original mesh. The following presents the construction of a precise representation of the boundary curves in the parameter field of the previous interpolation B-spline surface.

The B-spline surface interpolates all vertices of the extension mesh, including the boundary vertices of the original mesh. The parameter points of the boundary vertices can be determined in the parameter field from the interpolation parameter points. Two boundary curves can be computed by using a method similar to the one introduced in the previous section. A cubic B-spline curve with equidistant knots is chosen. The knots are the following:

- parameter knots for outside boundary curve:

  (0.0, 0.0, 0.0, 0.0, 1.0, 2.0, . . . , 112.0, 113.0,114.0, 114.0, 114.0, 114.0)

- parameter knots for inside boundary curve:

  (0.0, 0.0, 0.0, 0.0, 1.0, 2.0, . . . , 40.0, 41.0, 42.0, 42.0, 42.0, 42.0)

10.8.5 Texture mapping for the skirt

For the skirt surface, using a map from digital image field to parameter field of the surface can represent the texture mapping. This map can be constructed

by a map from image field $M \times N$ to the extension surface parameter field $(0,38) \times (0,42)$. To obtain texture mapping with different repeats in row and column, we combine a new large image as a texture image by iteratively combining the repeat image in row and column directions. Figure 10.28 is the texture mapping of the skirt with a single repeat and with 6×6 repeats. The size of a single repeat texture image is 256×256.

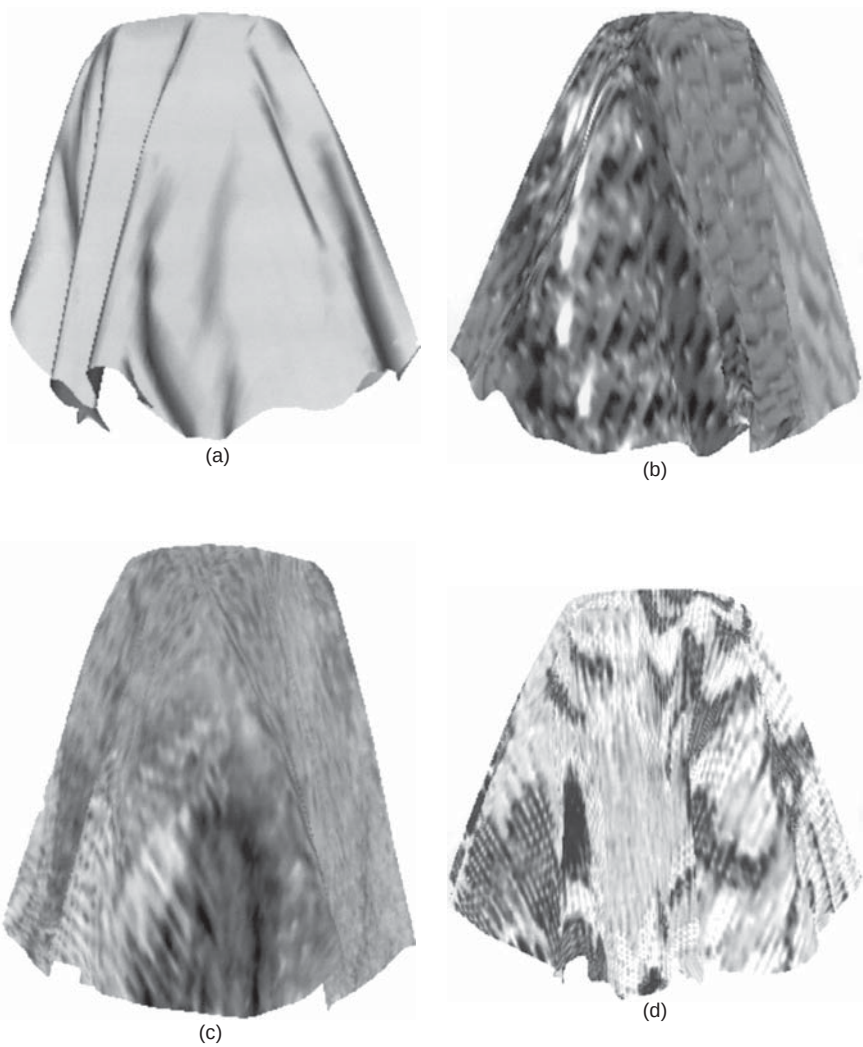

10.28 The texture mapping of skirt with a single repeat and 6×6 repeats. The size of single repeat texture image is 256×256: (a) skirt surface; (b)–(g) texture mapping of skirt with a single repeat; (h)–(m) texture mapping of skirt with 6×6 repeats.

(e)

(f)

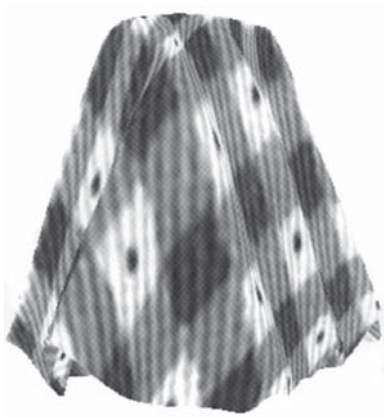

(g)

(h)

(i)

(j)

10.28 (cont.)

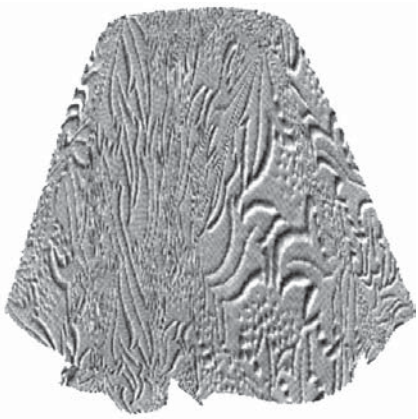

(k)

(l)

(m)

10.28 (cont.)

10.8.6 Summary

This part of the chapter presents a scheme for constructing a three-dimensional skirt surface with special texture. The scheme is an application of B-spline and texture mapping techniques to clothing modelling. Beginning with an initial three-dimensional skirt mesh, an extended regular rectangular mesh is constructed which includes the initial mesh. A B-spline surface is generated for interpolating the rectangular mesh vertices in which the boundary curves divide the interpolation surface into two parts, the initial and the extended

surface. Using B-spline curve in parameter field of B-spline interpolation surface represents the two boundary curves. They are determined by interpolating the boundary vertices. The three-dimensional skirt surface is constructed by trimming the rectangular B-spline surface along with the boundary curves. Finally, a three-dimensional texture mapping technique is used to put the image texture on the skirt surface. The texture size is changeable with repeating.

10.9 References

Barker R *et al* (1985 May, 1986 February & 1987 March), *Reports to North Carolina State University*, Raleigh, North Carolina 27695–8301, Kawabata Consortium, School of Textiles, North Carolina State University.

Chen B and Govindaraj M (1995), A physical based model of fabric drape using flexible shell theory, *Text Res J*, **65**(6), 324–330.

Crisfield, M (1997), *Non-linear Finite Element Analysis of Solids and Structures*, Volume II: Advanced Topics, Chichester, John Wiley & Sons.

Deng S (1994), *Nonlinear Fabric Mechanics Including Material Nonlinearity, Contact and an Adaptive Global Solution Algorithm* (Doctoral Dissertation, North Carolina State University, Raleigh, N C.

Dhande S G, Rao P V M and Moore C L (1993), Geometric modelling of draped fabric surfaces, *Graphics, design and visualization (Proc Int Conf on Computer Graphics)*, S P Mudur and S N Pattanaik (eds), Bombay, Jaico Publishing House, 173–180.

Gan L, Ly Ng and Steven G P (1995), A study of fabric deformation using non-linear finite elements, *Text Res J*, **65**(11), 660–668.

Hearle J W S, Grosberg P and Backer S (1969), *Structural Mechanics of Fibres, Yarns, and Fabrics: vol I*, New York, Wiley-Interscience, 340.

Hearle J W S, Thwaites J J and Amirbayat J (1980), *Mechanics of Flexible Fibres Assemblies (NATO Advanced Study Institute Series: E, Applied Sciences No 38*), The Netherlands, Alpen aan den Rijn, Sijthoff and Noordhoff.

Hu J L and Chung S P (1998), Investigation of drape behaviour on woven fabrics with seams, *Text Res J*, **68**(12), 913–919.

Kang T J and Yu W R (1995), Drape simulation of woven fabric by using the finite-element method, *J Text Inst*, **86**(4), 635–648.

Kawabata S (1975), *The Standardization and Analysis of Hand Evaluation*, Osaka, hand evaluation and standardization committee of the Textile Machinery Society of Japan.

Kawabata S (1980), Examination of effect of basic mechanical properties of fabric hand, in *Mechanics of Flexible Fibre Assemblies (NATO Advanced Study Institute Series: E, Applied Sciences No 38)*, Hearle J W S, Thwaites J J and Ambirbayat J (eds), The Netherlands, Alpen aan den Rijn, Sijthoff and Noordhoff 14–18.

Kawabata S (1980, July), *Standardisation and Analysis of Hand Evaluation, 2nd edition Osaka*, the Textile Machinery Society of Japan.

Kim J (1991), *Fabric Mechanics Analysis Using Large Deformation Orthotropic Shell Theory* (Doctoral Dissertation, North Carolina State University, Raleigh, NC).

Oloffson B (1967), Study of inelastic deformations of textile fabrics, *J Text Inst*, **58,** 221.

Peirce F T (1937), The geometry of cloth structure, *J Text Inst*, **28,** 45–96.

Skelton J (1974), Frictional effects in fibrous assemblies, *Text Res J*, **44**, 746–752.
Skelton J and Schoppee M M (1976), Frictional damping in multicomponent assemblies, *Text Res J*, **46**, 661–667.
Teng J G (1996), Buckling of thin shells: recent advances and trends, *Appl Mech Rev ASME*, **49**(4), 263–274.

Index